technische universität
dortmund

mpi
dortmund

Identification of small-molecule modulators that enhance the ability of the immune system to eliminate cancer cells

Dissertation

zur Erlangung eines akademischen Grades
des Doktors der Naturwissenschaften
(Dr. rer. nat.)

der Fakultät für Chemie und Chemischen Biologie
der Technischen Universität Dortmund

vorgelegt von

Elisabeth Hennes, M.Sc.
geboren am 16.08.1991 in Bonn

Dortmund, den 01.02.2022

Die vorliegende Dissertation wurde im Zeitraum vom März 2017 bis Januar 2022 unter der Anleitung von Prof. Dr. Dr. h.c. Herbert Waldmann und Dr. Slava Ziegler an der Fakultät für Chemie und Chemische Biologie der Technischen Universität Dortmund und dem Max-Planck-Institut für Molekulare Physiologie Dortmund verfasst.

1. Gutachter: Prof. Dr. Dr. h.c. Herbert Waldmann
2. Gutachter: Prof. Dr. Carsten Watzl

Results presented in this thesis contributed to the following publications:

E. Hennes, P. Lampe, L. Dötsch, N. Bruning, L-M. Pulvermacher, S. Sievers, Z. Ziegler, H. Waldmann, "Cell-Based Identification of New IDO1 Modulator", Angew. Chem. Int. Ed. **2021**, 60, 9869-9874.

Table of Contents

1. Summary / Zusammenfassung

Summary:

The ability of the immune system to fight cancer is long-established whereas an in-depth understanding of how cancer cells can escape from immunosurveillance has only emerged over the last 20 year. This led to the development of the first groundbreaking cancer immunotherapies. However, the variety of cancer cell escape mechanisms is still not entirely elucidated, e.g., how cancer cells establish their immunosuppressive tumor microenvironment (TME). Although key components of the TME have been identified, only a few could be established as drug targets for the development of novel small-molecule drugs.

To discover new small molecules modulating the immunosuppressive features of the TME, two chemical genetic approaches were developed in the course of this thesis.

The TME harbors various tumor-derived soluble suppressive factors that inhibit effector immune cells, like natural killer (NK) cells, from eliminating cancer cells. In order to prevent NK cell suppression within the TME and to identify proteins or pathways involved in NK cell inhibition, a phenotypic assay was developed that mimics the TME, as the addition of transforming growth factor beta (TGFβ) and prostaglandin E2 (PGE2) inhibited NK cell-mediated anti-tumor activity. A co-culture system of primary lymphocytes or NK cells and the lung cancer cell line A549 was established in a 1536-well format to monitor the restoration of NK cell-mediated cytotoxicity upon small-molecule treatment. A library of approximately 29,000 small molecules was screened and identified hit compounds included modulators targeting key components of the TME, such as TGF-beta receptor type-1 (TGFR-1) as well as compounds targeting proteins not yet linked to NK cell suppression, such as the autophagy-related PI3K kinase VPS34.

The second approach focused on the kynurenine (Kyn) metabolic pathway and its rate limiting enzyme indolamine 2, 3-dioxygenase (IDO1) as it plays a key role in immunosuppression within the TME. Currently investigated compounds in clinical studies exclusively inhibit the enzymatic activity of IDO1 and showed only limited success. Therefore, a new cell-based assay was established to identify novel small-molecule modulators of the whole Kyn pathway that may have benefits over direct IDO1 inhibitors. In the assay, Kyn levels were monitored by means of a fluorescent Kyn sensor in a 1536-well format. Screening over 150,000 small molecules led to the identification of several compounds targeting known key elements of the Kyn metabolic pathway, such as heme synthesis inhibitors or IDO1 expression modulators. In addition, a plethora of compounds with unknown targets or modes of action were identified, of

which four were selected for in-depth analysis. Three highly potent inhibitors of cellular Kyn production with IC_{50} values between 5 and 30 nM were found to directly inhibit the enzymatic activity of IDO1 by preventing heme cofactor incorporation. The fourth compound, iDeg-1, inhibits IDO1 activity with an IC_{50} of 0.8 µM and displays an unprecedented mode of action. iDeg-1 highly selectively induces the polyubiquitination and subsequent degradation of IDO1. iDeg-1 directly interacts with IDO1, presumably with its apo form, and may facilitate the recruitment of the polyubiquitination machinery.

Both cell-based phenotypic assays established in the course of this thesis led to the discovery of various novel bioactive small molecules that may enhance cancer immunosurveillance. These compounds may pave the way for both, the identification of new drug targets, thereby deepening our understanding of cancer immunosuppression, as well as the development of novel cancer immunotherapies.

Zusammenfassung:

Die Fähigkeit des Immunsystems, Krebs zu bekämpfen, ist seit langem bekannt, während die detaillierten Erkenntnisse darüber, wie Krebszellen der Immunüberwachung entkommen können, erst in den letzten 20 Jahren entstanden ist. Dies führte zur Entwicklung von ersten bahnbrechenden Immuntherapien gegen Krebs. Die Vielfalt der Fluchtmechanismen von Krebszellen ist jedoch noch nicht vollständig aufgeklärt, z.B. wie Krebszellen die immunsuppressive Tumor-Mikroumgebung (TMU) aufbauen. Obwohl Schlüsselkomponenten der TMU identifiziert wurden, konnten nur wenige als Zielmoleküle für die Entwicklung neuer niedermolekularer Medikamente etabliert werden.

Um neue Substanzen zu entdecken, die die immunsuppressiven Eigenschaften der TMU modulieren, wurden im Rahmen dieser Arbeit zwei chemisch-genetische Ansätze entwickelt. Die TMU besteht aus verschiedene Tumor-abstammenden löslichen Suppressionsfaktoren, wodurch die Effektor-Zellen des Immunsystems, wie z.B. natürliche Killerzellen (NK-Zellen), die normalerweise Krebszellen eliminieren, inhibiert werden. Um die NK-Zell-Suppression innerhalb der TMU zu verhindern und gleichzeitig zelluläre Proteine oder Signalwege zu identifizieren, die an der NK-Zell-Hemmung beteiligt sind, wurde ein phänotypisches Testverfahren entwickelt. Dieses Testverfahren ahmt die TMU nach, da die Zugabe des transformierenden Wachstumsfaktors Beta (TGFβ) und von Prostaglandin E2 (PGE2) die NK-Zell-vermittelte Anti-Tumor-Aktivität inhibiert. Ein Co-Kultursystem von primären Lymphozyten oder NK-Zellen und der Lungenkrebszellllinie A549 wurde verwendet, um die Wiederherstellung der NK-Zell-vermittelten Zytotoxizität nach Behandlung mit Substanzen in einem 1536-Well-Format zu analysieren. Eine Bibliothek von ungefähr 29.000 chemischen Substanzen wurde untersucht und identifizierte, bioaktive Verbindungen umfassten Substanzen, die auf Schlüsselkomponenten der TMU abzielen, wie den TGF-β-Rezeptor Typ-1 (TGFR-1), sowie Substanzen, die Proteine modulieren, die noch nicht mit der NK-Zell-Suppression in Verbindung gebracht wurden, wie die in Autophagie involvierte PI3K-Kinase VPS34.

Der zweite Ansatz konzentrierte sich auf den Kynurenin (Kyn)-Stoffwechselweg und das geschwindigkeitslimitierende Enzym Indolamin 2,3-Dioxygenase (IDO1) welches eine Schlüsselrolle bei der Immunsuppression innerhalb der TMU spielt. Derzeit sind Substanzen in klinischen Studien, die ausschließlich die enzymatische Aktivität von IDO1 hemmen, jedoch zeigen diese wenig Erfolg. Daher wurde ein neues zellbasiertes Testverfahren etabliert, um neuartige niedermolekulare Modulatoren des gesamten Kyn-Signalwegs zu identifizieren, die Vorteile gegenüber direkten IDO1-Inhibitoren haben könnten. In dem Testsystem wurden die Kyn-Mengen mittels eines fluoreszierenden Kyn-Sensors in einem 1536-Well-Format gemessen. Das Screening von über 150.000 chemischen Molekülen führte zur Identifizierung

mehrerer Verbindungen, die auf bekannte Schlüsselelemente des Kyn-Stoffwechselwegs abzielen, wie Häm-Synthese-Inhibitoren oder IDO1-Expressionsmodulatoren. Darüber hinaus wurde eine Vielzahl von Verbindungen mit unbekannten zellulären Zielproteinen oder Wirkungsweisen identifiziert, von denen vier für eine eingehende Analyse ausgewählt wurden. Es wurde festgestellt, dass drei sehr wirksame Inhibitoren, die die zelluläre Kyn-Produktion mit IC_{50}-Werten zwischen 5 und 30 nM inhibieren, die enzymatische Aktivität von IDO1 hemmen, indem sie den Einbau des Häm-Cofaktors von IDO1 verhindern. Die vierte Verbindung, iDeg-1, hemmt die IDO1-Aktivität mit einem IC_{50} von 0,8 µM und zeigt einen neuartigen Wirkmechanismus. iDeg-1 induziert hochselektiv die Mehrfachubiquitinierung und somit den anschließenden Abbau von IDO1. iDeg-1 interagiert direkt mit IDO1, vermutlich mit seiner Apo-Form, und vermittelt die Rekrutierung der zellulären Maschinerie, die die Ubiquitinierung von Proteinen vermittelt.

Beide im Rahmen dieser Dissertation etablierten zellbasierten phänotypischen Testsysteme führten zur Entdeckung von neuen bioaktiven Substanzen, die die immun-vermittelte Bekämpfung von Krebs verbessern könnten. Diese Verbindungen könnten neue Wege sowohl für die Identifizierung neuer molekularer Zielstrukturen, mit dessen Hilfe das Verständnis der Krebsimmunsuppression vertieft wird, als auch für die Entwicklung neuartiger Krebsimmuntherapien eröffnen.

2. Introduction

In the 20th century, life expectancy increased substantially due to advances in hygiene, medical care and sufficient food.[1] However, aging is one of the major risk factors for oncological diseases and cancer prevalence rose in the ageing Western population making cancer the second leading cause of death in Europe and the US.[2]

Traditional cancer treatments include radiotherapy, chemotherapy and surgery. In parallel, also new cancer therapy approaches have been developed to complement the traditional ones which led to an increase in survival rate. Nonetheless, the 10-year survival rate of cancer patients is only 57 % and varies between the different types of malignancies.[3] Hence, the need for innovative and more effective cancer treatments is high. Cancer immunotherapy arose as promising strategy to fight cancer by stimulating the patient's immune system and approved immunotherapeutics exhibit great effectiveness in some cancer types. However, those therapies target only a few immune pathways and alternative agents are demanded to increase patient survival.[4]

2.1 The Immune System and Cancer Development

The immune system is vital for every multicellular organism as it follows various strategies to counteract pathogens, such as bacteria and viruses. The immune system comprises innate and the adaptive immunity which tightly cooperates to successfully eliminate pathogens.[5]

However, the immune system cannot only fight foreign invaders, constant immunosurveillance also facilitates the recognition and eradication of precancerous or malignant cells within the body and, thus, prevents tumor development. Cytotoxic immune cells that exhibit cytolytic function to eliminate malignant cells are natural killer (NK) cells, which belong to the innate immune system, and cytotoxic T lymphocytes (CTLs), also known as CD8+ T cells, which are part of the adaptive immune system. NK cells show broad cytotoxic activity against cells under stress without prior sensitization whereas CTLs require priming by antigen-presenting cells, like dendritic cells (DCs), to become activated. Once activated, CTLs specifically eliminate cells presenting cancer-associated antigens. These two contrasting elimination strategies usually efficiently eradicate developing cancer cells within the body.[6, 7]

Nonetheless, the immune system cannot always prevent tumor progression. And during the development of cancer, immunosurveillance even plays an important role in sculpting the malignant disease, which was termed "cancer immunoediting" by Schreiber and colleagues (Figure 2.1).[8] In the elimination phase (Figure 2.1A) the selective pressure driven by the immune system can provoke tumor cell variants that are less immunogenic and can persist in

a steady state (equilibrium, Figure 2.1B). Eventually, these cells develop further mutations and thereby mechanisms to escape the immune control and promote tumor progression (Figure 2.1C).[8, 9]
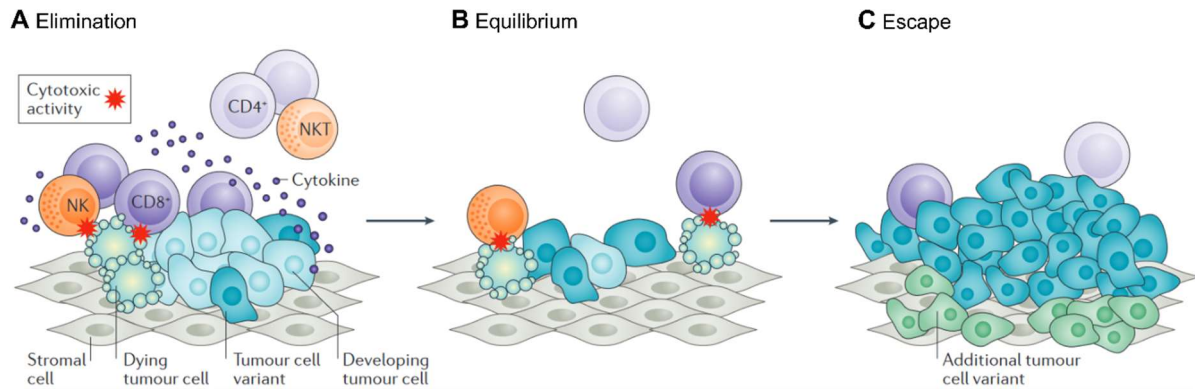

Figure 2.1: **The three phases of cancer immunoediting.** In the elimination phase (A) cytotoxic immune cells, namely natural killer (NK) cells and CD8^{+} T cells, eliminate developing tumor cells with support of cytokine releasing cells (NKT and CD4^{+} cells). In the second phase, the equilibrium (B), tumor cell variants that are less immunogenic persist and the accumulation of mutations can finally lead to cancer immune escape (C) and cancer progression. Reprinted by permission from Springer Nature: [9], Copyright © 2016.

Various mechanisms can lead to cancer cell variant persistence and immune escape despite an immunocompetent environment. Cancer cells may develop mechanisms to avoid immune recognition, like the loss of cancer-associated antigens or by directly inhibiting immune cell function, e.g. by expressing inhibitory ligands like the programmed death receptor ligand 1 (PD-L1).[10] In addition, dysregulated metabolism of cancerous cells leads to an enhanced consumption of nutrients and an elevated secretion of factors such as lactate, reactive oxygen species (ROS) and urea that reduce anti-tumor immunity.[11] Furthermore, during tumorigenesis cancer cells can also orchestrate an immunosuppressive network, known as tumor microenvironment (TME) that inhibits effector immune cells, NK cells and CTLs.[10]

2.2 Tumor Microenvironment (TME)

The tumor microenvironment (TME) is a multifaceted environment and is established to strengthen cancer development and progression.[12] The TME is composed of cancer cells as well as blood vessels, extracellular matrix, various types of stromal cells, such as fibroblasts, and mesenchymal stem cells (MSCs) and tumor-associated macrophages (M2) (Figure 2.2). Cancer cells constantly interact with and sculpture non-malignant cells in their surrounding. For example, fibroblasts are reprogrammed to cancer-associated fibroblasts (CAFs) to promote cancer growth. Moreover, regulatory immune cells, like regulatory T cells and

dendritic cells (DCs), can be recruited to support cancer growth.[10] Accordingly, the term tumor actually describes a complex environment including various cell types and not just an accumulation of cancer cells. The exact composition of the TME varies between different tumor types.[13]
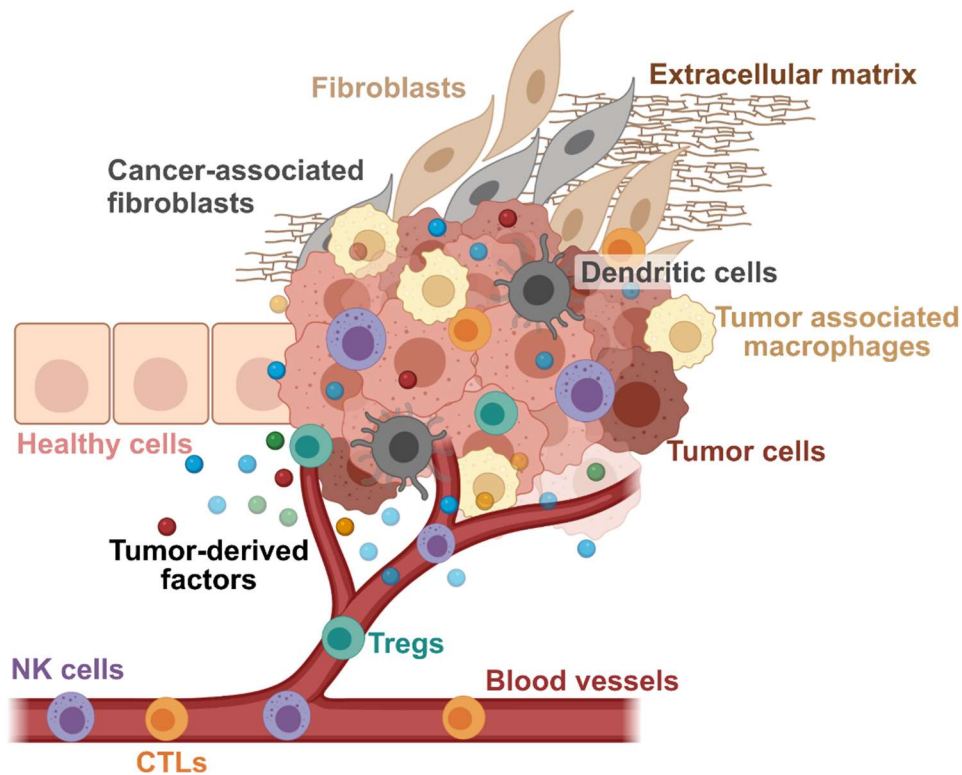

Figure 2.2: **Tumor microenvironment**. The TME is composed of cancer cells as well as fibroblasts, cancer-associated fibroblasts, extracellular matrix and immune cells. Blood vessels are recruited to maintain oxygen and nutrient supply. Various tumor-derived secreted factors are in the TME. Altogether, the TME supports cancer development and progression. Created with BioRender.com and based on Adams *et al.*[14]

Cancer cells together with the tumor-associated cells release multiple factors to orchestrate angiogenesis, proliferation, invasion as well as immunosuppression. In comparison to healthy cells, cancer cells have an altered metabolism, which causes the accumulation of lactate, reactive oxygen species (ROS) and kynurenine (Kyn), amongst others. Furthermore, some metabolic enzymes are upregulated within the TME, such as indolamine-2,3-dioxygenase (IDO1) and arginase which reduce the abundance of the amino acids tryptophan (L-Trp) and arginine (L-Arg), respectively which induces amino acid deprivation and, thus, immune cell inhibition. Moreover, tumor-derived immunosuppressive factors, like transforming growth factor β (TGFβ), interleukin-6 (IL-6), IL-10 and prostaglandin E2 (PGE2) are secreted into the extracellular space of the TME. Although effector immune cells (NKs and CTLs) infiltrate into the TME, tumor-derived suppressive factors substantially reduce immune cell-mediated cancer cell elimination and induce an anergic, suppressed immune cell phenotype.[10] Thus,

effector immune cells that are at the tumor site to eradicate malignant cells are inhibited by the multiple suppressive mechanisms within this tumor microenvironment. Consequently, the TME strengthens cancer immune escape and cancer progression.

2.2.1 Natural Killer Cells

Natural killer (NK) cells were first described by Kiessling *et al.*[15] as "naturally" occurring killer cells, hence their name. NK cells belong to the peripheral blood lymphocytes and exhibit powerful cytotoxic responses against viral infections and aberrant cells. The development and education of NK cells take place in the bone marrow and the secondary lymphoid organs. The education of NK cells is important to ensure self-tolerance. The major histocompatibility complex (MHC) class I is a constitutively expressed receptor on the surface of healthy cells and is the key player in self and nonself discrimination by NK cells. MHC class I molecules bind to inhibitory killer cell immunoglobulin-like receptors (KIRs) on NK cells and thereby prevent NK cell activation. Nevertheless, NK cell activity is tightly regulated not only by inhibitory signals (MHC) also activating receptors, e.g. natural killer group 2-member D (NKG2D) and natural killer protein (NKps) are present on NK cells and regulate NK cell function.[7, 16, 17] Moreover, NK cells respond to cytokines, such as IL-2, IL-12, IL-15, IL-18 and type I interferons (IFN) which are involved in NK cell maturation, activation and proliferation.[6] NK cells are activated by encountering malignant or virus-infected cells during immunosurveillance as well as by cytokines that are produced during immune response. Stimulation of NK cells by IL-2 or IL-15 enhances cytotoxic activity and the expression of effector molecules (granzymes and perforin) through the PI3K-AKT-mTOR- pathway. mTOR complex 1 (mTORC1) activity is crucial for NK cell activity as it regulates NK cell metabolism and effector functions.[17, 18] Activated NK cells also secret cytokines, such as interferon gamma (IFNγ) and tumor necrosis factor alpha (TNFα), elevating the immune response and recruiting effector immune cells. However, IFNγ exhibits pro- and anti-tumorigenic effects and can also strengthen cancer immune escape (see 2.2.2).[19]

As described above, NK cell cytotoxicity is critical as first-line of defense (innate immunity) against tumor development as no prior sensitization is required.[17] Stressed or transformed cells often downregulate or lose MHC class I molecules, whereas activating ligands, e.g. CD155 and MICA (MHC class I polypeptide-related sequence A), are elevated in multiple malignant cells.[20] Both mechanisms result in an activation of NK cells and elimination of diseased cells. Furthermore, a third mechanism to activate NK cells is facilitated by antibodies that are attached to target cells inducing antibody-dependent cell-mediated cytotoxicity (ADCC). Once, NK cells are activated, target cells cytolysis can be induced by two distinct

mechanisms: cytotoxic granules or death receptor ligation (FasL/TRAIL). Cytotoxic granules contain effector molecules like granzyme B and perforin, among others, and induce apoptosis of target cells. Similarly, death receptor ligation induces target cell apoptosis.[7, 21]

Although NK cells exhibit strong cancer cell elimination capability, cancer cells can escape from NK cell-mediated immunosurveillance. Evading NK cell recognition can be mediated by multiple factors in the TME. Tumor-derived suppressive factors, like TGFβ, IL-10, PGE2, and, amino acid as well as nutrient deprivation induce an anergic, suppressed NK phenotype which inhibits NK cell-mediated cancer cells lysis.[10, 17, 22]
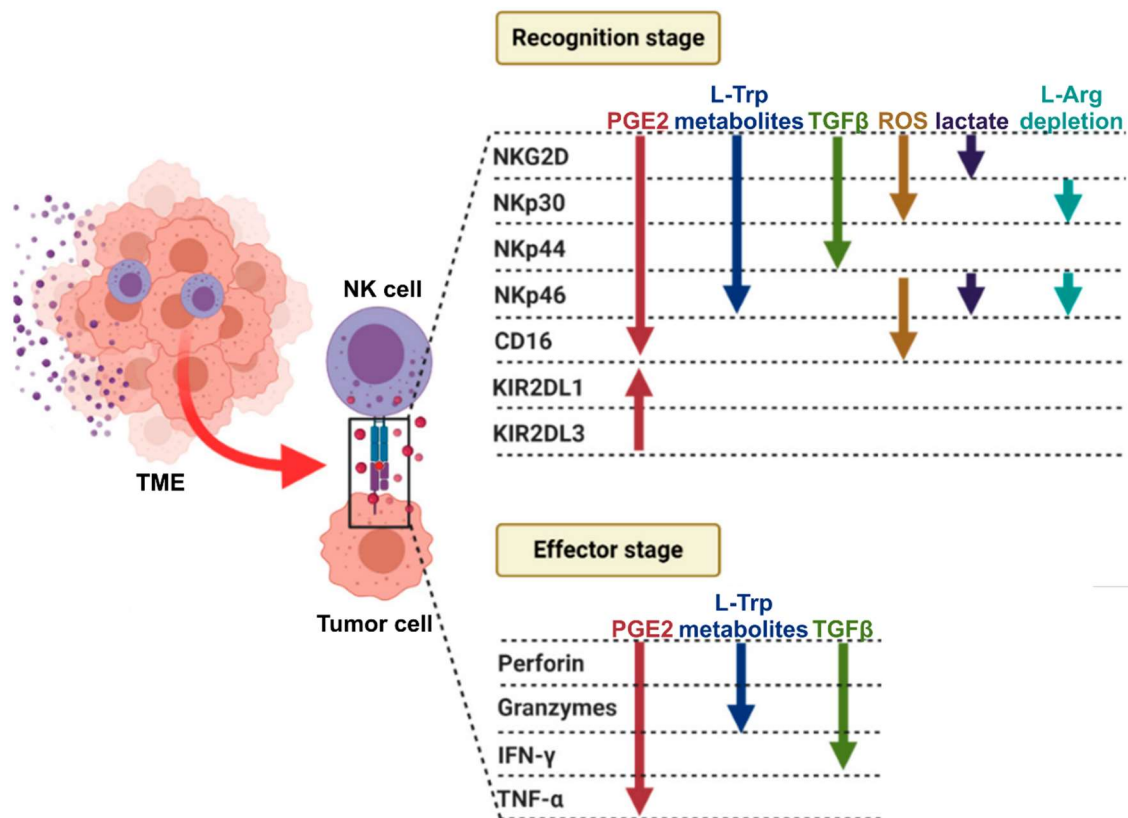
Figure 2.3: **NK cell inhibition mediated by the TME.** Tumor-infiltrating NK cells are inhibited by diverse tumor-derived suppressive factors which modulate NK cell target recognition and activating receptors as well as NK cell effector molecules. Adapted with permission from Domagala *et al.*[17]

TGFβ is a key player in immune homeostasis and tolerance and elevated secretion levels of TGFβ have been associated with poor prognosis in various cancer types, e.g. in gastric and bladder carcinoma.[18, 23] TGFβ is also a well-known suppressor of NK cell activity. The molecule binds to the TGF-beta receptor type-1 and 2 (TGFR-1/2) on NK cells and stimulates the TGFβ/SMAD pathway.[18] Activating TGFβ/SMAD signaling results in a downregulation of effector molecules like granzyme B and perforin that are essential for NK cell cytotoxicity. Furthermore, activating NK cell receptors are downregulated and, thus, target cell recognition

and elimination is diminished (Figure 2.3).[18] Moreover, it was demonstrated that TGFβ opposes mTOR activity that is critical in NK cell metabolism and effector functions.[17]

As shown in Figure 2.3, also PGE2 modulates NK cell activity and is associated with increased tumor burden *in vivo*.[24, 25] PGE2 acts independently of mTOR by binding to the PGE receptor EP1 - EP4 subtypes (PTGER1-4), of which PTGER2 and PTGER2 are expressed on NK cells. Receptor stimulation by PGE2 increases cAMP levels and activates the transcription factor CREB (cAMP response element-binding protein).[24] This leads to an increase in KIRs and decrease of activating NK cell receptors (Figure 2.3).[17, 26] Nutrient and amino acid metabolites also alter receptor and effector molecule expression which are, analogous to TGFβ, regulated via mTOR inhibition.[17] Consequently, NK cell activity is significantly hampered by multiple soluble factors released into the extracellular space of the TME. Strategies that would maintain NK cell activity within the TME might elevate anti-tumor immunity and, thus, may serve as starting point for therapeutic approaches for cancer.[27]

2.2.2 The Kynurenine Pathway and its Key Player Indolamine 2,3-dioxygenase 1

The kynurenine (Kyn) pathway is the main catabolic pathway of the essential amino acid L-tryptophan (L-Trp). Along the Kyn pathway, L-Trp is degraded to kynurenine which can be further transformed to kynurenic acid or quinolinic acid. The first and rate limiting step of the Kyn pathway is catalyzed by either one of the two isoforms of indoleamine 2,3-dioxygenase (IDO1 and IDO2) or by tryptophan 2,3-dioxygenase (TDO). Amongst the three, IDO1 displays the highest affinity to L-Trp and, thus, exhibits the highest catabolic activity.[28, 29] In 1998, Munn *et al.*[30] discovered that IDO1 is involved in the inhibition of CTL activity during pregnancy in mice[30, 31] which triggered the interest to investigate IDO1 and its potential immunoregulatory features. To date, IDO1 is well established for its capability to suppress the immune system. High IDO1 expression is associated with poor prognosis in various types of cancers.[32, 33]

IDO1 binds heme as a cofactor which is essential for the redox-reaction of L-Trp to *N*-formylkynurenine (NFK) and oxygen. IDO1 is an immunoregulatory enzyme and is not constitutively expressed in cells but can be induced by inflammatory cytokines. The strongest inducer of IDO1 expression is IFNγ, a cytokine which is secreted for example by active immune cells, like NK cells during immune responses (see 2.2.1). IFNγ activates JAK/STAT signaling resulting in IDO1 expression. Thereby, IDO1 is expressed first in its apo form (apo-IDO1) lacking heme. Subsequent heme incorporation results in the catalytically active holo form of IDO1 (holo-IDO1). The interaction between IDO1 and heme is non-covalent, allowing the heme to dissociate from the heme-binding pocket of IDO1.[34, 35]

Generally, the IFNγ–IDO1 axis restricts microbial growth and is especially important during viral infections.[36] Moreover, IDO1 is expressed in endothelial and epithelial cells in the female genital tract and is crucial for maternal tolerance to fetal tissue.[30, 33] IDO1 is also expressed in mature DCs and in lung endothelial cells, while in most other cells it can be induced by IFNγ.[22] In the TME, IDO1 is often highly expressed in endothelial cells, immune cells and in cancer cells, causing the depletion of L-Trp in the tumor environment. IDO1-mediated depletion of L-Trp limits the essential amino acid and induces cell cycle arrest and thereby inhibits NK cell and CTL proliferation. The accumulation of Kyn and other L-Trp metabolites reduces effector immune cell activity, including NK cell activity (see Figure 2.3, 2.2.1). Moreover, Kyn binds and activates the aryl hydrocarbon receptor (AhR) on naïve T lymphocytes, thereby inducing their differentiation to regulatory T cells (Tregs), which further weakens anti-tumor immunity.[10, 29, 37]
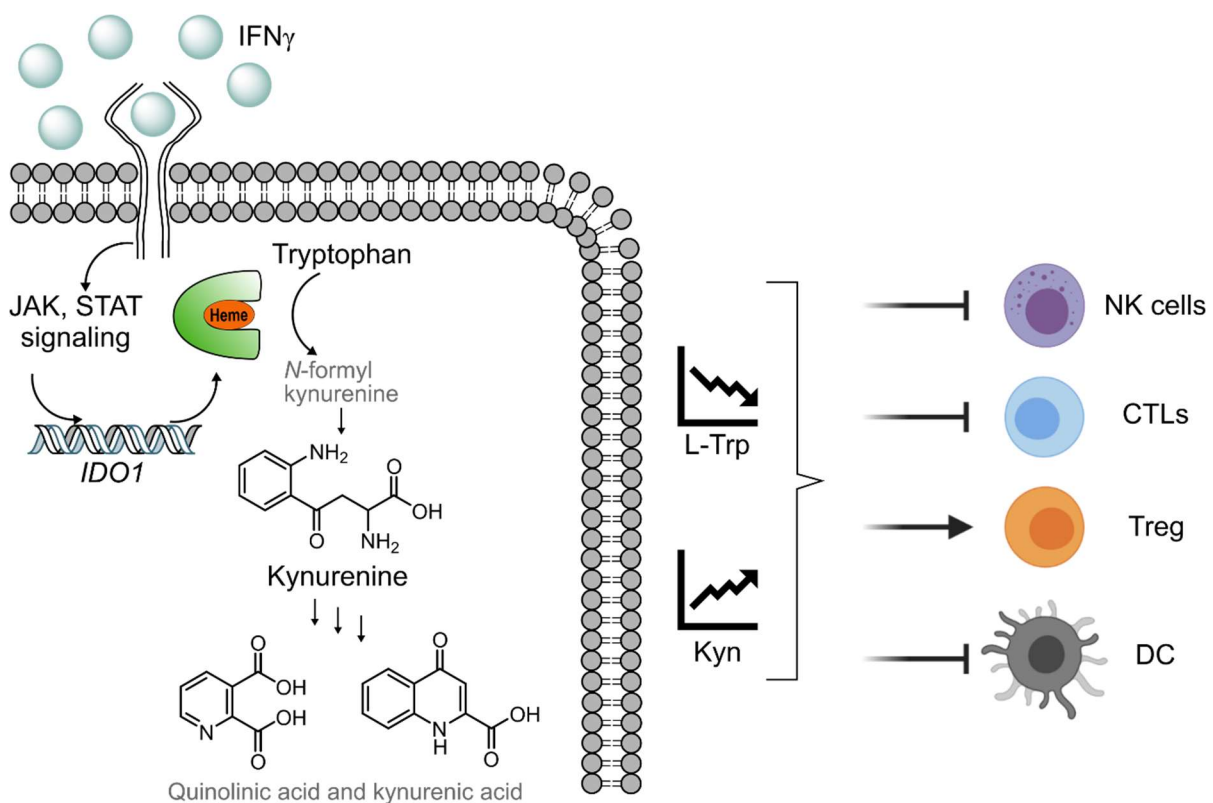
Figure 2.4: **IDO1 activity causes immunosuppression**. IDO1 expression is regulated in many cells by IFNγ and IDO1 activity causes L-Trp depletion and Kyn accumulation which reduces the activity of NK cells and CTLs. Furthermore, Kyn enhances the differentiation of Tregs and changes the DCs phenotype from immunogenic to tolerogenic. The figure was created with Chemdraw and BioRender.com and is based on Tang *et al.*[38]

Furthermore, IDO1 exhibits cellular signaling function beside its catalytic activity, which was observed in DCs and particularly investigated in plasmacytoid DCs (pDCs).[36, 39-41] Dendritic cells belong to the innate immune system and mainly regulate the responses of T lymphocytes, e.g. they can prime and activate CTLs via antigen presentation.[41] Moreover, DCs can integrate environmental cues and stimulate or suppress the immune responses

accordingly. And IDO1 as signaling molecule is involved in this functional plasticity of DCs as IDO1 expression induces a suppressive DC phenotype. Plasmacytoid dendritic cells are a subset of DCs that regulate immune responses mainly by the secretion of cytokines, like interferons that recruit and activate immune cells. However, in the presence of IFNγ, pDCs express IDO1, which leads to L-Trp depletion and immunosuppression. However, both the IDO1 expression and the immunosuppressive features of pDCs decline fast in the absence of IFNγ.[42] In contrast to IFNγ, the immunoregulatory factor TGFβ activates long-term expression of IDO1 in pDCs thereby establishing a regulatory, tolerogenic phenotype in pDCs.[36, 39, 40-42]

TGFβ signaling in pDCs leads to the phosphorylation of the immune tyrosine-based inhibitory motifs (ITIM1 and ITIM2) of IDO1. Upon phosphorylation, a conformational change of IDO1 is induced causing the transition from an enzymatically active protein to a catalytically inactive signaling molecule. Phosphorylated IDO1 activates the noncanonical, anti-inflammatory NF-κB pathway via the interaction with Src homology 2 domain phosphatases (SHP1 and SHP2), and thereby activates IDO1 expression. Activated NF-κB signaling not only maintains IDO1 expression, it increases IDO1 protein levels over time which results in IDO1s' self-amplification and, thus, it retains a suppressive phenotype of pDCs.[36]

Taken together, both the enzymatic function as well as the nonenzymatic signaling function of IDO1 contribute to an immunosuppressive milieu within the TME. Hence, inhibition of IDO1 may restore anti-tumor immunity.[31, 36, 37, 41, 43]

2.3 Cancer immunotherapy

In 1891, W. Coley provided the first evidence that activating the immune system by means of a bacterial vaccine could support malignant cell elimination.[44] However, at that time too little was known about the complexity of anti-tumor immunity and how cancer cells can evade the immune system to develop directed therapies. Over the last 100 years, the understanding of the immune system and the dynamic interplay between immune cells and cancer cells has increased significantly and various mechanisms on how cancer cells can escape from immunosurveillance have been explored in detail.[8, 10, 17, 29, 31, 41] This allowed the development of various cancer immunotherapies, among which the so-called immune checkpoint inhibitors were a breakthrough.[45]

Immune checkpoints are regulatory receptors that dampen immune responses to protect healthy cells. However, cancer cells and cells within the TME express higher levels of the inhibitory ligands for immune checkpoints thus suppressing cancer cell elimination. The most prominent examples that set the path for targeting immune checkpoints are the CTL-associated antigen 4 (CTLA-4) and programmed cell death receptor (PD-1) which are

expressed on CTLs. Stimulation of the receptors by their ligands B7 or PD-L1, respectively, produces an inhibitory signal reducing CTL effector function (Figure 2.5A). The ligand of CTLA-4, B7 is expressed on either antigen presenting cells, like DCs, while PD-L1 is expressed on antigen-presenting cells as well as cancer cells. By using antibodies against CTLA-4, PD-1 or PD-L1, the negative immune regulation is inhibited and CTL cytotoxicity against malignant cells is recovered (Figure 2.5B).[45, 46]

In 2011, Ipilimumab, an antibody targeting human CTLA-4, was approved by the FDA as the first checkpoint inhibitor for the treatment of metastatic melanoma followed by the approval of two antibodies targeting PD-1 in 2014 for squamous non-small cell lung cancer, renal cell carcinoma, colorectal cancer, hepatocellular carcinoma, among others. Moreover, three antibodies targeting PD-L1 were approved for the treatment of bladder cancer and non-small cell lung cancer. The success of the checkpoint inhibitors has profoundly revolutionized cancer therapies. Hence, in 2018 the Nobel prize was given to James P. Allison and Tasuku Honjo for the for the discovery of CTLA-4 and PD-1/L1, respectively.[47, 48]
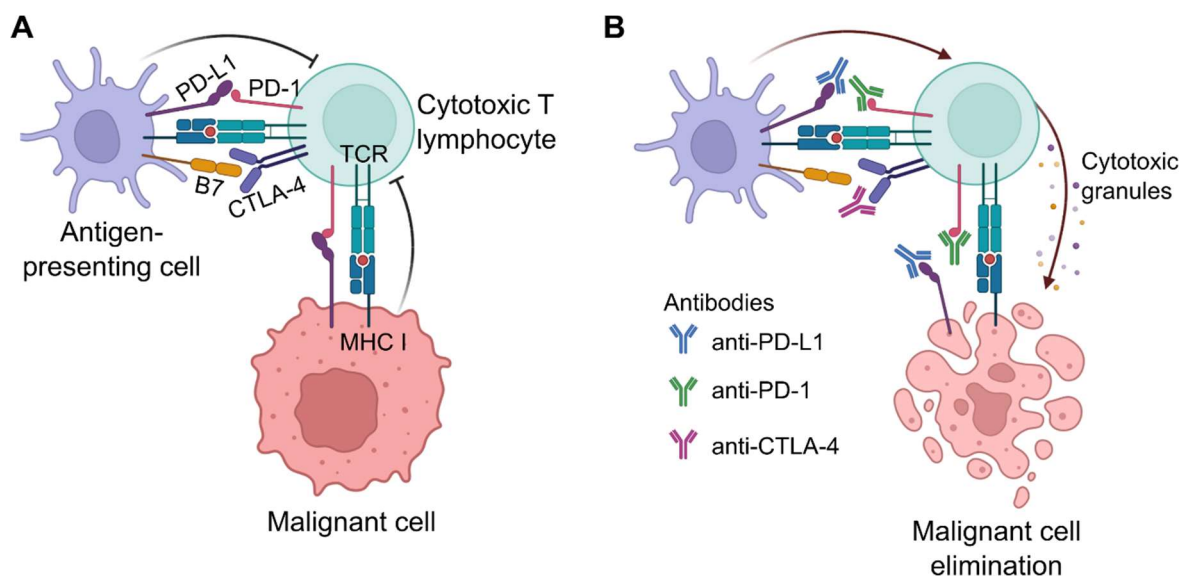
Figure 2.5: **Immune checkpoint inhibition activates CTLs.** A) In the absence of immune checkpoint inhibitors, antigen-presenting cells can inhibit CTLs via CTLA-4 and PD-1 stimulation at the tumor site. Moreover, malignant cells inhibit CTL cytotoxicity by expressing PD-L1. B) The addition of either of the checkpoint inhibitors (antibodies against CTLA-4, PD-1 or PD-L1) blocks the interaction of ligand and receptor and prevents CTL inhibition. Hence, CTLs get activated and eliminate malignant cells. The figure was created with BioRender.com. Based on Mohr *et al.*[49]

Furthermore, cell-based immunotherapies were developed like Sipuleucel-T and chimeric antigen receptor (CAR)-T cell therapy. Sipuleucel-T uses autologous dendritic cells that are primed with a recombinant protein to activate CTLs and enhance the immune response.[50] In

the case of CAR-T cells, CTLs of patients are genetically engineered to recognize malignant cells and shown effectiveness in lymphomas and leukemias.[51]

Current immunotherapies mainly focus on biological agents and only few small-molecule modulators are under investigation. Nevertheless, small molecules have the potential to modulate intracellular networks to enhance anti-tumor immunity. Moreover, it becomes increasingly apparent that combinational therapies are powerful and can strengthen the recovery of anti-tumor immunity.[14, 45] Hence, new approaches are required to reduce immunosuppression.

2.3.1 NK cell-based immunotherapies

In addition to the enhancement of the cytotoxicity of CTLs to eradicate cancer cells, also NK cells represent optimal features for cancer immunotherapies. In 1997, Rituximab was approved by the FDA to treat Non-Hodgkin lymphoma and represents the first immunotherapy that was approved. Rituximab is an antibody that binds to CD20, a specific surface protein found on Non-Hodgkin lymphoma cells and tags those cells for the recognition and elimination by NK cells via ADCC (Figure 2.6).[52]
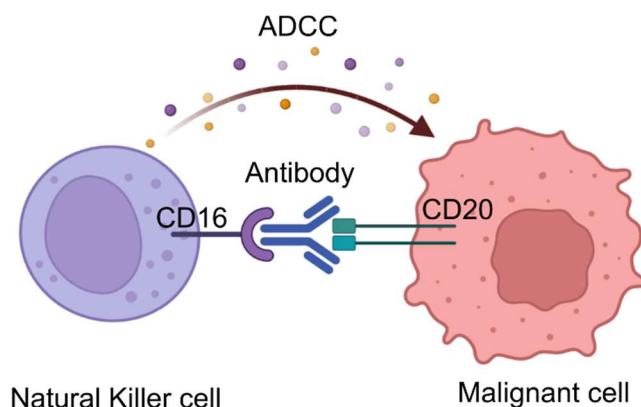
Figure 2.6: **Antibody-dependent NK cell-mediated cytotoxicity against malignant cells**. Antibody-based treatment tags malignant cells for elimination by NK cells via ADCC. The figure was created with BioRender.com.

In the following years, further antibodies were approved and strongly improved the treatments for various lymphomas.[53] Furthermore, IL-2, an NK cell-activating cytokine was approved for the treatment of metastatic renal cancer and melanoma. However, the response rate is relatively low with 12 to 20 %.[54]

Moreover, adoptive transfer of activated NK cells or CAR-NK cells has been investigated intensively, however it does not achieve significant efficiency *in vivo*.[55] The major obstacle is the TME which suppresses NK cell activity, also of *ex-vivo* activated NK cells.[56]

Hence, the modulation of NK cells to maintain NK cell cytotoxicity within the TME is highly demanded. This can be achieved by targeting NK cells directly or reducing tumor-derived suppressive factors.

2.3.2 IDO1 inhibition to increase anti-tumor immunity

To increase anti-tumor immunity within the TME, targeted approaches against overexpressed enzymes might be powerful to dampen their immunosuppressive properties.[14] Intensive research demonstrated that the inhibition of IDO1, which is often highly expressed in cancer, is a promising strategy to enhance anti-tumor immunity.[37, 57, 58] Consequently, multiple structurally diverse classes of IDO1 inhibitors were discovered including tryptophan derivatives, indole analogues, compounds based on imidazole, 1,2,3-triazole or tetrazole-based, further quinone- and iminoquinone-based inhibitors as well as small molecules with *N*-hydroxyamidine scaffold among many more.[35, 59-64] Five of those IDO1 inhibitors have already entered clinical trials (Figure 2.7), mostly in combination with checkpoint inhibitors or chemotherapy, for diverse malignancies, such as head and neck cancer, breast cancer, advanced malignancy, and various lung cancers.[38]

Epacadostat
clinical trial phase I and phase II

BMS-986205
clinical trial phase II and phase III

PF06840003
clinical trial phase I

Navoximod
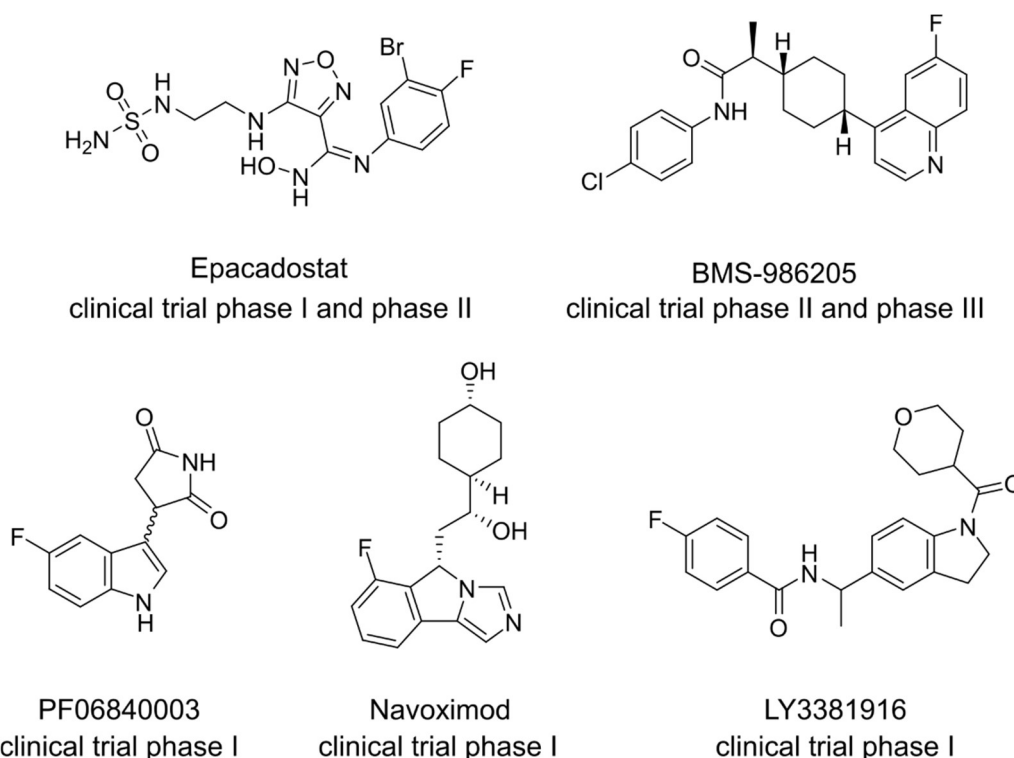clinical trial phase I

LY3381916
clinical trial phase I

Figure 2.7: **Inhibitors of IDO1 enzymatic activity in clinical trials.**

In 2016, epacadostat entered a phase III clinical study but, unfortunately, the treatment of unresectable or metastatic melanoma with epacadostat in combination with pembrozilumab,

an antibody that targets PD-1, had limited success.[58, 65] The combination did not outperform the treatment with pembrozilumab alone. However, several aspects of the study were addressed that may account for the failure. The selected patients were not evaluated for tumoral IDO1 expression.[58, 65] Moreover, the dosing of epacadostat might not have been sufficient, as only 1/4 of the dosing that is required to achieve 90 % inhibition of IDO1 in patients was used.[66] However, IDO1 activity was not evaluated during the study, e.g. by using a biomarker such as Kyn.[58, 65] Furthermore, IDO2 and TDO are often also expressed in cancer tissue and may contribute to L-Trp degradation or even substitute IDO1 when it is inhibited.[67] In addition, IDO1s' signaling activity may be relevant for immunosuppression which is not inhibited by enzymatic inhibitors like epacadostat.[68] Further trials are required to assess the effect of co-treatments by using higher doses, different IDO1 inhibitors as well as different types of tumors.[58, 65]

Indoximod
clinical trial phase I and phase II

NLG802 (Indoximod prodrug)
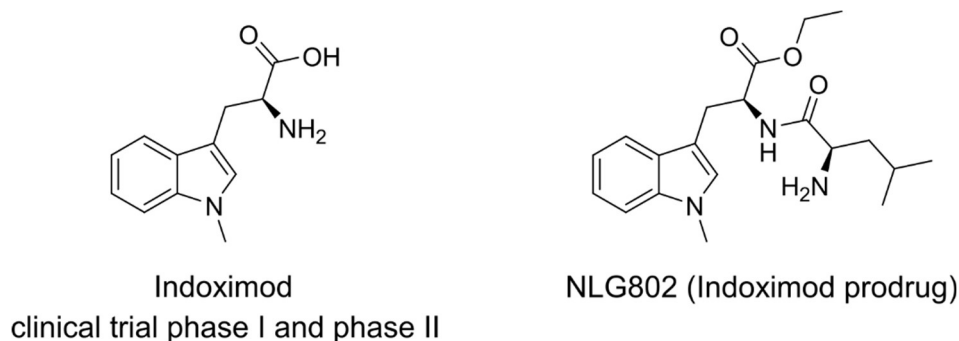
Figure 2.8: **Downstream IDO1 modulator Indoximod and its prodrug.**

The small molecule, indoximod (Figure 2.8) modulates the Kyn pathway independently of direct IDO1 inhibition and may offer a potential alternative strategy to stimulate the immune system.[38] Indoximod opposes the effects of L-Trp deprivation on immune cells as it mimics L-Trp. It could revert CTL proliferation and effector function and was able to reduce the non-enzymatic function of IDO1 in DCs.[68] Moreover, clinical trials using indoximod showed promising results. A phase II study in patients with advanced melanoma displayed enhanced antitumor efficacy of the co-treatment of indoximod with pembrolizumab when compared to pembrolizumab alone.[69]

Nonetheless, further strategies to reduce L-Trp depletion and Kyn accumulation are of high relevance to investigate the importance of IDO1 and the Kyn pathway for therapeutic approaches.

2.4 Chemical genetics

For a long-time, classical genetics was the only available method to elucidate gene function which was carried out by mutagenesis or gene deletion (Figure 2.9). However genetic alterations can have long-lasting effects in cells and might be even lethal.[70, 71]

In 1994, the chemical genetic approach was coined by Rebecca Ward at Harvard University.[72] The idea was to use small molecules as probes, instead of genetics, to change biological systems in order to understand biological processes (Figure 2.9).[73] In contrast to genetic alterations, chemical perturbation is a reversible method and can be fine-tuned in time and intensity.[70, 71]
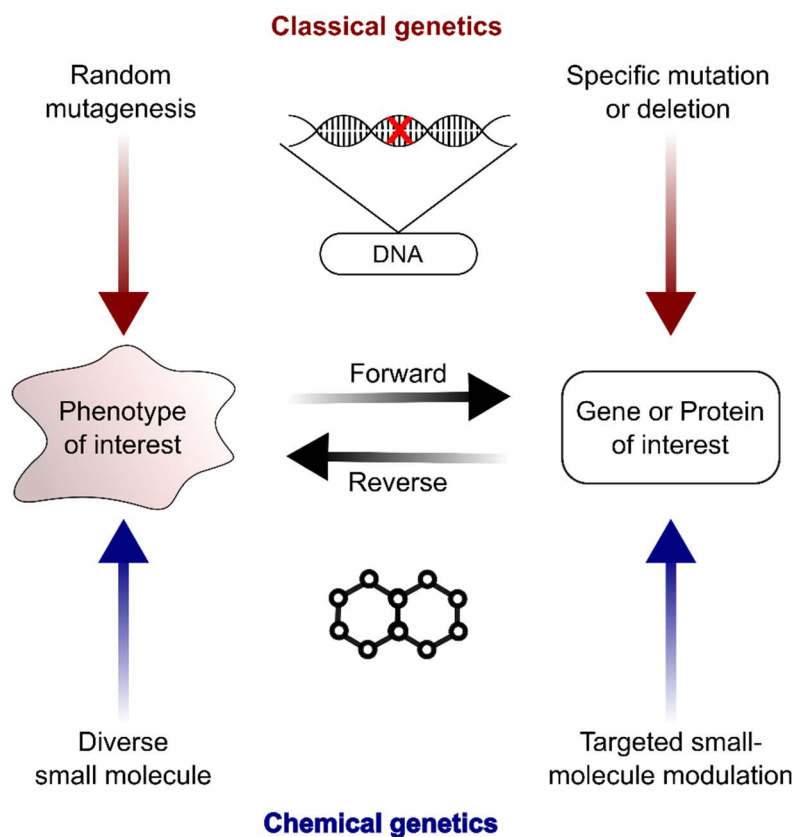
Figure 2.9: **Comparison of classical genetics and chemical genetics.** Classical and chemical genetics are used to explore the function of genes or proteins. Both, classical and chemical genetics can be further divided into forward and reverse studies. Reverse approaches modulate a gene or protein of interest to investigate its function while forward approaches examine desired changes in a phenotype by random genetic or chemical perturbation. The responsible target gene or protein which altered the phenotype is elucidated afterwards and may facilitate the identification of novel targets relevant to the phenotype of choice. Based on Lehár *et al.*[74]

The chemical genetic toolset can be divided into forward chemical genetics (or phenotype-based approaches) and reverse chemical genetics (or target-based approaches).[70] The latter

one evaluates small molecules for their potential to modulate the function of targets *in vitro*. Thereby, the focus is on a defined molecular target and the identification of a small-molecule modulator of its function which can be either inhibitors or activators of the targets' function. The identified hit compounds can be then used to study the function of the target in cells or organisms. Target-based approaches were proven successful since bioactive small molecules for diverse protein classes were discovered, such as enzymes or receptors.[70] Moreover, this strategy led to numerous life-saving drugs.[75] However, chemical modulators identified *in vitro,* e.g. by means of protein activity assays, not always show the corresponding effect in cells. Off-target activity or poor cell permeability might account for this, among other reasons. Furthermore, reverse chemical genetics is limited to known molecular targets with known activities or functions.[70, 76]

In contrast, forward chemical genetics explore the modulatory potency of small molecules directly in cells or tissue. Phenotypic assays are cell-based systems that can monitor changes of an e.g. disease phenotype or selected pathway of interest towards a desired outcome. Chemical modulators can be investigated in phenotypic assays to discover compounds that perturb the phenotype of choice. Therefore, chemical libraries are often used that contain on the one hand small molecules with already known protein targets and on the other hand compounds that display novel and diverse chemotypes. Phenotypic perturbation by compounds with known targets that were not yet been linked to the investigated phenotype may unravel novel molecular targets and involved signaling pathways. Thereby, chemical modulators can broaden the understanding of the analyzed phenotype and may reveal alternative targeted strategies for pharmacological approaches. Compounds with unknown cellular targets can reveal novel mechanisms to modulate known targets, but also can disclose new molecular targets for which functional modulators have not been identified yet.[70, 77] Hence, forward chemical genetics is an essential concept to explore the complexity and fundamental biology of a phenotype, e.g. of incompletely understood diseases, that cannot be realized with target-based approaches. Moreover, phenotypic-based approaches may identify novel target proteins and thereby expand the target scope as well as the toolbox of chemical probes.

The major challenge of phenotypic assays is the target deconvolution of active compounds with unknown target proteins. However, significant advances in e.g. in small molecule-based affinity chromatography, target engagement studies and computational-based methods allow to overcome this obstacle.[78-80]

Consequently, both forward and reverse chemical genetics have advantages and limitations, which in synergy enables to study the function of proteins *in vitro* and at the same time in complex cellular systems by using chemical probes.[81]

2.4.1 The development of phenotypic screening assays

To acquire meaningful phenotypic assays that empower the discovery of unprecedented molecular mechanism in health and diseases, the strategy of the phenotypic assay development is critical.[77, 82] In 2015, Vincent *et al.*[83] defined the 'rule of 3' for the design of physiological and disease-relevant phenotypic assays that refer to the assay system, the stimulus and the assay readout.[83]

Assay systems are traditionally based on cancer cell lines. However, those cells are genetically modified to achieve indefinite division which does not replicate phenotypes *in vivo*. Hence, applying primary cells or induced pluripotent stem cell (iPSC)–derived systems for a phenotypic assay may better represent human physiology. Moreover, experimental setups that display the cellular microenvironment by including two or more cell types or three-dimensional systems like organoids may further elevate the significance of the employed system. If disease-causing alterations are not intrinsically reflected by the selected assay system, usually a stimulus is applied to induce the desired phenotype. In case a stimulus is required, the physiological stimulus, e.g. the cytokine or growth factor, should be used to best recapitulate the complexity of the disease-relevant signaling networks. Transient overexpression of a disease relevant protein will not reflect the real phenotype of the disorder as mostly complex networks are responsible for the altered, diseased phenotypes. Last but not least, the assay readout is important for relevance of the assay system. Evaluating the phenotype after applying small molecules should be as close as possible to the clinical end point of a disease, e.g. by using a functional readout, like muscle function, cell viability or immune cell activity instead of readouts which are distal to the clinical end point e.g. gene expression.[83]

Together, these three aspects determine how relevant a phenotypic assay is in relation to the disease. Assay systems with low physiological relevance may lack translatability to the actual disease phenotype and to patients.[82]

To date, diverse, highly disease relevant phenotypic assays are available to investigate small molecules for bioactivity as well as for drug discovery. However, when employing phenotypic assays for medium to high-throughput screenings (HTS), some of the mentioned aspects might be challenging to maintain. The adaptation of the assays system to evaluate several 100,000 small molecules in an automated HTS procedure demands for miniaturization as well as robustness and reproducibility of the phenotypic assay. This might be not feasible for every phenotypic assay, especially complex experimental setups like tissue-, organism- or primary cell-based assays are sensitive to slight variabilities which affect reproducibility. Hence,

assessment between aspects required for disease relevance and the ones essential for HTS applicability have to be made.[77, 82]

To evaluate the robustness of an assay and assess its suitability for HTS the following statistical parameters are essential. The resolution of an assay is determined by the signal to background (S/B) ratio which represents the assay window (Equation 1).

$$(1) \qquad S/B = \frac{mean\ signal}{mean\ background}$$

The signal is the positive control that displays the highest value achievable in the assay while the background or a negative control represents the lowest value detectable. Hence, positive and negative controls are critical to assess reproducibility and signal variations of the assay window. However, the S/B does not incorporate the standard deviations (SD) of the obtained values and hence, determination of the assay quality by the S/B alone is not accurate. The overall performance of the assay is determined by the Z'-factor (Equation 2) which considers both, mean values as well as the standard deviation of the signal and the control.[84]

$$(2) \qquad Z' = 1 - \frac{3*SD\ of\ signal + 3*SD\ of\ control}{|mean\ of\ signal - mean\ of\ control|}$$

The Z' factor can result in values between 0 and 1, however, the higher the value the better the assay system. A value of <0 indicates that a screening is impossible while a Z' value of 0 displays high variation in sample and control, however, a yes or no answer might be possible. An increase of the Z' factor coincides with a decrease in the variation of sample and control values which enhances the assay quality. Z' values above 0.5 represent excellent assays, while Z' of 1 corresponds to an ideal assays.[84]

After the HTS is performed, orthogonal assays are key to confirm the hit compounds, independent of S/B and Z' factor, followed by mode-of-action studies.

3. Objectives

The aim of this thesis was to develop two distinct phenotypic assays as novel methods to find alternative ways to enhance anti-tumor immunity. The phenotypic assays should be suitable for automatization to screen a small-molecule library of more than 150,000 members.

Two distinct approaches will be taken since cancer cells display multiple mechanisms that cooperatively impede immune cell activity. Hence, to effectively reduce immunosuppression, diverse strategies will be required.

The first assay will investigate potential inhibition strategies for the immunoregulatory enzyme indoleamine 2,3-dioxygenase (IDO1) in its native cellular environment because IDO1 overexpression in cancer suppresses effector immune cells and correlates with poor survival. A cell-based assay should be developed that monitors kynurenine, the main product of IDO1 catalytic activity. This assay will facilitate the discovery of small molecules that impede IDO1 enzymatic activity not only directly but also indirectly.

In contrast to the first approach, the second assay will be an unbiased phenotypic assay focusing on the suppressive NK-cell phenotype that is induced by various tumor-derived suppressive factors. A co-culture assay of NK cells and cancer cells should be developed that monitors NK cell cytotoxicity in a suppressive environment. Hence, this assay will identify small molecules that can increase the efficiency of NK cell-mediated cytolysis of cancer cells even in a suppressive environment.

Once the phenotypic assays will be established and the screening campaigns completed, potent hit compounds should be selected for in-depth analysis including hit validation, chemical investigation, mode-of-action studies, and target identification.

Small molecules that reduce cancer immunosuppression may empower the development of innovative cancer immunotherapies, e.g. by elucidating novel drug target proteins. Moreover, the discoveries could contribute to expand the understanding of immunosuppression by cancer cells.

4. Experimental part

4.1 Materials

Name	Supplier
12-well plate, clear, flat bottom	Sarstedt AG & Co,
384-well plate, black, flat, clear bottom	Corning Inc.
384-well plate, clear, flat bottom	Greiner Bio-One
384-well plate, clear, non-binding	Greiner Bio-One
4-(2-hydroxyethyl)-1-piperazineethanesulfonic acid (HEPES)	Gerbu
6-well plate, clear, flat bottom	Sarstedt AG & Co
7-AAD Viability stain	Biolegend
96-well plate, black, clear flat bottom	Corning Inc.
96-well plate, clear, conical bottom	Sarstedt AG & Co
96-well plate, clear, flat bottom	Greiner falcon
96-well plate, clear, flat bottom, UV-Star	Greiner Bio-One
Acetonitrile	Fisher Chemical
Acrylamide / Bisacrylamide solution	AppliChem
Ammonium persulfate (APS)	Serva
Ascorbic acid	Sigma-Aldrich
Bacto agar	Fisher Scientific GmbH
Bacto Trypton	Fisher Scientific GmbH
Bacto Yeast Extract	Fisher Scientific GmbH
BMS-986205	Cayman Chemicals
Bovine serum albumin (BSA)	Serva
Bromophenol blue	Carl Roth
Buffy coats	DRK Hagen
Carfilzomib	Abcam
Catalase from bovine liver	Sigma-Aldrich
Cell culture dish, 10 cm	Sarstedt AG & Co
Cell culture dish, 15 cm	Sarstedt AG & Co
Cell culture flask T175	Sarstedt AG & Co
Cell culture flask T25	Sarstedt AG & Co
Cell culture flask T75	Sarstedt AG & Co
Chloroacetamide	Sigma-Aldrich
cOmplete™ protease inhibitor cocktail	Sigma-Aldrich
Cryovials	VWR International GmbH
DharmaFect 1 transfection reagent	Horizon Discovery Biosciences Limited
Dimethyl sulfoxide (DMSO)	Sigma-Aldrich
Disodium phosphate (Na_2HPO_4)	Merck
Dithioerythritol (DTE)	Gerbu
Dithiotreitol (DTT)	Gerbu
DNAse I	Serva
Epacadostat	Selleckchem
Ethanol (EtOH)	VWR

Name	Supplier
Ethylene diamine tetraacetic acid (EDTA)	Gerbu
Fetal bovine serum (FBS)	Gibco
Formaldehyde	AppliChem
Formic acid	J.T. Baker
FuGENE6	Promega Corporation
G418	Sigma Aldrich
Glucose	Carl Roth
Glycerol	Carl Roth
Glycine	Carl Roth
GST magnetic beads	Thermo Fisher
Guanidine hydrochloride (GndHCl)	VWR
Hemin BioXTRA from porcine	Sigma-Aldrich
High Fidelity (HF®) EcoRI	New England Biolabs
High Fidelity (HF®) SalI	New England Biolabs
Hoechst-33342	Invitrogen
Hydrochloric acid (HCl)	AppliChem
IFNγ, recombinant human	PeproTech
IL-15, recombinant human	StemCell
Iodacatamide	AppliChem
Lipofectamine 2000 transfection reagent	Thermo Fisher
L-Kynurenine	Sigma-Aldrich
Lys-C Endoproteinase	Wako Chemicals
MEM non-essential amino acids	PAN Biotech
Methanol (MeOH)	Sigma-Aldrich
Methylene blue	Fisher Scientific GmbH
Micro reaction tube, 0.5 mL	Sarstedt AG & Co
Micro reaction tube, 1.5 mL	Sarstedt AG & Co
Micro reaction tube, 1.5 mL, protein low-binding	Eppendorf AG
Micro reaction tube, 2.0 mL	Sarstedt AG & Co
Micro reaction tube, 2.0 mL, protein low-binding	Eppendorf AG
Micro reaction tube, 5.0 mL, protein low-binding	Eppendorf AG
Milk powder, non-fat dry	AppliChem
Monopotassium phosphate (KH_2PO_4)	Thermo Fisher
Mr. Frosty™	Thermo Fisher
N-methyl protoporphyrin IX	Cayman Chemicals
NP-40 alterative	Calbiochem
Pancoll human 1.077g/mL	Pan Biotech
Parafilm® M	Bemis Company Inc.
PBS tablets	Jena Bioscience
PBS-based Odyssey® Blocking buffer	Li-COR Biosciences
Prostaglandin E2 (PGE2)	SantaCruz
Phenylmethylsulfonyl fluoride (PMSF)	Thermo Fisher
PhosSTOP phosphatase inhibitors	Sigma-Aldrich
Pierce Protein A/G Magnetic Beads	Thermo Fisher
Piperazine-*N,N'*-bis(2-ethanesulfonic acid) (PIPES)	Sigma-Aldrich

Name	Supplier
Pipette tips, 10 µL	Sarstedt AG & Co
Pipette tips, 10 µL, protein low-binding	Sorenson Bioscience Inc.
Pipette tips, 100 µL, protein low-binding	Sorenson Bioscience Inc.
Pipette tips, 1000 µL	Diagonal GmbH & Co. KG
Pipette tips, 1000 µL, protein low-binding	Sorenson Bioscience Inc.
Pipette tips, 200 µL	Diagonal GmbH & Co. KG
Pipette tips, 200 µL, protein low-binding	Sorenson Bioscience Inc.
Polycarbonate ultracentrifugation tubes, 0.5 µL	Beckman Coulter Inc.
Polysorbate 20 (Tween® 20)	Sigma-Aldrich
Polystyrene Test Tube	Corning Falcon
Polyvinylidiene difluoride (PVDF) membrane	Merck KGaA
Potassium chloride (KCl)	J.T. Baker
RepSox	SelleckChem
Sample tube, 15 mL	Sarstedt AG & Co
Sample tube, 50 mL	Sarstedt AG & Co
Serological pipette, 1 mL	Sarstedt AG & Co
Serological pipette, 10 mL	Sarstedt AG & Co
Serological pipette, 25 mL	Sarstedt AG & Co
Serological pipette, 5 mL	Sarstedt AG & Co
Serological pipette, 50 mL	Sarstedt AG & Co
siRNA Buffer (5x)	Horizon Discovery Biosciences Limited
siRNA CRBN, human, on-target plus, smart pool	Horizon Discovery Biosciences Limited
siRNA Library Ubiquitin enzymes, human, on-target plus, smart pool	Horizon Discovery Biosciences Limited
siRNA VHL, on-target plus, smart pool	Horizon Discovery Biosciences Limited
siRNA, on-target plus, human, non-targeting pool	Horizon Discovery Biosciences Limited
siRNA, SIAH1, human, on-target plus, smart pool	Horizon Discovery Biosciences Limited
Sodium acetate	J.T. Baker
Sodium ascorbate	Sigma-Aldrich
Sodium chloride (NaCl)	VWR Chemicals
Sodium dodecylsulfate (SDS)	Gerbu
Sodium pyruvate solution	PAN Biotech
SsoAdvancedTM SYBR® green mix	Bio-Rad Laboratories GmbH
Staurosporine	Enzo
Succinylacetone	TCI
SYPRO orange dye	Thermo Fisher
Syringe, 1 mL	B. Braun Melsungen AG
T4 DNA ligase	New England Biolabs
T4 DNA ligase reaction buffer	New England Biolabs
tGFP mRNA	ThermoFischer
Transforming growth factor beta (TGFβ)	StemCell
Trichloroacetic acid (TCA)	Sigma-Aldrich
Triethanolamine	Sigma-Aldrich
Triethylammonium bicarbonate (TEAB) 1.0 M buffer	Sigma-Aldrich
Triethylene glycol diamine tetraacetic acid (EGTA)	VWR Chemicals
Trifluoroacetic acid (TFA)	Sigma-Aldrich

Name	Supplier
Tris((1-hydroxy-propyl-1H-1,2,3-	Sigma-Aldrich
Tris(2-cyrboxyethyl)phosphine) (TCEP)	Thermo Fisher
Tris-HCl	Carl Roth
Triton X-100	Serva
Trypsin, recombinant	Sigma-Aldrich
Trypsin/EDTA solution	PAN Biotech
Trypsin/Lys-C Mix, Mass spec. grade, 5x	Promega Corporation
Urea	J.T. Baker
UV-Star Plate, 96-well	Greiner Bio-One GmbH
Whatman® 3MM filter paper	Whatman GmbH
Q5® Reaction Buffer Pack	New England Biolabs

Chemical synthesis: All reagents were purchased from commercial sources and were used directly without further purification.

4.1.1 Buffer

Name	Composition
Buffer A (protein expression)	50 mM Tris-HCl pH 7.4 100 mM NaCl
Buffer B (protein expression)	50 mM Tris-HCl pH 7.4 200 mM KCl
Denaturation buffer:	50 mM Tris pH 7.5 8 M Urea 1 mM DTT
IDO1 assay buffer	50 mM Potassium phosphate pH 6.5
Immunoprecipitation lysis buffer	20 mM Tris-HCl pH 7.5 100 mM NaCl 0.1 mM EDTA 0.5 % NP-40 alternative Phosphatase and Protease inhibitors 10 mM N-ethylmaleimide (NEM)
Immunoprecipitation wash buffer	50 mM PIPES pH 7.4 150 mM NaCl 5 mM MgCl$_2$ 0.5 mM EGTA 0.1 % NP-40 alternative 0.1 % Triton X-100 0.1 % Tween® 20

Name	Composition
	1 mM DTT
IP alkylation solution	Denaturation Buffer + 50 mM Chloroacetamide
Kyn sensor buffer	50 mM H_3PO_4 , HCl pH=1
	120 mM NaCl
Lysogeny broth (LB) Medium	1 L H2O pH=7.4
	10 g Bacto Trypton
	5 g Bacto Yeast Extract
	10 g NaCl
LB agar plates	LB medium
	1.5 % Bacto Agar
NP-40 lysis buffer	50 mM Tris-HCl, pH 8.0
	150 mM NaCl
	1 % NP-40 alternative
Phosphate-buffered saline (PBS)	2.7 mM KCl
	1.5 mM KH_2PO_4
	136.9 mM NaCl
	8.1 mM Na_2HPO_4
	pH 7.4
PBS-T	PBS
	0.1 % (v/v) Tween® 20
PreScission protease cleavage buffer	50 mM Tris-HCl, pH 7.0
	150 mM NaCl
	1 mM DTE
	200 µM Hemin
Proteomics lysis buffer	PBS
	0.4 % (v/v) NP-40 alternative
SDS running buffer (10x)	250 mM Tris
	2.5 M glycine
	35 mM SDS
SDS sample buffer (5x)	0.5 M Tris-HCl, pH 6.8
	40 % (v/v) glycerol
	277 mM SDS
	400 mM DTE
	0.3 mM bromophenol blue
SDS separating gel buffer	1.5 M Tris
	pH 8.8
SDS stacking gel buffer	1.0 M Tris
	pH 6.8

Name	Composition
Stage-tip elution buffer	80 % (v/v) acetonitrile
	0.1 % (v/v) formic acid
Stage-tip wash buffer	0.1 % (v/v) formic acid
Transfer buffer	25 mM Tris
	188 mM glycine
	10 % (v/v) methanol
Tris-buffered saline (TBS)	50 mM Tris-HCl
	150 mM NaCl
	pH 7.5
TBS-T	TBS
	0.1 % (v/v) Tween® 20
TUBE buffer	20 mM Na_2HPO_4
	20 mM NaH_2PO_4
	1 % NP-40 alternative
	2 mM EDTA
	10 mM N-Ethylmaleimide (NEM)
	Protease inhibitors

4.1.2 Cell culture media

Name	Supplements	Product number	Supplier
DMEM-based growth medium	10 % (v/v) FBS 1 mM sodium pyruvate 1x MEM non-essential amino acids	P04-03550	PAN Biotech GmbH, Germany
DMEM-based growth medium w/o phenol red	10 % (v/v) FBS 1 mM sodium pyruvate 1x MEM non-essential amino acids	P04-03550	PAN Biotech GmbH, Germany
RPMI 1640-based growth medium	10 % (v/v) FBS (heat inactivated)	P04-18147	PAN Biotech GmbH, Germany
RPMI 1640-based growth medium w/o phenol red	10 % (v/v) FBS (heat inactivated) 2.5 mg/L D (+)-glucose 1 mM sodium pyruvate	P04-16515	PAN Biotech GmbH, Germany

Name	Supplements	Product number	Supplier
IMDM-based growth medium	10 % (v/v) FBS (heat inactivated)	P04-20150	PAN Biotech GmbH, Germany
McCoy's 5A-based growth medium	10 % (v/v) FBS (heat inactivated)	P04-05500	PAN Biotech GmbH, Germany
Opti-MEM™		11058-021	Thermo Fisher Scientific Inc., USA

4.1.3 Cell lines

Name	Description	Culture conditions	Source
A549^{Green}	Human lung carcinoma cells	DMEM-based growth medium, 5 % CO_2, 37 °C	DSMZ GmbH, Germany
BxPC3	Human pancreatic adenocarcinoma cells	RPMI1640-based growth medium, 5 % CO_2, 37 °C	DSMZ GmbH, Germany
SKOV3	Human ovary adenocarcinoma	McCoys 5A-based growth medium, 5 % CO_2, 37 °C	DKFZ, Heidelberg, Germany
HEK293T	Human embryonic kidney cells	DMEM-based growth medium, 5 % CO_2, 37 °C	DSMZ GmbH, Germany
HeLa	Human cervix carcinoma cells	DMEM-based growth medium, 5 % CO_2, 37 °C	DSMZ GmbH, Germany
PBMC	human peripheral blood mononuclear cells	IMDM-based growth medium	DRK Hagen, Germany

4.1.4 Kits

Name	Supplier
1-Step human coupled IVT Kit (88881)	Thermo Fischer
Bio-Rad Protein Assay	Bio-Rad Laboratories, Inc.
Click-iT HPG Alexa Fluor 488 Protein Synthesis Assay	Thermo Fischer
Dynabeads untouched human NK cell kit (11349D)	Thermo Fischer
IDO1 activity assay Kit (K972-100)	BioVision, Inc.
MycoAlert™ mycoplasma detection kit	Lonza Group AG
Nano-Glo® Dual-Luciferase® Reporter Assay Kit	Promega Corporation

Name	Supplier
Neon™ Transfection Kit (MPK10025)	Thermo Fisher Scientific Inc.
QuantiTect Rev. Transcription Kit (205313)	Qiagen
RNeasy Plus Kit (74104)	Qiagen
SuperSignal™ West Pico PLUS Substrate	Thermo Fisher Scientific Inc.

4.1.5 Antibodies

Antigen	Origin	Supplier	Blocking buffer	Dilution for immunoblotting	Product number
IDO1	rabbit	Abcam	5% milk (TBS)	1:3000	ab211017
IDO1	mouse	ThermoFisher	LI-COR buffer	1:3000	14-9750-80
Vinculin	mouse	ThermoFisher	5% milk (TBS)	1:10000	V9131
Granzyme B	rabbit	Abcam	5% milk (TBS)	1:2000	ab134933
Perforin	mouse	Thermo Fisher	Licor buffer	1:1000	PA587351
α-Tubulin	rabbit	Abcam	5% milk (TBS)	1:5000	ab4074
Mouse IgG (680RD)	donkey	LI-COR	LI-COR buffer	1:5000	926-68072
Mouse IgG (800CW)	goat	LI-COR	LI-COR buffer	1:5000	926-32210
Rabbit IgG (680RD)	donkey	LI-COR	LI-COR buffer	1:5000	926-68073
Rabbit IgG (HRP)	goat	Thermo Fisher	5% milk (TBS)	1:10000	Pierce 31460

Antigen	Origin	Supplier	Blocking buffer	Dilution for flow cytometry	Product number
CD3 PE-conjugated	mouse	Biolegend	FC buffer	1:200	300308
CD56 BV421-conjugated	mouse	BD Bioscience	FC buffer	1:100	562751

4.1.6 Plasmids

Name	Supplier	Backbone	Insert
pCMV3-IDO1	Sino Biological US Inc.	pCMV3	IDO1
pEGFP-H2Bj	Clontech, USA	pEGFP-N1	H2BJ
pGEX6p-GST-IDO1	A. Antoni[85], kindly gifted	pGEX6p-2rbs	IDO1
pT7CFE1-IDO1-His	Thermo Fisher	pT7CFE1-IDO1-CHis	IDO1
pXPG-IDO1	G. M. Doody[86], kindly gifted	pXPG	Firefly luciferase

4.1.7 Oligonucleotides

Name	Forward primer (5' to 3')	Reverse primer (3' to 5')	Supplier
IDO1	GCCTGATCTCATAGAGTCTGGC	TGCATCCCAGAACTAGACGTGC	Eurofins
GAPDH	GTCTCCTCTGACTTCAACAGCG	ACCACCCTGTTGCTGTAGCCAA	Eurofins
EcoRI-IDO1	AAAAAAGGATCCAAATGGCACAC GCTATGG		Eurofins
IDO1-SalI		AAAAAAGTCGACTTAACCTTCCT TCAAAAGGGA	Eurofins

4.1.8 Bacterial strains

Name	Description	Source
One Shot OmniMAX™ 2 T1	*Escherichia coli*	Thermo Fisher Scientific Inc.
BL21 DE2 RIL K+	*Escherichia coli*	Thermo Fisher Scientific Inc.

4.2 Instruments and software

4.2.1 Instruments

Description	Name	Supplier
Automated cell seeding	Multidrop Combi	Thermo Fisher Scientific Inc.
Automated Fluorescence Microscope	Axiovert 200M	Carl Zeiss AG
	IncuCyte S3	Sartorius AG
Automated screening robot	Spinnaker automation system	Thermo Fisher Scientific Inc.
Centrifuge	5810R	Eppendorf AG
	5417R	Eppendorf AG
	5424R	Eppendorf AG
	5430	Eppendorf AG

Description	Name	Supplier
	Minispin	Eppendorf AG
	Tomy mini personal	Sonation GmbH
Chromatography column	GSTTrap HP	GE Healthcare GmbH
	HiLoad 16/600 Superdex 200 pg	GE Healthcare GmbH
Chromatography system	ÄKTAprime Plus	GE Healthcare GmbH
Clean bench (Cell culture)	NU-437-400E	ibs tecnomara GmbH
Clean bench (Proteomics)	MSC-Advantage 1.2	Thermo Fisher Scientific Inc.
Precision scale	Analytical Plus	Sartorius AG
Flow cytometer Cell Sorter	BD FACSAria™ III	BD Biosciences
Flow cytometer	BD LSR II	BD Biosciences
Gel and blot documentation system	ChemiDoc™ MP	Bio-Rad Laboratories, Inc.
Gradient thermal cycler	Mastercycler ep gradient	Eppendorf AG
	CFX96 Real-Time System	Bio-Rad Laboratories, Inc.
High-content imaging system	Image Xpress XL	Molecular Devices, LLC
HPLC-MS/MS system	LCQ Fleet	Thermo Fisher Scientific Inc.
Incubator	Nuaire NU-5500E	Integra Biosciences GmbH
Liquid dispenser	Echo 520	Labcyte Inc.
Mass spectrometer	Q Exactive™ Plus	Thermo Fisher Scientific Inc.
	Q Exactive™ HF Hybrid Quadrupole-Orbitrap	Thermo Fisher Scientific Inc.
NanoDSF	Prometheus NT.48	NanoTemper Technologies
Nano-HPLC system	Ultimate™ 3000 RSLC nano-HPLC system	Thermo Fisher Scientific Inc.
Protein electroporation device	Neon™ Transfection System Pipette Station	Thermo Fisher Scientific Inc.
Plate reader	Sparks	Tecan Group AG
Spectrophotometer	Nanodrop 2000c	Thermo Fisher Scientific Inc.
UHPLC-MS/MS system	VelosPro	Thermo Fisher Scientific Inc.
Ultracentrifuge	Optima™ MAX-XP	Beckman Coulter Inc.
UV irradiation system	BLX-365	Vilber Lourmat Deutschland GmbH, Germany
Vacuum concentrator	Concentrator plus	Eppendorf AG

4.2.2 Software

Description	Name	Supplier
Chemical analysis software	ChemDraw	PerkinElmer, Inc.
Data analysis software	Prism	GraphPad Software
	Excel	Microsoft Corperation
Flow cytometry analysis	FlowJo v09	BD Biosciences
Gel / Immunoblot analysis software	ImageLab	Bio-Rad Laboratories, Inc.
Mass spectrometry analysis software	Xcalibur	Thermo Fisher Scientific Inc.
Microscopy & image analysis software	IncuCyte® S3 2019B Rev2	Sartorius AG
	MetaMorph	Molecular Devices, LLC
	MetaXpress	Molecular Devices, LLC
Screening analysis software	Quattro Software Suite	Quattro Research GmbH

Chemical synthesis: Proton nuclear magnetic resonance (1H-NMR) spectra were measured on Varian Mercury 400 (400 MHz) NMR spectrometer at room temperature. Proton (^{1}H) chemical shifts are specified as parts per million (ppm, δ-scale) and the spectra was referenced to the protium in the NMR solvent (CDCl3, δ7.26 ppm; DMSO-d_6, δ2.50 ppm). Data are characterized as follows: chemical shift, multiplicity (s = singlet, d = doublet, dd= doublet of doublets, ddd= doublet of doublet of doublets, t = triplet, q = quartet, m = multiplet), coupling constant (*J*) in Hertz (Hz) and integration

4.3 Methods

4.3.1 Cell culture methods

4.3.1.1 Cell culture and cell seeding

All cell lines were long-term cultivated at 37 °C and 5 % CO_2 in the respective medium listed in 2.2.1.2. Cells were sub-cultured when a confluence of 70 - 90 % was reached. Therefore, the growth medium was removed, cells were washed with 8 mL sterile PBS and detached using 1-1.5 mL trypsinization solution. After cell detachment, 6 mL of fresh growth medium was added and the cell suspension was transferred to a 50 mL tube. Cells were centrifuged at 300 x g for 5 min to separate death cells and debris. Subsequently, the cell pellet was resuspended in the required assay medium and the cell number was determined. Therefore, 10 µL of the cell suspension was mixed 1:1 with trypan blue solution to visualize dead cells and to determine live-cell number using the automated cell count device Countess™ II. Depending on the obtained cell number, the cell suspension was diluted in assay medium to

obtain the desired cell seeding density. Cells were seeded into 96-well plates (100 µL/well) or into 6-, 12- or 24-well plates. In case heat-inactivated FBS was required for the growth medium, FBS was incubated for 30 min at 56 °C and stored at -20 °C for further usage.

4.3.1.2 Cryopreservation of cells

For long term storage, cells were cryopreserved in growth medium containing 5 % (v/v) DMSO at a density of approximately 1×10^6 cells/mL. For this purpose, a cell suspension was prepared, the cell density was determined followed by a dilution to yield 1×10^6 cells/mL. 0.5 – 1 mL of the DMSO-supplemented cell suspension was transferred to a cryovial and subsequently placed in a freezing container (Mr. Frosty^{TM}), which ensures an even and slow reduction of the temperature. The freezing container was placed into a freezer of -80 °C for 24 h and afterwards cryopreserved cells were transferred into a liquid nitrogen tank until further usage. PBMCs were cryopreserved in FBS (heat inactivated (hi)) supplemented with 10 % (v/v) DMSO at a cell density between 5×10^6 and 2×10^7 cells/mL.

4.3.1.3 Compound treatment and controls

All compounds were dissolved in DMSO as 50 mM or 10 mM stock solution according to their solubility and stored at -20 °C in aliquots to reduce freeze-thaw cycles to a minimum. Cellular and biochemical assays that involved compound treatment always included a DMSO control at the same concentration of DMSO that was added with the compounds. The DMSO concentration for cellular assay was always below 0.5 % and in biochemical assay it did not exceed 2 %. For dose-response analyses, compounds were diluted in ten three-fold dilution steps in DMSO followed by a pre-dilution step (1:8 for biochemical assays and 1:50 for cellular assays) in either cell culture medium or assay buffer. The pre-dilution in either cell culture medium or assay buffer were added to the respective assay and was thereby further dissolved to the required concentration.

4.3.1.4 Generation of the A549^{Green} cell line

A549 cells were transfected with linearized pEGFP-N1-H2BJ using FuGENE6 transfection reagent. The plasmid was linearized because it increases the chances of productive integration. 24 h post transfection, cells were placed under selection pressure by adding medium containing 0.75 mg/ml G418. After two weeks of culturing cells in G418-containing medium, cells were sorted according to their fluorescence intensity using flow cytometry. Non-fluorescent cells were excluded. Single cells with a medium to high fluorescence intensity

compared to the wild-type cells were seeded in a 96-well plate. Single cells were expanded and one clonal cell line was chosen for the co-culture assay.

4.3.1.5 PBMC isolation from buffy coats

Buffy coats were obtained from the Deutsches Rotes Kreuz (DRK) Hagen and PBMC isolation was performed upon receival. Buffy coat content was diluted 1:2 with PBS and 50 mL tubes were filled with 20 mL of human Pancoll (PAN BioTech) density gradient solution. Afterwards, 30 mL of the diluted buffy coat was gently added on top of the human Pancoll layer and a centrifugation step at 800 x g for 25 min with brake-off was applied to separate PBMCs from red blood cells and plasma. The white mononuclear cell layer was collected and transferred to a new 50 mL tube. It is important to keep the samples of different donors separated. The obtained PBMCs were washed once with 40 mL PBS and twice with 10 mL PBS by and centrifugation at 300 x g for 12 min. Finally, cells were resuspended in FBS and counted for cryopreservation.

4.3.1.6 NK cell isolation

To isolate NK cells from PBMCs, cryopreserved PBMCs were thawed and cultivated overnight. Suspension cell fraction containing all lymphocytes are used for NK cell isolation while adherent cells (monocytes) remain in the cell culture flask. NK cells were isolated by means of Dynabeads™ Untouched™ Human NK Cells Kit according to the manufacturer's protocol.

4.3.1.7 Flow cytometry-based immune-cell characterization

Lymphocytes or isolated NK cells were collected, resuspended in FC Buffer at a cell density of 4 x 10^6 cells/mL and surface protein staining using fluorescently labelled antibodies was performed. For each staining condition, 50 µL of the cell suspension was used and anti-CD3-PE (1:200) and anti-CD56-BV421 (1:100) antibodies were added and incubated for 20 min on ice. Afterwards, cells were washed twice with 200 µL FC Buffer and finally resuspended in 150 µL FC Buffer. The cell suspension was transferred to a polystyrene test tube and the live/dead stain 7-AAD (1:50) was added. For fluorescence compensation, fluorophores were analyzed separately beforehand. Samples were excited using a 405 nm and a 488 nm laser and emission was detected by the following filters: 450/50, 575/26 and 695/40 nm. Prior to single-cell flow cytometry analysis, all samples were compensated using FlowJo™ software.

4.3.2 Phenotypic Screening Methods

4.3.2.1 Screening library

The compound library (3000 small molecules) used for the screening campaigns was composed of proprietary (10 %) as well as commercially available (90%) compounds. The LOPAC library, the Prestwick library the US drug collection, Selleckchem kinase and target-specific libraries and further hand-picked inhibitors include compounds with annotated bioactivity (2.5% of the whole library). Further screening compounds were obtained from ChemDiv and Enamine. Cheminformatic tools were applied to choose compounds having drug-likeness and compliance to rule of five. Compounds **6**, **7** and **8** were purchased from ChemDiv (ID: 5593-1162 (6); ID: G528-0384 (7); ID: E021-0159 (8))

4.3.2.2 Automated NK cell-mediated cancer cell cytolysis assay

The high-throughput screening to identify NK cell modulators was performed in phenol red-free RPMI 1640 medium supplemented with 10 % FBS (hi) in black multiwell plates. A549^{Green} cells (500 cells/well in 20 µl for 384-well plate and 400 cells/well in 4 µl for 1536-well plate) were seeded using Multidrop Combi (Thermo Fisher Scientific) and incubated overnight. Compound treatment (final concentration of 11 µM or serial dilutions for IC$_{50}$ values) was performed using an Echo550 dispenser (Labcyte) prior lymphocyte addition. First, lymphocytes of different donors were titrated to determine the E:T ratio that results in the best S/B value. Based on this, lymphocytes were prepared at the required cell density and were added together with 30 ng/mL IL-15 and suppressive factors TGFβ (30 ng/mL) and PGE2 (200 ng/mL) to each well. 5 or 20 µL of the lymphocyte cell suspension were added using Multidrop Combi (Thermo Fisher Scientific) to 1536-well or 384-well plate, respectively. The control samples, which were included on every screening plate, contained lymphocytes and 30 ng/mL IL-15 only. After brief centrifugation step, plates were incubated for 144 h at 37 °C and 5 % CO$_2$. Lymphocytes of different donors were used and are listed in Table 1. After 144 h, A549^{Green} cells were imaged (excitation: 465/40 nm, emission: 525/30 nm) using the ImageXpress Micro XL device (Molecular Devices). The obtained images were analyzed using MetaXpress and the Cell Proliferation HT module. The cell count of A549^{Green} cells was calculated relative to the cell count obtained in the co-culture with IL-15, TGFβ and PGE2 treated with DMSO.

Table 1: Lymphocytes of different donors were used for the initial screen in 1536-well format. The applied E:T ratios and the obtained S/B values are listed.

Compound library	Donor	E:T ratio	Signal to background (S/B)	Z'
In-house	9, 17, 28	40:1, 60:1, 60:1	3.9, 13.4, 2	0.16, 0.43, 0.31
Prestwick, Edelris, LOPAC	33	60:1	8.1	0.38
Kinase inhibitor collection	33	60:1	8.1	0.38
Chemdiv	33, 34	60:1, 60:1	2, 6.3	0.3, 0.28

Dose-response analyses of hit compounds that reduce A549[Green] cell count in the presence of lymphocytes were performed in 384-well plates in eight three-fold dilution steps starting from 17 µM. As toxic compounds will reduce A549[Green] cell count in dependently of NK cells, A549[Green] cells were incubated with the compounds without the addition of lymphocytes. Therefore, an A549[Green] cell count after 96 h was determined using 5 ng/mL Hoechst (33342). After incubation for 30 min at 37°C, cells were imaged (excitation: 377/50 nm, emission: 447/60 nm) using the ImageXpress Micro XL device (Molecular Devices). The obtained images were analyzed using MetaXpress and the Cell Proliferation HT module to obtain the cell count. The measurements were performed at least in technical triplicates. All HTS data was analyzed using the Quattro Software Suite (Quattro Research GmbH).

4.3.2.3 Automated cell-based Kyn assay

BxPC3 cells (1,000 cells/well in 2.5 µL) were seeded in phenol red-free RPMI 1640 medium in 1536-well plates (Greiner #782086) using Multidrop Combi (Thermo Fisher Scientific). After 24 h of incubation, plates were subjected to Spinnaker automation system (Thermo Fisher Scientific) for the transfer of 2.5 nL of compounds by an Echo550 dispenser (Labcyte) as well as for the addition of 1 µL of medium containing IFNγ (50 ng/mL) and L-Trp (380 µM). Subsequently, plates were centrifuged for 1 min at 500 x g and incubated at 37 °C and 5 % CO_2. After 48 h of incubation, TCA was added to a final concentration of 7 % and incubated for 10 min prior to a centrifugation step of 10 min at 1620 x g. Kyn levels were determined by means of the Kyn sensor[87] at a final concentration of 17.5 µM in sensor buffer. Fluorescence intensity (excitation: 535 nm, emission: 595 nm) was measured using a Spectramax Paradigm reader (Molecular Devices). Data was normalized to the values for cells that were treated with DMSO. All HTS data was analyzed using the Quattro Software Suite (Quattro Research GmbH).

The follow-up dose-response analyses of hit compounds were performed in 384-well plates in eight three-fold dilution steps starting from 10 µM. BxPC3 cells (4,000 cells/well) were seeded in phenol red-free medium supplemented with 10 % FBS (hi) in 384-well plates (Corning #3770) and treated as described above. In parallel, compound toxicity was evaluated prior to TCA addition and Kyn detection. Therefore, 5 ng/mL Hoechst-33342 were added to the cells and incubated for 30 min at 37°C. Afterwards, cells were imaged (excitation: 377/50 nm, emission: 447/60 nm) using the ImageXpress Micro XL device (Molecular Devices) followed by image analysis using MetaXpress and the Cell Proliferation HT module. All measurements were performed in technical triplicates.

4.3.2.4 Semi-automated siRNA screen in HeLa cells

To identify E3 ligases or other proteins involved in protein degradation of IDO1 a genetic screen was performed exploiting the Kyn assay. Therefore, all four subsets of the human ON-TARGETplus siRNA Library - ubiquitin enzymes were used. The Library contains 663 different genes that are involved in protein ubiquitination, e.g. E3 ligases, deubiquitinases as well as substrate receptors that can induce ubiquitination. To screen the siRNA library investigating their effect on the Kyn assay, 5 µL OptiMEM containing 1.05 % (v/v) Dharmafect transfection reagent 1 were added to each well of a 384-well plate followed by the addition of 0.15 µL of the respective siRNAs by means of an Echo550 dispenser (Labcyte). Each plate contained two wells of the same siRNA to directly compare treated and non-treated conditions. Afterwards, another 5 µL OptiMEM were added to ensure appropriate mixing and the solution was incubated 30 to 45 min at room temperature. HeLa cells (1300 cells / well) were added using Multidrop Combi (Thermo Fisher Scientific) and incubated for 48 h at 37°C and 5 % CO_2. Two days later, 50 ng/mL IFNγ and 170 µM L-Trp were added to each well and the two wells per plate that contain the same siRNA were treated with either 5 µM compound **12** or DMSO as a control and incubated for further 48 h at 37°C and 5 % CO_2. Kyn levels were determined as described for the automated Kyn assay (see 4.3.2.3). For each gene, at least two biological repetitions with three technical replicates were performed. Genes that showed significant differences upon knockdown in the two biological repetitions were evaluated a third time.

For data analysis, the percent of inhibition by **12** was calculated relative to cells that were treated with DMSO and the same siRNA. Afterwards, the inhibitory potency was normalized to the control condition (i.e., cells that were treated with non-targeting siRNA and **12**). Inhibitory potency of **12** in the conditions with non-targeting siRNA was set to 100 %. Genes whose knockdown reduced the inhibitory potency to approximately 80 % or more in at least two biological replicates were considered as hits.

$$(1) \qquad fold\ reduction\ in\ Kyn\ levels\ of\ \mathbf{12} = {}^{siRNA\ DMSO}\!/_{siRNA\ \mathbf{12}}$$

$$(2)\ Inhibitory\ potency = \left(\frac{\genfrac{}{}{0pt}{}{fold\ reduction\ (1)}{(siRNA)}}{\genfrac{}{}{0pt}{}{fold\ reduction\ (1)}{(non-targeting\ siRNA\ control)}}\right) * 100$$

Furthermore, genes whose knockdown changed Kyn levels in the absence of **12** were identified. Therefore, values for cells that were treated with DMSO and siRNA were normalized to the respective cell count and Kyn levels were calculated relative to cells that were treated with non-targeting siRNA and DMSO (100%).

$$(1)\ \ Kyn\ level\ normalization\ to\ cell\ count = {}^{Kyn\ level\ (siRNA)}\!/_{cell\ count\ (siRNA)}$$

$$(2) \qquad Kyn\ level = \left(\frac{\genfrac{}{}{0pt}{}{normalized\ Kyn\ level}{(siRNA)}}{\genfrac{}{}{0pt}{}{normalized\ Kyn\ level}{(non-targeting\ siRNA\ control)}}\right) * 100$$

4.3.3 Functional cell-based assays

4.3.3.1 Manual NK cell-mediated cancer cell cytolysis assay

A549[Green] cells (3,000 cell/well) were seeded in phenol red-free RPMI1640 in a 96-well plates 18 h prior to NK-cell or lymphocyte addition. Cryopreserved PBMCs were thawed and after a centrifugation at 300 x g for 5 min were transferred to a culture flask for lymphocyte (1*10^6/mL) separation. On the next day, A549[Green] cells were counted before immune-cell addition by means of the software IncuCyte® S3 2019B Rev2. According to the required E:T ratio, lymphocytes or NK cell density was adjusted in phenol red-free RPMI 1640 medium. Suppressive factors were added the medium obtaining a final concentration of 7.5 ng/mL IL-15, 7.5 ng/mL TGFβ and 200 µg/mL PGE2 (for NK cell) or 30 ng/mL IL-15, 30 ng/mL TGFβ and 200 µg/mL PGE2 (for lymphocytes). A549[Green] medium was aspired and 90 µL of the immune-cell suspension was added followed by 10 µL of either DMSO or compound pre-

dilution. A549^{Green} cell growth was monitored in real-time for up to 160 h by means of the IncuCyte® S3. To evaluate A549^{Green} cell count, the fluorescent nuclear count was analyzed determined in the acquired images using the provided software IncuCyte® S3 2019B Rev2 and plotted against the time using GraphPad Prism 6.0 (GraphPad software, USA). Calculation of cytolysis rate is based on the nuclear count. At the endpoint, the relative percentage of residual A549^{Green} cell number of each condition is calculated compared to the A549^{Green} cells in co-culture without any stimulatory or suppressive factors (unstimulated, medium control). Final subtraction from 100 % results in the cytolysis rate which reflects NK cell activity, and the number indicates how much of A549^{Green} cells were eliminated.

$$Cytolysis\ rate = 100 - \left(\frac{\begin{array}{c} A549\ cell\ count \\ (stimulated) \end{array}}{\begin{array}{c} A549\ cell\ count \\ (unstimulated) \end{array}} \right)$$

4.3.3.2 Manual cell-based Kyn assay

BxPC3 (6,000 cells/well or 20,000 cells/well) or SKOV3 cells (6,500 cells/well) were seeded in 384-well plates or 96-well plates, respectively, and incubated for 24 h at 37°C and 5 % CO_2. 50 ng/mL (BxPC3) or 5 ng/mL IFNγ (SKOV3 cells), 380 µM L-Trp or 450 µM L-Trp (SKOV3 cells) and compounds at indicated concentrations were added 48 h prior to the assay readout. After the incubation step, TCA was added to a final concentration of 7 % to each well and incubated for 10 min at 37 °C followed by centrifugation for 10 min at 1620 x g. Finally, for the detection of Kyn, either one volume of 2 % ((w/v)) of Ehrlich reagent in acetic acid or Kyn sensor at a final concentration of 20 µM in sensor buffer was added and fluorescence intensity (excitation: 555 nm, emission: 600 nm) or absorbance at 492 nm and at 650 nm as a background control was measured on a Sparks® multimode microplate plate reader. Absorbance values were corrected by subtracting the absorbance value at 650 nm and both readout values are presented relative to the DMSO control which was set to 100 %). Dose-response curves and IC$_{50}$ values were generated and fitted with GraphPad Prism 6.0 (GraphPad software, USA) using four-parameter variable slope non-linear regression curve fit.

4.3.3.3 Label-free Kyn detection

BxPC3 cells were seeded in 96-well plates 24 h prior to addition of 50 ng/mL IFNγ, 380 µM L-Trp and compounds at indicated concentrations and incubated for 48h. TCA was then added to each well and incubated for 10 min at 37 °C and samples were centrifuged for 10 min at

1620 x g. Afterwards, Kyn was detected in solution by HPLC-MS/MS using the LTQ Velos Pro and Dionex HPLC (Thermo Fisher Scientific). Assay was adapted from Xiao *et al.*.[88] Data were analyzed using Thermo Xcalibur[TM] (Thermo Fisher Scientific) and presented GraphPad Prism 6.0 (GraphPad software, USA).

4.3.3.4   HEK293T-based Kyn assay

HEK293T cells were reversely transfected with 1 µg pCMV3-IDO1 plasmid (for **9**, **10**, **11**) or 0.5 µg pCMV3-IDO1 plasmid (for **12**) using Lipofectamine 2000. While transfecting, cells were plated in a 96-well plate (25,000 cell/well) and incubated for 20 h at 37 °C and 5 % CO_2. Afterwards, 500 µM L-Trp and compounds at the indicated concentrations were added and cells were incubated for further 24 h prior to the addition of trichloroacetic acid to a final concentration of 7 %. Samples were incubated for 10 min at 37 °C and centrifuged for 10 min at 1620 x g. Finally, one volume of 2 % (w/v) of Ehrlich reagent in acetic acid was added to each well and absorbance at 492 nm and at 650 nm as a background control was measured on a Spark® multimode microplate plate reader (Tecan, Austria). Kyn levels were calculated by subtracting the absorbance value at 650 nm and presented relative to the DMSO control (which was set to 100 %). Dose-response curves and IC_{50} values were visualized and fitted with GraphPad Prism 6.0 (GraphPad software, USA) using four-parameter variable slope non-linear regression curve fit.

4.3.3.5   CHX pulse assay

BxPC-3 cells (200,000 cells/well) were seeded in a 12-well plate and supplemented with 50 ng/mL IFNγ. 24 h later, 5 µM cycloheximide (CHX) was added 30 min prior to the addition 5 µM of compound **12** and the co-treatment was performed for 24 h followed by immunoblotting (see 4.3.5.1).

4.3.3.6   Protein translation assay

BxPC3 cells (100,000 cells/well) were seeded in a 96-well plate and incubated at 37 °C and 5 % CO_2 overnight. Afterwards, 25 ng/mL IFNγ and compounds were added for 24 h followed by three washing steps using PBS and the addition of fresh medium containing the compounds as well as 50 µM L-homopropargylglycine (L-HPG). After 45 min of incubation at 37 °C and 5 % CO_2, cells were fixed using 4 % *para*-formaldehyde followed by L-HPG florescence labeling (click reaction) and cell nuclei staining as described by the manufacturer (Thermo Fisher). Cell image acquisition was performed at 10 x magnification by means of the

fluorescent microscope Axiovert 200M. Fluorescence microscopy pictures were analyzed via the MetaXpress software to quantify L-HPG-mediated fluorescence and cell count. The data was normalized to the cell count and visualized by Fiji ImageJ.

4.3.3.7 Electroporation of rhIDO1 into cells

HEK239T (3,000,000 cell/per electroporation) cells were mixed with 20 µg rhIDO1 (4.3.5.4) to a final volume of 120 µL electroporation buffer provided by the Neon™ transfection kit. 100 µL of the sample was transferred to the electroporation pipet tip and rhIDO1 were electroporated into cells applying 1000 V 2 pulses for 35 ms by means of the Neon™ transfection system pipette station. Afterwards, cells were transferred to 15 mL pre-warmed PBS and centrifuged at 300 x g for 5 min followed by resuspension in 3 mL trypsin/EDTA solution and incubated for 3 min at 37 °C to remove protein that might stick to the cell membrane. Afterwards cells were washed with 10 mL pre-warmed PBS and resuspended in phenol red-free growth medium at a density of 9×10^5 cells/mL. To determine IDO1 activity in cells, 90 µL cell suspension was plated per well in 96-well plates and 10 µL medium containing compounds as well as 150 µM L-Trp were added immediately and incubated for 24 h. Afterwards, Kyn levels were detected by 2 % ((w/v)) Ehrlich reagent in acetic acid as described above. For immunoblotting, 600 µL of the electroporated cell suspension were seeded in a 12-well plate and treated with the indicated compounds for 6, 14 or 24 h prior to immunoblotting. For lysate preparation, HEK239T cells were detached and washed twice with PBS followed by cell lysis in NP-40 lysis buffer for 30 min on ice. Insoluble material was removed by a centrifugation step at 100,000 x g at 4 °C for 15 min. Protein concentrations were determined by means of DC™ protein assay as described by the manufacturer (Bio-Rad). 30 µg of the protein lysate were subjected to immunoblotting (see 4.3.5.1).

4.3.3.8 TUBE pulldown

BxPC3 cells ($12*10^6$ / $4.6*10^6$ per dish) were seeded in either 15 or 10 cm^2 cell culture dishes, were supplemented with 40 ng/mL IFNγ 8 h later and incubated overnight. Next, fresh medium was added containing the respective compounds. For treatment with **12** alone, 50 µM **12** was added and incubated for 6 h at 37 °C and 5 % CO_2. For co-treatment experiments, 450 nM Carfilzomib (CFZ) was added 1 h prior to addition of compound **12**. After compound **12** was added cells were further incubated for 2 or 4 h at 37 °C and 5 % CO_2. Afterwards, cells were washed twice with PBS and scraped off the dish in 1 mL PBS followed by centrifugation at 300 x g for 5 min. 500 µL TUBE lysis buffer was added which was supplemented with the GST-tagged tandem ubiquitin binding entities (TUBE) protein (GST-Ubiquillin TUBE) at a

concentration of 100 µg/ml. Samples were kept on ice for 30 min followed by lysate clearance by centrifugation 30 min at 16,000 x g at 4°C and the determination of protein concentration by means of the DC assay. Samples were adjusted to the same concentration in 1 mL. 20 µL of the cleared lysate was used for the input analysis.

For the validation of ubiquitylated IDO1 species, the TUBE protein was not added during lysis. After determination of the protein concentration, samples were divided into three fractions of which one was supplemented with DTT (20 mM) and $ZnCl_2$ (2.5 mM), another one was supplemented with DTT and $ZnCl_2$ and the deubiquitinase USP2 (5 µM), which can remove polyubiquitin chains. Only the same amount of TUBE buffer was added to the third sample. The three samples were incubated 40 min at room temperature followed by the addition of the TUBE protein (100 µg/ml).

To pull down the polyubiquitinated proteins bound to the GST-tagged TUBE proteins, GST magnetic beads were washed with TUBE buffer and 40 µL of the beads were added per sample and rotated for 2 h at 4 °C. Supernatant was discarded and beads were washed four times with ice-cold PBS-T for 5 min. Finally, 20 µL 1x SDS sample buffer were added to the beads and incubated for 15 min at 55 °C to eluate bound proteins. Afterwards, 1x SDS sample buffer was added to all samples. Samples were boiled for 5 min at 98 °C and analyzed by immunoblotting (see 4.3.5.1).

4.3.3.9 IDO1 immunoprecipitation followed by MS analysis

BxPC3 cells ($4.6*10^6$ cells/dish) were seeded in 10 cm^2 dishes. 6 h later, 30 ng/mL IFNγ was added and cells were incubated overnight at 37 °C and 5 % CO_2. On the next day, the medium was exchanged and 5 mL medium with 20 µM of compound **12** or DMSO a as control were added for 6 h followed by cell detachment utilizing trypsin and two wash steps with PBS. Cells were lysed in 200 µL immunoprecipitation lysis buffer supplemented with fresh N-Ethylmaleimide. Three freeze and thaw cycles were performed followed by a centrifugation at 14,000 x g for 20 min at 4 °C. Protein concentration was determined by means of DC protein assay as described by the manufacturer (Bio-Rad) and 800 µg lysate was subjected to the immunoprecipitation.

For the following steps a magnetic rack was used to separate magnetic beads from its supernatant.

First, a pre-clearance step of the cell lysate was performed to reduce unspecific binding. Therefore, 25 µL of Pierce Protein A/G Magnetic beads per sample were washed twice with immunoprecipitation lysis buffer for 1 min followed by the addition of 800 µg lysate and an incubation of 1 h at 4°C while rotating. In parallel, 25 µL of Pierce Protein A/G Magnetic beads per sample were washed twice with immunoprecipitation lysis buffer for 1 min followed by the

addition of 400 µL immunoprecipitation lysis buffer and 8 µL IDO1 antibody (ab211017, abcam, 4.1.5) and continuous rotation for 1 h at 4 °C. Afterwards, the pre-cleared lysate was separated from the beads and added to the antibody containing beads. The immunoprecipitation was performed for 2 h at 4°C while rotating. Next, the supernatant was discarded and the beads were washed three times with immunoprecipitation wash buffer for 5 min while rotating. Afterwards, the beads were transferred to a fresh sample tube using three times 500 µL PBS to ensure complete transfer. Beads were washed further with 500 µL PBS (3 times) to remove all detergents followed by an on-bead digestion. Therefore, PBS was removed from the beads, 50 µL denaturation buffer was added and samples were incubated for 30 min while shaking. Afterwards 5.55 µL IP alkylation solution was added and incubated for another 30 min while shaking, followed by tryptic digestion. 1 µL LysC (stem solution of 0.5 µg/µL in water) was added for 1 h at 37 °C, while shaking. Afterwards, the LysC digestion supernatant was aspired from the beads and transferred to a fresh sample tube. 165 µL of 50 mM Tris (pH 7.5) containing 0.25 µg trypsin were added to the remaining beads and samples were incubated for 1 h at 37 °C, while shaking. The supernatants from the LysC- and trypsin-based digestion were combined and the remaining beads discarded. An another 0.5 µg trypsin were added and the digestion was performed overnight at 37 °C, while shaking. On the next day the enzymatic reaction was stopped by the addition of 20 µL 10 % TFA. Samples were desalted by means of stage tip purification. Therefore, for each sample a double layer of C18 chromatography matrix was placed into 200 µL pipette tip. The matrix was activated by adding 100 µL of 100 % methanol followed by one washing step with stage-tip elution buffer and two washing steps with stage-tip wash buffer. After each addition, a centrifugation in a tip centrifuge was performed. Finally, the samples were loaded on the tips and washed once with stage-tip wash buffer followed by sample elution using twice 20 µL stage-tip elution buffer. The samples were dried in a vacuum concentrator at 30 °C and submitted to the HRMS facility.

Following HPLC-MS/MS measurements and data analysis were performed by the HRMS facility of the MPI Dortmund.

The samples were analyzed by means of nano-HPLC-MS/MS and proteins were identified by database matching of a human reference proteome (Uniprot database) followed by a quantification using MaxQuant.[89]

4.3.3.10 Proteome profiling

HEK239T cells were electroporated with rhIDO1 (4.3.5.4) and treated with compounds at the indicated concentration for 6 h prior to lysate preparation. Cells were harvested and washed twice using PBS. Afterwards, cells were resuspended in PBS containing 0.4 % NP-40

alternative, and four freeze-thaw cycles were performed. Protein concentration was determined by means of DC protein assay as described by the manufacturer (Bio-Rad) and 2 µg of the lysates were mixed with an equal volume of 100 mM triethylammonium bicarbonate (TEAB) buffer and filled up to 150 µL with 50 mM TEAB. To reduce protein disulfide bridges, 7.5 µL of a 200 mM Tris(2-carboxyethyl)phosphine (TCEP) in 50 mM TEAB were added and samples were incubated at 55 °C for 1 h. Afterwards, 7.5 µL of 375 mM iodoacetamide in 50 mM TEAB were supplemented and samples were incubated for 30 min at room temperature in the dark. Subsequently, an acetone-based protein precipitation step was performed at -20 °C overnight. On the next day, the samples were centrifuged at 8,000 x g and 4 °C, the supernatant was removed and the samples were dried for 30 min at room temperature. Finally, the protein pellet was dissolved in 50 mM TEAB containing LysC/trypsin (25:1 protein:protease ratio (w/w), pre-dissolved in 1 mM HCl) followed by incubation at 37 °C overnight, while shaking. On the next day, samples were desalted by means of stage tip purification. Therefore, for each sample a double layer of C18 chromatography matrix was placed into 200 µL pipette tip. The matrix was activated by adding 100 µL of 100 % methanol followed by one washing step with stage-tip elution buffer and two washing steps with stage-tip wash buffer. After each addition, a centrifugation in a tip centrifuge was performed. Finally, the samples were loaded on the tips and washed once with stage-tip wash buffer followed by sample elution using twice 20 µL stage-tip elution buffer. The samples were dried in a vacuum concentrator at 30 °C and submitted to the HRMS facility.

Following HPLC-MS/MS measurements and data analysis were performed by the HRMS facility of the MPI Dortmund.

Samples were analyzed by means of Nano-HPLC-MS/MS. Protein identification and quantification was performed using MaxQuant.[89]

4.3.3.11 IDO1-promoter activity assay

HEK293T cells were transfected with pXPG-IDO-promoter plasmid for expression of firefly luciferase (Fluc) under the control of the *IDO1* promoter and the viability control plasmid pRL-TK for constitutive expression of *Renilla* luciferase (Rluc). After 24 h, cells were treated with 50 ng/mL IFNγ and the compounds at the indicated concentrations for 24 h. Afterwards, the luciferase activities were determined using the Dual-luciferase reporter assay system (Promega). Values for Fluc were normalized to the respective Rluc values and are presented relative to the DMSO control (which was set to 100 %).

4.3.3.12 Cellular thermal shift assay

SKOV3 ($1.3 * 10^6$ cells/well) cells were seeded into T-75 flask 48 h prior to compound addition. On day 3, 50 µM of compound **12** or DMSO as a control were added for 1 h. Afterwards, cells were washed with PBS and detached with trypsin, centrifuged for 5 min (4 °C, 1,200 rpm) and washed once more with PBS. After a second centrifugation step, cells were resuspended in PBS and then equally divided into ten different samples, which were subjected to a gradient heat treatment by means of the Mastercycler ep gradient (Table 2).

For the lysate-based thermal shift assay, SKOV3 ($1.3*10^6$ cells/well) cells were seeded into T-75 flask 48 h prior lysate preparation. cells were washed with PBS and detached with trypsin, centrifuged for 5 min (4 °C,1,200 rpm) and washed once more with PBS. After a second centrifugation step, cells were resuspended in PBS supplemented with 0.4 % NP40 alternative followed by freeze-thaw lysis and a final centrifugation step (50,000 x g, 4 °C). Cell lysates were equally divided into ten different samples, which were subjected to a gradient heat treatment by means of the Mastercycler ep gradient (Table 2).

Table 2: Temperatures applied for the thermal shift assay

Temperature	1	2	3	4	5	6	7	8	9	10
Intact cells/ lysates	37.0	40.8	44.1	47.4	50.0	53.4	55.7	56.3	61.0	63.7
rhIDO1	37.0	42.9	50.8	55.2	57.2	64.6	66.3	70.5	75.9	80.9

After 3 min of heat treatment, SKOV3 cells were lysed by adding NP-40 alternative to a final concentration of 0.4 % followed by freeze-thaw lysis and a subsequent centrifugation at 100,000 x g at 4 °C for 20 min. The supernatants were collected and subjected to immunoblotting as described in 4.3.5.1. An anti-IDO1 (rabbit, Abcam) was used to visualize IDO1 protein. The immunoblots were quantified using Image Lab software. Obtained band intensities were normalized to 37 °C and melting temperatures in presence or absence of the compound were determined via non-linear regression using Prism 7 (GraphPad, USA).

4.3.4 Molecular biology methods

4.3.4.1 Reverse transcription-quantitative PCR (RT-qPCR)

BxPC3 ($1*10^5$ cells/well) were seeded in 12-well plates 24 h prior to treatment with 50 ng/mL IFNγ and the respective compound concentrations or DMSO for 24 h. Afterwards, total RNA was isolated by means of RNeasy mini kit as described by the manufacturer (Qiagen) followed by reverse transcription with Quantitect Reverse transcriptase (Qiagen) according to the manufacturer's instructions. The obtained cDNA was diluted 5-fold and 3 μL diluted cDNA were utilized (in triplicates) for quantitative PCR using QuantiFast SYBR green PCR kit (Bio-Rad) and primers listed in 4.2.1.6. The experiment was performed using CFX96 Real-Time PCR Detection System (Bio-Rad). *IDO1* expression levels of each sample were normalized to the levels of the reference gene *GAPDH*. Relative quantification was performed using the $2^{-\Delta\Delta Ct}$ method.[90]

4.3.5 Biochemical and biophysical methods

4.3.5.1 Immunoblotting

For analysis of IDO1 protein levels, BxPC3 cells ($1*10^5$ cell/well) were seeded in 12-well plates 24 h prior to treatment with 50 ng/mL IFNγ and the indicated compounds or DMSO for 8 to 48 h. For analysis of perforin and granzyme B protein levels, lymphocytes were supplemented with either 30 ng/mL IL-15 or 30 ng/mL IL-15 and 30 ng/mL TGFβ for 48

For all samples subjected to immunoblotting, cell lysis was performed by means of NP-40 lysis buffer supplemented with protease and phosphatase inhibitors. Samples were incubated for 30 min on ice and the insoluble fraction was removed by a centrifugation step at 50,000 x g at 4 °C for 15 min. Protein concentrations were determined by means of DC protein assay as described by the manufacturer (Bio-Rad) followed by the addition of 1x SDS sample buffer. Samples were boiled for 5 min at 98 °C prior to protein separation by a 10 % SDS-PAGE. Afterwards, proteins were transferred to a polyvinylidene difluoride (PVDF) membrane using a wet-tank blotting system (Bio-Rad). Primary antibodies (4.2.1.4) were incubated at 4 °C overnight and detected with horseradish peroxidase-conjugated (Pierce) or IRDye-conjugated secondary antibodies (LI-COR Biosciences) for 1 h at room temperature. Wash steps were performed with TBS-T. Protein bands were visualized by the Odyssey Fc imaging system (LI-COR, USA) or ChemiDoc™ MP (Bio-Rad) using a chemiluminescent or fluorescent readout (4.1.5)

4.3.5.2 Kyn sensor titration

Absorbance and fluorescence spectra for the Kyn sensor were recorded at 20 °C using a Spark® multimode microplate reader (Tecan, Austria). L-Kynurenine was diluted in cell culture medium without phenol red and supplemented with 10 % FBS and an equal volume of sensor **6** was added at the indicated concentrations in assay buffer (50 mM H_3PO_4 and 120 mM NaCl, pH 1). Absorbance spectrum was measured between 500 and 620 nm in 2 nm increments. Fluorescence was measured by using an excitation wavelength of 555 nm. Emission spectrum was recorded between 585 nm and 650 nm or at 600 nm when L-Kyn was titrated.

4.3.5.3 Cloning of IDO1 into pGEX6p-2rbs

Full length human recombinant IDO1 protein sequence was cloned into the pGEX6p-2rbs-GST vector by means of the PCR cloning method using restriction digestion followed by ligation. Therefore, the full length IDO1 sequence was obtained from pCMV3-IDO1 utilizing the restriction primers for EcoRI-IDO1 and IDO1-SalI (4.1.7) together with the Q5® Reaction Kit by means of the gradient thermal cycler (40 cycles: 98 °C for 10 s, 50 °C for 30 sec. followed by 72 °C for 40 sec.). The PCR product were purified with the QIAquick PCR purification kit (QIAGEN) as described in the manufacturers protocol. Afterwards, the PCR product and the pGEX6p-2rbs-GST vector were digested by the two restrictions enzymes EcoRI and SalI for 3.5 h at 37 °C prior product purification by the QIAquick PCR purification kit (QIAGEN). The digested plasmid was mixed with a 5-fold excess of the IDO1 insert and the T4 DNA ligase in T4 DNA ligase reaction buffer and incubated at 4 °C for 2 days.

The ligation product was transformed into *E. coli* BL21 DE3 cells by heat shock. Therefore, *E. coli* cells were supplemented with 400 ng plasmid on ice followed by a heat shock at 42 °C for 60 sec after which cells were placed back on ice and incubated for 2 min. Afterwards, 800 µL lysogeny broth (LB) medium was added and cells were incubated for 1 h at 37 °C. To exclusively select cells containing the vector, cells were plated on agar plates containing ampicillin (100 µg/mL) and chloramphenicol (30 µg/mL) and incubated overnight at 37 °C. Single colonies were expanded and plasmid DNA was extraction according to the manufacturer protocol by the QIAGEN plasmid kit according.

Plasmid DNA sequence were determined by the Microsynth Seqlab GmbH (sanger sequencing).

4.3.5.4 Purification of recombinant IDO1 protein

Full length human recombinant IDO1 protein was expressed by means of pGEX6p-2rbs-GST-IDO1 vector. *E. coli* BL21 DE3 cells were transformed with the vector by heat shock (see

4.3.5.3). One colony originating from one clone was selected to infect 250 mL of LB medium (containing ampicillin (100 µg/mL) and chloramphenicol (30 µg/mL)) and incubated overnight at 37 °C while rotating. 50 mL were used to inoculate 2500 mL LB medium for final protein expression. IDO1 protein expression was induced by the addition of 200 µM IPTG and incubated at 18 °C overnight. Next, cells were sedimented by centrifugation 3600 x g for 20 min at 4 °C and the pellet was resuspended in 3 mL buffer A with DNase and phenylmethylsulfonyl fluoride (PMSF), a protease inhibitor. Cell suspension was homogenized by ultrasonication and cells were lysed mechanically. Insoluble fractions were separated by a centrifugation of 13,000 x g for 35 min at 10 °C. The soluble fraction was applied to a GST Trap HP column chromatography. GST-tagged IDO1 bound to the column was washed with buffer B followed by IDO1 cleavage from the column overnight using buffer B with freshly added PreScission protease (3.2 mg/mL) and 200 µM hemin.

Eluted IDO1 protein was finally subjected to a size exclusion column (HiLoad 16/600 Superdex 200 pg) to yield pure rhIDO1 protein. Heme load of IDO1 was between 55 and 80 % (A406/A280)
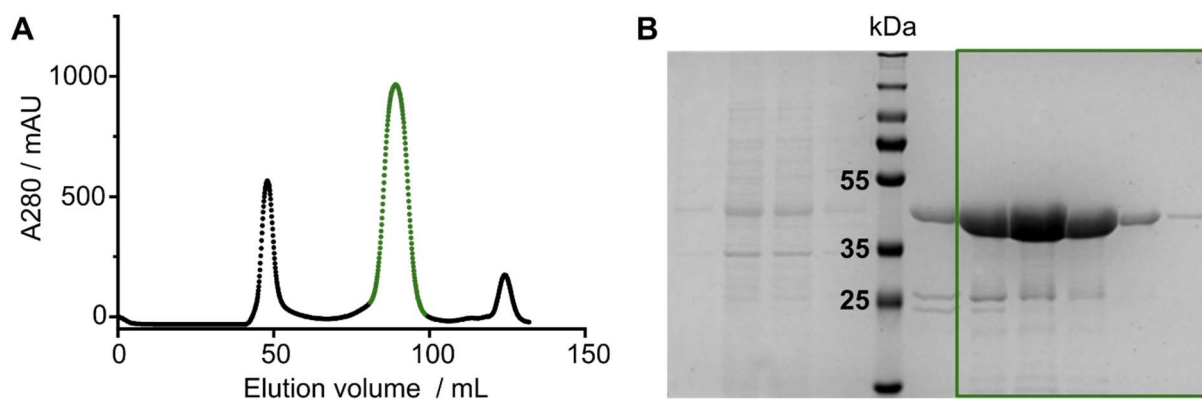
Figure 4.1: **Purified human IDO1 protein.** (A) Size exclusion chromatography and the fractions that were eluted. (B) SDS-PAGE of eluted protein fractions, protein stain was performed with Coomassie blue to visualize proteins. Highly pure IDO1 (45 kDa) was obtained with traces of GST protein (26 kDa) in the second elution peak (visualized in green).

4.3.5.5 IDO1 enzymatic assay

Enzymatic IDO1 activity was evaluated based on the conversion of L-Trp to NFK which was hydrolyzed by TCA to detect Kyn level. Therefore, rhIDO1 protein (1 µM) in IDO1 assay buffer was incubated with the respective compounds for 40 min at 37 °C or room temperature prior to the addition of 10 mM ascorbic acid, 10 µM methylene blue, 2 mM Trp and 100 µg/mL catalase. Enzymatic activity assay was monitored over 60 min followed by the addition of TCA to stop IDO1 enzymatic activity to a final concentration of 7 %. TCA supplemented reaction solution was incubated at 37 °C for 30 min to hydrolyze produced NFK to Kyn. Afterwards, an

equal volume of 2 % ((w/v)) of Ehrlich reagent in acetic acid or one volume of 40 µM sensor **6** in assay buffer was added and absorbance at 492 nm and at 650 nm as background control or fluorescence (excitation: 535 nm, emission: 595 nm) was measured. IDO1 activity was determined relative to the DMSO control. Dose-response curves and IC_{50} values were generated and fitted with GraphPad Prism 6.0 (GraphPad software, USA) using four-parameter variable slope non-linear regression curve fit.

4.3.5.6   UV/VIS analysis

To analyze the proportion of heme bound IDO1 in the presence of small molecules, the characteristic *'Soret band'* of IDO1 was measured. Compounds that compete with heme reduce the *'Soret band'*. [91, 92] Therefore, rhIDO1 (10 µM) in IDO1 assay buffer was incubated with the indicated compounds or DMSO (2 %) for 3 hours at 37°C prior a centrifugation step for 10 min at 4000 rpm was performed. The absorbance spectrum was measured at room temperature by means of the Spark® multimode microplate reader (Tecan, Austria) between 280 to 550 nm in 2 nm increments.

4.3.5.7   Differential scanning fluorimetry (DSF)

rhIDO1 (11 µM, 4.3.5.4) in IDO1 assay buffer supplemented with 20 mM sodium ascorbate and 5 µM methylene blue was mixed with the respective compound or DMSO. The protein solution was incubated for 30 min at 37 °C prior to addition of SYPRO orange dye (20,000 x) to a final concentration of 10 x. Fluorescence intensity was measured every 0.2 °C from 37 °C up to 95 °C by means of CFX96 Real-Time System. Melting temperatures were calculated using GraphPad Prism 6.0 (GraphPad software, USA).

4.3.5.8   nanoDSF

rhIDO1 (11 µM) in IDO1 assay buffer was mixed with the respective compound or DMSO as a control and incubated at 37 °C for 90 min. Afterwards the solution was added to a capillary and fluorescence intensities at 350 nm and 330 nm were measured every 0.045 °C from 20 °C up to 90 °C by means of the Prometheus NT.48 device. Melting temperatures were calculated by the Prometheus BT.48 software and melting curves were visualized by GraphPad Prism 6.0 (GraphPad software, USA).

4.3.5.9 IDO1 translation assay

pT7CFE1-IDO1 vector was cloned and utilized in the *in vitro* translation assay by means of 1-Step Human Coupled DNA IVT kit (Thermo Fisher). HeLa cell lysate was prepared according to the manual of the manufacturer to obtain the proteins required in protein translation. Lysates were mixed with the provided supplements and the pT7CFE1-IDO1 plasmid and samples were incubated for 3 h at 30 °C followed by IDO1 translation analysis by means of immunoblotting.

4.3.6 Chemical synthesis

All reactions were performed in evacuated standard laboratory glassware and under inert argon atmosphere. Commercially available reagents were used directly without further purification. Compounds were analyzed by thin-layer chromatography (TLC) using aluminum plates pre-coated with silica gel (Silica gel 60 254, Merck KGaA, Darmstadt, DE KGA). TLC plates were exposure to ultraviolet light (UV) to visualize reaction components. Flash column chromatography for the final purification step was performed manually using silica gel Acros Organics 60 (particle size 0.035–0.070 mm).

4.3.6.1 Synthesis of Diphenylmalonat (2)
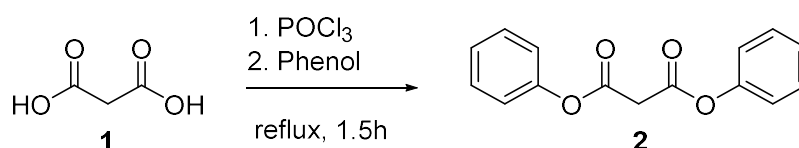
POCl$_3$ (10.8 mL, 115.3 mmol, 1.2 equiv) was added dropwise to the malonic acid (10.0 g, 96.1 mmol, 1 equiv) at 0 °C and the mixture was stirred for 60 min at room temperature. Then, Phenol (18.1 g, 192.2 mmol, 2 equiv) was added and the mixture was heated up to 125 °C for 60 min. After cooled to room temperature, the mixture was poured into 1 L water and afterwards extracted with EtOAc. The combined organic layers were dried and concentrated *in vacuo*. The obtained oil of diphenyl malonate (22.8 g 88.6 mmol, 92.1 %) was used further without additional purification steps.

^{1}H NMR (400 MHz, CDCl$_3$) δ 7.50 – 7.18 (m, 9H), 3.92 (s, 2H). The obtained NMR spectra matches with reported data.[93]

4.3.6.2 Synthesis of 7-(diethylamino)-4-hydroxy-2*H*-chromen-2-one (4)
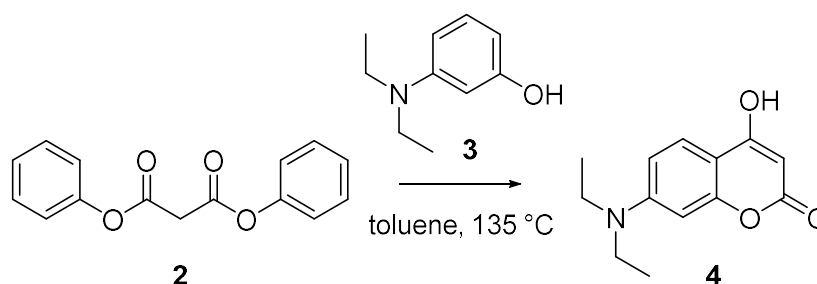
Diphenol malonate (6.36 g, 24.8 mmol, 1 equiv.) was dissolved in toluene and 3-(*N,N*-diethylamino)phenol (4.1 g, 24.8 mmol, 1 equiv.) was added dropwise. The reaction mixture was heated up to 135 °C for 5 h. The reaction was cooled down and the precipitated product was filtered and then washed with cold toluene. The crude product was dried and the yellow solid was obtained. (1.61 g, 27.8 % yield)

^{1}H NMR (400 MHz, DMSO-d_6) δ 11.88 (s, 1H), 7.54 (d, *J* = 9.0 Hz, 1H), 6.66 (ddd, *J* = 9.0, 2.5, 1.1 Hz, 1H), 6.45 (d, *J* = 2.4 Hz, 1H), 5.25 (s, 1H), 3.41 (q, *J* = 7.0 Hz, 4H), 1.19 – 1.05 (m, 6H). The obtained NMR spectra matches with reported data.[93]

4.3.6.3 Synthesis of 4-chloro-7-(diethylamino)-2-oxo-2*H*-chromene-3-carbaldehyde (5)
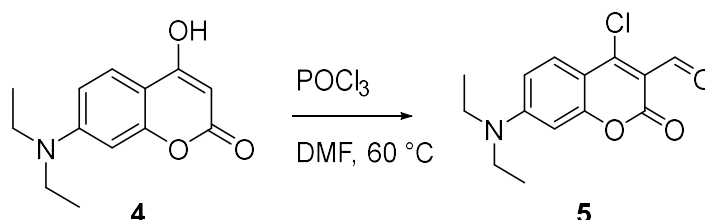
DMF was added dropwise to POCl$_3$ (4.38 mL, 46.8 mmol, 3 equiv.) at RT and stirred for 30 min. Afterwards **4** (3.64 g, 15.6, 1 equiv.) was dissolved in DMF and added slowly. The reaction mixture was stirred at 60 °C overnight. Subsequently, the mixture was poured into 50 mL of ice-cold water and NaOH was added to adjust the pH to 7.0. The precipitate was filtered followed by recrystallization in EtOH. A pure yellow solid was obtained. (3.05 g, 10.9 mmol, 70 % yield)

^{1}H NMR (400 MHz, DMSO-d_6) δ 10.08 (s, 1H), 7.82 (d, *J* = 9.3 Hz, 1H), 6.92 (dd, *J* = 9.4, 2.5 Hz, 1H), 6.63 (d, *J* = 2.5 Hz, 1H), 3.53 (q, *J* = 7.1 Hz, 4H), 1.16 (t, *J* = 7.0 Hz, 6H).The obtained NMR spectra matches with reported data.[93]

4.3.6.4 Synthesis of 7-(diethylamino)-4-(ethylthio)-2-oxo-2*H*-chromene-3-carbaldehyde (6)
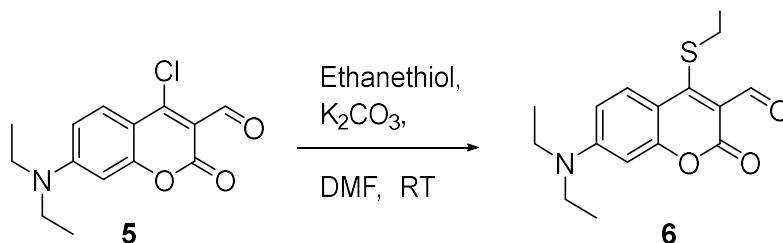
5 (3 g, 10.7 mmol, 1 equiv.) together with K_2CO_3 (5.9 g, 42.9 mmol, 4 equiv.) were dissolved in 0.1 M ethanethiol in DMF. The reaction mixture was stirred for 19 h at RT. Afterwards, DMF was removed in vacuo and the obtained solid was purified by chromatography using DCM/EtOAc (95:5). A yellow solid was obtained. (3.1 g, 10.2 mmol, 95 %)

^{1}H NMR (400 MHz, CDCl$_3$) δ 10.35 (s, 1H), 8.06 (d, *J* = 9.3 Hz, 1H), 6.63 (dd, *J* = 9.3, 2.6 Hz, 1H), 6.42 (d, *J* = 2.6 Hz, 1H), 3.46 (q, *J* = 7.1 Hz, 4H), 3.08 (q, *J* = 7.4 Hz, 2H), δ 1.26 (m, *J* = 14.4, 7.3 Hz, 9H). The obtained NMR spectra matches with reported data.[87]

5. Results

5.1 Phenotypic assay for small molecules that enhance NK cell-mediated elimination of cancer cells

5.1.1 Development of a phenotypic assay monitoring NK cell activity

To identify bioactive small molecules that can enhance NK cell-mediated elimination of cancer cells even in a suppressive TME, first a phenotypic screening assay was designed and established (Figure 5.1). The idea was to use a co-culture system in which a suppressed NK cell phenotype is induced by tumor-derived immunosuppressive factor. Hence, NK cell-mediated cancer cell cytolysis should be inhibited (Figure 5.1A and B). The addition of bioactive small molecules should prevent this NK phenotype and thus enable cancer cell cytolysis again (Figure 5.1C). To monitor NK cell activity, a direct cancer cell count would be optimal as readout, e.g., by fluorescently labelled cancer-cell nuclei (Figure 5.1D and E).
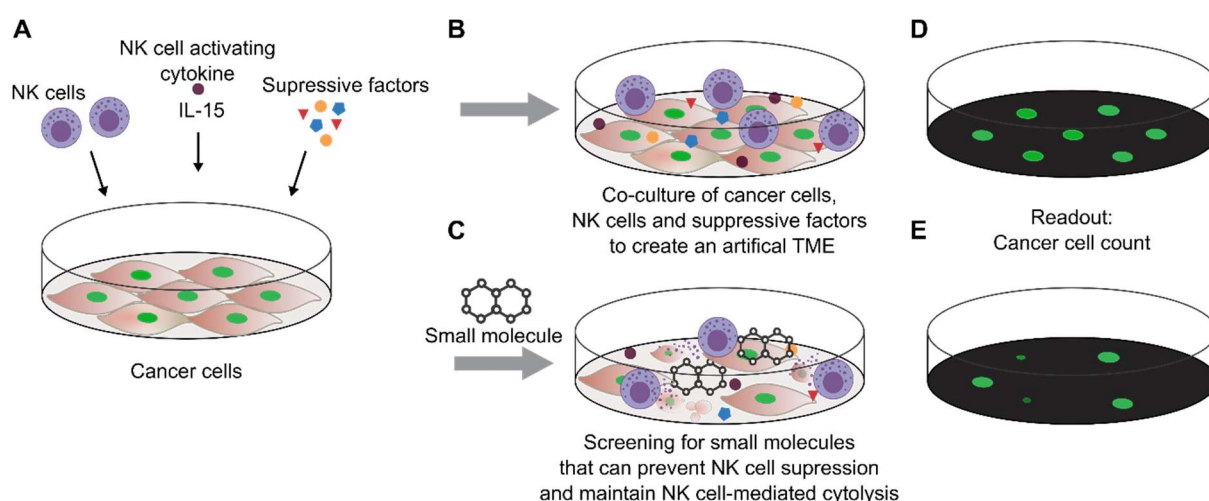
Figure 5.1 : **Phenotypic assay to identify small molecules that can induced NK cell-mediated cancer cell elimination.** Isolated human NK cells are co-cultured with cancer cells that contain fluorescently-tagged cell nucleus allowing for detection of cancer cell count and, thus, changes in cell count that occur in the co-culture. In addition, factors known to inhibit NK cells in the TME will be added to mimic the tumor surrounding (A). Under these conditions, NK cell-mediated cancer cell cytolysis is inhibited (B). Small-molecule modulators (C) could prevent NK cell inhibition and increase NK cell-mediated cancer cell elimination and will be identified by a reduction in cell count by means of the fluorescent nucleus (D and E).

For the assessment of NK cell-mediated cytolysis, the radioactive chromium 51 (^{51}Cr) release assay is usually used. For this, target cells are labelled with ^{51}Cr in advance and afterwards the released ^{51}Cr from the target cell due to NK cell-mediated cytotoxicity and reflects NK cell

activity. Free ^{51}Cr can be quantified in the cell culture supernatant after target cells separation.[94] However, radioactive assays are not suitable for screening due to acute health effects and further separation of cell supernatant from cells is technologically challenging. Fluorescently labelled cancer cells, for example by introducing a nuclear protein tagged with a green fluorescent protein (GFP), are an excellent alternative for the detection of NK cell-mediated cytolysis. The quantification of the nuclei count allows to determine target cell lysis similar to the ^{51}Cr release assay and additionally enables time-resolved measurements using live-cell imaging.

To realize this, the epithelial lung carcinoma cell line A549 was stably transfected with a Histone H2B type 1-J-eGFP (A549^{Green}) construct to label the cell nuclei green. A549 cells were chosen as target cells because they are known to be susceptible to NK cell cytolysis.[95] The introduced green label allowed to distinguish A549^{Green} cells from immune cells in a co-culture system (Figure 5.3C and D) and enables detection of A549^{Green} cell count in real time by live-cell imaging. A549^{Green} cell count directly correlates with NK cell activity and was used as readout. Active NK cells lyse A549^{Green} cells and reduce green nuclei count while suppressed NK cells will not alter A549^{Green} target cell count.

NK cells required for the co-culture assay were isolated from peripheral blood mononuclear cells (PBMCs). PBMCs are white blood cells containing monocytes, dendritic cells and naïve lymphocytes such as T cells, B cells, and NK cells. For PBMC isolation, buffy coats of human origin were obtained from a local blood bank. Buffy coats are a by-product of blood donations and contain PBMCs while most plasma and red blood cells were removed. By utilizing standard density gradient centrifugation, PBMCs were separated from the remaining red blood cells, plasma and granulocytes (e.g. eosinophils, neutrophils). The yielded PBMCs from diverse healthy donors were cryopreserved for storage. Subsequently, NK cells were isolated from cryopreserved PBMCs by means of a negative isolation method to obtain pure NK cells. The negative isolation protocol was based on magnet beads that were coated with specific antibodies that bind and, thereby, capture all PBMCs except NK cells, which remained untouched after magnetic separation. Obtaining unmodified NK cells was crucial to prevent NK cell modulation through the isolation process. Afterwards, isolated NK cells were assessed for their purity by flow cytometry. Immune cells are characterized by surface receptors that are specific for each immune cell subset and NK cells are defined as CD3$^-$/CD56$^+$ subset within the lymphocytes.[17] Hence, the obtained samples were stained for CD3 and CD56 and analyzed by flow cytometry to determine the percentage of CD3$^-$/CD56$^+$ cells which represent the NK cell subset. The resulting dot plots together with the applied gating strategy are shown in Figure 5.2. The displayed gating strategy (Figure 5.2A) was applied to all samples that were analyzed by flow cytometry.
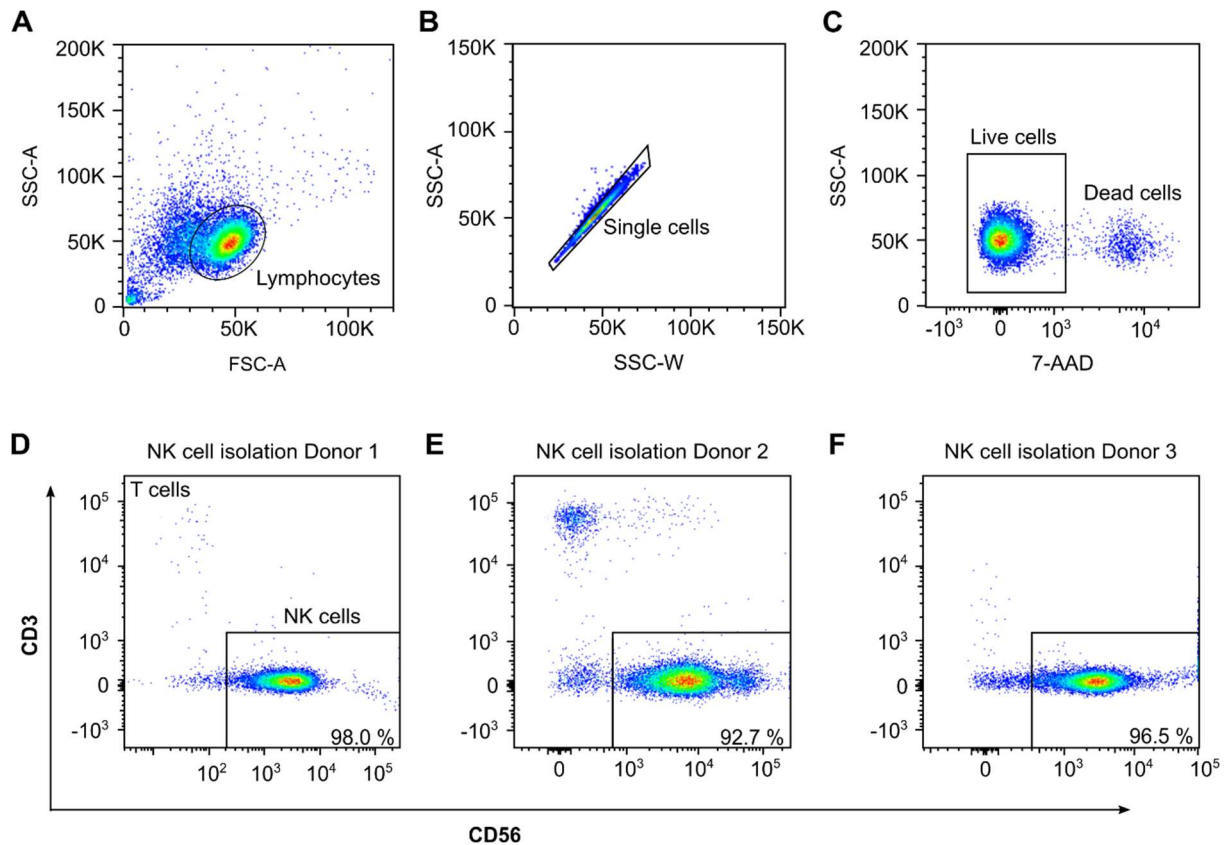
Figure 5.2: **Negative NK cell isolation yielded pure NK cells.** Isolated NK cell fractions of three different donors were stained for CD3 and CD56. 7-AAD was added for live/death discrimination and subjected to flow cytometry analysis. A), B) and C) Gating strategy. A) First the lymphocyte subset was selected by forward and side scatter gating, B) followed by the discrimination of doublets using SSC-A vs. SSC-W. C) Finally, only 7-AAD-negative cells were analyzed for CD3 and CD56 expression. D), E) and F) CD3 and CD56 expression analysis for NK cells of three different donors. CD3⁻/CD56⁺ NK cell fraction is represented with a box (lower right).

The isolated NK cells of three different donors were analyzed and displayed high purity between 92.7 and 98 % (Figure 5.2B). Thus, immune cell isolation and NK cell separation were established successfully. The freshly isolated NK cells were used to initiate the co-culture assay described above.

As specified in the introduction (see 2.2.1), TGFβ is one of the key players in NK cell suppression within the human body.[18, 96, 97] And it was already reported that NK cells stimulated with IL-15 and TGFβ display reduced cytotoxicity against cancer cells compared to NK cells stimulation with the activating cytokine IL-15 alone.[97, 98] This was the initial spark for the assay design. Most co-culture assays described in literature used freshly isolated NK cells that were pre-treated with the respective factors. After 16 to 48 h, the NK cells were added to the target cells to evaluate NK cell activity.[97, 98] Since the objective for this work was to stop NK cell inhibition utilizing small molecules, it was essential to include small molecules during the NK cell pre-treatment. However, a transfer of pre-treated NK cells to their target cells is not

feasible for a screening campaign with >1,000 small molecules because a robotic system that transfers reliably cell suspensions from well to well is not available. Therefore, a direct co-culture of NK cells and target cells was assessed. Freshly isolated NK cells together with IL-15 or IL-15 and TGFβ were added to A549[Green] cells at an effector to target ratio (E:T) of 10:1 and incubated for 120 to 150 h. To analyze the co-culture assay, the A549[Green] cell number was determined by counting the green fluorescent nuclei as represented in Figure 5.3D using the live-cell imaging device IncuCyte S3[®]. It is noteworthy, that not all green fluorescent objects, which were visible in the images, were counted by the software (counted objects are visualized by a purple mask, see Figure 5.3). Punctiform objects represent dead cells that had not yet lost their fluorescent stain and were excluded from the analysis. The results of the co-culture assay were analyzed in two ways: first based on the A549[Green] cell count at the end of the assay, the percentage of target cell cytolysis was determined. Cytolysis was calculated relative to the A549[Green] cell count obtained from the co-culture with NK cells that were not activated by IL-15 (see 4.3.3.1). This condition is defined as unstimulated conditions. Secondly, A549[Green] cell count was evaluated over time displaying target cell growth or reduction in the presence of NK cells under the different conditions. The analysis of NK cell-mediated cytolysis revealed that 51 - 97 % of the A549[Green] target cells were lysed in the presence of the activating cytokine IL-15 (Figure 5.3A). The addition of TGFβ to the co-culture decreased NK cell cytolysis by 34 ± 4 % compared to IL-15 alone represented by the grey bars in Figure 5.3A.
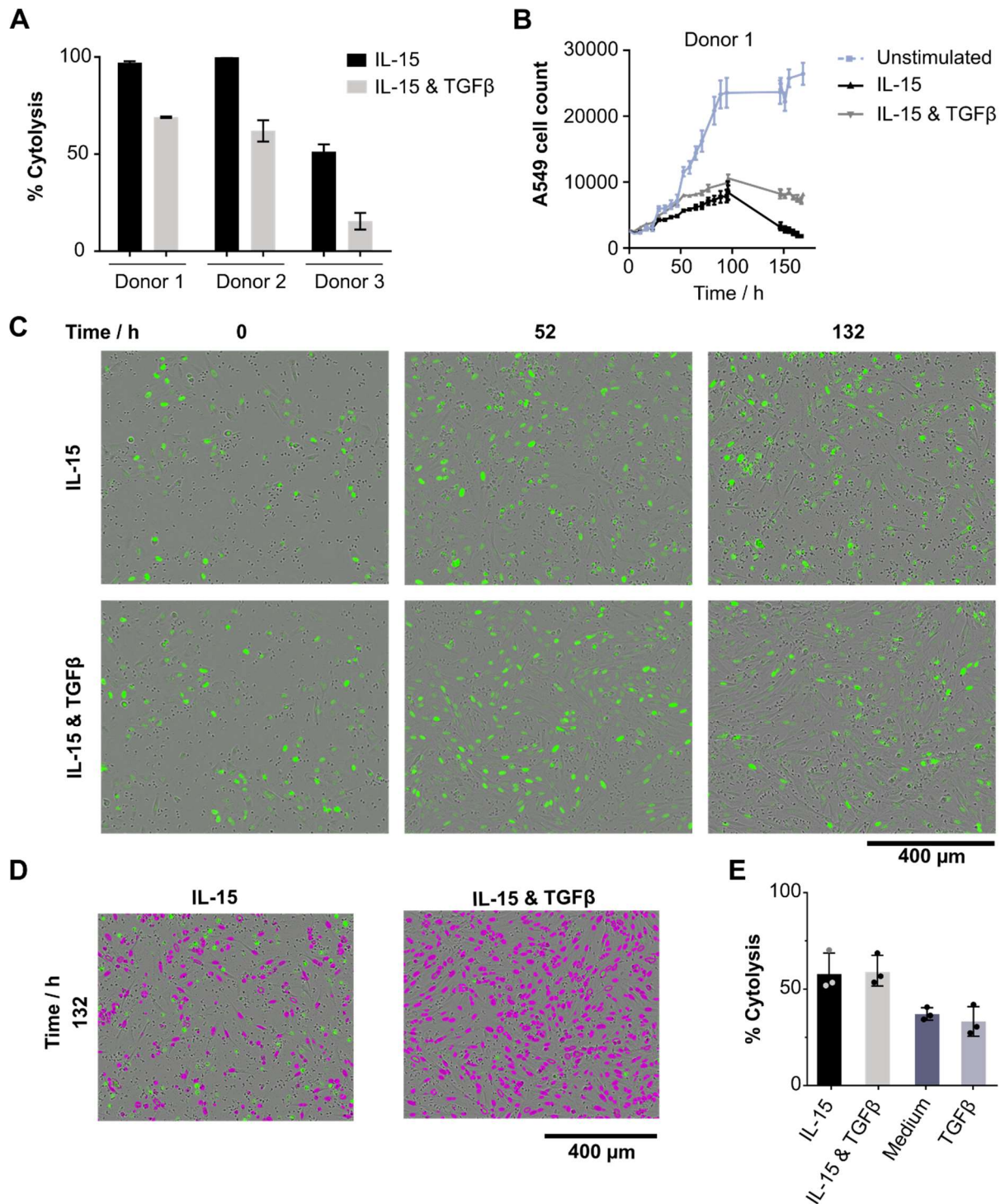
Figure 5.3: **Exogenous TGFβ reduces NK cell-mediated cytolysis of A549 cells**. Freshly isolated NK cells of three different healthy donors were added to A549[Green] cells at an E:T ratio of 10:1 together with only medium (unstimulated), 7.5 ng/ml IL-15 or IL-15 and 7.5 ng/ml TGFβ. A549[Green] cell count was monitored via live-cell imaging over 150-160 h using the IncuCyte S3®. Fluorescence of A549[Green] was used for the quantification of A549[Green] cell count. A) A549[Green] cell count was determined at the endpoint and the percentage of cytolysis relative to the co-culture with unstimulated NK cells was calculated. Data are mean ± SD, donors=3, N=3. B) Time-resolved A549[Green] cell count. Representative growth curve for donor 1. C) Representative images of A549[Green] cells in co-culture with NK cells. D) Representative images of A549[Green] cell count analysis method. Violet points represent each counted green nucleus. E) IL-2 expanded NK cells of three donors in co-culture with A549[Green] cells at an E:T

ratio of 1.5:1 treated with respective cytokines. A549[Green] cell count after 8 h as endpoint was determined and percentage of cytolysis relative to A549[Green] cells count only was calculated. Data are mean ± SD, donors=3, N=3.

Live-cell imaging of A549[Green] cell count over time in co-culture with NK cells (Figure 5.3B) showed that freshly isolated NK cells required approximately 50 h before target-cell cytolysis took place (Figure 5.3B). Freshly isolated NK cell were not immediately active after IL-15 addition and the time that was needed for NK cell activation is comparable to the pre-treatment time applied by Wilson *et al.*[97] Going into detail, A549[Green] target cells grew similarly in all three co-cultures (unstimulated, IL-15 or IL-15 and TGFβ) in the first 2 days. After 50 h, the A549[Green] cell count started to stagnate for the co-cultures treated with IL-15 or IL-15 and TGFβ (Figure 5.3B) while in the unstimulated condition A549[Green] cell growth continued to full confluence (Figure 5.3B). In the further time course, the A549[Green] cell count in the co-culture treated with only IL-15 was clearly reduced after 100 h (Figure 5.3B), while in the presence of IL-15 and the suppressive cytokine TGFβ, A549[Green] cell count still stagnated (Figure 5.3B grey curve). NK cell-mediated target cell cytolysis was partially inhibited in the presence of TGFβ (Figure 5.3B). The described growth behavior of the target cells is also reflected in the representative images in Figure 5.3D. At timepoint 132 h, a reduction in A549[Green] cell count was detected for the co-culture that was treated with IL-15 but not for the co-culture treated with IL-15 and TGFβ In parallel, IL-2-expanded NK cells (obtained from Watzl lab, IfADo, Dortmund) were tested in this co-culture setup. IL-2-expanded NK cells are freshly isolated NK cells that are first stimulated with feeder cells followed by continuous IL-2 addition for an expandable NK cell population. The proliferative property of expanded NK cells, in analogy to permanent cell lines, would be advantageous for screening. Furthermore, IL-2 expanded NK cells are already activated and NK cell-mediated cytolysis is immediate, which would significantly reduce the assay time to 6-8 h. However, IL-2 expanded NK cells in a co-culture with A549[Green] target cells treated with IL-15 and TGFβ did not exhibit reduced cytolysis compared to cells that were treated with IL-15 alone (Figure 5.3E). IL-15 and IL-2 are both NK cell activating cytokines and, thus, IL-2 expanded NK cells are pre-activated. For this reason, IL-15 was excluded from the assay and either only the inhibitory factor TGFβ or no stimulus was added to the co-culture and the cytolysis rate was evaluated. TGFβ could not inhibit NK cell-mediated cancer cell lysis. These results strongly indicated that IL-2-expanded NK cells are not suitable for this co-culture assay. Following, freshly isolated NK cells were used for the following assay optimization as tumor-derived suppressive factors could induce a suppressed NK cell phenotype mimicking the TME.

Considering that TGFβ only partially inhibits NK cell cytotoxicity (Figure 5.3A and B) and the initial idea was to mimic the TME, additional suppressive factors that are known to be involved in NK cell suppression in the TME were evaluated. It was important to define each single

suppressive factor separately. Each factor should have a distinct mode of suppression meaning that the combination of two or more suppressive factors should result in an additive inhibitory effect. Suppressive factors acting on the same pathway would not result in an additive inhibition of NK cell cytotoxicity.

TGFβ binds to the TGF-beta receptor type-1 and 2 (TGFR-1/2) receptor on NK cells and thereby modulates mTORC1 signaling resulting in a dysfunction of NK cell metabolism and decreased activity (see 2.2.1).[99] Another well-defined immunosuppressive molecule within the TME is PGE2 which binds to PTGER2 and PTGER4 on NK cells (see 2.2.1). Stimulated PTGER2/4 increases cAMP levels and, thus, activates the transcription factor CREB. Hence, the induced changes are distinct from mTORC1 signaling.[24] PGE2-mediated NK cell inhibition was demonstrated in literature before.[22, 26, 100]

To validate that PGE2 inhibits NK cell cytotoxicity in the established co-culture assay, freshly isolated NK cells were co-cultured with A549^{Green} target cells in the presence of IL-15 and PGE2. The A549^{Green} cell count was increased in the co-culture with IL-15 and PGE2 compared to the treatment with IL-15 alone (Figure 5.4A). NK cell activity was decreased equivalently to the condition of IL-15 and TGFβ. Consequently, both TGFβ and PGE2 inhibited NK cell cytolysis rate only partially when compared to the unstimulated co-culture condition. However, co-treatment with TGFβ and PGE2 in presence of IL-15 inhibited NK cell-mediated cytolysis substantially as the target cell proliferation was only slightly impacted. Comparing the relative cytolysis rate of IL-15 activated NK cells of all three donors with the one treated with IL-15, TGFβ and PGE2 yielded in an NK cell inhibition of 73.3 ± 6.5 %. NK suppression is also clearly represented by the increase in green fluorescent nuclei (Figure 5.4C). Hence, the aim to mimic the TME, in which NK cells are not able to eliminate cancer cells, was achieved.
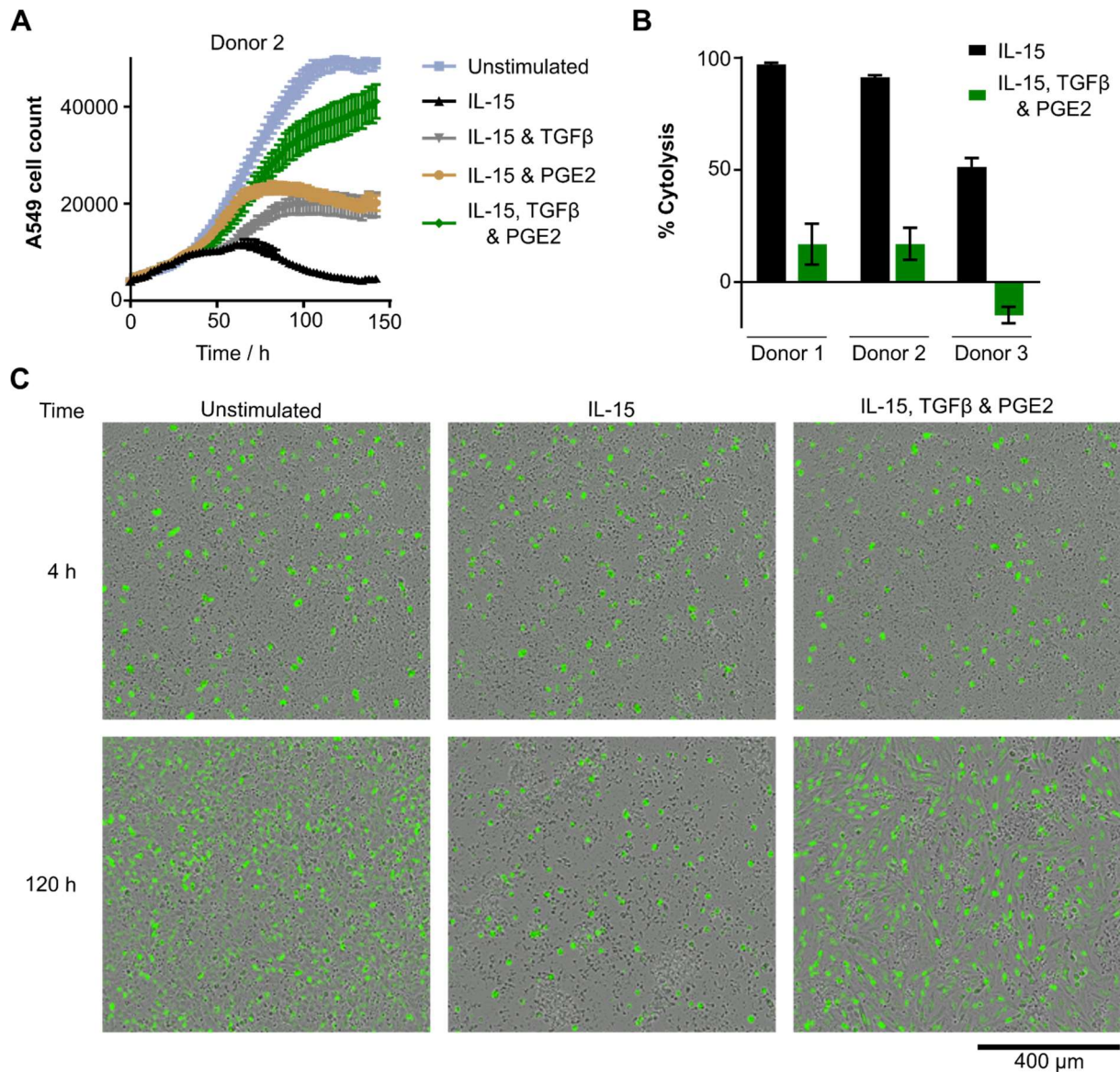
Figure 5.4: **The combination of TGFβ and PGE2 strongly inhibits NK cell-mediated target cell cytolysis.**
Freshly isolated NK cells of three different donors were added to A549[Green] cells at an E:T ratio of 10:1 together
with medium (unstimulated) or 7.5 ng/ml IL-15, 7.5 ng/ml TGFβ and / or 200 ng/ml PGE2. A549[Green] cell count was
monitored via live-cell imaging over 150-160 h using the IncuCyte S3®. The fluorescence of H2BeGFP was used
for the quantification of A549[Green] cell count. A) Time-resolved changes in A549[Green] cell count. Representative
growth curve for donor 2. B) A549[Green] cell count was determined at the assay endpoint (150 h) and the percentage
of cytolysis relative to the co-culture with unstimulated NK cells was calculated. Data are mean ± SD, donors=3,
N=3. C) Representative images of A549[Green] cells in co-culture with NK cells.

Utilizing freshly NK cells isolated from PBMCs is highly laborious when required for a
screening campaign. An alternative would be the use of the lymphocyte fraction of PBMCs.
PBMCs include lymphocytes (T cells, B cells an NK cells) as well as monocytes and dendritic
cells. The two latter cell types adhere onto surfaces of tissue culture flasks, while lymphocytes
are suspension cells. These opposing characteristics were exploited to isolate lymphocytes

from PBMCs by culturing them in tissue culture flasks overnight. Monocytes and dendritic cells adhered to the flask's surface while lymphocytes remained in suspension and could be easily separated. Although the lymphocyte fraction also contained T and B cells, the cytotoxic T cell subset is not able to contribute to A549[Green] cell cytolysis because naïve cytotoxic T cells require priming by antigen-presenting cells and cannot be activated by IL-15 alone (see 2.1).[101] B cells are immune cells without cytotoxic function.[102] Hence, lymphocytes can be utilized in the co-culture assay and the reduction of A549[Green] cells count is expected to be mediated solely by NK cells.
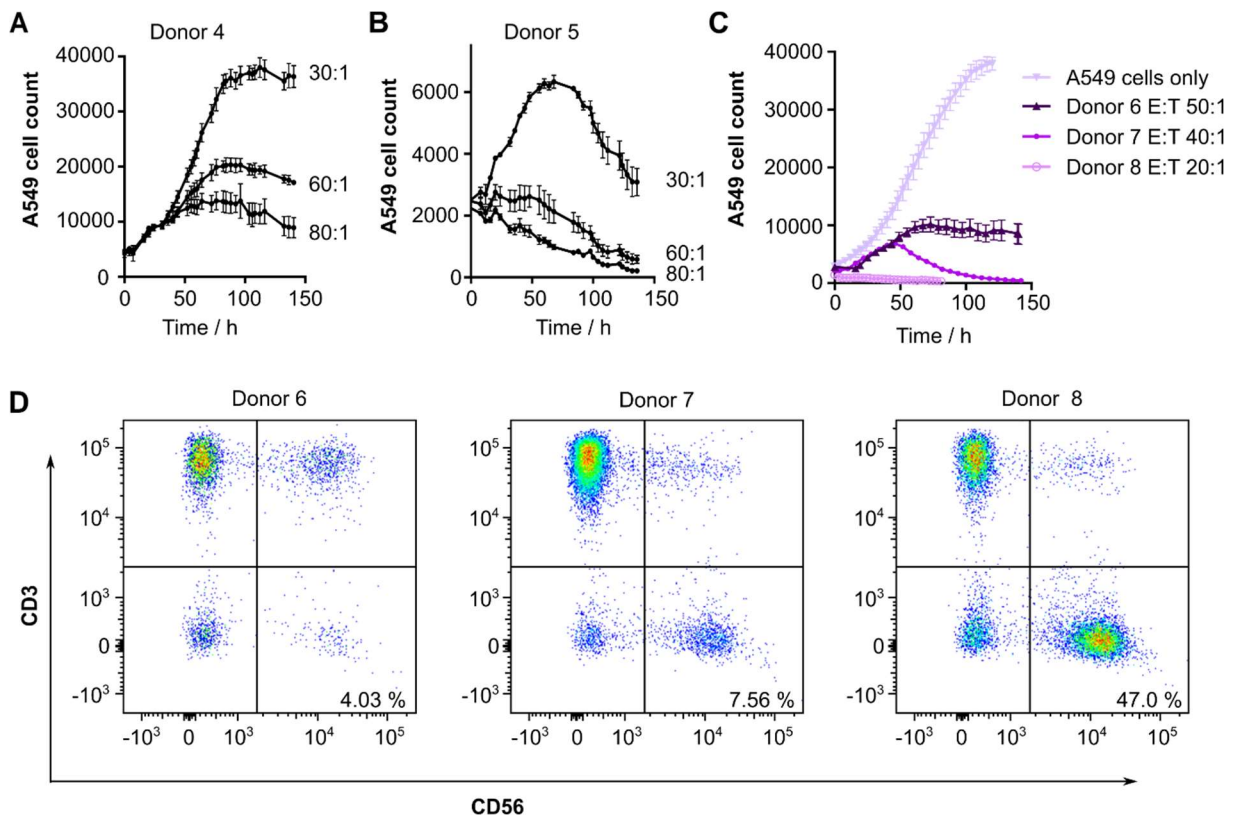
Figure 5.5: **The proportion of NK cells within the lymphocyte subset varies for individual donors.** A)-C) Lymphocytes of different donors were added to A549[Green] cells at E:T ratios between 20:1 and 80:1 and supplemented with 30 ng/mL IL-15. A549[Green] cell count was monitored via live-cell imaging over 140 h using the IncuCyte S3®. The fluorescence of H2BeGFP was used for the quantification of the A549[Green] cell count. D) Flow cytometry analysis of lymphocytes of three different healthy donors stained with CD3, CD56 and 7-AAD. Gating was performed as shown in Figure 5.2. CD3^{-}/CD56^{+} cells represent the NK cell subset and the percentage of NK cells is indicated in each plot.

In analogy to the assay setup using freshly isolated NK cells, lymphocytes and suppressive factors were added to A549[Green] cells and incubated for up to 150 h. However, first the required E:T value using lymphocytes were investigated in the presence of IL-15 alone because the lymphocyte subset is composed of different cells of which in average only 13.7 ± 6.5 % are NK cells.[103] Lymphocytes of different donors behaved very differently at the tested E:T ratios

as shown in Figure 5.5. Donor 4 for example could eliminate A549^{Green} target cells in the presence of IL-15 only at an E:T ratio higher then 60:1, while NK cells of donor 5 already lysed A549^{Green} cells at an E:T ratio of 30:1 efficiently. The varying efficiencies of NK cell-mediated elimination of different donors was highly dependent on the NK cell proportion within the lymphocyte fraction.

To directly relate the percentage of NK cells to the E:T ratio, different donors were analyzed for CD3$^-$/CD56$^+$ cells by flow cytometry. Three different donors were chosen that displayed clear differences in the efficiency of NK cell-mediated cytolysis (Figure 5.5D). Donor 6-derived lymphocytes stopped A549^{Green} cell growth only at an E:T of 50:1. Lymphocytes from Donor 7 reduced A549^{Green} cell count after the initial growth phase, while donor 8-derived lymphocytes prevented A549^{Green} cells growth immediately at low E:T ratio of 20:1.

Donor 6-derived lymphocytes exhibited 4 % of NK cells, while donor 7 contained 7.6 % NKs. In line with the high A549^{Green} elimination capacity, 47 % of the lymphocyte subset of donor 8 were identified to be NK cells, which is exceptionally high. Donor 8 may had carried an infection and therefore the NK cells were more abundant than usual. The investigation of the E:T ratio utilizing lymphocytes pointed out that the optimal proportion between lymphocytes and A549^{Green} cells is different for each donor. Hence, the optimal E:T ratio was determined in advance to achieve optimal assay conditions, i.e., high A549^{Green} cell elimination in presence of IL-15 while the unstimulated condition should not affect A549^{Green} cell growth. NK cells from donors that started to lyse the target cells without the required pre-activation (see donor 8 in Figure 5.5) were excluded from further assays.
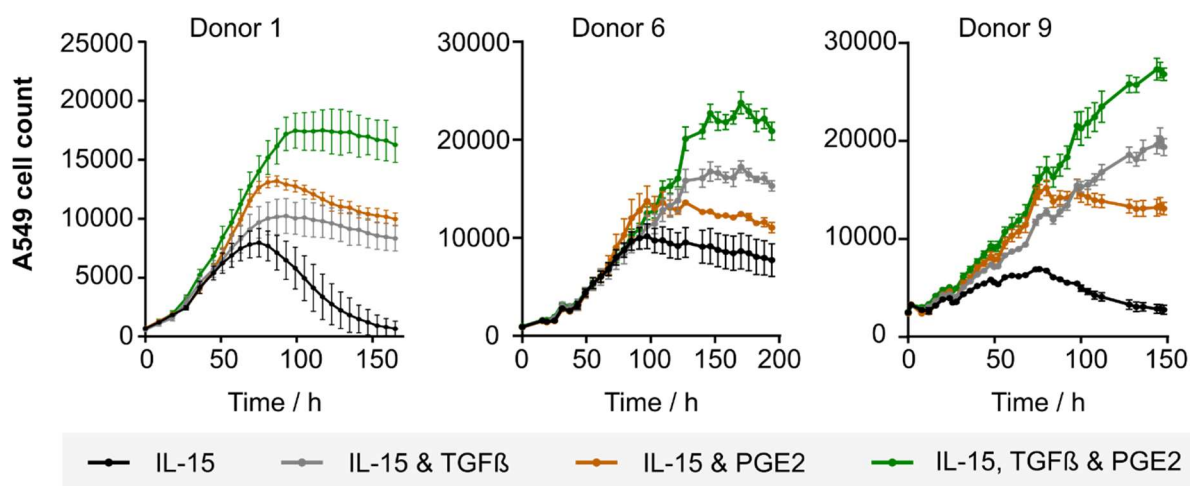
Figure 5.6: **Utilizing lymphocytes in the co-culture assay displays similar NK cell activities**. Lymphocytes of three healthy donors in co-culture with A549^Green target cells were treated with the indicated conditions (30 ng/mL IL-15, 30 ng/mL TGFβ, 200 ng/mL PGE2) and incubated for up to 190 h. Donor 1 was used with an E:T of 40:1, donor 6: E:T 50:1 and donor 9: E:T 30:1. A549^Green cell count was monitored via live-cell imaging up to 200 h using the IncuCyte S3®. The fluorescence of H2BeGFP was used for the quantification of A549^Green cells count. Data are mean ± SD, donor=3, representative donors, N=3.

Subsequently, the addition of the suppressive factors TGFβ and PGE2 were studied in the co-culture assay utilizing lymphocytes instead of freshly isolated NK cells. As shown in Figure 5.6, the co-culture of lymphocytes and cancer cells displayed similar growth curves for A549^Green cells as observed for isolated NK cells. IL-15 alone induced NK cell activation after 50 h resulting in a decreased A549^Green cell count (Figure 5.6). Treatment with IL-15 and TGFβ or IL-15 and PGE2 inhibited NK cell-mediated cytolysis partially while an additive NK cell inhibition was observed by combining the three. NK cell cytotoxicity was clearly reduced and A549^Green cell could proliferate further (Figure 5.6).

Finally, to ensure that TGFβ and PGE2 effect NK cell activity directly and do not increase A549^Green cell growth, A549^Green cells were treated with IL-15 or IL-15, TGFβ and PGE2 in the absence of immune cells and the cell count was monitored over time (Figure 5.6). The two treatment conditions did not influence A549^Green cell proliferation. Therefore, the differences in the two treatment conditions on A549^Green cell count in presence of NK cells (see Figure 5.6 and Figure 5.7) originated from NK cell activity.
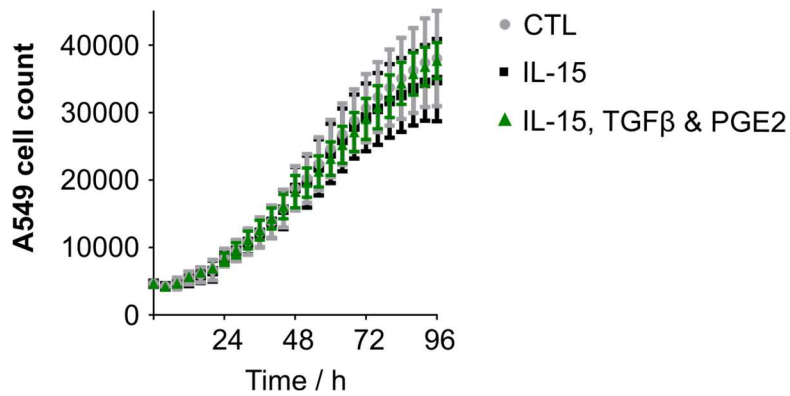
Figure 5.7: **A549^{Green} cell growth is not changes by IL-15, TGFβ and PGE2.** A A549^{Green} cell growth in the presence of 30 ng/mL IL-15 alone or in combination with 30 ng/mL TGFβ, 200 ng/mL PGE2 over 96 h. A549^{Green} cell count was monitored via live-cell imaging using the IncuCyte S3®. The fluorescence of H2BeGFP was used for the quantification of A549^{Green} cells count. Data are mean valued ± SD, n=3.

In Summary, utilizing lymphocytes instead of isolated NK cells can be used for further investigation, particularly, to identify small molecules that enhance NK cell-mediated elimination of cancer cells.

5.1.2 Proof-of-concept

NK cells eliminate target cells by secreting lytic granules that contain granzyme B and perforin that mediate NK cell cytotoxicity, and it was demonstrated that TGFβ reduces the expression of the two proteins.[18]
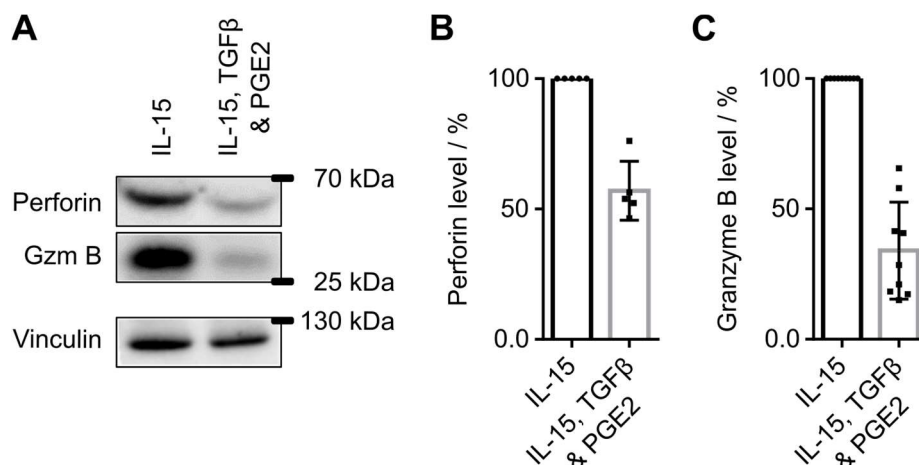
Figure 5.8: **TGFβ and PGE2 reduced cytotoxic effector proteins of NK cells**. A)-C) Detection of perforin and gramzyme B (GzmB) in lysates of Lymphocytes. Representative immunoblot of lymphocytes treated with either 30 ng/mL IL-15 or IL-15, 30 ng/mL TGFβ and 200 ng/mL PGE2. Vinculin was used as a loading control. C) and D) Quantification of perforin (C) and granzyme B levels (D) of lymphocytes originating from different healthy donors. Data are mean ± SD of different donors, donor ≥ 5.

To determine the effect of TGFβ and PGE2 on granzyme B and perforin levels when using lymphocytes, protein levels were evaluated following 48 h of lymphocyte incubation with IL-15 or IL-15, TGFβ and PGE2 *as part of the Master thesis of Alisa Reich*. The suppressive factors clearly reduced granzyme B and perforin protein abundance (see Figure 5.8).

To prove the concept that bioactive small molecules may prevent the suppressed phenotype of NK cells, the small molecule RepSox (Figure 5.9A) was studied in the co-culture assay. RepSox is a selective TGFR-1 modulator with an IC_{50} of 18 nM for the inhibition of TGFβ-induced signaling cascade in cells.[104] Thus, addition of RepSox to the co-culture with IL-15, TGFβ and PGE2 should preserve NK cell cytotoxicity. Indeed, TGFR-1 inhibition maintained the function of NK cells as depicted in Figure 5.9. The addition of 1 µM RepSox together with IL-15, TGFβ and PGE2 increased NK cell-mediated cytolysis rate of freshly isolated NK cells by 54, 61 or 78 %, respectively, compared to IL-15, TGFβ and PGE2 alone (Figure 5.9B). Time-resolved A549[Green] cell count for the co-culture treated with IL-15, TGFβ, PGE2 and RepSox showed a similar curve as observed for IL-15 alone (Figure 5.9C).
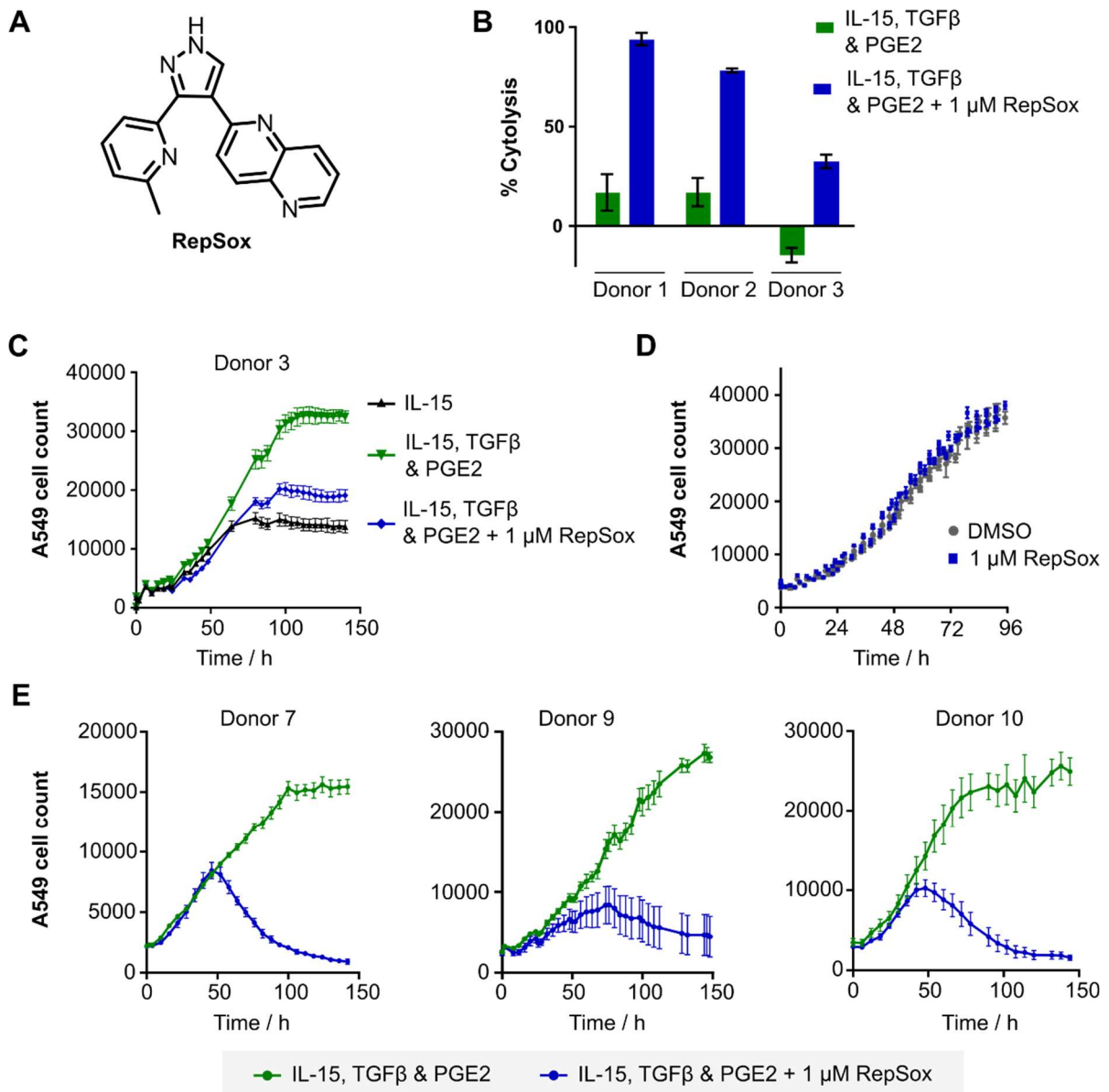
Figure 5.9: The **TGFβR-1 inhibitor RepSox prevents NK cell suppression.** A) Chemical structure of RepSox. B) NK cell-mediated cytolysis rate in co-culture with A549^Green cells treated with either 7.5 ng/mL IL-15, 7.5 ng/mL TGFβ and 200 ng/mL PGE2 with or without 1 µM RepSox. Freshly isolated NK cells of three different donors were used. C) Time-depended analysis of A549^Green cell count in co-culture with freshly isolated NK cells of donor 3 treated with IL-15, TGFβ and PGE2 alone or in the presence of 1 µM RepSox. D) A549^Green cell count in the presence of 1 µM RepSox or DMSO as control. E) Time-depended analysis of A549^Green cell count in co-culture with lymphocytes treated with either 30 ng/mL IL-15, 30 ng/mL TGFβ and 200 ng/mL PGE2 with or without 1 µM RepSox. Three representative donors are shown: donor 6 with E:T 40:1, Donor 9:E:T 30:1 and Donor 10: E:T 50:1. A549^Green cell count was monitored via live-cell imaging up to 150 h using the IncuCyte S3®. Fluorescence of H2BeGFP was used for the quantification of A549^Green cells count. Data are mean ± SD, donor=3 representative donors, N=3.

Similar results were obtained for the co-culture assay using lymphocytes, the addition of 1 µM RepSox to the suppressive factors clearly prevented NK cell inhibition (Figure 5.9E) compared

to the co-culture treated with IL-15, TGFβ and PGE2. In the absence of NK cells or lymphocytes, the A549^{Green} cell count was not reduced by RepSox as depicted in Figure 5.9D. Hence, the bioactive small molecule RepSox was capable of preventing NK cell suppression in the presence of tumor-derived suppressive factors. Interestingly, RepSox was able to fully block NK cell suppression induced by TGFβ as well as PGE2 although it inhibits TGFR-1 which is mechanistically unrelated to PGE2-mediated signaling.

In summary, small molecules are able to preserve NK cell activity in the co-culture assay mimicking the TME. Hence, the developed assay meets the requirement to be applicable for the identification of small-molecule modulators that can prevent NK cell inhibition.

5.1.3 Screening for small molecules that enhance NK cell-mediated elimination of cancer cells

In collaboration with the COmpound MAnagement and Screening center (COMAS) in Dortmund, the co-culture assay monitoring NK cell-mediated cancer cell cytolysis using lymphocytes (Figure 5.10) was miniaturized to 384-well format to determine the half-maximal inhibitory concentration (IC$_{50}$) of the hit compounds and even further to 1536-well format for the initial screening campaign. The read out of the assay was the A549^{Green} cell count by means of high-content analysis after 144 h.
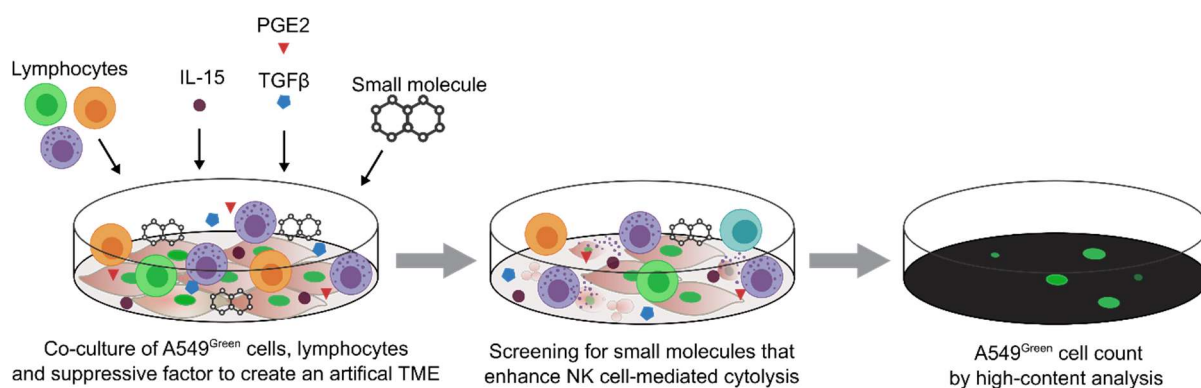
Figure 5.10: **NK cell-mediated cancer cell cytolysis assay for the screening campaign.** Lymphocytes, the NK cell activating cytokine IL-15 and the suppressive factors TGFβ and PGE2 are added to A549^{Green} target cells. At the same time, small molecules are added and A549^{Green} cell count is determined after 144 h.

Prior to screening, a sufficient number of lymphocytes were isolated from buffy coats and cryopreserved. Furthermore, obtained lymphocytes of each donor were pre-evaluated to determine the individual E:T ratio that delivered the highest signal-to-background value, i.e., A549^{Green} cell count with IL-15 (signal) and with IL-15, TGFβ and PGE2 (background).

69

The NK cell-mediated cancer cell cytolysis assay was performed for 29,306 selected compounds at a concentration of 11 µM using 1536-well format. The selected compounds comprised the LOPAC® library of pharmacologically active compounds, Prestwick Chemical Library® of FDA-approved & EMA-approved drugs, Edelris library containing natural product-like small molecules (Keymical Collections™), selected small molecules purchased from ChemDiv and the unique in-house compound library (synthesized within the Waldmann group). In parallel, A549^{Green} cells were treated with the respective compounds in the absence of lymphocytes and suppressive factors to identify toxic compounds that reduce A549^{Green} cell count independent of NK cell cytotoxicity. Compounds that reduce the A549^{Green} cell count by ≥70 % in the absence of lymphocytes were excluded from further analysis.

For the initial screening in 1536-well format, lymphocytes from seven different donors were used whereby varying signal-to-background (S/B) values were monitored. The calculated S/B values were between 2 and 14.6. Screening assays should have robust and high S/B values to exclude the accumulation of false positive hits. However, in the condition of active NK cells treated with IL-15, the A549^{Green} cell count was approximately 8,000 cells (96-well plate) which in the presence of TGFβ and PGE2 increased to around 35,000 cells. Although the S/B was only 4.4, the difference in total cells number was actually 27000. This differences clearly allowed to identify compounds that prevent NK cell inhibition and, thus, mediate the reduction of A549^{Green} cell count. Furthermore, the Z' value in 1536-well format was mostly between 0.3 and 0.4 which also indicates that the assay allowed to distinguish between hit and no hit (see 2.4). The initial screen in 1536-well format yielded a high hit rate of 1.4 % at a compound concentration of 17 µM. Compounds were identified as hits when a reduction of A549^{Green} cell count was ≥ 60 % compared to A549^{Green} cell count in the co-culture with lymphocytes, IL-15, TGFβ and PGE2. Compounds that reduce the A549^{Green} cell count also in the absence of lymphocytes by more than 70 % were excluded from further analysis. Remaining hit compounds were subjected to dose-response measurements to determine their respective IC$_{50}$ value (384-well format). The IC$_{50}$ determination strongly reduced the hit rate because several additional compounds showed toxicity as well. To evaluate toxicity further, two distinct approached were utilized, on the one hand a cell count analysis by means of Hoechst 33342 and on the other hand a CellTiter-Glo® assay. The obtained results reduced the hit rate by 92 % to 0.11 %. The screening campaign is still ongoing and intensive toxicity evaluations and hit compound validation by using lymphocytes of different donors will be performed.

IC$_{50}$ values of the hit compounds were evaluated in 384-well plates using five different donors with S/B values between 4.3 and 39.9 and a satisfying Z'-factor of 0.59 ± 0.12 (see 2.4). Thereby, a preliminary hit list with the respective IC$_{50}$ values was already obtained employing the NK cell-mediated cancer cell cytolysis assay (Table 3).

Table 3: **Identified compounds with known targets that revert NK cell inhibition in the automated NK cell-mediated cancer cell cytolysis assay**. Data are mean values ± SD, N=3. Viability was evaluated using either ([a]) Hoechst 33342 or ([b]) CellTiter-Glo® for compound's cytotoxicity. Data are mean values, N=3. D1: donor 1, D2: donor2.

Compound	Cytolysis IC_{50} [µM]	Viability IC_{50} [µM]	Mode of action
RepSox	D1: 0.14 ± 0.07 D2: 0.19 ± 0.09 D3: 0.22 ± 0.08	inactive	Inhibitor of TGFR-1/ALK5
SB-505124	D1: 0.26 ± 0.14 D2: 0.28 ± 0.10	> 3.4 [a]	Inhibitor of TGFR-1/ALK4/5
BI-4659	0.26 ± 0.14	inactive [a]	Inhibitor of TGFR-1/ALK5
SB-525334	0.28 ± 0.09	3.98 [a]	Inhibitor of TGFR-1/ALK5
GW788388	0.52 ± 0.10	inactive [a]	Inhibitor of TGFR-1/ALK5
TP-008	0.70 ± 0.20	inactive [a]	Inhibitor of TGFR-1/ALK4/5
LY2157299	1.53 ± 0.66	inactive [a]	Inhibitor of TGFR-1/ALK5
LY2109761	3.06 ± 0.21	inactive [a]	Dual inhibitor of TGF-β receptor type 1/2 (TGFR-1/2)
VPS34-IN1	0.72 ± 0.22	6.60[a]	Inhibitor of the lipid kinase VPS34
PIK-III	1.30 ± 0.27	15.21[a]	Inhibitor of the lipid kinase VPS34
SAR405	1.42 ± 0.34	inactive[a]	Kinase inhibitor of PIK3C3 /VPS34
Compound 19, PIK-III analogue	1.60 ± 0.37	> 17[a]	Inhibitor of VPS34
MZ1	0.13 ± 0.04	1.33[a]	PROTAC based on JQ-1. Induces proteasomal degradation of bromodomain-containing protein 4 (BRD4).
R406	D1: 0.28 ± 0.08 D2: 0.14 ± 0.04	inactive[b]	Inhibitor of Syk tyrosine kinase
BI1002494	D1: 0.54 ± 0.17 D2: 0.75 ± 0.21	12.5 [b]	Inhibitor of Syk tyrosine kinase
BI-2492	3.27 ± 0.50	13.3 [b]	Negative control of BI1002494 780-fold less potent
PRT318	1.26 ± 0.06	inactive [b]	Inhibitor of Syk tyrosine kinase
PRT505-15	D1: 1.35 ± 0.20 D2: 1.91 ± 0.18	inactive [b]	Inhibitor of Syk tyrosine kinase
NU7441	D1: 0.80 ± 0.41 D2: 0.39 ± 0.22	inactive [b]	Inhibitor of DNA-PK, also inhibits mTOR and PI3K

Concentrating on the hit compounds with annotated target, several TGFβR-1 inhibitors were identified. Furthermore, diverse kinase inhibitors with inhibitory activities against the phosphatidylinositol 3-kinase VPS34, the tyrosine kinase Syk and an inhibitor of the serine/threonine protein kinase DNA-PK were identified and showed only moderate or no toxicity. In addition, a bromodomain-containing protein 4 (BRD4) degrader was highly active with an IC_{50} of 130 nM, however, it displayed toxicity towards A549 cells already at low

concentrations. Future hit validation and mode-of-action analysis will further elucidate the compounds' effects.

5.2 Cell-based assay for Indolamine 2,3-dioxygenase modulators

5.2.1 Development of a cell-based screening assay to identify novel modulators of IDO1

To identify novel small molecule modulators reducing IDO1 activity, a cell-based screening assay was established that monitors IDO1-mediated Kyn production. A fundamental aspect of a screening assay is a robust readout, such as fluorescence or luminescence.[106] Currently employed cell-based assays monitoring Kyn levels utilize mainly *p*-dimethylamino benzaldehyde (*p*-DMAB)[107] for a colorimetric-based detection of Kyn levels. However, *p*-DMAB-mediated Kyn detection requires a transfer of cell culture supernatant[107] which is technologically challenging in screening assays. Nonetheless, *p*-DMAB was exploited in the course of this project for initial optimization studies and for the validation and mode-of-action (MoA) studies due to commercial availability. Alternatively, cellular Kyn production can be measured by means of high-performance liquid chromatography (HPLC).[108] HPLC-based techniques also require a transfer of cell culture supernatant[108] that is incompatible for automated screenings as mentioned above. Alternatively, Kyn levels in the culture medium can be detected by NFK Green™[109] using a fluorescent-based readout. However, it only offers a limited dynamic detection range in cells.[109] Therefore, a novel cell-based screening assay should be developed to overcome the before mentioned limitations of the existing techniques.
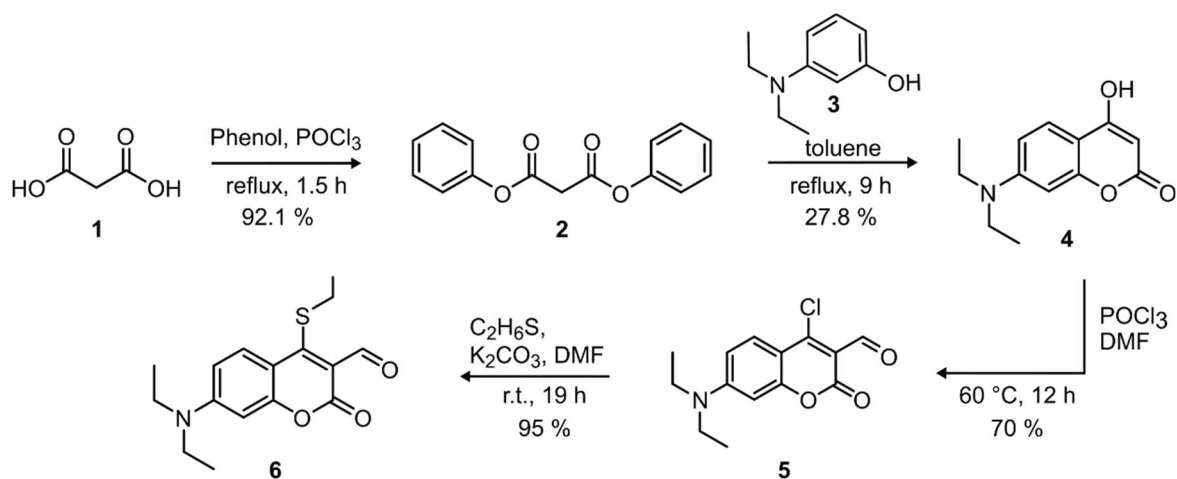
Figure 5.11: **Synthesis route to obtain the coumarin-based Kyn sensor (6)**. Isolated yield in percent (%).

To measure Kyn levels by means of a fluorescence readout, the previously developed coumarin-based Kyn sensor **6**[87] was synthesized via a four-step synthesis starting from malonic acid (Figure 5.11).

Previously, Klockhoff and Glass[87] showed that aldehyde **6** reversibly reacts in aqueous buffers with the aniline moiety of Kyn, but not with other biological amines like glycine and adenosine yielding a fluorescent adduct (Figure 5.12A).[87] As **6** has not been employed in enzymatic or cell-based assays yet, the synthesized Kyn sensor was validated for its use in a cell culture setting *as part of the Bachelor thesis of Nora Bruning*. Therefore, the spectral properties of **6** in the presence of Kyn were analyzed in cell culture medium containing fetal bovine serum (FBS).
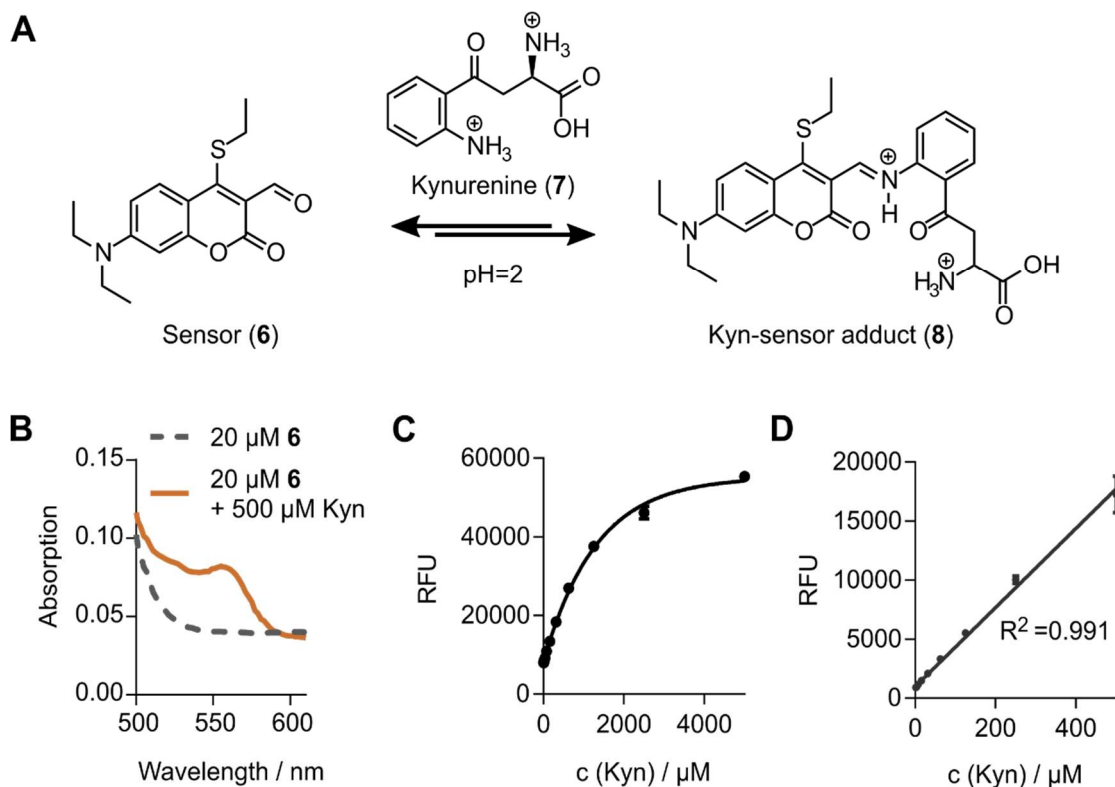
Figure 5.12: **Validation of a coumarin-based molecule as selective fluorescent sensor for kynurenine (7, Kyn).** A) Schematic representation of the reversible reaction between Kyn sensor (**6**) and Kyn. B) Absorbance scan of **6** in the absence or presence of 500 µM Kyn in cell culture medium. C) Kyn titration for determination of the linear detection range of sensor **6**. Detection of **8** by means of fluorescence (ex: 555 nm, em: 600 nm) in the presence of different Kyn concentrations (0-5000 µM) or D (0-500 µM) in cell culture medium.

In the absence of Kyn, the sensor absorbs light in a range below 500 nm in cell culture medium, while in the presence of Kyn the Schiff base **8** (Figure 5.12) is formed and a corresponding absorbance peak between 525 nm and 560 nm was observed (Figure 5.12B). Performing fluorescence intensity measurements (ex/em 555/600 nm), various Kyn concentrations ranging from 20 to 5000 µM were detected in cell culture medium by means of **6** (Figure 5.12C and D). A linear concentration-dependent increase in fluorescence was observed for Kyn concentrations up to 500 µM (Figure 5.12D) represented by the excellent correlation of 99.1 % (Figure 5.12D), allowing for a robust measurement within this

concentration range. To further validate this assay setup, Kyn levels in cell supernatants of IFNγ-stimulated cancer cells were analyzed *as part of the Bachelor thesis of Nora Bruning*. The human pancreas adenocarcinoma cell line BxPC3 was selected for the cell-based assay as these cells displayed the highest IDO1 expression upon stimulation with IFNγ. BxPC3 cells, as most cell lines, do not express IDO1 constitutively. Yet, stimulation with IFNγ significantly induced IDO1 expression in these cells (Figure 5.13A). IDO1 protein levels were already detectable after 8 h of IFNγ treatment and reached a maximum at 24 h which remained stable for at least 48 h as shown in Figure 3A.
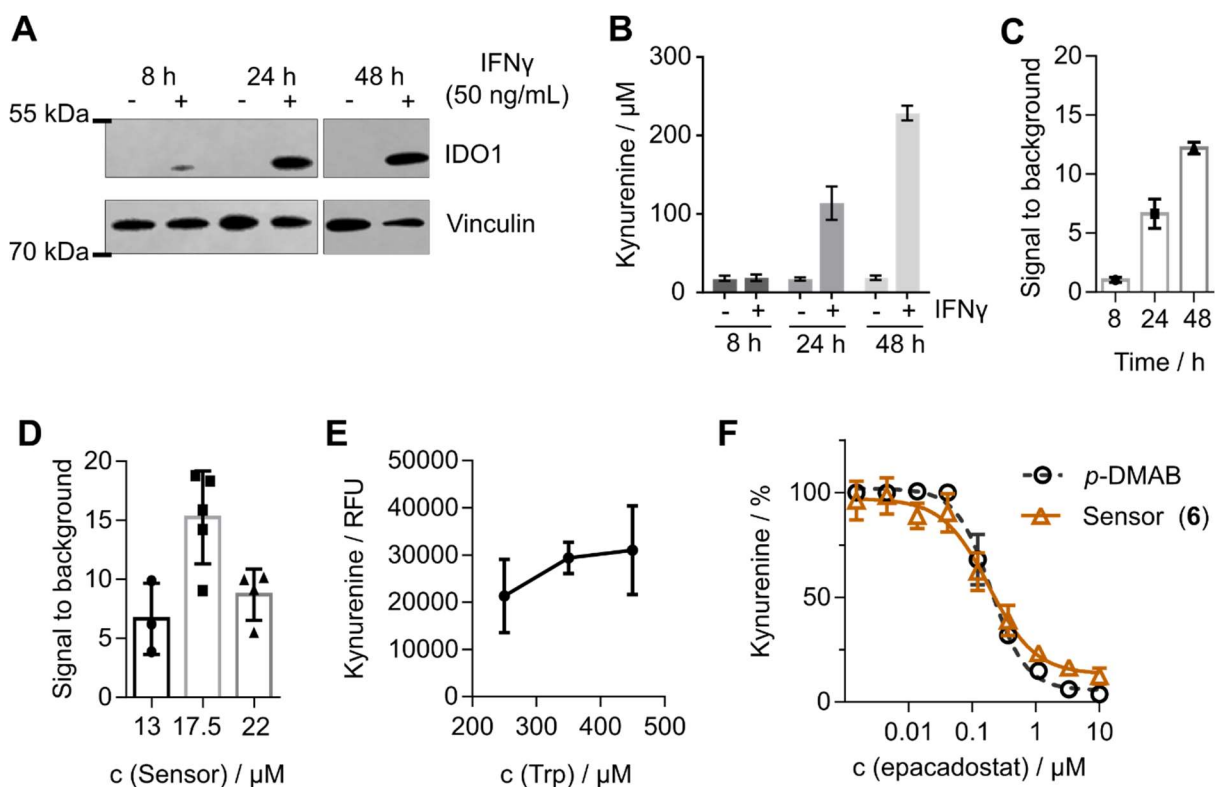
Figure 5.13: **Kyn sensor (6) detects cellular Kyn levels reliably**. A) IDO1 expression in BxPC3 cells after induction by IFNγ for 8, 24 and 48 h. Representative immunoblot for IDO1 and vinculin as a loading control. B) Time course of cellular Kyn production. The Kyn assay was performed in BxPC3 cells upon stimulation with IFNγ for 8, 24 and 48 h prior to detection of Kyn using LC-MS/MS. Kyn concentrations were obtained by a calibration curve. C) Calculation of signal to background ratios based on (B) to evaluate assay performance. S/B: signal to background ratio. Data are mean values ± SD, n = 3. D) Titration of sensor **6**. The Kyn assay was performed in BxPC3 cells treated with IFNγ for 48 h prior the detection of Kyn levels with diverse sensor concentrations. E) Titration of L-Trp. The Kyn assay was performed in BxPC3 cells treated with IFNγ and different L-Trp concentrations for 48 h prior to detection of Kyn levels using 17.5 μM sensor. Data are mean values ± SD, n = 2. F) Kyn assay in BxPC3 cell treated with IFNγ and epacadostat for 48 h prior the detection of Kyn levels utilizing *p*-DMAB or sensor **6**. Data are mean values ± S.D, n = 3.

In parallel, cellular Kyn levels were evaluated after 8, 24 and 48 h using LC-MS/MS (Figure 5.13B). 48 h were required for adequate Kyn production of approximately 230 μM Kyn together

with a high signal to background (S/B) ratio of 12. Hence, 48 h were set as assay incubation time. To further adjust the assay, the optimal Kyn sensor and L-Trp concentration were determined (Figure 5.13D and E, respectively). The following assay conditions were chosen for compound investigations: BxPC3 cells were stimulated with IFNγ and the assay medium was supplemented with 380 µM L-Trp. 48 h later, Kyn levels were detected using a final sensor concentration of 17.5 µM. To validate the chosen assay conditions, the known IDO1 inhibitor epacadostat was used as control compound. BxPC3 cells were treated with IFNγ, L-Trp and epacadostat for 48 h. For comparison, Kyn levels were detected by means of *p*-DMAB and sensor **6** (Figure 5.13F). Importantly, the usual transfer of cell supernatant into a fresh plate previously reported as required for Kyn detection by means of *p*-DMAB[107] was successfully omitted to adapt the assay for automated screenings. Using the known IDO1 inhibitor epacadostat, sensor **6** detected a dose-dependent decrease in Kyn levels similar to those detected by *p*-DMAB (Figure 5.13F), which is also reflected in the comparable IC_{50} values of 198 ± 9 nM (**6**) and 196 ± 4 nM (*p*-DMAB), respectively.
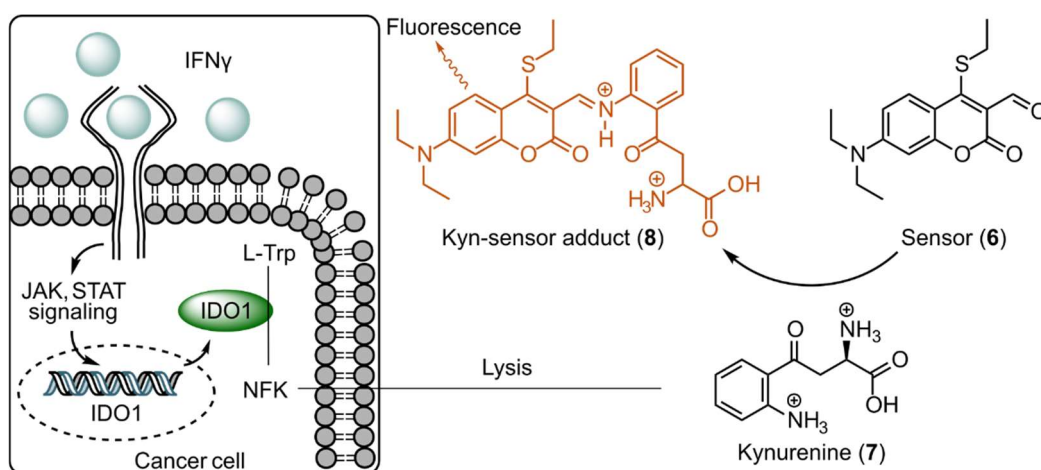
Figure 5.14: **Established fluorescent-based screening assay monitoring IDO1 activity in cells.** BxPC3 cancer cells are treated with IFNγ to induce IDO1 expression via JAK/STAT signaling. Cells are supplemented with IDO1's substrate L-Trp and Kyn levels are detected 48 h after IDO1 induction. Cells are lysed by means of TCA to release Kyn and Kyn levels are detected by means of sensor **6**.

Hence, **6** was validated as suitable fluorescent sensor to monitor Kyn levels in cells. A new cell-based assay, termed Kyn assay, was established. The underlying assay mechanism is illustrated in Figure 5.14. The Kyn assay was miniaturized and automated in collaboration with COMAS for screening large small-molecule libraries.
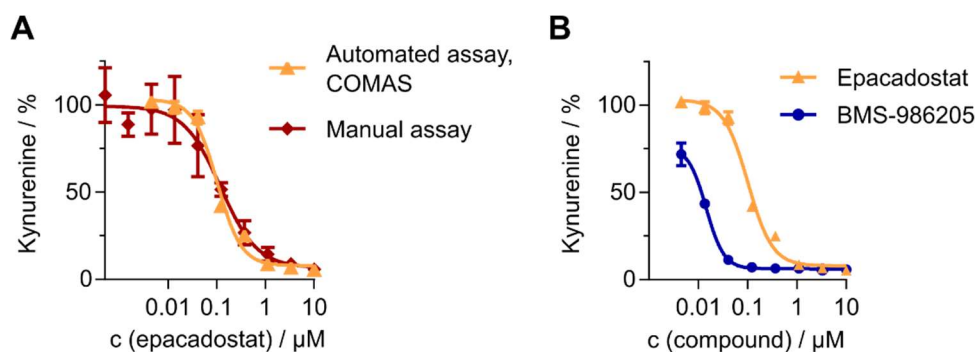
Figure 5.15: **Miniaturization and automatization of the Kyn assay**. BxPC3 cells were treated with IFNγ, L-Trp and compounds for 48 h prior to Kyn level detection using sensor **6**. The assay was performed in 384-well plates. A) Comparison of manual and automated Kyn assay. B) Automated Kyn assay for epacadostat and BMS-986205. Data are mean values ± S.D, n = 3.

Therefore, the assay was first adapted to a 384-well format. The minimization to 384-well format resulted in a comparable IC_{50} value of 119 ± 25 nM for the manual assay using epacadostat (Figure 5.15A) as obtained in 96-well format (IC_{50} = 198 ± 9 nM, Figure 5.13F). The assay was also performed in an automated fashion and comparable results were achieved as depicted in Figure 5.15B. A concentration-dependent decrease in Kyn levels was not only detected for epacadostat, also the mechanistically and chemically different IDO1 inhibitor BMS-986205 showed a reduction in Kyn levels with increasing concentration (IC_{50} = 14 ± 0.1 nM, Figure 5.15B).

The automated Kyn assay displayed robust assay characteristics with a Z'-factor of 0.76 and a signal-to-background ratio (S/B) of 14.2. The S/B ratio was calculated for IFNγ-stimulated BxPC3 cells and cells without IFNγ. To achieve an even higher throughput for the initial screening campaign (one-point measurements), downsizing to 1536-well format was successful (Z'-factor: 0.53 and S/B: 14.3). Thus, a robust, automated cellular Kyn assay with a high fluorescence dynamic range applicable for high-throughput analysis was developed. Employing the Kyn assay, a library comprising 157,332 chemically diverse compounds was screened at a final assay concentration of 7.1 µM (1536-well format), which resulted in a hit rate of 0.62 % applying a threshold of 50 % inhibition. Compounds that reduced cell viability by more than 25 %, small molecules with pan-assay interference (PAINS) features [5] as well as compounds that are frequently identified as hits in other screening campaigns were excluded from further analysis. The remaining hit compounds that reduce Kyn levels by ≥ 70 % were subjected to dose-response measurements to determine their respective IC_{50} values (384-well format). Thereby, 98.5 % of the small molecules were confirmed as Kyn level modulators and several potent hits with an IC_{50} value < 2 µM were identified.

As the enzymatic activity of IDO1 directly influences cellular Kyn levels[110], hit compounds with an IC_{50} value < 5 µM were tested for direct enzymatic inhibition of IDO1. For this, a biochemical assay using recombinantly expressed human IDO1 (rhIDO1) was established and performed. Interestingly, only 3.9 % of the compounds were identified as direct IDO1 modulators ($IC_{50} \geq$ 0.33 µM). Nonetheless, several chemotypes that have not been linked to IDO1 inhibition before were discovered including the most potent hit compounds **9**, **10** and **11** (Figure 5.16). These three hits were selected for further characterization (see below 5.2.2).
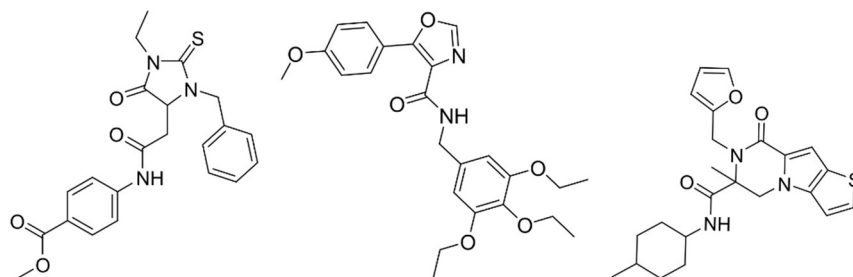
Compound	9	10	11
Kyn assay IC$_{50}$ / µM	0.006 ± 0.003	0.005 ± 0.001	0.05 ± 0.02
IDO1 activity assay IC$_{50}$ / µM	0.44 ± 0.18	0.73 ± 0.45	2.35 ± 1.83
Cell count IC$_{50}$ / µM	inactive	inactive	inactive
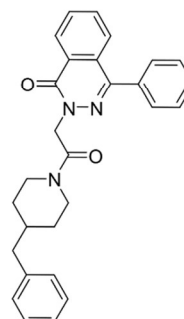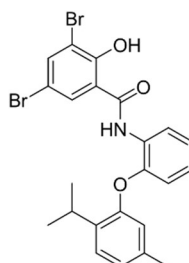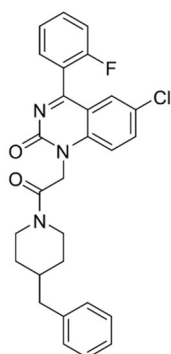
Compound	12	13	14
Kyn assay IC$_{50}$ / µM	0.08 ± 0.01	0.08 ± 0.001	0.10 ± 0.02
IDO1 activity assay IC$_{50}$ / µM	0.33 ± 0.02	0.36 ± 0.02	1.88 ± 0.32
Cell count IC$_{50}$ / µM	inactive	inactive	inactive
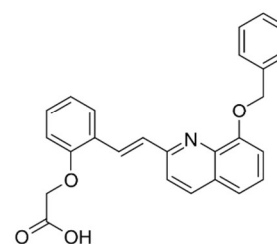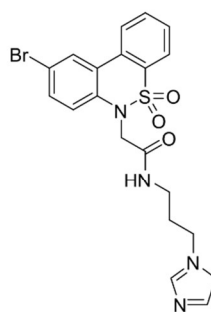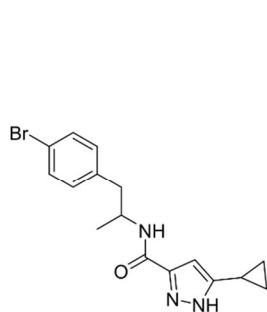
Compound	15	16	17
Kyn assay IC$_{50}$ / µM	0.35 ± 0.06	1.30 ± 0.22	2.00 ± 0.14
IDO1 activity assay IC$_{50}$ / µM	8.91 ± 1.32	9.91 ± 1.00	6.89 ± 1.99
Cell count IC$_{50}$ / µM	inactive	inactive	inactive

Figure 5.16: **Hit compounds directly inhibiting IDO1 enzymatic activity.** Structures and IC$_{50}$ values of IDO1 inhibitors identified in the HTS. IC$_{50}$ values in the Kyn assay were determined in BxPC3 cells. To exclude cytotoxic compounds, the cell count was evaluated via Hoechst-33342 staining in a dose dependent manner after 48 h, inactive compounds did not reduce cell count up to 10 µM. IC$_{50}$ values in the IDO1 activity assay were determined with rhIDO1 protein. Data are mean values ± SD, n ≥ 3.

Hit compounds that did not modulate IDO1 enzymatic activity were considered as indirect inhibitors. Within the subgroup of compounds with annotated cellular targets, two mechanistically distinct groups were identified (Table 4).

Table 4: **Selected hits of the Kyn screening with known targets.** Cell count was evaluated using Hoechst 33342 for compound's cytotoxicity. Data are mean values ± SD, n≥3.

Compound	Kyn assay IC$_{50}$ [µM]	Cell count IC$_{50}$ [µM]	Mode of action	
Momelotinib (CYT387)	0.29 ± 0.06	inactive	ATP competitive inhibitor of Janus kinases JAK1 and JAK2	JAK kinase inhibitors
Tofacitinib	0.59 ± 0.008	inactive	Irreversible inhibitor of Janus kinases JAK1 and JAK3	
Ruxolitinib	0.08 ± 0.005	inactive	ATP competitive inhibitor of Janus kinases JAK1 and JAK2	
Tofacitinib citrate	0.28 ± 0.03	inactive	Irreversible inhibitor of Janus kinases JAK1 and JAK3	
CEP-33779	0.45 ± 0.04	inactive	ATP competitive inhibitor of Janus kinase JAK2	
GSK1324726A	0.01 ± 0.005	> 2 µM	Inhibitor of bromodomain and extra-terminal (BET) family proteins BRD2, BRD3, and BRD4.	BRD/BET inhibitors
(+)-JQ1	0.03 ± 0.004	> 2 µM	Inhibitor of BRD4 (1/2)).	
OTX015	0.03 ± 0.01	> 2 µM	Inhibitor for BRD2, BRD3, and BRD4	
I-BET151	0.07 ± 0.002	inactive	Pan BET family inhibitor	
MZ1	0.09 ± 0.04	1.24	Proteolysis-targeting chimera (PROTAC) based on JQ-1. Induces proteasomal degradation of bromodomain-containing protein 4 (BRD4).	
PFI-1	0.51 ± 0.06	inactive	Inhibitor of BRD4	
I-BRD9	> 10 µM	inactive	Selective cellular chemical probe for BRD9.	
Succinylacetone	0.41 ± 0.22	inactive	Irreversible inhibitor of δ-aminolevulinic acid dehydratase which produces porphobilinogen, the precursor of heme.	Heme biosynthesis inhibitors
N-methyl protoporphyrin IX (1-NMPP)	2.61 ± 1.64	inactive	Inhibitor of protoporphyrin IX ferrochelatase which is involved in heme biosynthesis.	

Group 1 is comprised of JAK1/2 inhibitors and bromodomain-containing protein 4 (BRD4) inhibitors, which reduced Kyn levels by downregulating IFNγ-mediated IDO1 expression in BxPC3 cells. The JAK1/2 inhibitor ruxolitinib was selected as representative compound to analyze the influence of JAK1/2 inhibition (Figure 5.17A) on IDO1 expression. Ruxolitinib potently inhibited IDO1 promoter activity in a dose dependent manner. In line with this, IDO1 mRNA levels are significantly reduced by 2 µM of the JAK1/2 inhibitor leading to reduced IDO1 protein levels (Figure 5.17C-E).
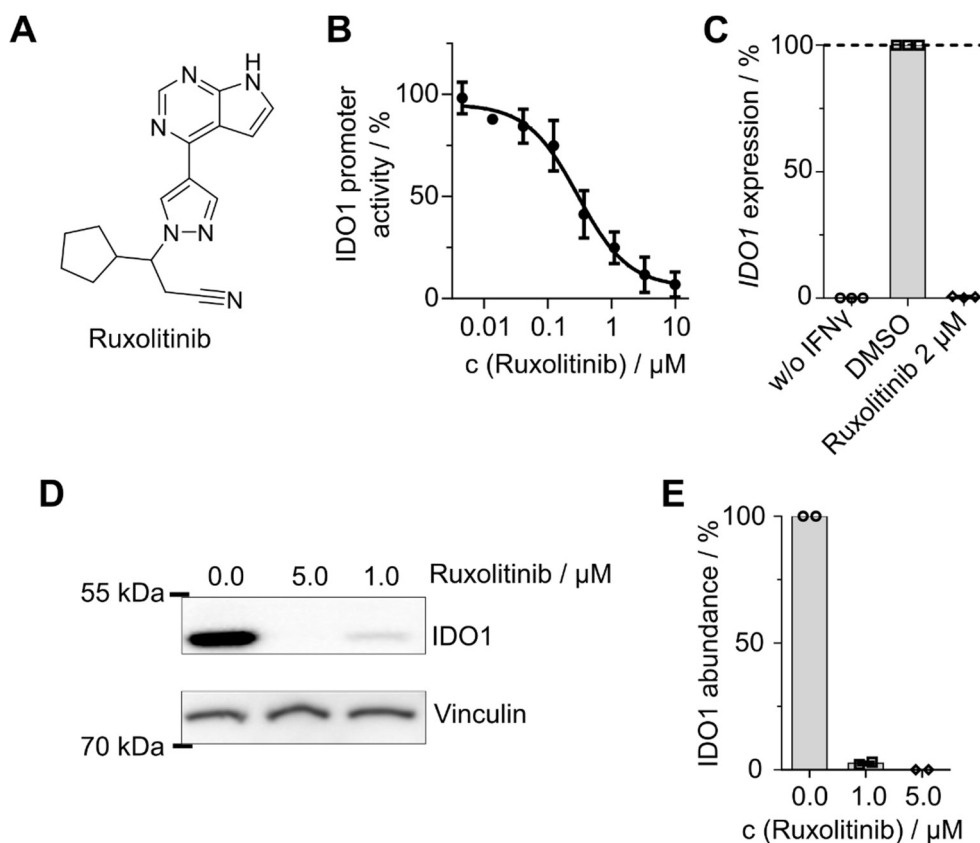
Figure 5.17: **JAK1/2 inhibitor ruxolitinib reduces IDO1 expression and thus diminishes cellular Kyn levels.**
A) Chemical structure of the JAK1/2 inhibitor ruxolitinib. B) IDO1 promoter reporter gene assay in HEK293T cells transiently transfected with a firefly luciferase construct under the control of the IDO1 promoter and a plasmid for constitutive *Renilla* luciferase expression upon treatment with IFNγ and ruxolitinib or IFNγ and DMSO for 24 h. The experiment was performed by Lara Dötsch. C) IDO1 mRNA level in BxPC3 cells treated with IFNγ and 2 µM ruxolitinib or DMSO for 24 h. Expression levels are determined using RT-qPCR. Data are mean values ± SD, n=3. D) Analysis of IDO1 expression in BxPC3 cells upon stimulation with IFNγ and ruxolitinib treatment at indicated concentrations for 24 h. Representative immunoblots for IDO1 and vinculin as a loading control. E) Normalized data of IDO1 abundance from D. Data are mean values ± SD, n=2.

The second group of hit compounds were inhibitors of cellular heme synthesis, namely succinylacetone and N-methyl protoporphyrin IX (Table 4). Heme is a cofactor that binds to IDO1 and is essential for IDO1 catalytic activity. Thus, decrease in cellular heme levels impairs

IDO1 activity (Table 4).[111, 112] Both compounds were validated as heme synthesis inhibitors as hemin cofactor supplementation completely abolished the inhibitory effect of both, succinylacetone and 1-NMPP (Figure 5.18C, D).
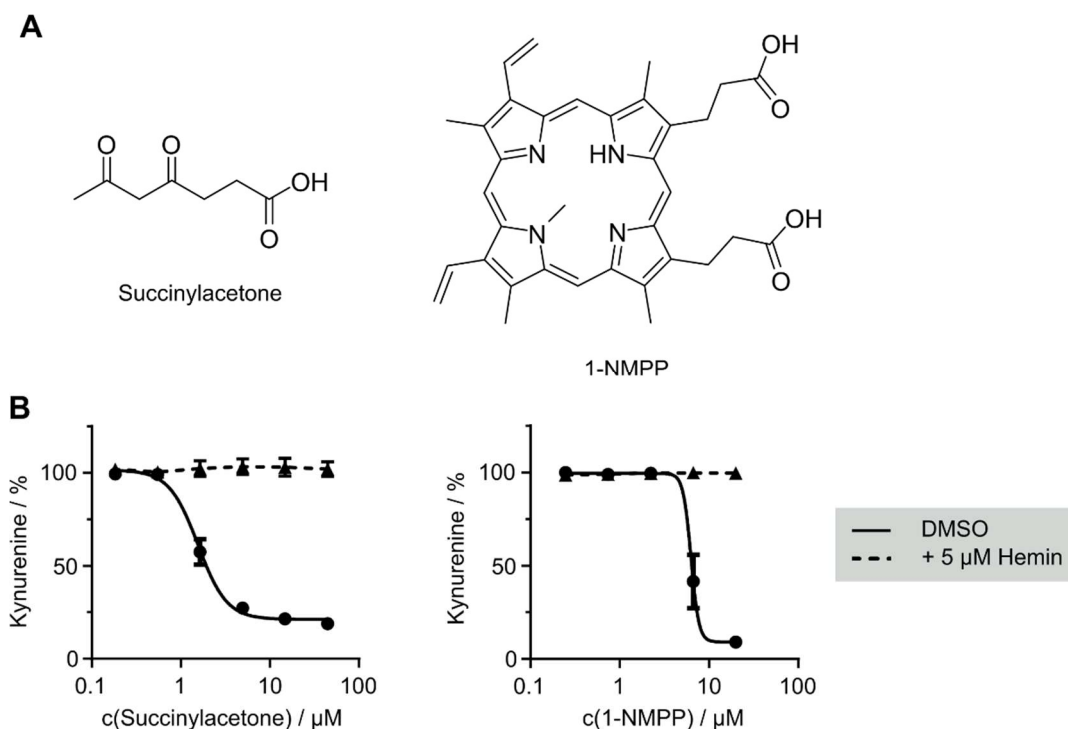
Figure 5.18: **Reduction of cellular Kyn levels by heme synthesis inhibitors is reversed by addition of hemin.** A) Chemical structures of succinylacetone and 1-NMPP. B) BxPC3 cells were treated with IFNγ, L-Trp and compounds for 48 h prior to Kyn level detection using *p*-DMAB. Data are mean vales ± SD, n = 3.

Additionally, several uncharacterized compound classes potently inhibited Kyn production. Of those, four hit compounds were selected for further MoA studies. On the one hand, the three most potent hit compounds in the screen, which inhibited IDO1 enzymatic activity, were chosen to be investigated in more detail. These are the thiohydantoin-based inhibitor **9** (IC_{50} = 6.3 ± 2.2 nM), the oxazole-4-carboxamide-based inhibitor **10** (IC_{50} = 4.8 ± 1.2 nM) and the piperazin-2-one-based inhibitor **11** (IC_{50} = 29.8 ± 13 nM, Figure 5.19A and B, see Figure S1 for further derivatives). On the other hand, hit compound **12** (IC_{50} = 0.83 ± 0.31 µM, Figure 5.19A and B) was selected for in-depth studies as it did not inhibit IDO1 enzymatic function and also because it is part of the department's in-house library and originated from a NP-inspired synthesis and, thus, has a unique structure.
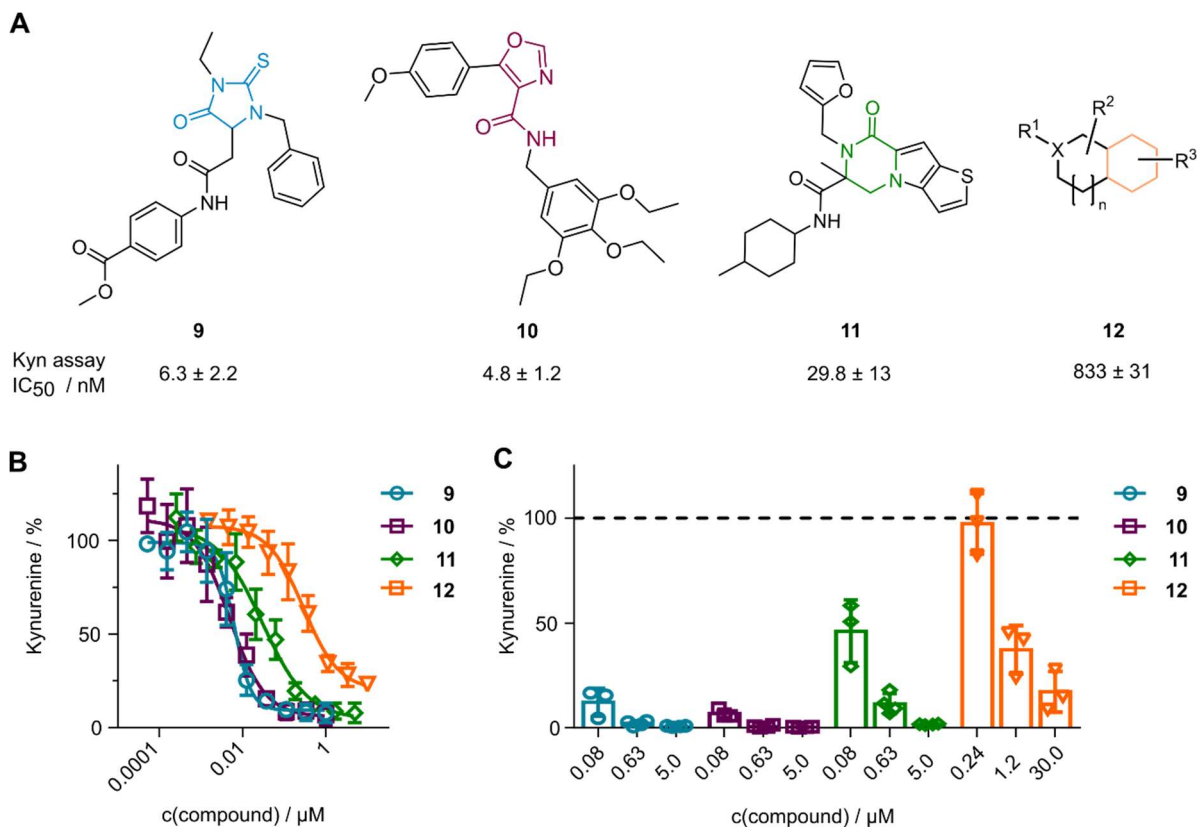
Figure 5.19: **Decrease of cellular Kyn production by identified hit compounds.** A) Structures of hit compounds **9**, **10**, **11** and **12** together with $IC_{50} \pm$ SD values in Kyn assay. B) Kyn assay using **6** in BxPC3 cells treated with the respective compounds for 48 h. C) Detection of Kyn levels using LC-MS/MS. Cells were treated as described in B. Data are mean values $\pm$ S.D, n$\geq$3.

Before investigating the mechanism in more detail, the four compounds were validated manually in the Kyn assay as well as by LC-MS/MS analysis as orthogonal method. Together, Kyn level reduction was confirmed for all four hit compounds in BxPC3 cells (Figure 5.19C).

5.2.2 Novel apo-IDO1 inhibitors

To investigate compounds **9**, **10** and **11** in more detail, additional validation assays were performed. First, the dose-dependent effect of compounds **9**, **10** and **11** was evaluated using a *p*-DMAB-based Kyn assay in BxPC3 cells and the human ovarian carcinoma cell line SKOV3 upon stimulation with IFNγ.
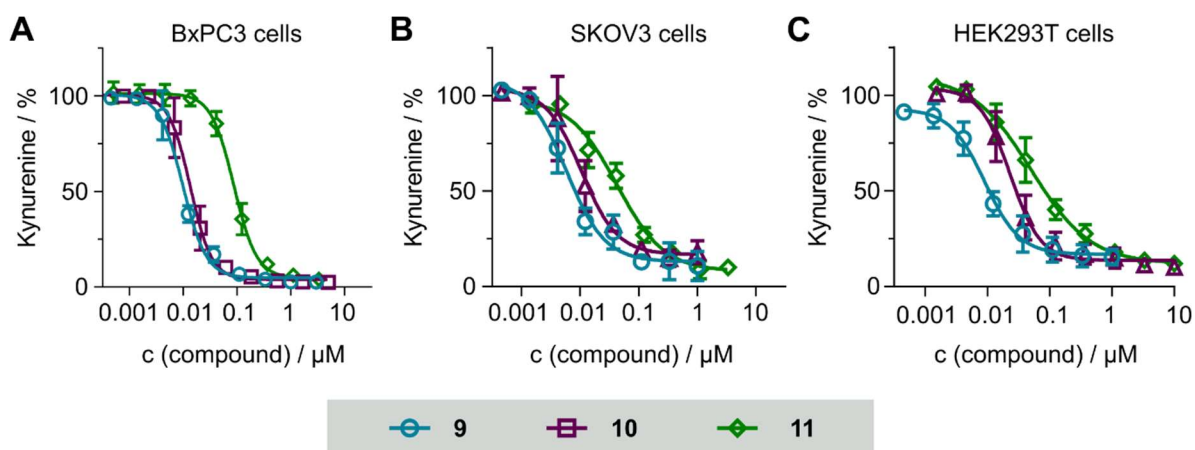
Figure 5.20: **Hit compounds inhibit cellular Kyn production.** A) Kyn assay in BxPC3 cells and B) in SKOV3 cells treated with IFNγ for 48 h prior to detection of Kyn levels using *p*-DMAB. C) Kyn assay in HEK293T cells that transiently express human IDO1 utilizing pCMV3-IDO1 plasmid. Compound addition was performed 24 h prior to Kyn levels determination using *p*-DMAB. Data are mean values ± SD, n=3.

As depicted in Figure 5.20A and B, Kyn levels decreased with increasing compound concentration confirming that compounds **9**, **10** and **11** are modulators of cellular IDO1 activity. Furthermore, the hit compounds were tested in HEK293T cells that transiently express human IDO1. IDO1 expression in HEK293T cells is independent of JAK/STAT signaling and, hence, allowed to discriminate between IDO1 expression inhibitors and IDO1 activity modulators. In line with the enzymatic inhibition of IDO1 observed for **9**, **10** and **11**, all three compounds induced a concentration-depended decline in Kyn levels in HEK293T cells (Figure 5.20C). The measured IC_{50} values of 9 ± 2.6 nM (**9**), 23 ± 5.4 nM (**10**) and 50 ± 9.8 nM (**11**) are in line with the ones detected in BxPC3 cells.

To explore the mechanism of IDO1 activity reduction of compounds **9**, **10** and **11**, enzymatic inhibition was further investigated. Compounds **9**, **10** or **11** (30 µM) were incubated with recombinant human IDO1 protein (rhIDO1, see 4.3.5.4) at different temperatures prior to the determination of IDO1 activity. Interestingly, pre-incubation of IDO1 with the compounds at 37 °C substantially decreased IDO1 activity while at 20 °C no changes of IDO1 activity occurred (Figure 5.21A). The same was observed for the heme-competitive apo-IDO1 inhibitor

BMS-986205.[34] In contrast, epacadostat, an L-Trp-competitive IDO1 binder[113], inhibited IDO1 activity after pre-incubation at both 37 °C and 20 °C (Figure 5.21A).
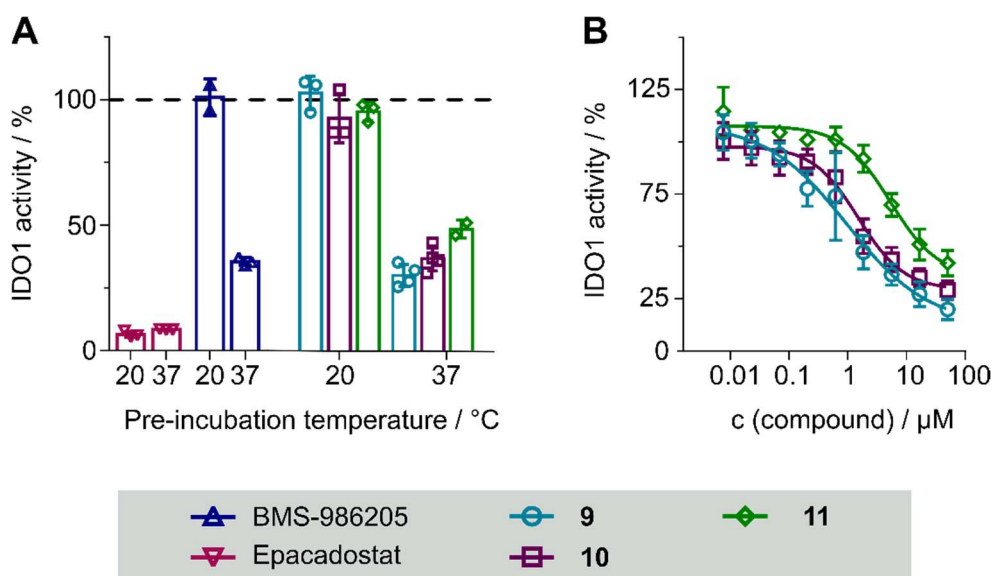
Figure 5.21: **Compounds 9, 10 and 11 target IDO1.** A) Influence of the pre-incubation temperature on IDO1 activity. IDO1 was incubated with **9**, **10** or **11** at 20°C or 37°C for 30 min prior to detection of Kyn levels using **6**. Epacadostat and BMS-986205 were used as controls. B) IDO1 enzymatic assay at 37°C. IDO1 was pre-incubated with the compounds at 37°C for 40 min prior to the detection of Kyn levels using *p*-DMAB. Data are mean values ± S.D., n ≥ 3.

As compounds **9**, **10** and **11** did not inhibit IDO1 when pre-incubated at 20 °C, IC_{50} values were determined after a pre-incubation with IDO1 at 37 °C. Thereby, IC_{50} values of 0.97 ± 0.59 µM (**9**), 1.52 ± 1.09 µM (**10**) and 5.28 ± 0.92 µM (**11**) were determined (Figure 5.21B). As **9**, **10** and **11** showed similar characteristics to BMS-986205 in terms of interfering with the enzymatic activity of IDO1, hit compounds **9**, **10** and **11** most likely inhibit IDO1 in a similar fashion as BMS-986205.

BMS-986205 is a heme-competitive inhibitor that binds to apo-IDO1. Apo-IDO1 is the immature form of IDO1 that lacks the cofactor heme (see 2.2.2). Upon incorporation of the heme cofactor, IDO1 is enzymatically active and hence in its mature form which is termed holo-IDO1.[34, 114] Heme-competitive inhibitors bind to the heme binding site and prevent heme incorporation, IDO1 maturation (= holo-IDO1 formation) as well as IDO1 enzymatic activity.

To confirm the direct binding of the compounds to IDO1, the influence of 9, 10 or 11 on the thermal stability of IDO1 was explored.
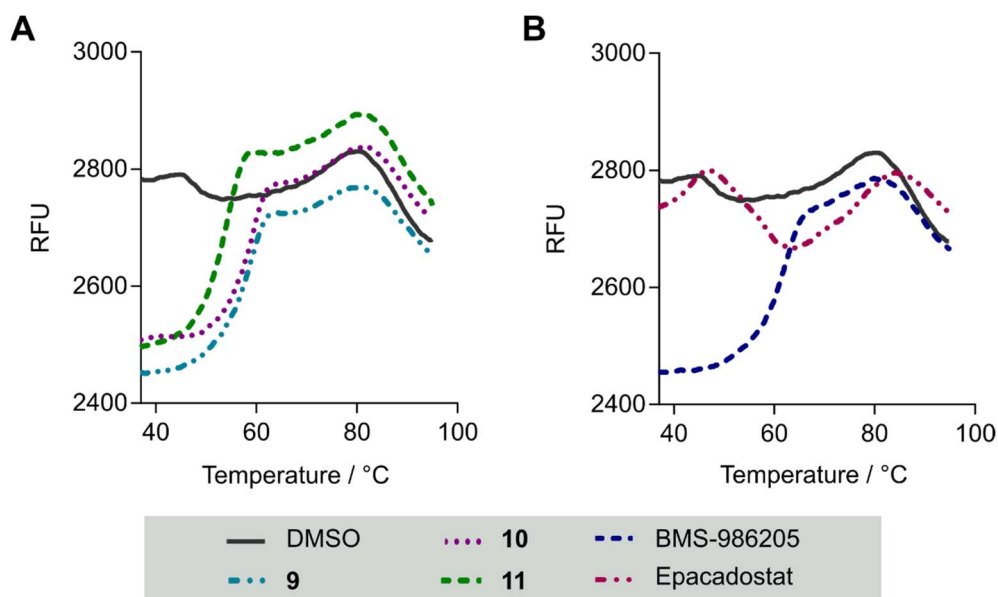
Figure 5.22: **Hit compounds bind to IDO1 and change the melting behavior of IDO1.** A) and B) IDO1 was pre-incubated with 30 µM of **9**, **10** or **11** (A) or 30 µM BMS-986205 or epacadostat (B) at 37 °C for 30 min prior to addition of SYPRO orange. Representative melting curves of IDO1 are shown, n = 3.

The melting behavior of IDO1 was monitored by means of differential scanning fluorimetry (DSF) and revealed that compound **9, 10** and **11** caused a distinct change in the melting curve compared to the DMSO control (Figure 5.22A) and the same was observed for BMS-986205 (Figure 5.22B). The melting curve of the IDO1 protein alone showed a biphasic shape with rather small changes in relative fluorescence within the curve course. However, the addition of **9, 10, 11** or BMS-986205 caused a considerable reduction in relative fluorescence at low temperatures and shifted the first melting peak of the biphasic curve substantially from 42.5 °C to 64.0 °C (**9**), 65.6 °C (**10**), 59.2 °C (**11**) or 66.6 °C (BMS-986205), respectively. Epacadostat did not affect the curve shape to the same extent, but led to a clear thermal stabilization of IDO1 with a shift in melting temperature of $\Delta T_m = 4.1 \pm 1.2$ °C considering the sharper, second melting peak (Figure 5.22B).

The high similarity of compound **9, 10** and **11** to BMS-986205 in this assay supports the assumption that the three compounds inhibit the enzymatic activity of IDO1 by binding to its apo-form, and thereby preventing heme incorporation, a mechanism analogous to BMS-986205.

To explore whether compound **9, 10** and **11** inhibit IDO1 enzymatic activity by heme displacement, the spectroscopic properties of IDO1 were analyzed in the presence of the compounds. Heme-containing IDO1 exhibits a characteristic absorbance peak between 400 and 410 nm depending on the protein buffer. This distinct peak is called ‚*Soret band*‘ and corresponds to the electronic state of the iron ion in the heme.[91, 92] Changes in the *Soret band* can be induced by protein-ligand interaction. Furthermore, the displacement of heme may be

reflected in an intensity decrease of the respective peak.
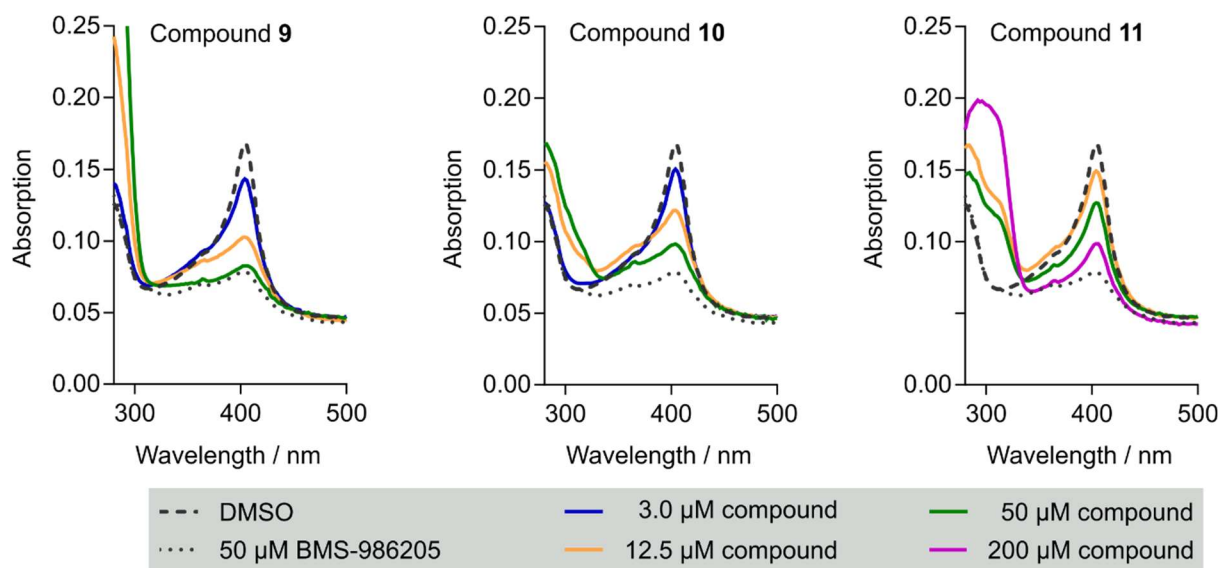
Figure 5.23: **Hit compounds affect the heme-binding properties of IDO1**. UV/Vis spectrum of IDO1. Human IDO1 was pre-incubated with test compounds at 37°C for 120 min prior detection of the UV/VIS spectrum. Representative spectrum (n=3).

To confirm this hypothesis, compound **9**, **10** or **11** were pre-incubated with IDO1 protein at 37 °C for 3 h to reach equilibrium. If **9**, **10** and **11** replaced the heme cofactor, the heme needs to dissociate from IDO1 before a small molecule can bind. It is known that the dissociation of heme from IDO1 is a slow process, hence the long incubation time.[62] The results of the UV/Vis spectral analysis in the presence of **9**, **10** or **11** are shown Figure 5.23. For all three compounds, a clear, concentration-depended reduction in the *Soret band* intensity indicated binding of the compounds to apo-IDO1. To confirm heme-competitive binding of **9**, **10** and **11** to IDO1, the enzymatic activity assay was repeated in the presence of 14 µM hemin. Indeed, the addition of hemin substantially reduced the inhibitory potency of **9**, **10** and **11** by at least 6.5-fold (Figure 5.24). The respective IC_{50} values increased from 0.97 ± 0.59 µM to 8.2 ± 1.4 µM (**9**), from 1.52 ± 1.09 µM to 9.7 ± 0.5 µM (**10**), and from 5.28 ± 0.92 to > 30 µM (**11**) in the presence of 14 µM hemin (Figure 5.24).
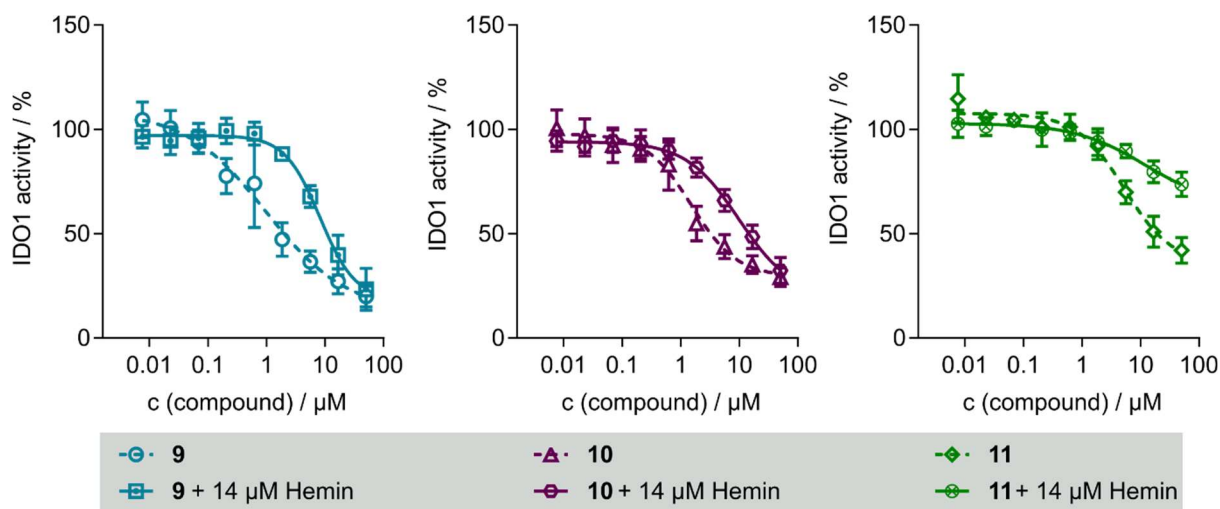
Figure 5.24: **Hit compounds 9, 10 and 11 bind to the heme pocket of IDO1.** Human IDO1 was pre-incubated with the compounds or the compounds and 14 µM hemin at 37°C for 40 min prior to detection of Kyn levels using *p*-DMAB. All data are mean values ± S.D, n ≥ 3.

Taken together, this data strongly suggest that the identified hit compounds **9**, **10** and **11** reduce cellular Kyn levels by binding to apo-IDO1 into the same pocket as the heme co-factor and, thereby, inhibiting the enzymatic activity of IDO1.

5.2.3 Small molecule degrader of IDO1

5.2.3.1 Biological characterization of the small molecule

Besides the investigation of the three novel IDO1 inhibitors, also hit compound **12** was of particular interest as it did not inhibit the enzymatic activity of IDO1, as depicted in Figure 5.25A. Hence, **12** acts as an indirect IDO1 modulator whose MoA was to be elucidated. First, the reduction of cellular Kyn levels by **12** was further validated in BxPC3 cells and SKOV3 cells.
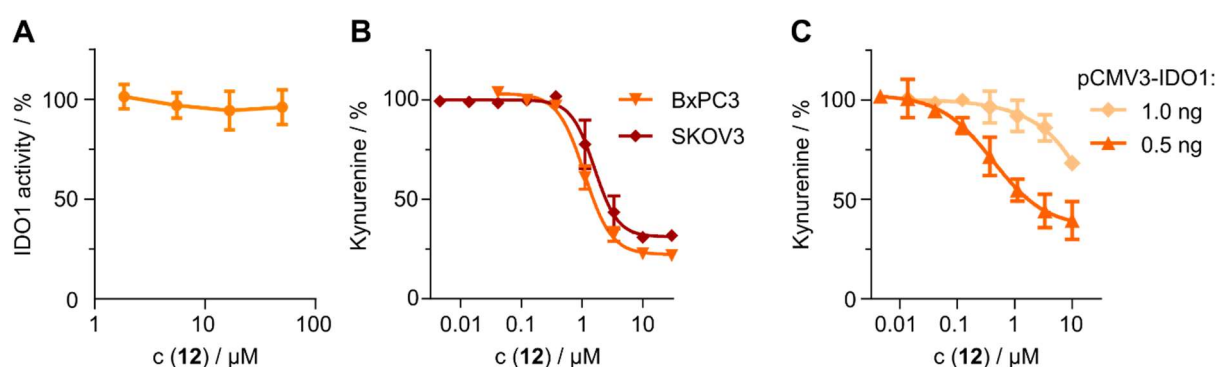
Figure 5.25: **Compound 12 decreases cellular Kyn levels without affecting the enzymatic activity of IDO1.** A) IDO1 enzymatic assay. IDO1 was pre-incubated with the compound at 37°C for 40 min prior to the detection of Kyn levels using *p*-DMAB. B) Kyn assay in different cell lines. BxPC3 and SKOV3 cells were treated with compound **12** and 50 or 5 ng/mL IFNγ, respectively, for 48 h prior to detection of Kyn levels utilizing *p*-DMAB. C) HEK293T cells were transiently transfected with pCMV3-IDO1 24 h prior to compound addition. Another 24 h later, Kyn levels were detected utilizing *p*-DMAB (experiments utilizing 1 ng pCMV3-IDO1 were performed by Lara Dötsch). Data were normalized to DMSO and all data are mean values ± S.D., n = 3.

A dose-dependent inhibition of cellular Kyn production was detected for both, BxPC3 and SKOV3 cells upon stimulation with IFNγ (Figure 5.25B). An IC_{50} value of 1.1 ± 0.13 µM was determined in BxPC3 and is in good agreement with the results from the automated assay (IC_{50} = 0.83 ± 0.31 µM). A similar IC_{50} value of 1.6 ± 0.32 µM was determined in SKOV3 cells. Furthermore, **12** was tested in HEK293T cells that transiently express human IDO1 independently of IFNγ. Interestingly, compound **12** reduces Kyn levels by only 30 % at 10 µM in cells transfected with 1 ng of the IDO1 expression plasmid as depicted in Figure 5.25C. In contrast, lowering the amount of the IDO1 expression plasmid by half, **12** inhibited cellular Kyn production dose-dependently with an IC_{50} of 0.42 ± 0.2 µM (Figure 5.25C). However, Kyn levels were solely downregulated to 39 ± 7.8 % at 10 µM whereas in BxPC3 cells Kyn levels were reduced to 22 ± 2.4 % at 10 µM. Transient IDO1 expression in HEK239T cells affected the potency of compound **12** strongly, which was not observed for direct IDO1 inhibitors (Figure 5.20). Nonetheless, **12** inhibited cellular Kyn production in HEK293T cells that express IDO1 independently of JAK/STAT signaling. Compounds, which interfere with the signaling

pathway inducing IDO1 expression, would not influence Kyn levels in HEK239T cells as they express IDO1 independently of IFNγ. Hence, **12** may not modulate the JAK/STAT signaling. However, the observed changes indicated IDO1 expression levels as a critical parameter that influences the potency of compound **12**.

Subsequently, the influence of **12** on IDO1 protein abundance was examined in BxPC3 cells upon stimulation with IFNγ. As shown in Figure 5.26, IDO1 protein levels were reduced by compound **12** concentration dependently to 55 % at 10 μM (D_{max} = 45 %) after 24 h with a half-maximal degrading concentration (DC_{50}) of 0.36 ± 0.23 μM.
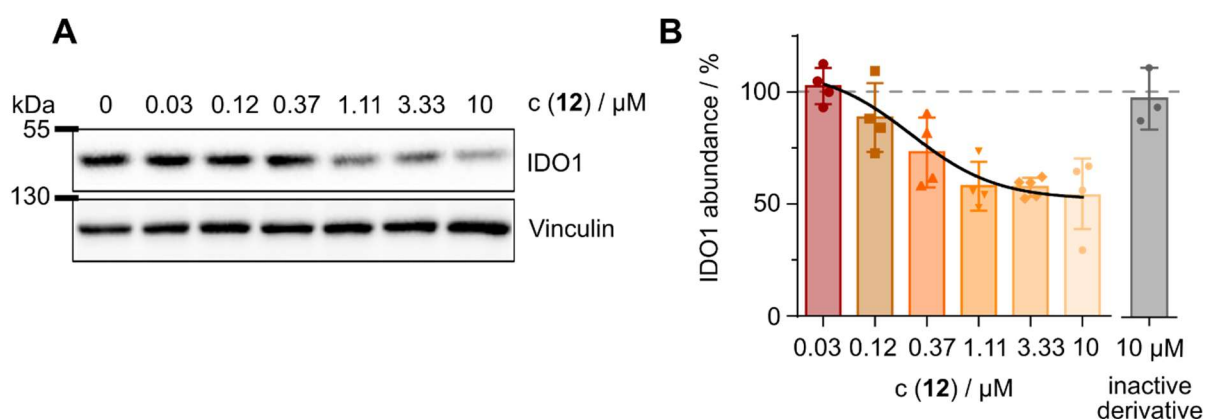
Figure 5.26: **Compound 12 reduces IDO1 protein levels.** A) Analysis of IDO1 expression in BxPC3 cells upon stimulation with IFNγ and treatment with **12** at the indicated concentrations for 24 h. Representative immunoblot for IDO1 and vinculin as a loading control. B) Normalized data of quantified band intensities from (A) and of a derivate of **12** that was inactive in the Kyn assay (inactive derivative). Data are mean values ± S.D., n = 3.

A derivate of **12** that was inactive in the Kyn assay (inactive derivative, Figure 5.26B) did not affect IDO1 protein levels at a concentration of 10 μM (Figure 5.26B) suggesting that compound **12** reduces Kyn levels by lowering IDO1 protein abundance. In line with the partial inhibition in the Kyn assay, **12** caused an incomplete protein depletion.

In theory, a small molecule can reduce the abundance of a protein either by decreasing protein transcription or translation or enhancing its degradation.[115] To further investigate the MoA of compound **12**, first *IDO1* transcription upon stimulation with IFNγ was studied in BxPC3 cells by means of RT-qPCR. Compound **12** did not lower *IDO1* mRNA levels (Figure 5.27A).These results suggest a MoA independent of JAK/STAT signaling, which is in line with the results obtained in HEK239T cells (Figure 5.25C). Next, global protein translation in cells in presence of **12** was investigated by utilizing the non-canonical amino acid analog of methionine, L-homopropargylglycine (HPG).[116] After incorporation into newly synthesized proteins, HPG can be fluorescently tagged by means of a click reaction and facilitates the quantification of translation. Cycloheximide (CHX), an inhibitor of protein translation that binds to the 60S ribosomal unit[117], was used as a control.
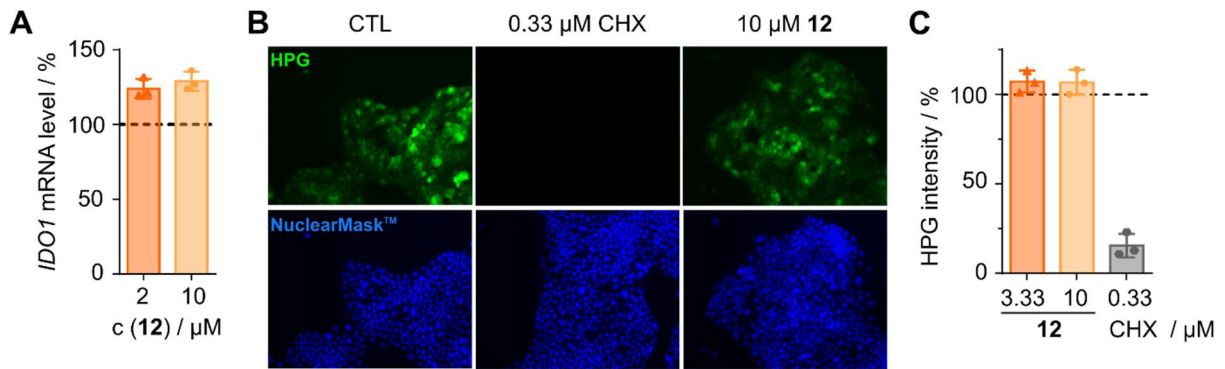
Figure 5.27: **Protein transcription and translation is not reduced by compound 12.** A) mRNA expression level of IDO1 in BxPC3 cells treated with IFNγ and **12** for 24 h. Expression levels were determined using RT-qPCR. Data are mean values ± SD, n=3. B) Analysis of global protein translation in cells 24 h after compound treatment by means of HPG detection. Representative images of HPG intensities displaying protein translation (green) and nuclear stain (blue) as a control. C) Normalized data of HPG signal intensities of the images in (B). Data are mean values ± S.D., n = 3.

CHX strongly suppressed protein translation in cells reflected by the absence of HPG fluorescence. In contrast, **12** did not inhibit HPG incorporation and, thus, global protein translation was not impacted by the hit compound (Figure 5.27B and C). To ensure that IDO1-specific protein translation was neither diminished by **12**, an *in vitro* translation assay utilizing *IDO1* mRNA was performed. IDO1 translation efficiency was not impacted by **12** at concentrations up to 50 µM as shown in Figure 5.27A and Figure 5.27B while CHX, as expected, significantly interfered with IDO1 translation.
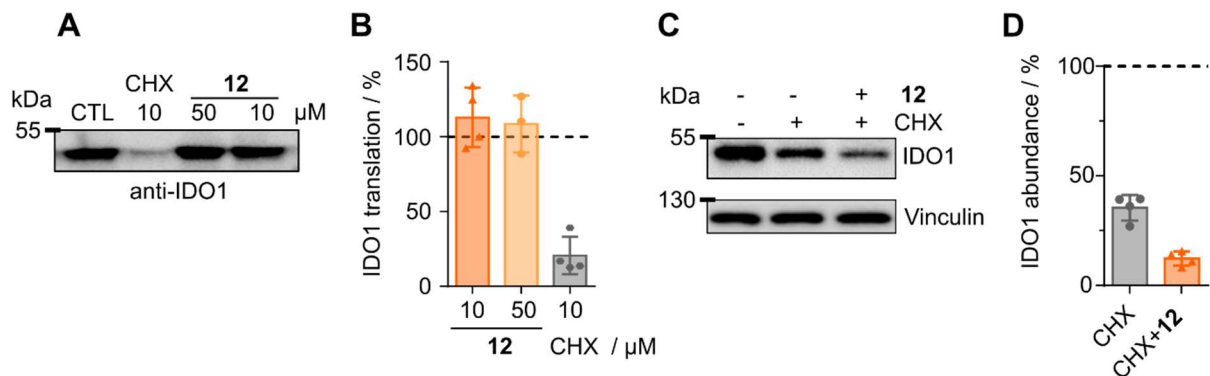
Figure 5.28: **IDO1 translation is not affected by compound 12.** A) and B) Analysis of IDO1 protein translation *in vitro*. *IDO1* mRNA translation was analyzed in cell lysates in the presence of **12**, CHX or DMSO as a control (CTL). Representative immunoblot for IDO1 protein (A) and quantified band intensities (B). C) CHX chase assay. BxPC3 cells were treated with 50 ng/mL IFNγ for 24 h prior to addition of 5 µM CHX or 5 µM CHX and 10 µM **12**. Representative immunoblot for IDO1 protein levels and vinculin as a control. D) Normalized data of quantified band intensities from (C). All data are mean values ± SD, n ≥ 3.

To determine the influence of **12** on IDO1 protein translation, a CHX chase assay was performed. IFNγ-stimulated BxPC3 cells were co-treated with CHX and **12** followed by IDO1

protein levels analysis. Co-treatment of CHX with compound **12** lowered IDO1 abundance even further compared to the treatment with the single agent CHX (Figure 5.28C and D). Considering that **12** did not inhibit the translation of IDO1 *in vitro* and IDO1 protein levels were further reduced in the presence of **12** together with the translation inhibitor (CHX) strongly indicates that the hit compound modulates IDO1 protein levels downstream of protein translation, e.g., by enhancing protein decay.

5.2.3.2 Investigation of IDO1 degradation induced by the small molecule

The majority of cytosolic proteins are degraded by the ubiquitin-proteasome-system (UPS). For this purpose, lysine residues of proteins are posttranslationally modified with polyubiquitin chains that tag them for proteasomal degradation.[118] As IDO1 is a cytosolic protein and gets degraded by the UPS, the compound may lower IDO1 levels by enhancing IDO1 polyubiquitination resulting in a higher rate of proteasomal IDO1 degradation.[119]

To test this hypothesis, a tandem ubiquitin binding entity (TUBE)-based pulldown was performed. TUBE proteins are artificial proteins containing domains that specifically bind polyubiquitin chains and can be used to enrich polyubiquitinated proteins from cell lysates.[120]
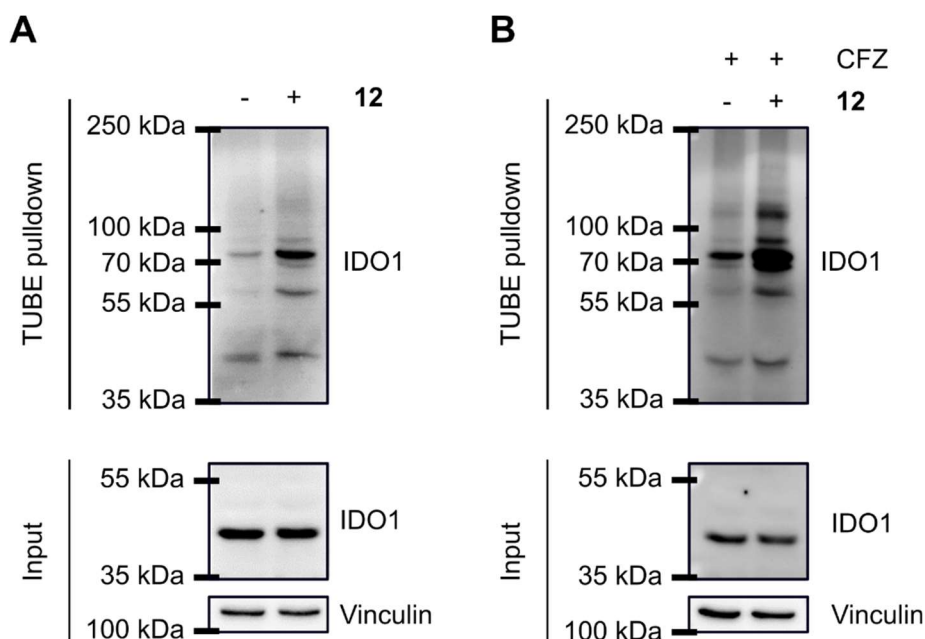
Figure 5.29: **IDO1 ubiquitination is enhanced in the presence of compound 12.** TUBE pulldown after treatment of IFNγ-stimulated BxPC3 cells with compound **12** or DMSO as a control. A) Cells were treated for 6 h with 50 μM **12** prior to lysate preparation and TUBE pulldown. B) Cells were first treated for 1 h with the proteasome inhibitor carfilzomib (CFZ, 450 nM) followed by 50 μM **12** for 4 h prior to lysate preparation and TUBE pulldown. Representative immunoblots for IDO1 and vinculin as a loading control (A and B), n=3.

Interestingly, treatment of IFNγ-stimulated BxPC3 cells for 6 h with **12** or DMSO as a control followed by a TUBE pulldown and IDO1 protein visualization revealed a clear increase in cellular IDO1 polyubiquitination in the presence of **12** compared to the control (Figure 5.29A). IDO1 specific bands with elevated intensities were observed at the height of 60 kDa and 80 kDa (Figure 5.29A). Monomeric ubiquitin (Ub) and IDO1 have molecular weights of 8.5 and 45 kDa, respectively. Accordingly, the band at 60 kDa may show IDO1 conjugated with two Ub molecules while 80 kDa might display IDO1 modified with a polyubiquitin chain of four to five Ub molecules. Moreover, a strong accumulation of polyubiquitinated IDO1 species was detected upon co-treatment of **12** with carfilzomib (CFZ) (Figure 5.29B). CFZ is an inhibitor of the proteasome and immunoproteasome and prevents the degradation of polyubiquitinated proteins.[121] Consequently, polyubiquitinated proteins accumulate in cells which was reflected by the TUBE pulldown for IDO1 in the presence of CFZ (Figure 5.29B). Polyubiquitinated IDO1 species were increased not only in cells treated with **12**, also for the cells treated with CFZ alone (Figure 5.29A). These observations suggest that **12** lowers cellular IDO1 protein levels by enhancing its polyubiquitination which leads to its increased proteasomal degradation.

However, sharp bands after a TUBE pulldown that can be ascribed to the conjugation of a specific length of polyubiquitin chains on a protein, as illustrated in Figure 5.29, is non-typical for polyubiquitinated proteins. Usually, a high molecular weight smear is detected for the protein of interest that represents various lengths of polyubiquitin chains.[122]

To confirm that the observed bands represent polyubiquitinated IDO1, a deubiquitinating enzyme (USP2) was exploited. USP2 removes polyubiquitin chains from proteins. Accordingly, the addition of USP2 to cell lysate treated with **12** should remove polyubiquitinated IDO1 species.

Therefore, IFNγ-stimulated BxPC3 cells were treated with **12** for 6 h and the obtained lysate was supplemented with USP2 prior to the TUBE pulldown. DTT and $ZnCl_2$ were essential for USP2 activity and, thus, added simultaneously.
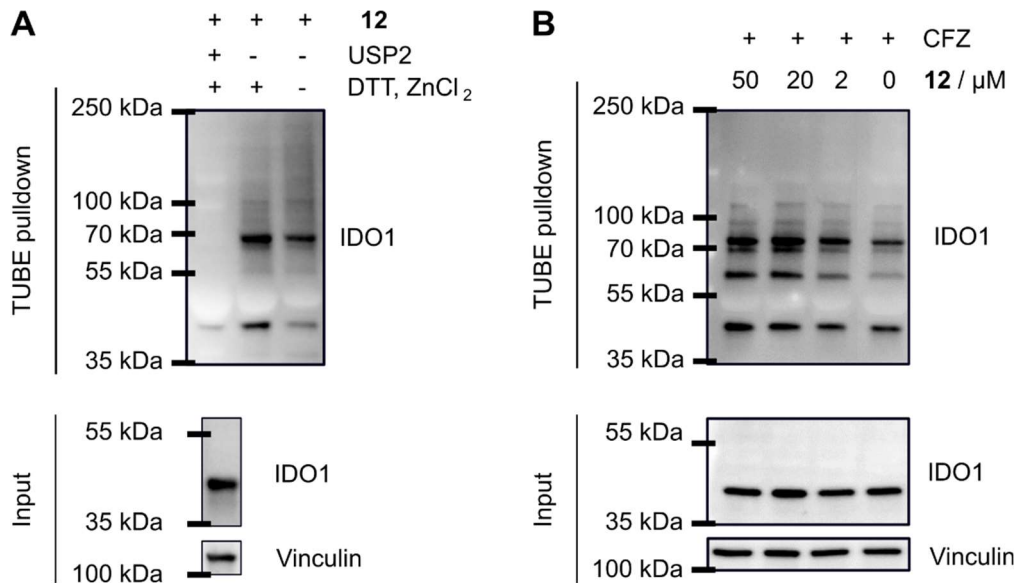
Figure 5.30: **12 induces polyubiquitination of IDO1**. A) Validation of IDO1 polyubiquitination bands by adding 5 µM USP2 prior to TUBE pulldown. IFNγ-stimulated BxPC3 cells were treated with **12** for 6 h. Lysates were supplemented with either buffer or DTT and ZnCl$_2$ or DTT, ZnCl$_2$ and USP2 and incubated for 40 min at room temperature. Afterwards, a TUBE pulldown was performed followed by immunoblotting. Representative immunoblot, n=3. B) IFNγ-stimulated BxPC3 cells were treated with 2, 20, 50 µM **12** or DMSO as a control for 2 h followed by lysate preparation and TUBE pulldown. Representative immunoblot, n=3.

The addition of USP2 abolished the detection of polyubiquitinated IDO1 as no IDO1-specific bands could be detected by immunoblotting anymore (Figure 5.30A). In contrast, the control conditions, in which the lysate was untreated, or supplemented with just DTT and ZnCl$_2$, still displayed IDO1-specific bands above 45 kDa. (Figure 5.30A). Consequently, the bands detected for IDO1 after the TUBE pulldown represent polyubiquitinated IDO1 protein. Moreover, small molecule-induced IDO1 polyubiquitination could also be detected already after shorter treatment times of 2 h and in a dose dependent manner(Figure 5.30B).

As **12** induces IDO1 polyubiquitination followed by its degradation, the small molecule was named iDeg-1 for **i**nduced I**D**O **deg**radation compound-**1**.

To determine which lysine of IDO1 is ubiquitinated and to find potential interaction partners, an IDO1 co-immunoprecipitation (Co-IP) experiment was performed and analyzed by means of mass spectrometry (MS). MS identifies proteins within a complex mixture by means of a peptide fingerprint. Protein samples that are subjected to an MS-based analysis are first digested by proteolytic enzymes such as trypsin. The derived peptides are then analyzed and assigned to the original protein. Additionally, a so-called diglycine (diGly) analysis was performed to detect protein ubiquitination on the primary amine of lysine side chains. After a tryptic digest, two glycines (=diGly) remain on the lysine (K) side chain that was ubiquitinated

before the digest and peptides that contain this characteristic diGly-modified lysine can be identified by an increase in mass.[123]
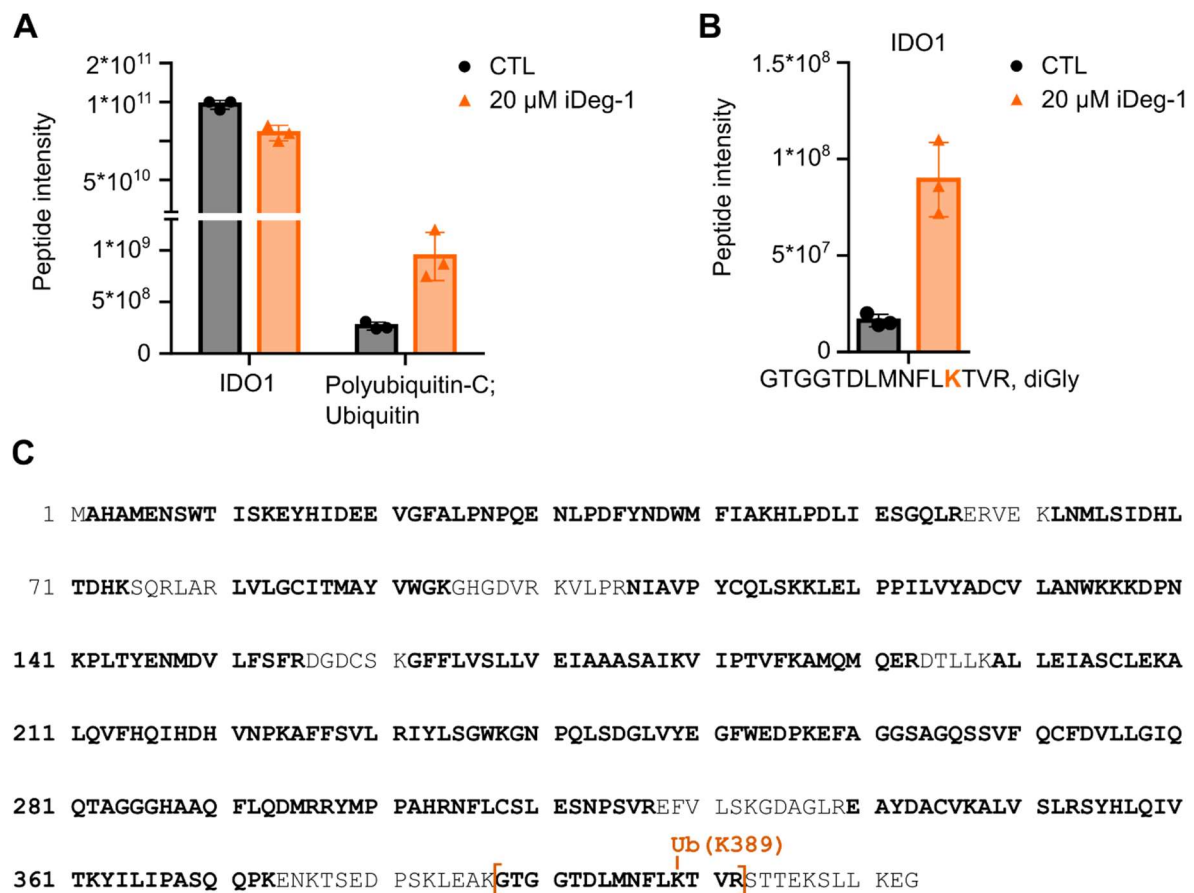

Figure 5.31: **iDeg-1 induces polyubiquitination of Lysine 389 of IDO1**. IFNγ-stimulated BxPC3 cells were treated with iDeg-1 or DMSO as a control (CTL) for 6 h prior to lysate preparation. IDO1 was immunoprecipitated and the enriched fraction was digested and analyzed by MS. A) Measured relative peptide intensity for IDO1 and polyubiquitin-C. B) Identified peptide of IDO1 with diGly modification. C) IDO1 protein sequence. Amino acids in bold illustrate regions identified using MS. K389, the identified ubiquitination site of IDO1, is highlighted in orange. Data are mean values ± SD, n=3.

IFNγ-stimulated BxPC3 cells were treated with iDeg-1 or DMSO as a control for 6 h prior to IDO1 immunoprecipitation. MS-based analysis of the Co-IP samples identified IDO1 with high intensity in both samples as depicted in Figure 5.31. Interestingly, cells treated with 20 µM iDeg-1 showed a 3.5-fold increase in polyubiquitin-C compared to the control sample which confirmed that iDeg-1 induces IDO1 ubiquitination. A diGly analysis revealed that IDO1 is ubiquitinated at the lysine residue K389. The intensity of the diGly modified peptide containing K389 was elevated by 5.5-fold in the presence of iDeg-1 compared to the control samples (Figure 5.31B). As after MS analysis the sequence coverage of IDO1 was 78 %, not every lysine within IDO1 was identified. In total, 20 lysines were identified while 10 lysines were within the undetected sequence area (Figure 5.31C). Ubiquitination on those undetected

lysines might additionally be possible. Besides, a diGly analysis was also performed for peptides originating from polyubiquitin-C (Figure 5.32).

Figure 5.32: **Polyubiquitin chains are connected by lysine 48 of Ub monomers.** IFNγ-stimulated BxPC3 cells were treated with iDeg-1 for 6 h prior to lysate preparation. IDO1 was immunoprecipitated and the enriched fraction was digested and analyzed by MS. A) Identified peptide of ubiquitin with diGly modification. B) Ub protein sequence. The bold letters illustrate identified regions while the other regions could not be identified. K48, the identified ubiquitination site of Ub, is highlighted in orange. Data are mean values ± SD, n=3.

For polyubiquitin-C, a diGly modification was detected at K48 which was substantially increased in the presence of iDeg-1 (Figure 5.32A). K48 connected ubiquitin chains are associated with protein degradation via the UPS.[83] This is in line with the previous observation that a co-treatment with iDeg-1 and CFZ led to an accumulation of polyubiquitinated IDO1 species in cells. (Figure 5.29). Of note, the sequence coverage for ubiquitin was with 44.7 % relatively low and K6, K11, K29 and K33 could not be identified. These lysine residues are also known to be involved in ubiquitin chain branching.[124] Thus, the diGly analysis of polyubiquitin-C is not comprehensive and a complete prediction of the branching of the polyubiquitin chains attached to IDO1 cannot be derived from the obtained data.
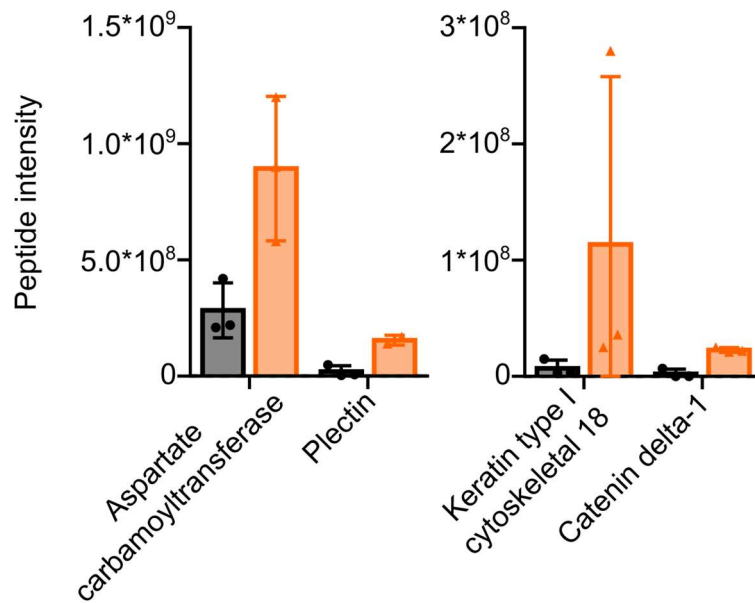
Figure 5.33: **Proteins that are enriched by co-immunoprecipitation display no link to the UPS.** IFNγ-stimulated BxPC3 cells were treated with iDeg-1 for 6 h prior to lysate preparation. IDO1 was immunoprecipitated and the enriched fraction was digested and analyzed by MS. Data are mean values ± SD, n=3.

Apart from polyubiquitin-C, the IDO1 Co-IP experiment did not revealed any other protein which is related to the UPS or protein degradation, like an E3 ubiquitin ligase (Figure 5.33). none of the four proteins which were enriched in the samples treated with iDeg-1 compared to the control samples are linked to protein degradation (Figure 5.33).

Together, the experimental data suggest that iDeg-1 induces ubiquitination and degradation of IDO1 which can be observed already after 2 h of compound treatment. Nontheless, changes in IDO1 protein levels by means of immunoblotting were only detectable after 24 h using IFNγ-stimulated BxPC3 cells. However, these cells continue to express IDO1 during the incubation time although IFNγ was removed after a pre-incubation of 16 h and was not present during compound treatment. Therefore, the effect of iDeg-1 on IDO1 protein levels is partly shielded by high IDO1 expression in BxPC3 cells. To focus exclusively on IDO1 degradation, recombinant human IDO1 (rhIDO1) was electroporated into HEK239T cells. As HEK293T cells do not express IDO1 constitutively, HEK239T-rhIDO1 cells can be used to investigate the changes in IDO1 protein levels that are only related to protein decay.

First, a cellular Kyn assay in HEK239T-rhIDO1 cells was performed to investigate the influence of iDeg-1 on rhIDO1 functionality.
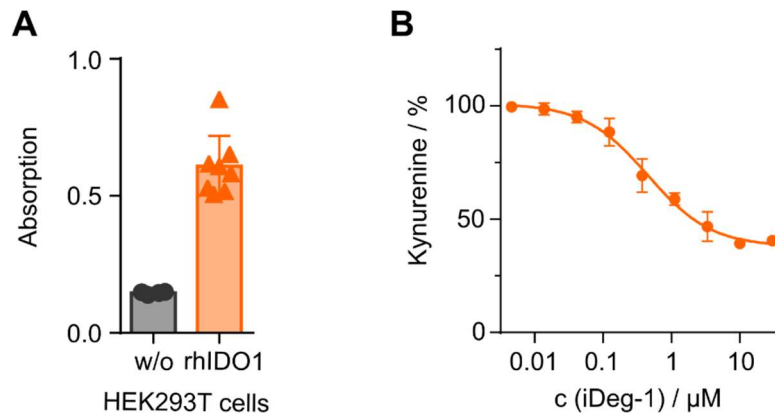
Figure 5.34: **iDeg-1 reduces Kyn levels in electroporated HEK293T cells.** HEK239T cells are electroporated with rhIDO1 protein and Kyn levels were detected by means of *p*-DMAB 24 h after treatment with 150 µM L-Trp and iDeg-1. A) Absorbance measurement of Kyn using *p*-DMAB in HEK239T cells electroporated with rhIDO1 compared to HEK293T cells without (w/o) rhIDO1. B) Dose dependent analysis of iDeg-1. Data are mean values ± SD, n=3.

The activity of electroporated IDO1 was determined using a Kyn assay which confirmed the introduced rhIDO1 into HEK293T cells as active (Figure 5.34A). iDeg-1 reduced cellular Kyn levels in HEK293T-rhIDO1 cells dose-dependently with an IC_{50} value of 0.45 ± 0.1 µM (Figure 5.34B) which is in agreement with the IC_{50} observed in HEK239T cells that transiently express IDO1 (IC_{50} = 0.42 ± 0.2 µM, Figure 5.25C).
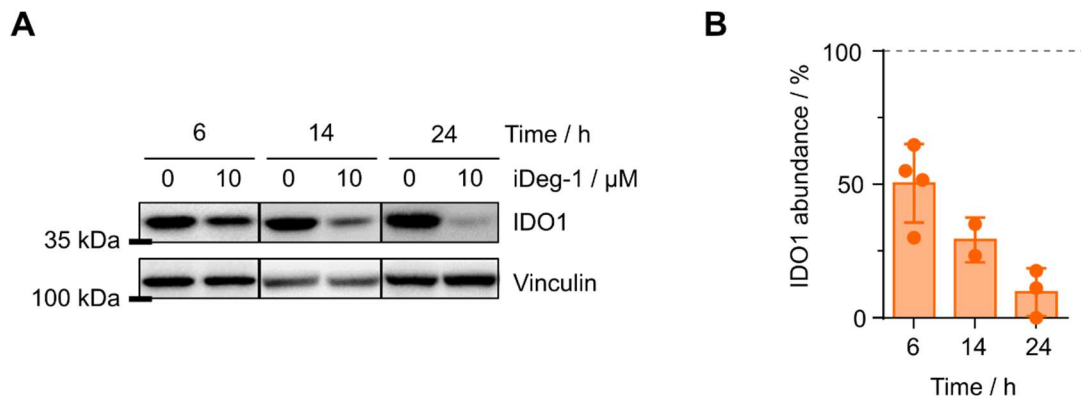
Figure 5.35: **IDO1 protein levels are erased over 24 h by iDeg-1**. HEK239T cells are electroporated with rhIDO1 protein followed by the treatment with iDeg-1 for 6, 14 or 24 h. A) IDO1 protein levels were determined via immunoblotting. Representative immunoblots for IDO1 and vinculin as a control. B) Normalized data from quantified band intensities from B. Data are mean values ± SD, n≥2.

Moreover, iDeg-1 treated HEK239T-rhIDO1 cells showed a clear reduction in IDO1 protein levels of approximately 50 % already after 6 h and protein levels decreased even further after 14 h and 24 h (Figure 5.35A and B). Hence, IDO1 protein levels could be reduced by 90 % after 24 h in HEK293T-rhIDO1 cells while in IFNγ-stimulated BxPC3 cells a D_{max} of 45 % was detected (Figure 5.26).

To identify the IDO1 degradation pathway induced by iDeg-1, HEK239T cells were electroporated with rhIDO1 and co-treated with either iDeg-1 and CFZ or iDeg-1 and MLN4924. MLN4924 is an inhibitor of the NEDD8-activating enzyme (NAE) that is essential for the posttranslational modification (PTM) of proteins with NEDD8, also known as neddylation.[125] NEDD8 conjugation is crucial for the enzymatic function of cullin-RING E3 ligases (CRLs) which are key enzymes in protein degradation. CRLs are multi-subunit protein complexes that transfer ubiquitin onto proteins and thereby assign them for proteasomal degradation. Inhibition of neddylation decreases the activity of CRLs and thereby interferes with protein ubiquitination and subsequent degradation of the respective target proteins.[125, 126] In contrast to MLN4924, the proteasome inhibitor CFZ interferes with the degradation of proteins that are already polyubiquitinated.[121] Both, the TUBE pulldown and IDO1 immunoprecipitation experiments suggest that the iDeg-1-induced IDO1 degradation is UPS-dependent.
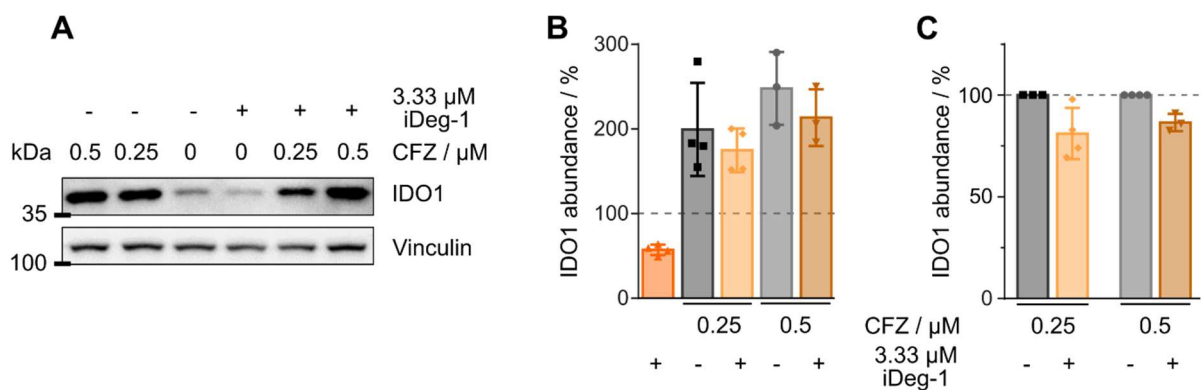
Figure 5.36: **iDeg-1 induces IDO1 degradation via the UPS**. HEK239T cells were electroporated with rhIDO1 protein. A pre-treatment with CFZ was performed for 30 min prior to the addition of 3.33 µM iDeg-1 for further 6 h followed by immunoblotting. A) Representative immunoblot for IDO1 and vinculin as a control. B) Normalized data quantified band intensities from of (A) relative to DMSO as control. C) Normalized data of quantified band intensities from (A) relative to the treatment of CFZ alone. Data are mean values ± SD, n = 3.

Experiments performed with HEK239T-rhIDO1 cells treated with the proteasome inhibitor CFZ revealed diverse aspects about IDO1 degradation. Interestingly, in the presence of CFZ alone, IDO1 protein levels were increased by 2- to 2.5-fold compared to the control (Figure 5.36A and B). Cells that were co-treated with iDeg-1 and CFZ still showed elevated IDO1 protein levels of up to 200 % of the control sample (Figure 5.36A and B). Hence, the efficiency of iDeg-1 to reduce IDO1 was clearly abolished by the addition of CFZ (Figure 5.36C). iDeg-1 alone reduced IDO1 protein levels by 40 % (Figure 5.36), while in the presence of 0.25 or 0.5 µM CFZ a reduction of only 23 % or 10 %, respectively, was detected (Figure 5.36C). Conclusively, iDeg-1-induced IDO1 degradation is mediated by the UPS.

The same experiments were performed with MLN4924 instead of CFZ. MLN4924 treatment alone also increased IDO1 protein levels compared to control condition by approximately 2-fold (Figure 5.37A and B) analogous to the treatment with CFZ alone (Figure 5.36). Together, these findings demonstrate that physiologically IDO1 is degraded via a neddylation-dependent E3 ligase and the UPS.
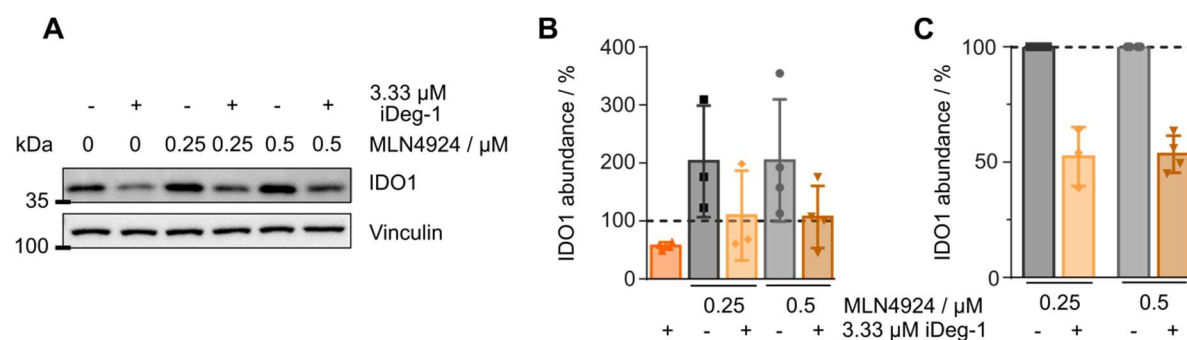

Figure 5.37: **iDeg-1-induced IDO1 degradation is neddylation independent.** HEK239T cells were electroporated with rhIDO1 protein. A pre-treatment with MLN4924 was performed for 30 min prior the addition of 3.33 µM iDeg-1 for further 6 h followed by immunoblotting. A) Representative immunoblot for IDO1 and vinculin as control. B) Normalized data of quantified band intensities (A) relative to DMSO as control. C) Normalized data of (A) relative to the treatment of MLN4924 alone. Data are mean values ± SD, n = 3.

However, co-treatment with the neddylation inhibitor and iDeg-1 could not diminish iDeg-1-induced degradation of IDO1 compared to the single treatments with MLN4924. Even in the presence of either 0.25 or 0.5 µM MLN4924, iDeg-1 reduced IDO1 protein levels by 48 % and 47 %, respectively (Figure 5.37B and C). Hence, iDeg-1-induced IDO1 degradation is neddylation independent and, thus, unrelated to IDO1's physiological degradation pathway which is neddylation dependent.

5.2.3.3 Interaction studies of IDO1 and the small molecule

To further investigate how degradation of IDO1 is induced by iDeg-1, the specificity of iDeg-1 for IDO1 was explored. For this, a proteome-wide study in HEK293T-rhIDO1 cells was performed after treatment with iDeg-1 for 6 h. A treatment for 6 h should ensure that observed alterations in protein levels are due to protein degradation or stabilization and not affected by changes in protein expression.

The proteome-wide analysis identified IDO1 as the only protein out of 2904 proteins whose abundance was significantly decreased after the treatment with 10 µM iDeg-1 compared to the control (Figure 5.38).
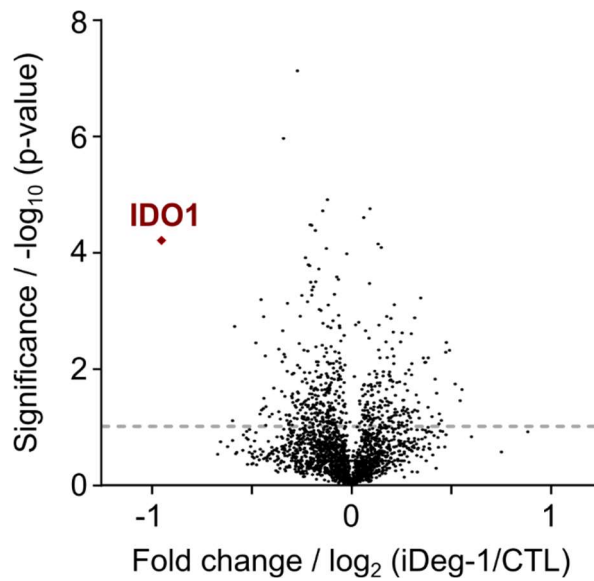
Figure 5.38: **Degradation of IDO1 by iDeg-1 is highly specific.** HEK239T cells were electroporated with rhIDO1 protein followed by the treatment with 10 µM iDeg-1 or DMSO as a control (CTL) for 6 h. Afterwards, cell lysates were generated and subjected to a trypic digest for MS analysis. Data are mean values ± SD, n=3.

These results strongly suggest that iDeg-1 may bind directly to IDO1 and thereby induce its ubiquitination and degradation because, if iDeg-1 would e.g. activate an E3 ligase without interacting with IDO1, also other proteins would be degraded to a higher extent. Similarly, if deubiquitination would be impeded by iDeg-1, this would not only effect IDO1.

To explore such potential interactions, the thermal stability of IDO1 was analyzed by means of nanoDSF, which detects the intrinsic tryptophan fluorescence of proteins. Tryptophan residues are highly sensitive to changes in their surroundings, such as thermal unfolding of proteins, which is reflected in the fluorescence intensity.[127]
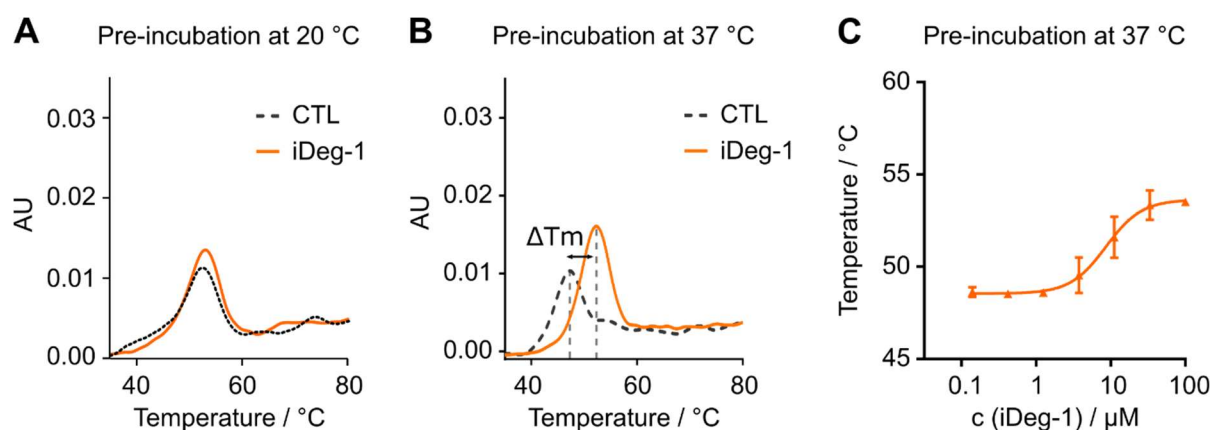
Figure 5.39: **iDeg-1 interacts directly with IDO1.** A) rhIDO1 treated with either 100 µM iDeg or DMSO as a control (CTL) for 90 min at room temperature prior to nanoDSF measurement. Representative curves, n=2. B) Analysis of rhIDO1 thermal stability in the presence of 100 µM iDeg-1 or DMSO as a control (CTL) utilizing nanoDSF. rhIDO1 and compounds were pre-incubated for 90 min at 37°C prior to the measurement. Representative result, n=3. C) Determination of the dissociation constant of iDeg-1 for IDO1 using nanoDSF. rhIDO1 and compounds were pre-incubated for 90 min at 37°C prior to the measurement. Data are mean values ± SD, n=3.

Interestingly, the melting behavior of IDO1 was not affected in the presence of iDeg-1 when IDO1 was pre-incubated with the compound at 20 °C compared to the control (Figure 5.39A). However, pre-incubating IDO1 with iDeg-1 or the control at 37 °C substantially increased in melting temperature of IDO1 by 4.9 ± 0.3 °C in the presence of iDeg-1 compared to the control condition (Figure 5.39B).

As deciphered in the course of the in-depth analysis of **9**, **10** and **11**, the dynamic binding of heme to IDO1 is highly temperature dependent. Only at higher temperatures, such as 37 °C, heme dissociation from IDO1 can be seen and small molecules binding to apo-IDO1 cannot interact with the enzyme at lower temperature, e.g., 20 °C. As the binding of iDeg-1 to IDO1 was only observed at 37 °C, it indicates that iDeg-1 binds to apo-IDO1.

IDO1 stabilization by iDeg-1 was also monitored dose-dependently using a pre-incubation temperature of 37 °C. Thereby, a dissociation constant (K_D) of 8.6 ± 2.96 µM was calculated for iDeg-1 (Figure 5.39C).

To investigate the interaction between iDeg-1 and IDO1 also in cells, cellular thermal shift assays (CETSA) were conducted *in the course of Lisa-Marie Pulvermacher's Master thesis*.
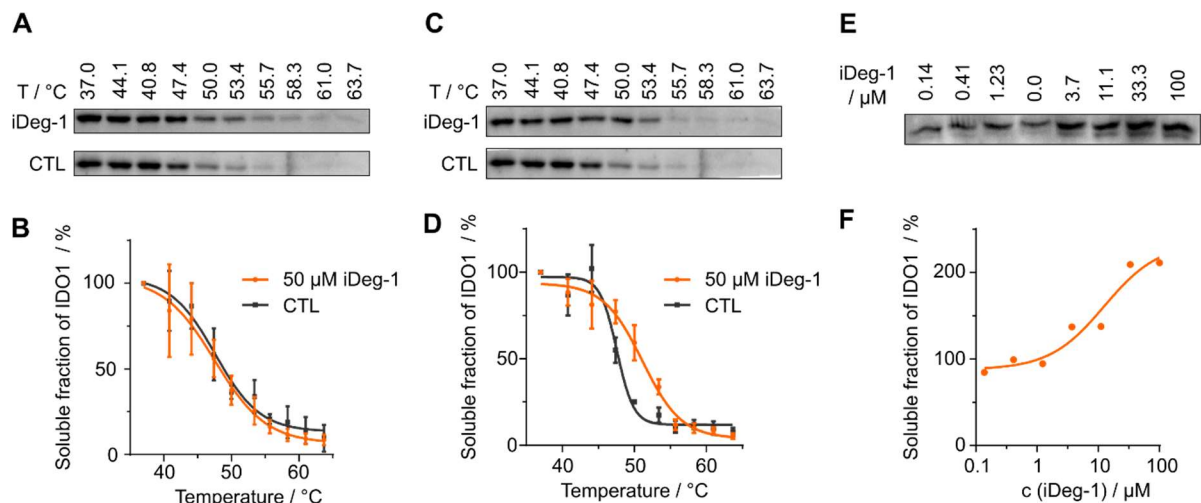
Figure 5.40: **Cellular thermal stability of IDO1 is increased by iDeg-1.** A) and B) CETSA in SKOV3 cell lysate treated with 50 µM iDeg-1 or DMSO as a control (CTL) for 15 min at room temperature prior to heat treatment. A) Representative immunoblot for IDO1. B) Quantification of band intensities from (A). Data are mean values ± SD, n=3. C) and D) CETSA in intact SKOV3 cells treated with iDeg-1 or DMSO as control for 1 h at 37°C at 5 % CO_2. C) Representative immunoblot for IDO1. D) Quantification of band intensities from (C). Data are mean values ± SD, n=3. E) and F) Isothermal shift assay at 50 °C. Representative immunoblot (E) and respective melting curve (F), n=3.

In line with the interaction studies conducted for rhIDO1, the thermal stability of IDO1 in cellular lysates was not altered by treatment with iDeg-1 and a pre-incubation step at room temperature prior heat treatment (Figure 5.40A). However, a thermal stabilization of IDO1 was observed in cells after iDeg-1 treatment. CETSA in SKOV3 cells that were treated with iDeg-1 for 1 h at 37 °C revealed a stabilization of IDO1 by ΔT_m 3.53 ± 0.4 °C compared to the control samples (Figure 5.40B). In addition, thermal stability of IDO1 was investigated in the presence of different iDeg-1 concentrations at 50 °C because at this temperature the stabilization of IDO1 by iDeg-1 was most pronounced (Figure 5.40D). In agreement, thermal stability of IDO1 increased concentration dependent. (Figure 5.40E and F).

Moreover, iDeg-1 was evaluated in the Kyn assay supplemented with additional hemin, the cofactor of IDO1 bound to an iron in its ferric state.
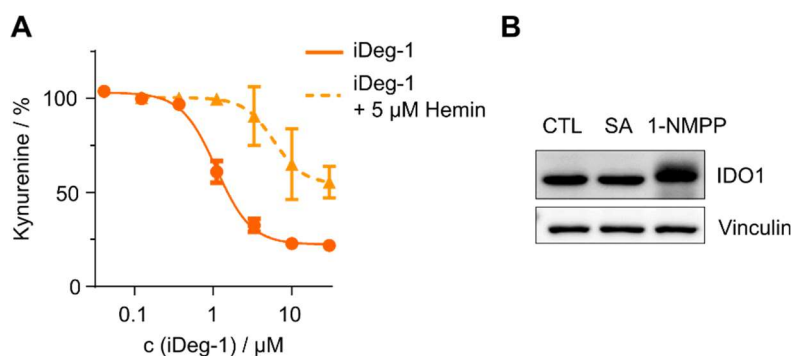

Figure 5.41: **Addition of heme, the cofactor of IDO1, reduces cellular potency of iDeg-1.** A) Kyn assay in BxPC3 cells for iDeg-1 in the presence or absence of 5 µM hemin. Data are mean values ± SD, n=3 B) Influence of heme synthesis inhibition on IDO1 protein levels. IFNγ -simulated BxPC3 cells were treated with 10 µM of the heme synthesis inhibitors succinylacetone (SA) or 1-NMPP for 24 h prior to IDO1 protein analysis. Representative immunoblot, n=2.

The potency of iDeg-1 in the Kyn assay was strongly reduced in the presence of hemin (Figure 5.41A). In case of the heme synthesis inhibitors, succinylacetone (SA) and 1-NMPP the addition of hemin completely abolished the inhibitory potency of the two, even at high concentrations (Figure 5.18). This was not the case for iDeg-1. Furthermore, neither SA nor 1-NMPP reduce IDO1 protein levels (Figure 5.41B). Hence, in presence of additional heme cofactor the interaction of iDeg-1 and IDO1, presumable apo-IDO1 might be impeded as the equilibrium might be shifted towards holo-IDO1.

This finding together with the observation that the incubation temperature of 37 °C was essential for IDO1 thermal stabilization by iDeg-1 indicate that iDeg-1 may bind to apo-IDO1 and thus induces ubiquitination and degradation. To prove apo-IDO1 binding, the UV/Vis spectrum of IDO1 after the incubation with iDeg-1 at 37°C was measured and revealed a slight reduction of the specific absorbance peak, i.e., the *Soret* band, of holo-IDO1. The optimized apo-IDO1 binder BMS-986205 reduced the characteristic absorbance peak of holo-IDO1 much stronger. However, BMS-986205 binds rapidly[34, 62] and with a high affinity (K_D of 164 nM, Figure 5.42) to IDO1 while iDeg-1 displayed only a K_D value of 8.6 ± 2.96 µM that might explain the smaller effect on the *Soret* band intensity.
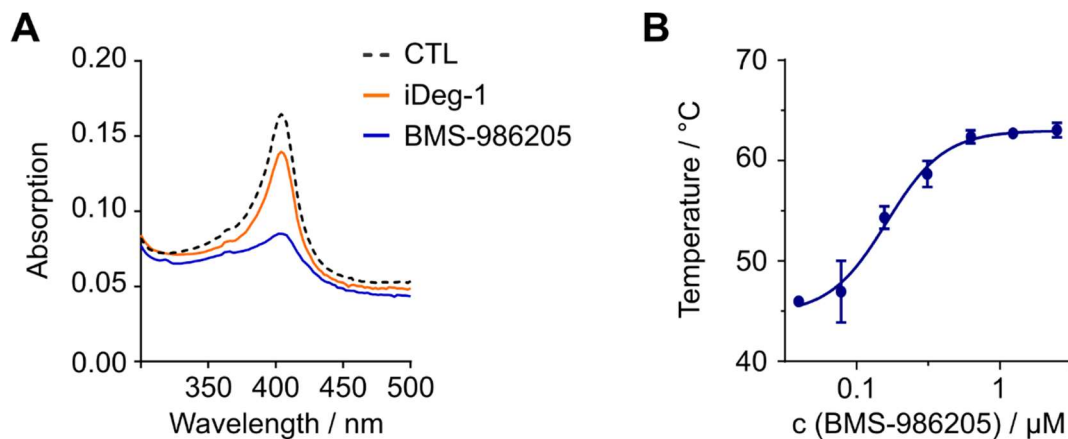
Figure 5.42: **iDeg-1 slightly reduces the *Soret* band intensity.** A) UV/Vis spectral analysis of rhIDO1 treated with either 100 μM iDeg, 50 μM BMS-986205 or DMSO as control (CTL) for 3 h at 37°C. Representative spectrum, n=3. B) Determination of the dissociation constant of BMS-986205 for IDO1 using nanoDSF. rhIDO1 and compounds were pre-incubated for 90 min at 37°C prior to the measurement. Data are mean values ± SD, n=3.

However, if iDeg-1 binds to apo-IDO1 and thereby induces IDO1 degradation, IDO1 enzymatic activity should be impacted as heme displacement results in inactive IDO1. To investigate a potential IDO1 inhibition by iDeg-1, enzymatic IDO1 activity in cells was measured by means of LC-MS/MS analysis as it can detect smaller changes in Kyn levels with an enhanced sensitivity compared to the Kyn sensor or *p*-DMAB.
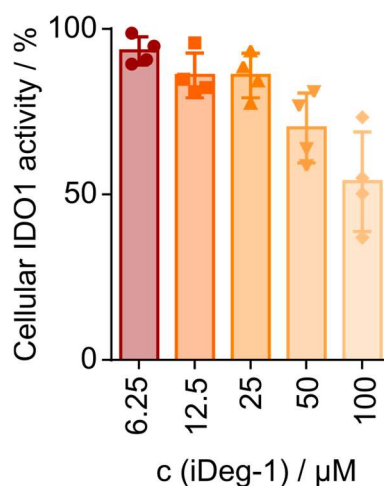

Figure 5.43: **IDO1 activity is slightly inhibited by high concentrations of iDeg-1**. IFNγ-stimulated BxPC3 cells were cultured in L-Trp-free medium for 48 h. iDeg-1 or DMSO as a control was added and pre-incubated for 30 min at 37 °C 5 % CO_2 followed by the addition of 100 μM L-Trp. 1 h after iDeg-1 addition, Kyn levels were measured by LC-MS/MS. Data are mean values ± SD, n=4.

For this, IFNγ-stimulated BxPC3 cells were treated with iDeg-1 and incubation for 30 min at 37 °C prior to the addition of L-Trp. Kyn levels were determined after 30 min of L-Trp addition by LC-MS/MS analysis. Interestingly, in cells, iDeg-1 slightly reduced IDO1 enzymatic activity (Figure 5.43). However, reduced enzymatic activity was only observed for concentrations 50- to 100-fold above the IC_{50} determined in the Kyn assay for iDeg-1 (Figure 5.43). This indicates

that although iDeg-1 might bind to apo-IDO1, the relevant mechanism for reducing Kyn level is not impeding heme to bind to apo-IDO1 as it is the case for heme-competitive inhibitors. iDeg-1 inhibits cellular Kyn production by IDO1 degradation.

5.2.3.4 siRNA screen to elucidate the degradation machinery

As the interaction of iDeg-1 and apo-IDO1 on its own does not explain IDO1 degradation, the involvement of an E3 ubiquitin ligase was explored. Co-treatment experiments clearly revealed that the neddylation-dependent CRLs are not involved in iDeg-1-induced IDO1 degradation (see Figure 5.37). Protein ubiquitination is mediated by an ubiquitin-conjugating enzyme (E2) and an E3 ubiquitin ligase (E3). The E3 binds the substrate protein and at the same time an E2 enzyme and catalyzes the transfer of ubiquitin from E2 to the substrate protein.[128] Human cells have over 600 E3 ligases divided in four families, namely the HECT-type, RING-finger, U-box and PHD-finger E3 ligases. Of those, only the six CRL and three further E3 ligases (SMURF1, MDM2, Parkin) are known to be NEDD8 dependent.[128, 129] Hence, the majority of E3 ligases are potential candidates for involvements in the iDeg-1 induced degradation of IDO1.

To elucidate which E3 ligase is involved in iDeg-1-mediated IDO1 degradation, a ubiquitin specific siRNA library was obtained (Horizon Discovery Biosciences Limited) and screened in the Kyn assay. The siRNAs library targets 663 proteins known to be involved in protein ubiquitination and degradation and allowed to study genes that are involved in the physiological IDO1 degradation pathway and to elucidate those proteins that mediate ubiquitination and degradation of IDO1 in the presence of iDeg-1. To screen the siRNAs, the Kyn assay was performed in HeLa cells as these cells are well established for effective siRNA transfection and could be easily adapted for the Kyn assay. IDO1 expression in HeLa cells is also inducible by IFNγ, and iDeg-1 inhibited Kyn production dose-dependently with an IC_{50} value of 1.1 ± 0.8 µM *which was investigated in the course of Lara Dötsch's PhD thesis* (Figure 5.44).
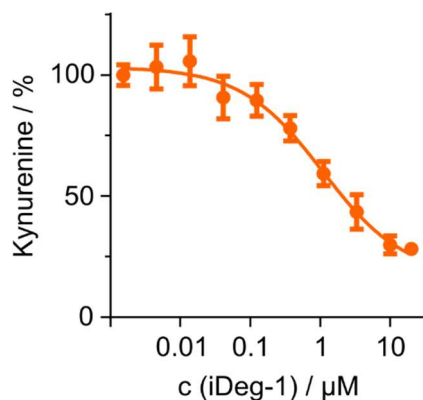
Figure 5.44: **iDeg-1 inhibits cellular Kyn production in HeLa cells.** Kyn assay in HeLa cells treated with 50 ng/mL IFNγ, L-Trp and iDeg-1 for 48 h prior to detection of Kyn levels using *p*-DMAB. (Performed by Lara Dötsch) Data are mean values ± SD, n=3.

For the final siRNA screening assay, HeLa cells were transfected with the siRNAs 48 h prior to the Kyn assay to ensure siRNA-mediated protein reduction during the assay. The effect of each gene in the Kyn assay was evaluated in the presence or absence of 5 µM iDeg-1. siRNAs that increase cellular Kyn production in the control conditions (i.e. in the absence of iDeg-1) might represent proteins involved in the physiological IDO1 degradation pathway, while siRNAs that increase Kyn production through reducing the inhibitory potency of iDeg-1 might be a prerequisite for iDeg-1-induced degradation.

The genetic screen identified two groups of proteins: one group of proteins that are potentially involved in the physiological degradation of IDO1, as their knockdown increased Kyn levels up to 140 % compared to samples treated with non-targeting siRNA in the absence of iDeg-1 (Table 5). A second group of proteins whose knockdown reduced the inhibitory potency of iDeg-1 (Table 6). The first group (Table 5) is composed of three proteins that are part of the CRL multisubunit complex: S-phase kinase-associated protein 2 (SKP2), E3 ubiquitin-protein ligase RBX1 (RBX1) and cullin 2 (CUL2). SKP2 is a F-Box protein and functions as a substrate receptor within the CRL complex.[130] RBX1 is the E3 ubiquitin ligase that mediates substrate ubiquitination, and CUL2 is the scaffold protein of the complex. The involvement of a NEDD8-dependent E3 in the physiological IDO1 degradation pathway was already indicated by previous experiments (Figure 5.37) and, hence, validates the siRNA screen as functional.

Table 5: **List of genes that effect Kyn levels in cells**. Knockdown of six genes was found to increase Kyn levels compared to Kyn levels in the control conditions (treatment with non-targeting siRNA). HeLa cells were transfected with siRNA 48 h prior to IFNγ, L-Trp and compound or DMSO addition. Kyn levels were determined after 48 h of treatment using sensor **6**. Data are mean values ± SD, n≥2, N=3.

Gene	Protein name	Hit in Kyn assay	Kyn level / % ±S.D.
CUL2	Cullin 2	2/3	134.5 ± 23
RBX1	E3 ubiquitin-protein ligase RBX1	3/3	132.2 ± 5
SKP2	S-phase kinase-associated protein 2	3/3	140.1 ± 2.6
PEX10	Peroxisome biogenesis factor 10	2/3	133.0 ± 11.2
PSMD14	26S proteasome non-ATPase regulatory subunit 14	3/3	126.5 ± 5.5
USP44	Ubiquitin carboxyl-terminal hydrolase 44	2/2	138 ± 7

Moreover, the knockdown of the 26S proteasome non-ATPase regulatory subunit 14 (PSMD14) increased Kyn levels and is part of the first group. PSMD14 is a subunit of the proteasome with metalloprotease activity and is involved in protein deubiquitination and ubiquitin recycling of polyubiquitin chains.[131] Inhibition of PSMD14 was shown to increase polyubiquitinated protein abundance due to reduced proteasome activity[132]. Therefore, PSMD14 knockdown might decrease proteasome activity and, thus, increase IDO1 protein levels and Kyn production.

The other two proteins, PEX10 and USP44, whose knockdown increased Kyn levels compared to non-targeting siRNA in DMSO treated cells could be connected to IDO1 stabilization or the Kyn signaling pathway.

Table 6: **List of genes that reduce the inhibitory potency of iDeg-1 in the Kyn assay**. 9 genes were found to reduce inhibitory potency of iDeg-1 treated cells relative to non-targeting siRNA treated cells with 5 µM iDeg-1 (= 100 % inhibitory potency). HeLa cells were transfected with siRNA 48 h prior IFNγ, L-Trp and compound or DMSO addition. Kyn levels were determined after 48 h of treatment using **6**. Data are mean values ± SD, n≥2, N=3.

Gene	Protein name	Hit in Kyn assay	relative inhibitory potency / % ± S.D. @ 5 µM iDeg-1
CUL2	Cullin 2	2/3	71.0 ± 4.7
PHF1	PHD finger protein 1	2/3	72.8 ± 5.2
PRICKLE1	Prickle-like protein 1	2/2	71.2 ± 7.0
RBX1	E3 ubiquitin-protein ligase RBX1	2/3	66.2 ± 7.1
RFPL4AL1	Ret finger protein-like 4A-like protein 1	2/2	75.0 ± 4.2
SIAH2	Seven in Absentia Homolog 2, E3 ubiquitin-protein ligase	3/4	82.5 ± 8.7
SOCS3	Suppressor of cytokine signaling 3	3/4	77.4 ± 7.3
TRIP12	Thyroid hormone Receptor Interacting Protein 12; E3 ubiquitin-protein ligase	3/3	71.6 ± 10.8
UBA6	Ubiquitin-like modifier-activating enzyme 6	3/3	78.1 ± 12.1

Table 6 shows the proteins that were found to influence the inhibitory potency of iDeg-1. Interestingly, two proteins that elevated cellular Kyn levels in the absence of iDeg-1 also reduced its inhibitory potency, namely CUL2 and RBX1. Although, as mentioned previously, CUL2 and RBX1 are members of the CRL complex which require a neddylation for protein ubiquitination.[125, 126] Hence, iDeg-1-mediated IDO1 degradation is not influenced by them. Furthermore, the knockdown of suppressor of cytokine signaling 3 (SOCS3) was identified to reduce iDeg-1 inhibition by 22 % compared to the treatment with control siRNA and iDeg-1. SOCS proteins including SOCS3 are negative regulators of JAK/STAT signaling.[133]

Knockdown of SOCS3 might decrease feedback inhibition of the signaling pathway and thus lead to enhanced JAK/STAT signaling and IDO1 expression. It was already demonstrated in HEK293T cells that IDO1 expression levels are critical for the compound's potency (Figure 5.25C). Additionally, SOCS3 was also described by Orabona *et al.*[134] to be involved in IDO1 degradation. SOCS3 binds IDO1 if the immunoreceptor tyrosine-based inhibitory motifs (ITIMs) of IDO1 are phosphorylated.[134] Bound to substrate proteins, SOCS3 can act as a substrate receptor in the CRL complex. It was reported that proteins that contain the SOCS-box structural motif interact with either cullin 2 or cullin 5 of the CRL.[135] Nonetheless, NEDD8 modification is required for CRL activity[136, 137] and, thus, involvement of SOCS3 as substrate receptor in iDeg-1-mediated IDO1 degradation is unlikely. Apart from SOCS3, no other proteins were reported to be involved in IDO1 degradation.

In addition, two other E3 ligases were identified to potentially be involved in the iDeg-1-induced degradation of IDO1, namely TRIP12 and SIAH2. Both are E3 ligases that act independently of an E3 complex and do not require NEDD8 modification to be active.[206, 207] Neither of the two are mechanistically linked to IDO1 or the Kyn pathway. TRIP12 is a HECT-type E3 ligase that plays an important role in the cell cycle as well as during degradation in response to DNA damage.[138] Recently, TRIP12 was found to be involved in PROTAC-mediated degradation of BRD4 which strongly indicates that TRIP12 can be hijacked by small molecules to promote targeted protein ubiquitination.[139]

SIAH2 is a member of the RING finger E3 ligases and mediates ubiquitination of various proteins, like CHK2 and Nrf2.[140, 141] SIAH2 and the isoform SIAH1 bind to their substrate proteins via a common binding motif of which the core residues VxP display highest degree of conservation. The IDO1 protein sequence contains three of these VxP motifs. One VxP motif was found close to the heme pocket to which the compound might bind (Figure 5.45 and Figure S 3). Hence, SIAH2 could be involved in iDeg-1-induced IDO1 degradation.
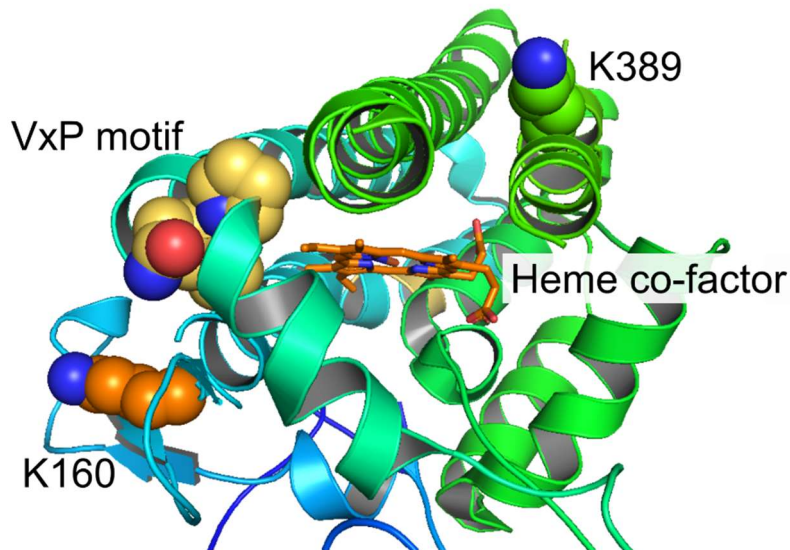
Figure 5.45: **IDO1 contains a VxP motif close to the catalytic pocket**. Crystal structure of IDO1 (PDB: 5ek4) in which residues of interest are highlighted. K389 is the lysine residue that was found to be polyubiquitinated. K160 was not identified by the MS analysis. VxP motif is highlighted in yellow, for all VXP motifs see Figure S 3. The heme cofactor of IDO1 is shown in the catalytic pocket.

Furthermore, knockdown of PRICKLE1 weakened iDeg-1-mediated Kyn inhibition. PRICKLE1 is not characterized as an E3 ligase, nonetheless PRICKLE1 was reported to mediate Dishevelled (DVL3) ubiquitination and degradation. DVL3 is a positive regulator of the Wnt/β-catenin pathway.[142] Whether PRICKLE1 can be hijacked by small molecules, like iDeg-1 to degrade also other proteins, has to be further investigated.

Intriguingly, UBA6 knockdown reduced iDeg-1 inhibition by approximately 22 % compared to the control conditions. Together with UBE1, UBA6 is one of the two ubiquitin-activating enzymes. They are essential for ubiquitin activation and, thus, E2 ubiquitin loading. However, ubiquitin activation is not rate-limiting in the protein ubiquitination process and thus reduced activity of UBA6 should not reduce protein ubiquitination as UBE1 is active.[143, 144] However, UBA6 also activates the ubiquitin-like protein FAT10 and FAT10ylation of lysine residues also targets proteins for proteasomal degradation.[145] IFNγ stimulation was shown to increase the cellular level of FAT10 and, thus, also UBA6-mediated activation of FAT10.[146] Hence, downregulation of UBA6 may reduce FAT10ylation as UBA6 is the only protein that can activate FAT10.[145] Nevertheless, IDO1 immunoprecipitation and MS analysis solely identified polyubiquitin modified IDO1 and not FAT10. Hence, the role of UBA6 in iDeg-1-dependent IDO1 degradation should be further elucidated.

The remaining two proteins RFPL4AL1 and PHF1 are zinc finger proteins and literature search could neither reveal any potential function in the IDO1 degradation pathway nor any role in the Kyn pathway.

Ultimately, the performed siRNA screening did not reveal an E3 ligase whose knockdown substantially reduced iDeg-1 inhibition. Nonetheless, the proteins that potentially be involved in iDeg-1-mediated IDO1 degradation have to be validated mainly by investigating IDO1 protein levels as a direct evaluation method upon the knockdown.

Several factors might account for the inconclusive results: first, the knockdown efficiency for target proteins are unknown and might not be sufficient to detect changes. Moreover, even a reduced abundance of the E3 ligase responsible for iDeg-1-mediated IDO1 degradation may be enough to catalyze IDO1 ubiquitination, solely the degradation rate might be reduced. Hence, iDeg-1-induced degradation can still take place. Furthermore, using the Kyn assay as an indirect readout for IDO1 abundance might be challenging considering the fast turnover of IDO1. The assay system might not be sensitive enough to detect changes in protein abundance by means of Kyn levels. In addition, iDeg-1 only slightly reduced IDO1 enzymatic activity in cells since iDeg-1 most likely binds to the heme pocket and prevents heme incorporation and IDO1 catalytic activity. Investigating IDO1 protein levels after knockdown would most likely lead to more precise results. However, a knockout of the responsible E3 ligase may be required instead of a knockdown to clearly identify the involved E3 ligase.

In summary, the siRNA screen suggested several E3 ligases, which might be involved in the physiological degradation pathway of IDO1 and in iDeg-1-induced IDO1 degradation. Further studies are required to validate either of the proteins. Importantly, IDO1 protein levels should be evaluated after the knockdown or knockout of the above listed proteins.

6. Discussion

6.1 Phenotypic assay for small molecules that enhance NK cell-mediated elimination of cancer cells

The indispensable role of the immune system in anti-tumor activity has become of great interest and intensive research is ongoing for the development of meaningful cancer immunotherapies and their implementation. Some immunotherapy approaches are already approved by the FDA and show great success, such as CAR-T cells as well as the so-called checkpoint inhibitors. Checkpoint inhibitors are antibodies that block inhibitory receptors, such as CTLA-4 (cytotoxic T lymphocyte-associated antigen 4) or PD-1 (programmed cell death protein 1) on cytotoxic T lymphocytes (CTL) and thereby diminish cancer cell-mediated T cell inhibition.[45, 46] Hence, the current cancer immunotherapies utilize CTL activity to eliminate cancer cells. However, also natural killer (NK) cells exhibit great anti-cancer activity and strategies to enhance NK-cell tumoricidal activity are in development. Approaches mainly focus on adoptive NK cell therapy. *Ex-vivo* activated and expanded NK cells or genetically engineered CAR-NK cell are currently in clinical trials. However, adoptive cell therapies are highly laborious. Moreover, the *in-vivo* persistence of transferred NK cells as well as absent trafficking towards the tumor tissue is an obstacle. The tumor microenvironment (TME) might be responsible for this because tumor-derived suppressive factors, such as TGFβ, kynurenines and PGE2 strongly interfere with NK cell activity and proliferation. For this reason, methods to elucidate how to enhance NK cell activity and their persistence within the TME are of high relevance, e.g. by utilizing phenotypic screening assays. However, at the beginning of the work described on this thesis no phenotypic assay was available that studied NK cell activity in an environment similar to the TME. Solely NK cell activity in the presence of individual tumor-derived immunosuppressive factors, such as TGFβ[97], kynurenines[147, 148] or PGE2[22, 100] were studied. At the same time established NK cell cytolysis evaluation methods were not adaptable for screening campaigns, such as chromium release assay or flow cytometry.[149] In contrary, automated high-content analysis was highly advanced for screenings in drug discovery.[150]

Hence, a phenotypic screening assay was developed that monitors NK cell activity by high-content analysis. The developed co-culture assay (lymphocytes and cancer cells) was supplemented with tumor-derived immune-suppressive factors (TGFβ and PGE2) to mimic the TME. Together, it enables the investigation of NK cell cytotoxicity in highly disease relevant phenotypic assay. Below, this assay will be referred to as TME-like NK cytolysis assay to be able to distinguished the assay from the further discussed NK cell-based assay.

Till recently, assays that are suitable for HTS were not available to discover small molecules that can modulate NK cell activity. Nevertheless, compounds that enhance NK cell cytotoxicity were of high interest and highly laborious evaluation methods were performed to identify immunomodulatory small molecules.[149, 151, 152] For instance, 502 natural products were investigated for their ability to enhance NK cell activity by monitoring IFNγ secretion.[151] IFNγ is secreted by active NK cells and usually correlates with cytolytic activity. This property was exploited to screen for NK cell activators, however only andrographolide could be identified and validated as natural product enhancing NK cell-mediated cancer cell cytolysis.[151] Andrographolide was also investigated in the TME-like NK cytolysis assay, however, no increase in NK cell activity was observed. Two years later, the Prestwick Chemical Library (1,200 compounds) was screened by means of europium release assays monitoring NK cell-mediated target cell cytolysis.[152] A great advantage of this assay was that it monitored NK cell cytotoxicity directly, however, the use of the non-radioactive europium to assess NK cell cytotoxicity never became prevalent because of low reproducibility.[153] Within the screen, the antibiotic amphotericin B was identified and validation as enhancer of NKL (human natural killer cell leukemic cell line) cytotoxicity.[152] Amphotericin B enhanced NK cell activity by approximately 50 % at 5 μM, it was also tested in the TME-like NK cytolysis assay but could not enhance NK cell activity.

Remarkably, in the last years, several new detection methods were developed to monitor target cell survival in a direct co-culture with NK cells. All with the same motivation: to enable automated screening of small molecule libraries aiming for the discovery of enhancers of NK cell cytotoxicity (Table 7).[154-157] This clearly highlights the demand of platforms to further investigate NK cells and their ability to eradicate cancer cells. A NanoLuc® luciferase release assay was developed to quantify target cell lysis by means of a bioluminescent signal. Luciferase-produced bioluminescence is an established and robust readout for high-throughput screens.[158] Target cells stably express the NanoLuc® luciferase which is release upon target cell lysis. However, NanoLuc® luciferases are proteins and protein stability is essential for luciferase activity. Thus, the NanoLuc® luciferase release assay is limited to short assay times to ensure luciferase activity in the cell culture supernatant.[158] Moreover, compounds might interfere with the luciferase activity and can result in false negatives. An alternative assay might be a fluorescence-based calcein release assay which was established for screening.[155] However, transient cellular stains, such as calcein have several disadvantages. On the one hand the fluorescence intensity is diluted upon target cell proliferation and on the other hand divergent loading efficiency as well as spontaneous release can lead to false positives.[159] Another assay that was developed recently by Xu *et al.*[156] used a luminescence-based ATP readout to quantify target cell survival as ATP reflects the

114

proportion of metabolically active cells.[156] This assay readout can be adapted to all assay incubation times, however, small molecule that change cellular metabolism without enhancing NK cell activity might interfere with an ATP-based readout. Furthermore, a time-resolved analysis is not possible.

In contrast, the utilization of stable, fluorescently-tagged target cell lines as used in the TME-like NK cytolysis assay empowers time-resolved analysis, makes the assay adaptable to any incubation time required and does neither require the addition of a luminescence substrate nor pre-labeling of cancer target cells. Moreover, the fluorescence intensity of the target cells does not decline over time.

Table 7: **Published co-culture assays to evaluate NK cell cytolysis activity by monitoring target cell lysis.**

Effector cells	Target cells	Relevant additives	Readout	Investigated small molecules	Reference
PBMCs, healthy donors	K562-NL	None	NanoLuc (NL) release assay [a]	782 (TMIC Human Metabolome Library)	Hayek *et al.* [154] **2019**
Expanded NK cells	OVCAR-3	None	Calcein release [b]	20,000	Lee *et al.* [155] **2019**
Expanded NK cells	H1299	None	ATP-based luminescence [b]	2,880 (natural products)	Xu *et al.*[156] **2020**
NK 92	K562-NL	None	NL release assay [a]	1,200 (Prestwick Chemical Library®)	Cortés-Kaplan *et al.* [157] **2021**
Lymphocytes	A549[Green]	IL-15, TGFβ & PGE2	Target cell count (fluorescence nucleii) [b]&[c]	3,000 (Prestwick Chemical Library® Keymical Collections™ pseudo-natural products)	Not published **2021**

Screening format: [a] 96-well [b] 384-well and [c] 1536-well.

The recently reported assays share the objective to identify compounds that enhance NK cell-meditated cancer cell cytolysis.[154-157] NK cells within human PBMCs, IL-2 expanded NK cells or the NK cell line NK 92 were used as effector cells (Table 7). The effector cells were either pre-incubated with the small molecules (16 h) prior to target cell addition[154, 155] or directly co-cultured with the target cells in the presence of small molecules[156, 157]. The incubations times of the co-cultures are rather short with 2 h, 4 h, 5 h and only Xu *et al.*[156] investigated the effect of the small molecules in co-culture over 24 h[156]. The short assay times restrict the identification to fast acting small molecules, modulators inducing transcriptional changes that enhance NK cytotoxicity cannot be identified in assays that last only few hours. Moreover, the suppressive properties of the TME are not reflected in either of the assays (Table 7).[154-157]

The number of identified small molecules that were shown to enhance NK cell cytotoxicity by means of the above described assays is limited. Xu *et al.* could confirm that the hit compound DI3A (20-deoxyingenol 3-angelate) increases NK cell activity.[156] Screening of the Prestwick Chemical Library® by Cortés-Kaplan *et al.* [157] discovered initially 14 compounds that enhanced target cell cytolysis by 30 % or more, however only colistin sulfate salt could be validated using K562 target cells, but not when 786O or A375 were used as target cells.[157] In line, colistin sulfate salt was not active in the TME-like NK cytolysis assay as A549[Green] were used as target cells. Contradictory, amphotericin B, which was identified to be an enhancer of NKL cytolysis[152] was not active utilizing NK 92 cells[157]. The evaluation of 20,000 small molecules in the calcein release assay disclosed the pan-ROCK inhibitor, Y-27632 as small molecule modulator of NK cell activity. Target cell (OVCAR-3) cytolysis was increased by 30 %.[155] Y-27632 was also included in the TME-like NK cytolysis assay and enhanced NK cell activity by 45 %, however the small molecule also reduced A549[Green] cell count by 32 %. Further investigations are required to validate Y-27632 in the TME-like NK cytolysis assay. The utilization of the TMIC Human Metabolome Library did not identify enhancers NK cell activity, only inhibitors were discovered.

Nevertheless, not many small molecules that could increase NK cell activity towards cancer cells were revealed by the four described screening assays (Table 7) and neither was the suppressive nature of the TME considered. Adapting one of the described assays to include tumor-derived suppressive factors to reflect the TME would not have been possible. The inhibitory effect of TGFβ towards NK cell activity was not observed when using expanded NK cells (same is true for NK cell lines). However, as evidently represented in the literature, TGFβ is a key suppressive factor and inhibits NK cells.[18, 56, 97, 99] Expanded NK cells are constantly stimulated with the activating cytokine IL-2 to maintain proliferation but the cytotoxic activity is also induced. TGFβ inhibitory effects are mediated by transcriptional changes, e.g., granzyme B and perforin protein reduction, as well as metabolic changes.[18, 99] Alterations in protein levels, which are induced by transcriptional changes, take approximately 24 h.[160] However, expanded NK cells are immediately active and NK cell-mediated target cell occurs within approximately 7-10 h. Hence, transcriptional changes might not affect cytolysis rate.

Therefore, lymphocytes from healthy human donors were used for the TME-like NK cytolysis assay as TGFβ reduced NK cell activity. Combining TGFβ and PGE2 clearly induced a strong suppressed NK cell phenotype in the co-culture and may represent the TME. The utilization of primary cells (lymphocytes) in co-culture with target cells and disease-relevant suppressive factors (TGFβ and PGE2)[26, 56, 99, 161, 162] increases the physiological relevance of the assay and may improve translational relevance.

Although the phenotypic TME-like NK cytolysis assay has several advantages compared to aforementioned phenotypic NK cell activity assay, it also has its limitations. The use of primary human lymphocytes for the co-culture assay required a pre-investigation of each donor as the percentage of NK cells within the lymphocyte fraction of different donors varies due to genetic and environmental conditions.[163, 164] Moreover, the duration of the assay may elevate toxicity of small molecules, as represented in the results.

Exploiting the established phenotypic assay for the biological evaluation of around 3,000 small molecules identified several TGFR-1 inhibitors as hit compounds with diverse chemotypes. Interestingly, not all compounds that inhibit TGFR-1 increased NK cell cytolysis, less active derivatives only partially elevated NK activity or were inactive. Only highly potent TGFR-1 inhibitors that display low IC_{50} values > 50 nM for TGFR-1 could maintain NK cell cytolysis. The utilization of the TGFR-1 inhibitor RepSox in co-culture with IL-15, TGFβ and PGE2 evidently prevented NK cell inhibition. Importantly, TGFR-1 inhibitors were already reported as promising small molecules in combination with adoptive NK cell transfer to preserve cytotoxic function of *ex-vivo* activated NK cells also *in-vivo* when encountering the TME.[56]

Interestingly, RepSox recovered NK cytolysis activity to a similar level of NK cells that were only treated with IL-15. Hence, TGFβR1 inhibition not only impacted TGFβ-mediated NK cell inhibition, but also seemed to abolished PGE2-mediated NK cell suppression. Both suppressive factors alone inhibited NK cell activity only partially and the combination of TGFβ and PGE2 showed an additive effect. Accordingly, modulating the effect of one suppressive factor should revert NK cell activity only partially. The observed influence may be explained by the secretome analysis of A549 cells. A549 cells secret TGFβ, which is further elevated under hyperglycemic conditions (25 mM glucose).[165, 166] 25 mM glucose is a standard concentration in cell culture growth medium.

In addition, VPS34 inhibitors, Syk inhibitors, a DNA-PK inhibitor and a PROTAC for BRD4 were found to preserve NK cell activity for which no direct mechanistical link to either TGFβ nor PGE2 can be made. Generally, the accumulation of kinase inhibitors is noticeable. Often, ATP-competitive kinase inhibitors lack selectivity since they bind to a well conserved binding site within the kinase family.[167] Hit evaluation for potential inhibition of the kinase TGFR-1 is mandatory.

The target protein VPS34 is known to be involved in autophagy and its inhibition prevents autophagy. PGE2 activates EP2 and EP4 which results in an increase of cAMP. PGE2-mediated activation of EP2/4 as well as increased cAMP were reported to activate autophagy.[168, 169] Grisan *et al.* showed that the cAMP-dependent protein kinase (PKA) induces

autophagy that resembles that of starvation.[168] In line, VPS34 inhibitors also reduce starvation induced autophagy.[170] It might be worthwhile to explore NK cell autophagy in in this context.

Interestingly, iTeos Therapeutics developed an immunosuppressive cell line/T cell co-culture assay and screened the Selleck compound library containing 1,902 compounds which led to the identification of 42 compounds which modulate the metabolism, epigenetics, autophagy, and TGFβ signaling.[171] More information about the hit compounds is not disclosed. In line, the identified hit compounds in the TME-like NK cytolysis assay modulate autophagy (VPS34), epigenetics (BRD4) and the TGFβ signaling (TGFR-1).

In summary, the developed novel phenotypic assay is characterized by high physiological relevance and screening of a small molecule library might enable the discovery of target proteins that were not linked to NK cell suppression yet. Thereby, the understanding of immunosuppression by cancer cells can be expanded and may empower the development of innovative cancer immunotherapies that preserve NK cell cytotoxicity in the TME.

6.2 Cell-based assay for Indolamine 2, 3-dioxygenase 1 modulators

The development and approval of diverse immune checkpoint inhibitors against PD-1 or CTLA4 displays a breakthrough in cancer immunotherapies. However, in the tumor microenvironment (TME), multiple mechanisms cooperatively impede effector immune cell activity, and, thus, prevent cancer cell elimination. Hence, co- or even multiplex-treatment approaches of diverse immune modulatory agents may improve therapeutic outcomes Indolamine 2, 3-dioxygenase 1 (IDO1) was found to be overexpressed in the TME in multiple tumor types and mediates immunosuppression by depleting L-Trp and producing kynurenine metabolites. Subsequently, IDO1 has emerged as a promising target for cancer immunotherapies.

The combination of already approved checkpoint inhibitors, like an anti-PD1 antibody with IDO1 inhibitors displayed enhanced efficacy in mouse models and early clinical trials while IDO1 inhibitors as single agents are less promising. Phase III clinical trials of the IDO1 inhibitor epacadostat in combination with pembrozilumab peculiarly showed limited success in the treatment of unresectable or metastatic melanoma. To deepen the understanding of the role of the immunosuppressive enzyme IDO1 and to discover more efficient ways to reduce Kyn production, novel chemotypes as well as alternative ways of modulating IDO1 activity should be explored.

To date, modulators of IDO1 enzymatic activity originate from target-based screening campaigns and many different scaffolds were disclosed as IDO1 inhibitors.[59, 109, 172-175] However, IDO1 is a redox sensitive protein, which bears major challenges if enzymatic inhibition assays are used for inhibitor discovery. Activity assays of redox-sensitive proteins require several additives, such as catalase and ascorbic acid, to maintain the redox cycle. Adverse interference with these additives makes the assay vulnerable to false-positive screening hits, such as redox-cycling compounds.[60, 113, 173] Moreover, IDO1s' cofactor heme was revealed as an obstacle in biochemical assays as IDO1 activity can be diminished by heme-competitive inhibitors. However, binding and, thus, IDO1 inhibition by those inhibitors are highly dependent on the temperature as well as the presence or absence of reductants during IDO1-compound pre-incubation.[34, 62, 113] Furthermore, it was recognized that the validation of inhibitory potency for many IDO1 inhibitors from *in vitro* to *in cellulo* is poor.[172, 173] For instance, Röhrig *et al.*[173] investigated the Prestwick Chemical Library (1,200 compounds) and the Maybridge HitFinder Collection (14,000 compounds) in a target-based screen for enzymatic IDO1 activity inhibitors.[173] Initially, 60 compounds were identified to inhibit IDO1 enzymatic activity, however only four compounds displayed a dose-dependent inhibition in cells.[173] Moreover, 2,000 natural products were screened for IDO1 inhibition, and only 30 %

of the initial hit compounds also displayed cellular IDO1 inhibition. Compounds' off-target activity or promiscuous enzymatic inhibition might account for this.[176]

To circumvent these challenges, a phenotypic approach was developed in the course of this thesis to identify IDO1 activity modulators in the native cellular environment of IDO1. Phenotypic assays empower the identification of small-molecule modulators of diverse target proteins that are involved in the signaling pathway of interest and can elucidate cellular mechanism that were not yet linked to the explored phenotype. Consequently, the developed cell-based Kyn assay allows unraveling alternative mechanisms to downregulate IDO1 activity in contrast to a target-based approach that would identify direct IDO1 inhibitors solely. To date, no phenotypic HTS has been performed to find IDO1 modulators in cells as neither suitable Kyn detection agents nor appropriate cell-based setups for automatization were available. The screening assay that was developed in the course of this thesis is the first HTS conducted to find IDO1 modulators in cells.

As IDO1 is not ubiquitously expressed in cells, IDO1 induction was required for the phenotypic assay. In the tumor microenvironment, IDO1 expression is mainly stimulated by IFNγ.[37] To maximize physiological relevance of the assay, cellular IDO1 expression was induced via the physiological stimulus IFNγ as it mimics an important disease feature. In addition, other IFNγ-inducible proteins will be co-expressed, which might be essential for IDO1 regulation and Kyn pathway modulation, such as SOCS proteins which are negative regulators of IFNγ signaling that interfere with the JAK/STAT pathway.[177]

Screening a small molecule library of more 150,000 members in the Kyn assay underscored the potential of the assay to uncover modulators of cellular Kyn production with diverse mechanisms reducing IDO1 activity as illustrated by Figure 6.1, e.g. IDO1 expression inhibitors, heme synthesis inhibitors, and IDO1 degraders. IDO1 expression was reduced by JAK1/2 inhibitors which prevent IFNγ signaling as well as BRD4 inhibitors as BRD4 is involved in the epigenetic regulation of *IDO1*.[178] These findings provide targets that can be beneficial for dual treatment approaches to enhance the effectiveness of checkpoint inhibitors as for example BET inhibitors are under investigation in several clinical trials.[179]
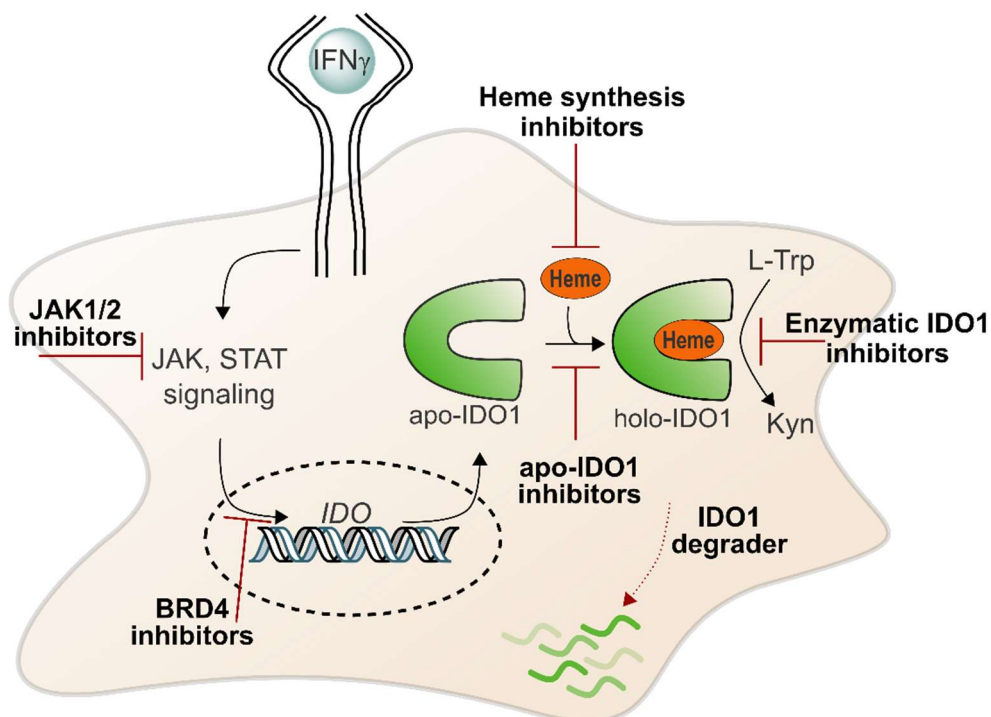
Figure 6.1: **Cellular pathways targeted by the identified hit compounds**. Cellular Kyn levels were decreased by hit compounds with multiple mechanism: 1. targeting IDO1 transcription (JAK and BRD4 inhibitors) 2. preventing heme cofactor incorporation into IDO1 (apo-IDO1 binders and heme synthesis inhibitors) and, thus, inhibition IDO1 catalytically, 3. Direct holo-IDO1 enzymatic inhibitor and 4. IDO1 degradation (iDeg-1).

Moreover, small molecules that interfere with cellular heme synthesis reduce the abundance of the cofactor essential for IDO1 activity and thereby reduce IDO1 activity and cellular Kyn levels.[112] Interestingly, reduction of heme synthesis does not display cellular cytotoxicity after 48 h of treatment. Most heme-containing proteins, such as peroxidases, cytochromes and hemoglobin, bind the cofactor heme covalently and their protein half-life expands over several days.[180-183] In contrast, IDO1 binds heme dynamically (non-covalent) and has a rather short half-life, as elucidated in the course of this thesis. Hence, reduced heme levels in cells for up to 48 h might affect solely proteins that do not covalently bind the heme cofactor, such as IDO1, IDO2 and TDO. Nonetheless, heme shortage might affect heme-responsive sensor proteins which are regulated by heme abundance, and reduced heme levels may alter cellular transcription or redox signaling.[184] Moreover, free heme correlates with the production of reactive oxygen species (ROS), which also contributes to immunosuppression in the TME and promotes cancer cell survival.[185, 186] Together, inhibiting heme synthesis might be interesting alternative approach to reduce Kyn production, however, heme is vital for hemoglobin which is involved in oxygen transport and, thus, respiration.[187] Hence, a TME-specific delivery strategies should be considered to avoid disorders, like anemia, which are caused by malfunctional heme synthesis.[187]

Several biologically uncharacterized hit compounds were identified to decrease cellular Kyn levels by reducing IDO1 enzymatic activity directly: a thiohydantoin-based inhibitor (**9**), the oxazole-4-carboxamide-based inhibitor (**10**) and the piperazin-2-one-based inhibitor (**11**). All three compounds are novel chemotypes which inhibit IDO1 activity by competing with the heme cofactor and, thus, act similarly to BMS-986205. The outstanding potency of apo-IDO1 inhibitors like BMS-986205 as well as **9** and **10** compared to epacadostat highlights the efficacy in reducing cellular Kyn levels by targeting apo-IDO1 in cells. Therefore, the interruption of heme incorporation and, thus, the inhibition of IDO1 activity might be an effective approach for the reduction of cellular Kyn production. Moreover, targeting apo-IDO1 may be advantageous as substrate-competitive binders often display structural similarities to L-Trp and Kyn and may activate the aryl hydrocarbon receptor (AhR). The AhR is a transcription factor and can be activated by kynurenines, among other ligands and promotes the differentiation of regulatory T cells and, thus, inhibits effector immune cells.[188]

Throughout the mechanistic studies for the apo-IDO1 binders **9**, **10** and **11,** a significant discrepancy of approximately 100-fold between the IC_{50} values in the enzymatic assay compared to the cell-based assay was detected. To elucidate this observation, the focus has to be on the heme co-factor. *In vitro*, recombinant human holo-IDO1 was used to evaluate IDO1 activity. Hence, IDO1 was loaded with its cofactor heme to facilitate substrate conversion. Small molecules that interact only with apo-IDO1 require heme dissociation from holo-IDO1 in order to bind and inhibit IDO1 enzymatic activity. Heme dissociation, however, only occurs at temperatures of 30 °C or higher.[62] Even at appropriate incubation temperatures, heme dissociation and, thus, formation of apo-IDO1 *in vitro* is a reversible and slow process.[35] Thus, heme-competitive IDO1 inhibitors are inactive at 20 °C as heme dissociation only occurs at 30 °C or higher. Furthermore, the slow nature of heme dissociation results in a remaining fraction of active holo-IDO1 even in the presence of heme-competitive inhibitors and a pre-incubation at 37 °C, and explains the discrepancy between the cellular and biochemical IC_{50} values. In cells, heme-competitive IDO1 inhibitors are more potent because IDO1 is expressed in its apo-form and heme-competitive modulators can bind and prevent IDO1 maturation and, thus, heme incorporation. Moreover, cellular assays are performed at 37 °C at which apo- and holo-IDO1 are in an equilibrium. The opposite is the case when working with the recombinant protein as holo-IDO1 is used and heme needs to dissociate first before compound binding can occur.

Subsequently, IDO1's native cellular environment was important to detect the three highly potent apo-IDO1 inhibitors. Intriguingly, not only the three most potent hit compounds of the screen were heme-competitive binders, also other investigated hit compounds were identified to be heme-competitive (results obtained within the Waldmann group). Substrate-competitive

IDO1 inhibitors were not identified among the in-depth investigated hit compounds with $IC_{50} >$ 2 µM. On the contrary, although diverse IDO1 target-based assays have been conducted, a low number of chemotypes inhibiting IDO1 heme-competitively was described compared to substrate-competitive IDO1 inhibitors.[189] The above defined challenges of biochemical IDO1 activity assays might account for this observation. Target-based HTS have been conducted by different groups, however, the enzymatic reaction was performed at room temperature and, noteworthy, without a pre-incubation step of IDO1 and the compounds which limited the outcome.[109, 172-175, 190] The identification of apo-IDO1 binders is not possible without a pre-incubation at > 30°C and should be considered for the identification and confirmation of apo-IDO1 binders.[62]

The native cellular environment of IDO1 was not only key for the identification of apo-IDO1 binders but also for the identification of hit compound named iDeg-1 (**12**). iDeg-1 was an exceptional finding because it is the first monovalent degrader for IDO1. The identified compound specifically binds to IDO1 and induces its ubiquitination followed by proteasomal degradation.

In the last decade, research and development in the field of targeted protein degradation (TPD) has increased noticeably because TPD has great potential as new therapeutic modality. Traditional small-molecule modulators change the activity of disease-related proteins, e.g. by enzymatic inhibition. In contrast, TPD enables the reduction of cellular protein levels of the protein of interest and this significantly has expanded the target scope as "undruggable" proteins, e.g. transcription factors which do not have an enzymatic function or even defined binding pockets, could be downregulated using TPD.[191] For induced protein degradation, the cellular protein degradation mechanisms are exploited such as the ubiquitin-proteasome-system (UPS).

IDO1's catalytic activity is successfully modulated by conventional small-molecule inhibitors or activators[34, 62, 63, 189, 192, 193], however, when IDO1 gets phosphorylated, its enzymatic activity is lost and IDO1 functions as signaling molecule.[42, 194, 195] IDO1 as signaling molecule promotes its self-amplification leading to continuous IDO1 expression and an increase in IDO1 protein abundance in dendritic cells (DC), particularly shown for plasmacytoid DCs (pDCs) which causes the initiation of a long-term tolerogenic phenotype in pDCs.[39, 42, 194, 195] The signaling activity of IDO1 was considered as relevant for the failure of the clinical phase III trial of epacadostat in combination with pembrolizumab.[176] IDO1 inhibitors like epacadostat were selected based on their inhibitory potency, however, do not inhibit IDO1's signaling activity.[68] Epacadostat binds in a substrate-competitive manner into the catalytic pocket of IDO1.[113] As phosphorylation of IDO1 results in a conformational change, binding of epacadostat to IDO1

signaling protein might therefore not be possible. This is supported by experimental data demonstrating that epacadostat could not disrupt IDO1 self-amplification in DCs.[68]

Hence, the development of compounds that can block both, the catalytic and signaling activity of IDO1 is of high interest. IDO1 protein degradation as an alternative approach may serve both. However, the identification of compounds that induce protein degradation is still an obstacle. Most single-ligand molecules that enhance protein degradation like the discovered iDeg-1 are serendipitously identified. The development of approaches to monitor changes in ubiquitination or protein levels within the whole proteome, e.g. for chemical screening, has proven to be very challenging. Highly laborious analysis methods are still required to identify TPD by small molecules.[196]

Nonetheless, in the last decade diverse compounds were discovered for TPD and the number of available protein degraders is increasing significantly.[197] Depending on the mode of action of the chemical entities, target degradation can be classified into three groups: small-molecule degraders, molecular glues and bifunctional degraders (Figure 6.2).
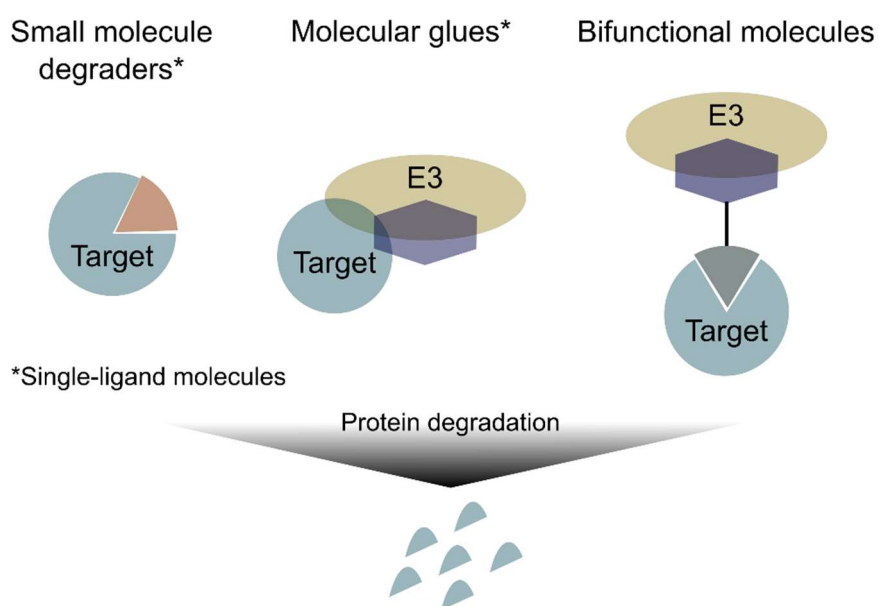
Figure 6.2: **Classification of small molecules that induce degradation of target proteins**. Adapted from Naito *et al*.[198]

Small-molecule degraders directly interact with their targets and induce ubiquitination and degradation however without interacting with the hijacked E3 ligase.[198] A successful example for a small-molecule degrader is Fulvestrant, a selective estrogen receptor downregulator (SERD) which is approved as drug for breast cancer.[199] In contrast to small molecule

degraders, molecular glues mainly interact with an E3 ubiquitin ligase altering its substrate specificity and thereby inducing neo-substrate degradation.[198] The most noted molecular glues are the IMiDs (immunomodulatory imide drugs) such as thalidomide which bind to the substrate receptor cereblon (CRBN). CRBN is part of the CRL complex and the interaction with thalidomide changes the substrate recognition pocket of CRBN and, thus, elevates the degradation of transcription factors Ikaros and Aiolos.[200]

iDeg-1 is a new chemotype identified as a single-ligand molecule that binds to IDO1 and induces its degradation by hijacking a E3 ligase that acts independent of NEDD8. Based on the presented experimental data in this thesis combined with the classification from literature, it is not clear yet, if iDeg-1 is a small molecule degrader or might acts as a molecular glue. The small molecule clearly interacts with IDO1, however, an enhanced interaction of IDO1 with an E3 or substrate receptor in the presence of iDeg-1 could not be identified by immunoprecipitation. To prove the mode of action of iDeg-1, the identification of the involved E3 is essential as well as interaction studies of E3, IDO1 and iDeg-1.

The third class of molecules for TPD are bifunctional molecules containing a functional group that binds to the E3 ligase and one that binds to the target protein generating a chimeric molecule (Figure 6.2). The close proximity of the target protein to the E3 induces target ubiquitination and degradation.[198] To date, the so-called PROTACs, proteolysis-targeting chimera are extensively used to induce degradation of diverse proteins, such as transcription factors and kinases.[179, 201] In 2019, the first PROTAC for targeted degradation of the androgen receptor entered the clinic for the treatment of metastatic castration-resistant prostate cancer.[202] Most developed PROTACs connect the IMiDs, which bind to the substrate receptor CRBN, with a binder for a protein of interest.[197] The protein of interest can be any protein for which a small molecule binder is available which makes this technique an extremely attractive tool as available building blocks can be combined in any way needed.[179, 197, 198, 203, 204] The toolbox of bifunctional molecules is rapidly expanding and not only the UPS is exploited for protein degradation by means of PROTACs anymore. Similar strategies use autophagy degradation pathways by autophagy-targeting chimera molecules (AUTAC) or the lysosomal degradation pathway by lysosome-targeting chimera (LYTAC).[197]

Accordingly, a PROTAC was developed to degrade cellular IDO1. The known IDO1 inhibitor epacadostat was linked to the small molecule lenalidomide, which binds to CRBN and mediates IDO1 degradation via the cullin-RING E3 complex 4 ($Cul4^{CRBN}$). The IDO1-specific PROTAC showed effective degradation of IDO1 with a maximal degradation (D_{max}) of 93 %

and half-maximal degrading concentration DC_{50} of 2.84 µM in IFNγ-(5 ng/mL) stimulated HeLa cells after 24 h.[204]

The small molecule degrader iDeg-1 displays higher potency with a DC_{50} of 0.36 µM in IFNγ-stimulated (50 ng/mL) BxPC3 cells after 24 h, but the D_{max} is substantially lower with 54 %. However, comparing two different cell lines with a 10-fold difference in the IFNγ concentration used for IDO1 expression might be not appropriate. Moreover, IDO1's half-life is rather short and high IDO1 expression levels induced by a high concentration of IFNγ may mask degradation strength. A clear advantage of iDeg-1 compared to the PROTAC is the molecular weight as bifunctional molecules exhibit a higher molecular weight which leads to reduced cellular permeability. Low cell permeability might account for the high DC_{50} value compared to inhibitory potency of epacadostat alone.[204] Moreover, the epacadostat-based PROTAC binds substrate-competitive to IDO1 and, hence, presumably only degrades holo-IDO1.[113] Nevertheless, IDO1 as signaling molecule is enzymatically inactive due conformational changes within the substrate binding pocket and therefore, epacadostat might not be able to bind to IDO1 anymore.[195] In contrast, the here presented results demonstrate that iDeg-1 does not bind substrate competitive to IDO1 as no enzymatic inhibition is observed. Furthermore, the findings during the dissertation strongly indicate that iDeg-1 binds to apo-IDO1 to induce IDO1 degradation. Therefore, the utilization of iDeg-1 might be highly beneficial to reduce IDO1 signaling in pDC cells and thereby restore anti-tumor immunity. Experimental work is ongoing to investigate this hypothesis. Moreover, crystallization studies will be performed to analyze the binding mode of iDeg-1 to IDO1.

So far, intensive research on the role of IDO1 in DCs and pDCs was conducted and collectively highlights the potential of reducing IDO1 protein levels in pDCs to disrupt IDO1 self-amplification, reduce the tolerogenic phenotype of DCs and, thus, elevate antitumor immunity.[42, 68, 194] siRNA-mediated IDO1 silencing in DCs enhanced the antitumor effect of DC-based therapy against immunogenic tumors in mice.[205] Moreover, the small molecule, indoximod (1-methyl-D-tryptophan) which modulates the Kyn signaling pathway but not IDO1 enzymatic activity, also effected IDO1 expression in DC. Indoximod downregulates IDO1 protein expression in DCs with an IC_{50} of 20 µM and reduces the regulatory phenotype of DCs (similar trends were observed for pDCs).[39, 68] Furthermore, indoximod was able to mediate T cell proliferation by opposing L-Trp deprivation-mediated mTORC1-activation. In summary, indoximod exhibits various Kyn pathway inhibitory functions by blocking both, the enzymatic effects of L-Trp depletion and Kyn accumulation as well as the non-enzymatic signaling function of IDO1.[68] Phase II clinical trials in patients with advanced melanoma displayed enhanced antitumor efficacy of indoximod in combination with anti-PD1 antibody

pembrolizumab when compared to pembrolizumab alone.[69] Nonetheless, it might be of high interest to investigate the influence of iDeg-1 in comparison to indoximod on pDC.

To conclude, with the identification of iDeg-1 the TPD toolkit has now been expanded by a monovalent small-molecule degrader for IDO1. Furthermore, the discussed findings indicate that the degradation of IDO1 in DCs as well as in cancer cells might be highly beneficial for treatment approaches to enhance anti-tumor immunity. Hence, it provides an alternative approach to downregulate IDO1 activity in cells. Moreover, iDeg-1 might contribute to deepen the understanding of IDO1 as signaling molecule in tolerance and immunity.

7. Perspective

Herein, two forward chemical genetic screening assays were developed: The NK cell-mediated cancer cell cytolysis assay and the Kyn assay. Both assays were designed to closely mimic the respective disease phenotype and they led to the identification of several bioactive immunomodulatory small molecules.

Among the small molecules identified in the NK cell-mediated cancer cell cytolysis assay were inhibitors targeting the autophagy related PI3K kinase, VPS34. VPS34 activity has neither been linked to NK cell suppression nor to the maintenance of NK cell activity before. Hence, follow up studies should be performed to investigate autophagy in NK cells and the influence of TGFβ and PGE2. Furthermore, a few novel chemotypes were found to stimulate NK cell activity. Their respective targets and modes of action are yet to be elucidated.

Secondly, the Kyn assay identified the small molecule iDeg-1 which bind to IDO1 and induce its degradation. It was found that iDeg-1 presumably interact with apo-IDO1. To confirm this assumption, co-crystallization of IDO1 and iDeg-1 should be performed. Moreover, the crystal structure will reveal the exact binding configuration of iDeg-1 in IDO1 which should be used to chemically optimize the compound to obtain derivatives that degrade IDO1 with higher potency. Furthermore, as iDeg-1 most likely interact with apo-IDO1, which fulfils signaling functions in e.g. dendritic cells, the influence of iDeg-1 on IDO1-mediated immune cell signaling should be investigated. In addition, it remains to be elucidated if iDeg-1 acts as a molecular glue or a small molecule degrader. To further unravel the MoA of iDeg-1 the identification of respective E3 ligase is critical. For this, candidate proteins identified in the siRNA screen should be validated for their involvement in iDeg-1-mediated IDO1 degradation by investigating IDO1 protein levels instead of the Kyn assay. Therefore, either siRNA-mediated knockdown of the respective proteins can be performed or knockout cell lines can be used. Once the E3 ligase responsible for iDeg-1-induced IDO1 degradation is identified, interaction studies should be performed to elucidate if iDeg-1 may induce the interaction between IDO1 and the E3 ligase. In case the interaction between IDO1 and the E3 ligase is promoted in the presence of iDeg-1, the compound acts as a molecular glue. If iDeg-1 does not increase the interaction, the compound is more likely a small molecule degrader. Moreover, iDeg-1 should be investigated for its potential to degrade TDO and IDO2 as IDO1s' isoform IDO2 as well as TDO also contribute to L-Trp depletion and show structural similarities.

Altogether, the obtained results in the curse of this thesis demonstrates that phenotypic assays are powerful tools to discover new drug targets and alternative mechanisms of action to revert

a disease phenotype. Thus, phenotypic assays deepen our understanding of cancer immunosuppression and may pave the way for the development of novel cancer immunotherapies.

8. References

1.	Brown, G. C., Living too long: the current focus of medical research on increasing the quantity, rather than the quality, of life is damaging our health and harming the economy. *EMBO reports* **2015,** *16* (2), 137-141.

2.	Sung, H.; Ferlay, J.; Siegel, R. L.; Laversanne, M.; Soerjomataram, I.; Jemal, A.; Bray, F., Global Cancer Statistics 2020: GLOBOCAN Estimates of Incidence and Mortality Worldwide for 36 Cancers in 185 Countries. *CA Cancer J Clin* **2021,** *71* (3), 209-249.

3.	Brenner, H., Long-term survival rates of cancer patients achieved by the end of the 20th century: a period analysis. *Lancet* **2002,** *360* (9340), 1131-5.

4.	Wang, S.; Xie, K.; Liu, T., Cancer Immunotherapies: From Efficacy to Resistance Mechanisms - Not Only Checkpoint Matters. *Front Immunol* **2021,** *12*, 690112.

5.	Nicholson, Lindsay B., The immune system. *Essays in Biochemistry* **2016,** *60* (3), 275-301.

6.	Zwirner, N. W.; Domaica, C. I., Cytokine regulation of natural killer cell effector functions. *BioFactors* **2010,** *36* (4), 274-288.

7.	Prager, I.; Liesche, C.; van Ooijen, H.; Urlaub, D.; Verron, Q.; Sandström, N.; Fasbender, F.; Claus, M.; Eils, R.; Beaudouin, J.; Önfelt, B.; Watzl, C., NK cells switch from granzyme B to death receptor–mediated cytotoxicity during serial killing. *Journal of Experimental Medicine* **2019,** *216* (9), 2113-2127.

8.	Schreiber, R. D.; Old, L. J.; Smyth, M. J., Cancer Immunoediting: Integrating Immunity's Roles in Cancer Suppression and Promotion. *Science* **2011,** *331* (6024), 1565-1570.

9.	van der Burg, S. H.; Arens, R.; Ossendorp, F.; van Hall, T.; Melief, C. J. M., Vaccines for established cancer: overcoming the challenges posed by immune evasion. *Nature Reviews Cancer* **2016,** *16* (4), 219-233.

10.	Rabinovich, G. A.; Gabrilovich, D.; Sotomayor, E. M., Immunosuppressive strategies that are mediated by tumor cells. *Annu Rev Immunol* **2007,** *25*, 267-296.

11.	Villalba, M.; Rathore, M. G.; Lopez-Royuela, N.; Krzywinska, E.; Garaude, J.; Allende-Vega, N., From tumor cell metabolism to tumor immune escape. *The International Journal of Biochemistry & Cell Biology* **2013,** *45* (1), 106-113.

12.	Hanahan, D.; Weinberg, Robert A., Hallmarks of Cancer: The Next Generation. *Cell* **2011,** *144* (5), 646-674.

13.	Anderson, N. M.; Simon, M. C., The tumor microenvironment. *Current Biology* **2020,** *30* (16), R921-R925.

14.	Adams, J. L.; Smothers, J.; Srinivasan, R.; Hoos, A., Big opportunities for small molecules in immuno-oncology. *Nat Rev Drug Discov* **2015,** *14* (9), 603-22.

15.	Kiessling, R.; Klein, E.; Wigzell, H., "Natural" killer cells in the mouse. I. Cytotoxic cells with specificity for mouse Moloney leukemia cells. Specificity and distribution according to genotype. *Eur J Immunol* **1975,** *5* (2), 112-7.

16.	Watzl, C., Chapter Five - How to Trigger a Killer: Modulation of Natural Killer Cell Reactivity on Many Levels. In *Advances in Immunology*, Alt, F. W., Ed. Academic Press: 2014; Vol. 124, pp 137-170.

17.	Domagala, J.; Lachota, M.; Klopotowska, M.; Graczyk-Jarzynka, A.; Domagala, A.; Zhylko, A.; Soroczynska, K.; Winiarska, M., The Tumor Microenvironment—A Metabolic Obstacle to NK Cells' Activity. *Cancers* **2020,** *12* (12), 3542.

18.	Viel, S.; Marçais, A.; Guimaraes, F. S.-F.; Loftus, R.; Rabilloud, J.; Grau, M.; Degouve, S.; Djebali, S.; Sanlaville, A.; Charrier, E.; Bienvenu, J.; Marie, J. C.; Caux, C.; Marvel, J.; Town, L.; Huntington, N. D.; Bartholin, L.; Finlay, D.; Smyth, M. J.; Walzer, T., TGFbeta inhibits the activation and functions of NK cells by repressing the mTOR pathway. *Science Signaling* **2016,** *9* (415), ra19.

19.	Castro, F.; Cardoso, A. P.; Goncalves, R. M.; Serre, K.; Oliveira, M. J., Interferon-Gamma at the Crossroads of Tumor Immune Surveillance or Evasion. *Front Immunol* **2018,** *9*, 847.

20.	Textor, S.; Dürst, M.; Jansen, L.; Accardi, R.; Tommasino, M.; Trunk, M. J.; Porgador, A.; Watzl, C.; Gissmann, L.; Cerwenka, A., Activating NK cell receptor ligands are differentially expressed during progression to cervical cancer. *International Journal of Cancer* **2008,** *123* (10), 2343-2353.

21.	Prager, I.; Watzl, C., Mechanisms of natural killer cell-mediated cellular cytotoxicity. *J Leukoc Biol* **2019,** *105* (6), 1319-1329.

22.	Joshi, P. C.; Zhou, X.; Cuchens, M.; Jones, Q., Prostaglandin E2 suppressed IL-15-mediated human NK cell function through down-regulation of common gamma-chain. *J Immunol* **2001,** *166* (2), 885-91.

23.	Drake, C. G.; Jaffee, E.; Pardoll, D. M., Mechanisms of immune evasion by tumors. *Adv Immunol* **2006,** *90*, 51-81.

24.		Holt, D.; Ma, X.; Kundu, N.; Fulton, A., Prostaglandin E(2) (PGE (2)) suppresses natural killer cell function primarily through the PGE(2) receptor EP4. *Cancer Immunol Immunother* **2011,** *60* (11), 1577-86.

25.		Ma, X.; Holt, D.; Kundu, N.; Reader, J.; Goloubeva, O.; Take, Y.; Fulton, A. M., A prostaglandin E (PGE) receptor EP4 antagonist protects natural killer cells from PGE2-mediated immunosuppression and inhibits breast cancer metastasis. *OncoImmunology* **2013,** *2* (1), e22647.

26.		Park, A.; Lee, Y.; Kim, M. S.; Kang, Y. J.; Park, Y. J.; Jung, H.; Kim, T. D.; Lee, H. G.; Choi, I.; Yoon, S. R., Prostaglandin E2 Secreted by Thyroid Cancer Cells Contributes to Immune Escape Through the Suppression of Natural Killer (NK) Cell Cytotoxicity and NK Cell Differentiation. *Front Immunol* **2018,** *9,* 1859.

27.		Du, N.; Guo, F.; Wang, Y.; Cui, J., NK Cell Therapy: A Rising Star in Cancer Treatment. *Cancers* **2021,** *13* (16), 4129.

28.		Ball, H. J.; Jusof, F. F.; Bakmiwewa, S. M.; Hunt, N. H.; Yuasa, H. J., Tryptophan-catabolizing enzymes - party of three. *Front Immunol* **2014,** *5,* 485.

29.		Pallotta, M. T.; Rossini, S.; Suvieri, C.; Coletti, A.; Orabona, C.; Macchiarulo, A.; Volpi, C.; Grohmann, U., Indoleamine 2,3-dioxygenase 1 (IDO1): an up-to-date overview of an eclectic immunoregulatory enzyme. *The FEBS Journal* **2021**.

30.		Munn, D. H.; Zhou, M.; Attwood, J. T.; Bondarev, I.; Conway, S. J.; Marshall, B.; Brown, C.; Mellor, A. L., Prevention of Allogeneic Fetal Rejection by Tryptophan Catabolism. *Science* **1998,** *281* (5380), 1191-1193.

31.		Mellor, A. L.; Munn, D. H., Tryptophan catabolism and T-cell tolerance: immunosuppression by starvation? *Immunology Today* **1999,** *20* (10), 469-473.

32.		Godin-Ethier, J.; Pelletier, S.; Hanafi, L. A.; Gannon, P. O.; Forget, M. A.; Routy, J. P.; Boulassel, M. R.; Krzemien, U.; Tanguay, S.; Lattouf, J. B.; Arbour, N.; Lapointe, R., Human activated T lymphocytes modulate IDO expression in tumors through Th1/Th2 balance. *J Immunol* **2009,** *183* (12), 7752-60.

33.		Théate, I.; van Baren, N.; Pilotte, L.; Moulin, P.; Larrieu, P.; Renauld, J. C.; Hervé, C.; Gutierrez-Roelens, I.; Marbaix, E.; Sempoux, C.; Van den Eynde, B. J., Extensive profiling of the expression of the indoleamine 2,3-dioxygenase 1 protein in normal and tumoral human tissues. *Cancer Immunol Res* **2015,** *3* (2), 161-72.

34.		Nelp, M. T.; Kates, P. A.; Hunt, J. T.; Newitt, J. A.; Balog, A.; Maley, D.; Zhu, X.; Abell, L.; Allentoff, A.; Borzilleri, R.; Lewis, H. A.; Lin, Z.; Seitz, S. P.; Yan, C.; Groves, J. T., Immune-modulating enzyme indoleamine 2,3-dioxygenase is effectively inhibited by targeting its apo-form. *Proc Natl Acad Sci U S A* **2018,** *115* (13), 3249-3254.

35.		Pradhan, N.; Akhtar, N.; Nath, B.; Pena-Garcia, J.; Gupta, A.; Perez-Sanchez, H.; Kumar, S.; Manna, D., Inhibition of immunosuppressive indoleamine 2,3-dioxygenase by targeting the heme and apo-form. *Chem Commun (Camb)* **2021,** *57* (3), 395-398.

36.		Pallotta, M. T.; Orabona, C.; Volpi, C.; Vacca, C.; Belladonna, M. L.; Bianchi, R.; Servillo, G.; Brunacci, C.; Calvitti, M.; Bicciato, S.; Mazza, E. M. C.; Boon, L.; Grassi, F.; Fioretti, M. C.; Fallarino, F.; Puccetti, P.; Grohmann, U., Indoleamine 2,3-dioxygenase is a signaling protein in long-term tolerance by dendritic cells. *Nature Immunology* **2011,** *12* (9), 870-878.

37.		Prendergast, G. C.; Malachowski, W. P.; DuHadaway, J. B.; Muller, A. J., Discovery of IDO1 Inhibitors: From Bench to Bedside. *Cancer Res* **2017,** *77* (24), 6795-6811.

38.		Tang, K.; Wu, Y.-H.; Song, Y.; Yu, B., Indoleamine 2,3-dioxygenase 1 (IDO1) inhibitors in clinical trials for cancer immunotherapy. *Journal of Hematology & Oncology* **2021,** *14* (1), 68.

39.		Chen, W.; Liang, X.; Peterson, A. J.; Munn, D. H.; Blazar, B. R., The indoleamine 2,3-dioxygenase pathway is essential for human plasmacytoid dendritic cell-induced adaptive T regulatory cell generation. *J Immunol* **2008,** *181* (8), 5396-404.

40.		Chen, W., IDO: more than an enzyme. *Nature Immunology* **2011,** *12* (9), 809-811.

41.		Mellor, A. L.; Munn, D. H., Ido expression by dendritic cells: tolerance and tryptophan catabolism. *Nature Reviews Immunology* **2004,** *4* (10), 762-774.

42.		Fallarino, F.; Grohmann, U.; Puccetti, P., Indoleamine 2,3-dioxygenase: from catalyst to signaling function. *Eur J Immunol* **2012,** *42* (8), 1932-7.

43.		Dolšak, A.; Gobec, S.; Sova, M., Indoleamine and tryptophan 2,3-dioxygenases as important future therapeutic targets. *Pharmacology & Therapeutics* **2021,** *221,* 107746.

44.		Ehrlich, P. R., *The Collected Papers of Paul Ehrlich*. Pergamon Press: 1956; Vol. 1.

45.		Barbari, C.; Fontaine, T.; Parajuli, P.; Lamichhane, N.; Jakubski, S.; Lamichhane, P.; Deshmukh, R. R., Immunotherapies and Combination Strategies for Immuno-Oncology. *International journal of molecular sciences* **2020,** *21* (14), 5009.

46.   Parry, R. V.; Chemnitz, J. M.; Frauwirth, K. A.; Lanfranco, A. R.; Braunstein, I.; Kobayashi, S. V.; Linsley, P. S.; Thompson, C. B.; Riley, J. L., CTLA-4 and PD-1 receptors inhibit T-cell activation by distinct mechanisms. *Mol Cell Biol* **2005,** *25* (21), 9543-9553.

47.   The Nobel Prize in Physiology or Medicine 2018. NobelPrize.org. Nobel Prize Outreach AB 2022. Fri. 7 Jan 2022. <https://www.nobelprize.org/prizes/medicine/2018/summary/>

48.   Robert, C., A decade of immune-checkpoint inhibitors in cancer therapy. *Nature Communications* **2020,** *11* (1), 3801.

49.   Mohr, R.; Jost-Brinkmann, F.; Ozdirik, B.; Lambrecht, J.; Hammerich, L.; Loosen, S. H.; Luedde, T.; Demir, M.; Tacke, F.; Roderburg, C., Lessons From Immune Checkpoint Inhibitor Trials in Hepatocellular Carcinoma. *Front Immunol* **2021,** *12*, 652172.

50.   Gardner, T.; Elzey, B.; Hahn, N. M., Sipuleucel-T (Provenge) autologous vaccine approved for treatment of men with asymptomatic or minimally symptomatic castrate-resistant metastatic prostate cancer. *Human Vaccines & Immunotherapeutics* **2012,** *8* (4), 534-539.

51.   Nair, R.; Westin, J., CAR T-Cells. *Adv Exp Med Biol* **2020,** *1244*, 215-233.

52.   Phelps, M. A., Rituximab immunotherapy: it's getting personal. *Blood* **2017,** *129* (19), 2595-2596.

53.   Cheng, M.; Chen, Y.; Xiao, W.; Sun, R.; Tian, Z., NK cell-based immunotherapy for malignant diseases. *Cellular & Molecular Immunology* **2013,** *10* (3), 230-252.

54.   Achkar, T.; Arjunan, A.; Wang, H.; Saul, M.; Davar, D.; Appleman, L. J.; Friedland, D.; Parikh, R. A., High-dose interleukin 2 in patients with metastatic renal cell carcinoma with sarcomatoid features. *PLOS ONE* **2017,** *12* (12), e0190084.

55.   Sendker, S.; Reinhardt, D.; Niktoreh, N., Redirecting the Immune Microenvironment in Acute Myeloid Leukemia. *Cancers (Basel)* **2021,** *13* (6).

56.   Otegbeye, F.; Ojo, E.; Moreton, S.; Mackowski, N.; Lee, D. A.; de Lima, M.; Wald, D. N., Inhibiting TGF-beta signaling preserves the function of highly activated, in vitro expanded natural killer cells in AML and colon cancer models. *PLoS One* **2018,** *13* (1), e0191358.

57.   Prendergast, G. C.; Smith, C.; Thomas, S.; Mandik-Nayak, L.; Laury-Kleintop, L.; Metz, R.; Muller, A. J., Indoleamine 2,3-dioxygenase pathways of pathogenic inflammation and immune escape in cancer. *Cancer Immunol Immunother* **2014,** *63* (7), 721-35.

58.   Muller, A. J.; Manfredi, M. G.; Zakharia, Y.; Prendergast, G. C., Inhibiting IDO pathways to treat cancer: lessons from the ECHO-301 trial and beyond. *Semin Immunopathol* **2019,** *41* (1), 41-48.

59.   Wang, X. X.; Sun, S. Y.; Dong, Q. Q.; Wu, X. X.; Tang, W.; Xing, Y. Q., Recent advances in the discovery of indoleamine 2,3-dioxygenase 1 (IDO1) inhibitors. *Medchemcomm* **2019,** *10* (10), 1740-1754.

60.   Rohrig, U. F.; Majjigapu, S. R.; Vogel, P.; Zoete, V.; Michielin, O., Challenges in the Discovery of Indoleamine 2,3-Dioxygenase 1 (IDO1) Inhibitors. *J Med Chem* **2015,** *58* (24), 9421-37.

61.   Nelp, M. T.; Kates, P. A.; Hunt, J. T.; Newitt, J. A.; Balog, A.; Maley, D.; Zhu, X.; Abell, L.; Allentoff, A.; Borzilleri, R.; Lewis, H. A.; Lin, Z.; Seitz, S. P.; Yan, C.; Groves, J. T., Immune-modulating enzyme indoleamine 2,3-dioxygenase is effectively inhibited by targeting its apo-form. *Proceedings of the National Academy of Sciences* **2018,** *115* (13), 3249-3254.

62.   Ortiz-Meoz, R. F.; Wang, L.; Matico, R.; Rutkowska-Klute, A.; De la Rosa, M.; Bedard, S.; Midgett, R.; Strohmer, K.; Thomson, D.; Zhang, C.; Mebrahtu, M.; Guss, J.; Totoritis, R.; Consler, T.; Campobasso, N.; Taylor, D.; Lewis, T.; Weaver, K.; Muelbaier, M.; Seal, J.; Dunham, R.; Kazmierski, W.; Favre, D.; Bergamini, G.; Shewchuk, L.; Rendina, A.; Zhang, G., Characterization of Apo-Form Selective Inhibition of Indoleamine 2,3-Dioxygenase**. *ChemBioChem* **2020,** *21* (n/a), 1-8.

63.   Hennes, E.; Lampe, P.; Dötsch, L.; Bruning, N.; Pulvermacher, L.-M.; Sievers, S.; Ziegler, S.; Waldmann, H., Cell-Based Identification of New IDO1 Modulator Chemotypes. *Angewandte Chemie (International ed. in English)* **2021,** *60* (18), 9869-9874.

64.   Markwalder, J. A.; Seitz, S. P.; Blat, Y.; Elkin, L.; Hunt, J. T.; Pabalan, J. G.; Jure-Kunkel, M. N.; Vite, G. D.; Covello, K., Identification and optimization of a novel series of indoleamine 2,3-dioxygenase inhibitors. *Bioorganic & Medicinal Chemistry Letters* **2017,** *27* (3), 582-585.

65.   Eynde, B. J. V. d.; Baren, N. v.; Baurain, J.-F., Is There a Clinical Future for IDO1 Inhibitors After the Failure of Epacadostat in Melanoma? *Annual Review of Cancer Biology* **2020,** *4* (1), 241-256.

66.   Beatty, G. L.; O'Dwyer, P. J.; Clark, J.; Shi, J. G.; Bowman, K. J.; Scherle, P. A.; Newton, R. C.; Schaub, R.; Maleski, J.; Leopold, L.; Gajewski, T. F., First-in-Human Phase I Study of the Oral Inhibitor of Indoleamine 2,3-Dioxygenase-1 Epacadostat (INCB024360) in Patients with Advanced Solid Malignancies. *Clinical Cancer Research* **2017,** *23* (13), 3269-3276.

67.   Opitz, C. A.; Somarribas Patterson, L. F.; Mohapatra, S. R.; Dewi, D. L.; Sadik, A.; Platten, M.; Trump, S., The therapeutic potential of targeting tryptophan catabolism in cancer. *British Journal of Cancer* **2020,** *122* (1), 30-44.

68.   Brincks, E. L.; Adams, J.; Wang, L.; Turner, B.; Marcinowicz, A.; Ke, J.; Essmann, M.; Mautino, L. M.; Allen, C. V.; Kumar, S.; Vahanian, N.; Link, C.; Mautino, M. R., Indoximod opposes the immunosuppressive effects mediated by IDO and TDO via modulation of AhR function and activation of mTORC1. *Oncotarget* **2020,** *11* (25), 2438-2461.

69.   Zakharia, Y.; McWilliams, R. R.; Rixe, O.; Drabick, J.; Shaheen, M. F.; Grossmann, K. F.; Kolhe, R.; Pacholczyk, R.; Sadek, R.; Tennant, L. L.; Smith, C. M.; Kennedy, E. P.; Link, C. J., Jr.; Vahanian, N. N.; Yu, J.; Shen, S. S.; Brincks, E. L.; Rossi, G. R.; Munn, D.; Milhem, M., Phase II trial of the IDO pathway inhibitor indoximod plus pembrolizumab for the treatment of patients with advanced melanoma. *J Immunother Cancer* **2021,** *9* (6).

70.   Spring, D. R., Chemical genetics to chemical genomics: small molecules offer big insights. *Chem Soc Rev* **2005,** *34* (6), 472-82.

71.   Choi, H.; Kim, J. Y.; Chang, Y. T.; Nam, H. G., Forward chemical genetic screening. *Methods Mol Biol* **2014,** *1062*, 393-404.

72.   Horton, B., Developing 'chemical genetics'. *Nature* **1998,** *391* (6669), 819-819.

73.   Schreiber, S. L., The small-molecule approach to biology. *C & E N* **2003,** *81* (9), 9.

74.   Lehár, J.; Stockwell, B. R.; Giaever, G.; Nislow, C., Combination chemical genetics. *Nature Chemical Biology* **2008,** *4* (11), 674-681.

75.   Gashaw, I.; Ellinghaus, P.; Sommer, A.; Asadullah, K., What makes a good drug target? *Drug Discovery Today* **2011,** *16* (23), 1037-1043.

76.   Croston, G. E., The utility of target-based discovery. *Expert Opinion on Drug Discovery* **2017,** *12* (5), 427-429.

77.   Eggert, U. S., The why and how of phenotypic small-molecule screens. *Nature Chemical Biology* **2013,** *9* (4), 206-209.

78.   Shangguan, Z., A Review of Target Identification Strategies for Drug Discovery: from Database to Machine-Based Methods. *J. Phys.: Conf. Ser* **2021,** *1893* (012013).

79.   Ziegler, S.; Pries, V.; Hedberg, C.; Waldmann, H., Target Identification for Small Bioactive Molecules: Finding the Needle in the Haystack. *Angewandte Chemie International Edition* **2013,** *52* (10), 2744-2792.

80.   Comess, K. M.; McLoughlin, S. M.; Oyer, J. A.; Richardson, P. L.; Stöckmann, H.; Vasudevan, A.; Warder, S. E., Emerging Approaches for the Identification of Protein Targets of Small Molecules - A Practitioners' Perspective. *J Med Chem* **2018,** *61* (19), 8504-8535.

81.   Heilker, R.; Lessel, U.; Bischoff, D., The power of combining phenotypic and target-focused drug discovery. *Drug Discov Today* **2019,** *24* (2), 526-532.

82.   Vincent, F.; Loria, P.; Pregel, M.; Stanton, R.; Kitching, L.; Nocka, K.; Doyonnas, R.; Steppan, C.; Gilbert, A.; Schroeter, T.; Peakman, M. C., Developing predictive assays: the phenotypic screening "rule of 3". *Sci Transl Med* **2015,** *7* (293), 293ps15.

83.   Chau, V.; Tobias, J. W.; Bachmair, A.; Marriott, D.; Ecker, D. J.; Gonda, D. K.; Varshavsky, A., A Multiubiquitin Chain Is Confined to Specific Lysine in a Targeted Short-Lived Protein. *Science* **1989,** *243* (4898), 1576-1583.

84.   Zhang, J. H.; Chung, T. D.; Oldenburg, K. R., A Simple Statistical Parameter for Use in Evaluation and Validation of High Throughput Screening Assays. *J Biomol Screen* **1999,** *4* (2), 67-73.

85.   Petrovic, A.; Mosalaganti, S.; Keller, J.; Mattiuzzo, M.; Overlack, K.; Krenn, V.; De Antoni, A.; Wohlgemuth, S.; Cecatiello, V.; Pasqualato, S.; Raunser, S.; Musacchio, A., Modular assembly of RWD domains on the Mis12 complex underlies outer kinetochore organization. *Mol Cell* **2014,** *53* (4), 591-605.

86.   Barnes, N. A.; Stephenson, S. J.; Tooze, R. M.; Doody, G. M., Amino acid deprivation links BLIMP-1 to the immunomodulatory enzyme indoleamine 2,3-dioxygenase. *J Immunol* **2009,** *183* (9), 5768-77.

87.   Klockow, J. L.; Glass, T. E., Development of a Fluorescent Chemosensor for the Detection of Kynurenine. *Organic Letters* **2013,** *15* (2), 235-237.

88.   Xiao, C.; Chen, Y.; Liang, X.; Xie, Z.; Zhang, M.; Li, R.; Li, Z.; Fu, X.; Yu, X.; Shi, W., A modified HPLC method improves the simultaneous determination of plasma kynurenine and tryptophan concentrations in patients following maintenance hemodialysis. *Exp Ther Med* **2014,** *7* (4), 907-910.

89.   Tyanova, S.; Temu, T.; Sinitcyn, P.; Carlson, A.; Hein, M. Y.; Geiger, T.; Mann, M.; Cox, J., The Perseus computational platform for comprehensive analysis of (prote)omics data. *Nat Methods* **2016,** *13* (9), 731-40.

90.   Livak, K. J.; Schmittgen, T. D., Analysis of relative gene expression data using real-time quantitative PCR and the 2(-Delta Delta C(T)) Method. *Methods* **2001,** *25* (4), 402-8.

91.   Lewis-Ballester, A.; Pham, K. N.; Batabyal, D.; Karkashon, S.; Bonanno, J. B.; Poulos, T. L.; Yeh, S. R., Structural insights into substrate and inhibitor binding sites in human indoleamine 2,3-dioxygenase 1. *Nat Commun* **2017,** *8* (1), 1693.

92.   Terentis, A. C.; Thomas, S. R.; Takikawa, O.; Littlejohn, T. K.; Truscott, R. J.; Armstrong, R. S.; Yeh, S. R.; Stocker, R., The heme environment of recombinant human indoleamine 2,3-dioxygenase. Structural properties and substrate-ligand interactions. *J Biol Chem* **2002,** *277* (18), 15788-94.

93.   Liu, J.; Sun, Y. Q.; Huo, Y.; Zhang, H.; Wang, L.; Zhang, P.; Song, D.; Shi, Y.; Guo, W., Simultaneous fluorescence sensing of Cys and GSH from different emission channels. *J Am Chem Soc* **2014,** *136* (2), 574-7.

94.   Dunkley, M.; Miller, R. G.; Shortman, K., A modified 51Cr release assay for cytotoxic lymphocytes. *Journal of Immunological Methods* **1974,** *6* (1), 39-51.

95.   Mou, X.; Zhou, Y.; Jiang, P.; Zhou, T.; Jiang, Q.; Xu, C.; Liu, H.; Zheng, T.; Yuan, G.; Zhang, Y.; Chen, D.; Mao, C., The regulatory effect of UL-16 binding protein-3 expression on the cytotoxicity of NK cells in cancer patients. *Sci Rep* **2014,** *4*, 6138.

96.   Viel, S.; Marçais, A.; Guimaraes, F. S.-F.; Loftus, R.; Rabilloud, J.; Grau, M.; Degouve, S.; Djebali, S.; Sanlaville, A.; Charrier, E.; Bienvenu, J.; Marie, J. C.; Caux, C.; Marvel, J.; Town, L.; Huntington, N. D.; Bartholin, L.; Finlay, D.; Smyth, M. J.; Walzer, T., TGFbeta inhibits the activation and functions of NK cells by repressing the mTOR pathway. *Science Signaling* **2016,** *9* (415), ra19-ra19.

97.   Wilson, E. B.; El-Jawhari, J. J.; Neilson, A. L.; Hall, G. D.; Melcher, A. A.; Meade, J. L.; Cook, G. P., Human tumour immune evasion via TGF-beta blocks NK cell activation but not survival allowing therapeutic restoration of anti-tumour activity. *PLoS One* **2011,** *6* (9), e22842.

98.   Kopp, H. G.; Placke, T.; Salih, H. R., Platelet-derived transforming growth factor-beta down-regulates NKG2D thereby inhibiting natural killer cell antitumor reactivity. *Cancer Res* **2009,** *69* (19), 7775-83.

99.   Slattery, K.; Woods, E.; Zaiatz-Bittencourt, V.; Marks, S.; Chew, S.; Conroy, M.; Goggin, C.; MacEochagain, C.; Kennedy, J.; Lucas, S.; Finlay, D. K.; Gardiner, C. M., TGFbeta drives NK cell metabolic dysfunction in human metastatic breast cancer. *J Immunother Cancer* **2021,** *9* (2).

100.   Van Elssen, C. H.; Vanderlocht, J.; Oth, T.; Senden-Gijsbers, B. L.; Germeraad, W. T.; Bos, G. M., Inflammation-restraining effects of prostaglandin E2 on natural killer-dendritic cell (NK-DC) interaction are imprinted during DC maturation. *Blood* **2011,** *118* (9), 2473-82.

101.   Frauwirth, K. A.; Thompson, C. B., Activation and inhibition of lymphocytes by costimulation. *Journal of Clinical Investigation* **2002,** *109* (3), 295-299.

102.   LeBien, T. W.; Tedder, T. F., B lymphocytes: how they develop and function. *Blood* **2008,** *112* (5), 1570-1580.

103.   Elena Kokuina, M. C. B.-F., Carlos A. Villegas-Valverde, Isabel Mora-Díaz Normal Values of T, B and NK Lymphocyte Subpopulations
in Peripheral Blood of Healthy Cuban Adults. *MEDICC Review* **2019,** *21* (2-3), 6.

104.   Gellibert, F.; Woolven, J.; Fouchet, M.-H.; Mathews, N.; Goodland, H.; Lovegrove, V.; Laroze, A.; Nguyen, V.-L.; Sautet, S.; Wang, R.; Janson, C.; Smith, W.; Krysa, G.; Boullay, V.; de Gouville, A.-C.; Huet, S.; Hartley, D., Identification of 1,5-Naphthyridine Derivatives as a Novel Series of Potent and Selective TGF-β Type I Receptor Inhibitors. *Journal of Medicinal Chemistry* **2004,** *47* (18), 4494-4506.

105.   Mark-Anthony Bray, A. C., Advanced Assay Development Guidelines for Image-Based High Content Screening and Analysis. In *Assay Guidance Manual*, S. Markossian, A. G., K. Brimacombe Ed. Bethesda (MD): Eli Lilly & Company and the National Center for Advancing Translational Sciences: 2004.

106.   Judson, R.; Kavlock, R.; Martin, M.; Reif, D.; Houck, K.; Knudsen, T.; Richard, A.; Tice, R. R.; Whelan, M.; Xia, M.; Huang, R.; Austin, C.; Daston, G.; Hartung, T.; Fowle, J. R., 3rd; Wooge, W.; Tong, W.; Dix, D., Perspectives on validation of high-throughput assays supporting 21st century toxicity testing. *ALTEX* **2013,** *30* (1), 51-56.

107.   Richards, T.; Brin, E., Cell based functional assays for IDO1 inhibitor screening and characterization. *Oncotarget* **2018,** *9* (56), 30814-30820.

108.   Koblish, H. K.; Hansbury, M. J.; Bowman, K. J.; Yang, G.; Neilan, C. L.; Haley, P. J.; Burn, T. C.; Waeltz, P.; Sparks, R. B.; Yue, E. W.; Combs, A. P.; Scherle, P. A.; Vaddi, K.; Fridman, J. S., Hydroxyamidine inhibitors of indoleamine-2,3-dioxygenase potently suppress systemic tryptophan catabolism and the growth of IDO-expressing tumors. *Mol Cancer Ther* **2010,** *9* (2), 489-98.

135

109.   Seegers, N.; van Doornmalen, A. M.; Uitdehaag, J. C.; de Man, J.; Buijsman, R. C.; Zaman, G. J., High-throughput fluorescence-based screening assays for tryptophan-catabolizing enzymes. *J Biomol Screen* **2014,** *19* (9), 1266-74.

110.   Munn, D. H.; Mellor, A. L., Indoleamine 2,3 dioxygenase and metabolic control of immune responses. *Trends Immunol* **2013,** *34* (3), 137-143.

111.   Thomas, S. R.; Salahifar, H.; Mashima, R.; Hunt, N. H.; Richardson, D. R.; Stocker, R., Antioxidants inhibit indoleamine 2,3-dioxygenase in IFN-gamma-activated human macrophages: posttranslational regulation by pyrrolidine dithiocarbamate. *J Immunol* **2001,** *166* (10), 6332-40.

112.   Ebert, P. S.; Hess, R. A.; Frykholm, B. C.; Tschudy, D. P., Succinylacetone, a potent inhibitor of heme biosynthesis: Effect on cell growth, heme content and δ-aminolevulinic acid dehydratase activity of malignant murine erythroleukemia cells. *Biochemical and Biophysical Research Communications* **1979,** *88* (4), 1382-1390.

113.   Rohrig, U. F.; Reynaud, A.; Majjigapu, S. R.; Vogel, P.; Pojer, F.; Zoete, V., Inhibition Mechanisms of Indoleamine 2,3-Dioxygenase 1 (IDO1). *J Med Chem* **2019,** *62* (19), 8784-8795.

114.   Austin, C. J.; Kosim-Satyaputra, P.; Smith, J. R.; Willows, R. D.; Jamie, J. F., Mutation of cysteine residues alters the heme-binding pocket of indoleamine 2,3-dioxygenase-1. *Biochem Biophys Res Commun* **2013,** *436* (4), 595-600.

115.   Hausser, J.; Mayo, A.; Keren, L.; Alon, U., Central dogma rates and the trade-off between precision and economy in gene expression. *Nat Commun* **2019,** *10* (1), 68.

116.   Su Hui Teo, C.; Serwa, R. A.; O'Hare, P., Spatial and Temporal Resolution of Global Protein Synthesis during HSV Infection Using Bioorthogonal Precursors and Click Chemistry. *PLOS Pathogens* **2016,** *12* (10), e1005927.

117.   Schneider-Poetsch, T.; Ju, J.; Eyler, D. E.; Dang, Y.; Bhat, S.; Merrick, W. C.; Green, R.; Shen, B.; Liu, J. O., Inhibition of eukaryotic translation elongation by cycloheximide and lactimidomycin. *Nat Chem Biol* **2010,** *6* (3), 209-217.

118.   Lecker, S. H.; Goldberg, A. L.; Mitch, W. E., Protein degradation by the ubiquitin-proteasome pathway in normal and disease states. *J Am Soc Nephrol* **2006,** *17* (7), 1807-19.

119.   Mondanelli, G.; Albini, E.; Pallotta, M. T.; Volpi, C.; Chatenoud, L.; Kuhn, C.; Fallarino, F.; Matino, D.; Belladonna, M. L.; Bianchi, R.; Vacca, C.; Bicciato, S.; Boon, L.; Ricci, G.; Grohmann, U.; Puccetti, P.; Orabona, C., The Proteasome Inhibitor Bortezomib Controls Indoleamine 2,3-Dioxygenase 1 Breakdown and Restores Immune Regulation in Autoimmune Diabetes. *Front Immunol* **2017,** *8*, 428.

120.   Hjerpe, R.; Aillet, F.; Lopitz-Otsoa, F.; Lang, V.; England, P.; Rodriguez, M. S., Efficient protection and isolation of ubiquitylated proteins using tandem ubiquitin-binding entities. *EMBO Rep* **2009,** *10* (11), 1250-8.

121.   Zhang, X.; Linder, S.; Bazzaro, M., Drug Development Targeting the Ubiquitin-Proteasome System (UPS) for the Treatment of Human Cancers. *Cancers (Basel)* **2020,** *12* (4).

122.   Emmerich, C. H.; Cohen, P., Optimising methods for the preservation, capture and identification of ubiquitin chains and ubiquitylated proteins by immunoblotting. *Biochem Biophys Res Commun* **2015,** *466* (1), 1-14.

123.   Kim, W.; Bennett, E. J.; Huttlin, E. L.; Guo, A.; Li, J.; Possemato, A.; Sowa, M. E.; Rad, R.; Rush, J.; Comb, M. J.; Harper, J. W.; Gygi, S. P., Systematic and quantitative assessment of the ubiquitin-modified proteome. *Mol Cell* **2011,** *44* (2), 325-40.

124.   Tracz, M.; Bialek, W., Beyond K48 and K63: non-canonical protein ubiquitination. *Cell Mol Biol Lett* **2021,** *26* (1), 1.

125.   Soucy, T. A.; Smith, P. G.; Milhollen, M. A.; Berger, A. J.; Gavin, J. M.; Adhikari, S.; Brownell, J. E.; Burke, K. E.; Cardin, D. P.; Critchley, S.; Cullis, C. A.; Doucette, A.; Garnsey, J. J.; Gaulin, J. L.; Gershman, R. E.; Lublinsky, A. R.; McDonald, A.; Mizutani, H.; Narayanan, U.; Olhava, E. J.; Peluso, S.; Rezaei, M.; Sintchak, M. D.; Talreja, T.; Thomas, M. P.; Traore, T.; Vyskocil, S.; Weatherhead, G. S.; Yu, J.; Zhang, J.; Dick, L. R.; Claiborne, C. F.; Rolfe, M.; Bolen, J. B.; Langston, S. P., An inhibitor of NEDD8-activating enzyme as a new approach to treat cancer. *Nature* **2009,** *458* (7239), 732-6.

126.   Brownell, J. E.; Sintchak, M. D.; Gavin, J. M.; Liao, H.; Bruzzese, F. J.; Bump, N. J.; Soucy, T. A.; Milhollen, M. A.; Yang, X.; Burkhardt, A. L.; Ma, J.; Loke, H. K.; Lingaraj, T.; Wu, D.; Hamman, K. B.; Spelman, J. J.; Cullis, C. A.; Langston, S. P.; Vyskocil, S.; Sells, T. B.; Mallender, W. D.; Visiers, I.; Li, P.; Claiborne, C. F.; Rolfe, M.; Bolen, J. B.; Dick, L. R., Substrate-assisted inhibition of ubiquitin-like protein-activating enzymes: the NEDD8 E1 inhibitor MLN4924 forms a NEDD8-AMP mimetic in situ. *Mol Cell* **2010,** *37* (1), 102-11.

127. Strutz, W., Exploring Protein Stability by NanoDSF. *Biophysical Journal* **2016,** *110* (3, Supplement 1), 393a.

128. George, A. J.; Hoffiz, Y. C.; Charles, A. J.; Zhu, Y.; Mabb, A. M., A Comprehensive Atlas of E3 Ubiquitin Ligase Mutations in Neurological Disorders. *Frontiers in Genetics* **2018,** *9* (29).

129. Zhou, L.; Jiang, Y.; Luo, Q.; Li, L.; Jia, L., Neddylation: a novel modulator of the tumor microenvironment. *Molecular Cancer* **2019,** *18* (1), 77.

130. Gong, J.; Huo, J., New insights into the mechanism of F-box proteins in colorectal cancer (Review). *Oncol Rep* **2015,** *33* (5), 2113-2120.

131. Gu, Z. C.; Enenkel, C., Proteasome assembly. *Cellular and Molecular Life Sciences* **2014,** *71* (24), 4729-4745.

132. Song, Y.; Ray, A.; DAS, D. S.; Chauhan, D.; Anderson, K. C., Targeting 19S-Proteasome Deubiquitinase Rpn11/POH1/PSMD14 in Multiple Myeloma. *Blood* **2015,** *126* (23), 1811-1811.

133. Collins, A. S.; McCoy, C. E.; Lloyd, A. T.; O'Farrelly, C.; Stevenson, N. J., miR-19a: An Effective Regulator of SOCS3 and Enhancer of JAK-STAT Signalling. *PLOS ONE* **2013,** *8* (7), e69090.

134. Orabona, C.; Pallotta, M. T.; Volpi, C.; Fallarino, F.; Vacca, C.; Bianchi, R.; Belladonna, M. L.; Fioretti, M. C.; Grohmann, U.; Puccetti, P., SOCS3 drives proteasomal degradation of indoleamine 2,3-dioxygenase (IDO) and antagonizes IDO-dependent tolerogenesis. *Proceedings of the National Academy of Sciences* **2008,** *105* (52), 20828.

135. Kamura, T.; Maenaka, K.; Kotoshiba, S.; Matsumoto, M.; Kohda, D.; Conaway, R. C.; Conaway, J. W.; Nakayama, K. I., VHL-box and SOCS-box domains determine binding specificity for Cul2-Rbx1 and Cul5-Rbx2 modules of ubiquitin ligases. *Genes Dev* **2004,** *18* (24), 3055-65.

136. Soucy, T. A.; Smith, P. G.; Milhollen, M. A.; Berger, A. J.; Gavin, J. M.; Adhikari, S.; Brownell, J. E.; Burke, K. E.; Cardin, D. P.; Critchley, S.; Cullis, C. A.; Doucette, A.; Garnsey, J. J.; Gaulin, J. L.; Gershman, R. E.; Lublinsky, A. R.; McDonald, A.; Mizutani, H.; Narayanan, U.; Olhava, E. J.; Peluso, S.; Rezaei, M.; Sintchak, M. D.; Talreja, T.; Thomas, M. P.; Traore, T.; Vyskocil, S.; Weatherhead, G. S.; Yu, J.; Zhang, J.; Dick, L. R.; Claiborne, C. F.; Rolfe, M.; Bolen, J. B.; Langston, S. P., An inhibitor of NEDD8-activating enzyme as a new approach to treat cancer. *Nature* **2009,** *458* (7239), 732-6.

137. Brownell, J. E.; Sintchak, M. D.; Gavin, J. M.; Liao, H.; Bruzzese, F. J.; Bump, N. J.; Soucy, T. A.; Milhollen, M. A.; Yang, X.; Burkhardt, A. L.; Ma, J.; Loke, H. K.; Lingaraj, T.; Wu, D.; Hamman, K. B.; Spelman, J. J.; Cullis, C. A.; Langston, S. P.; Vyskocil, S.; Sells, T. B.; Mallender, W. D.; Visiers, I.; Li, P.; Claiborne, C. F.; Rolfe, M.; Bolen, J. B.; Dick, L. R., Substrate-assisted inhibition of ubiquitin-like protein-activating enzymes: the NEDD8 E1 inhibitor MLN4924 forms a NEDD8-AMP mimetic in situ. *Mol Cell* **2010,** *37* (1), 102-11.

138. Larrieu, D.; Brunet, M.; Vargas, C.; Hanoun, N.; Ligat, L.; Dagnon, L.; Lulka, H.; Pommier, R. M.; Selves, J.; Jády, B. E.; Bartholin, L.; Cordelier, P.; Dufresne, M.; Torrisani, J., The E3 ubiquitin ligase TRIP12 participates in cell cycle progression and chromosome stability. *Scientific Reports* **2020,** *10* (1), 789.

139. Kaiho-Soma, A.; Akizuki, Y.; Igarashi, K.; Endo, A.; Shoda, T.; Kawase, Y.; Demizu, Y.; Naito, M.; Saeki, Y.; Tanaka, K.; Ohtake, F., TRIP12 promotes small-molecule-induced degradation through K29/K48-branched ubiquitin chains. *Molecular Cell* **2021,** *81* (7), 1411-1424.e7.

140. Baba, K.; Miyazaki, T. In *Novel Function of E3 Ubiquitin Ligase Siah2 to Regulate ROS Metabolism*, 2016.

141. Garcia-Limones, C.; Lara-Chica, M.; Jimenez-Jimenez, C.; Perez, M.; Moreno, P.; Munoz, E.; Calzado, M. A., CHK2 stability is regulated by the E3 ubiquitin ligase SIAH2. *Oncogene* **2016,** *35* (33), 4289-301.

142. Chan, D. W.; Chan, C. Y.; Yam, J. W. P.; Ching, Y. P.; Ng, I. O. L., Prickle-1 Negatively Regulates Wnt/β-Catenin Pathway by Promoting Dishevelled Ubiquitination/Degradation in Liver Cancer. *Gastroenterology* **2006,** *131* (4), 1218-1227.

143. Ronchi, V. P.; Haas, A. L., Measuring rates of ubiquitin chain formation as a functional readout of ligase activity. *Methods Mol Biol* **2012,** *832*, 197-218.

144. Groettrup, M.; Pelzer, C.; Schmidtke, G.; Hofmann, K., Activating the ubiquitin family: UBA6 challenges the field. *Trends in Biochemical Sciences* **2008,** *33* (5), 230-237.

145. Pelzer, C.; Groettrup, M., FAT10 : Activated by UBA6 and Functioning in Protein Degradation. *Subcell Biochem* **2010,** *54*, 238-46.

146. Raasi, S.; Schmidtke, G.; de Giuli, R.; Groettrup, M., A ubiquitin-like protein which is synergistically inducible by interferon-γ and tumor necrosis factor-α. *European Journal of Immunology* **1999,** *29* (12), 4030-4036.

147. Bellora, F.; Castriconi, R.; Dondero, A.; Reggiardo, G.; Moretta, L.; Mantovani, A.; Moretta, A.; Bottino, C., The interaction of human natural killer cells with either unpolarized or polarized

macrophages results in different functional outcomes. *Proc Natl Acad Sci U S A* **2010,** *107* (50), 21659-64.

148. Park, A.; Yang, Y.; Lee, Y.; Kim, M. S.; Park, Y. J.; Jung, H.; Kim, T. D.; Lee, H. G.; Choi, I.; Yoon, S. R., Indoleamine-2,3-Dioxygenase in Thyroid Cancer Cells Suppresses Natural Killer Cell Function by Inhibiting NKG2D and NKp46 Expression via STAT Signaling Pathways. *J Clin Med* **2019,** *8* (6).

149. Theorell, J.; Gustavsson, A. L.; Tesi, B.; Sigmundsson, K.; Ljunggren, H. G.; Lundback, T.; Bryceson, Y. T., Immunomodulatory activity of commonly used drugs on Fc-receptor-mediated human natural killer cell activation. *Cancer Immunol Immunother* **2014,** *63* (6), 627-41.

150. Li, Z.; Cvijic, M. E.; Zhang, L., 2.15 - Cellular Imaging in Drug Discovery: Imaging and Informatics for Complex Cell Biology. In *Comprehensive Medicinal Chemistry III*, Chackalamannil, S.; Rotella, D.; Ward, S. E., Eds. Elsevier: Oxford, 2017; pp 362-387.

151. Gong, C.; Ni, Z.; Yao, C.; Zhu, X.; Ni, L.; Wang, L.; Zhu, S., A High-Throughput Assay for Screening of Natural Products that Enhanced Tumoricidal Activity of NK Cells. *Biol Proced Online* **2015,** *17*, 12.

152. Kim, N.; Choi, J.-W.; Park, H.-R.; Kim, I.; Kim, H. S., Amphotericin B, an Anti-Fungal Medication, Directly Increases the Cytotoxicity of NK Cells. *International Journal of Molecular Sciences* **2017,** *18* (6), 1262.

153. Fassy, J.; Tsalkitzi, K.; Salavagione, E.; Hamouda-Tekaya, N.; Braud, V. M., A real-time digital bio-imaging system to quantify cellular cytotoxicity as an alternative to the standard chromium-51 release assay. *Immunology* **2017,** *150* (4), 489-494.

154. Hayek, S.; Bekaddour, N.; Besson, L.; Alves de Sousa, R.; Pietrancosta, N.; Viel, S.; Smith, N.; Jacob, Y.; Nisole, S.; Mandal, R.; Wishart, D. S.; Walzer, T.; Herbeuval, J. P.; Vidalain, P. O., Identification of Primary Natural Killer Cell Modulators by Chemical Library Screening with a Luciferase-Based Functional Assay. *SLAS Discov* **2019,** *24* (1), 25-37.

155. Lee, G.; Karunanithi, S.; Jackson, Z.; Wald, D., Small Molecule Screening Identifies Rho-Associate Protein Kinase (ROCK) As a Regulator of NK Cell Cytotoxicity Against Cancer. *Blood* **2019,** *134* (Supplement_1), 3607-3607.

156. Xu, Z.; Zhu, X.; Su, L.; Zou, C.; Chen, X.; Hou, Y.; Gong, C.; Ng, W.; Ni, Z.; Wang, L.; Yan, X.; Zhu, Y.; Jiao, X.; Yao, C.; Zhu, S., A high-throughput assay for screening natural products that boost NK cell-mediated killing of cancer cells. *Pharmaceutical Biology* **2020,** *58* (1), 357-366.

157. Cortés-Kaplan, S.; Hasim, M. S.; Kaczmarek, S.; Taha, Z.; Maznyi, G.; McComb, S.; Lee, S.-H.; Diallo, J.-S.; Ardolino, M., A small molecule drug screening identifies colistin sulfate as an enhancer of Natural Killer cell cytotoxicity. *bioRxiv* **2021**, 2021.08.20.457155.

158. Fan, F.; Wood, K. V., Bioluminescent assays for high-throughput screening. *Assay Drug Dev Technol* **2007,** *5* (1), 127-36.

159. Somanchi, S. S.; McCulley, K. J.; Somanchi, A.; Chan, L. L.; Lee, D. A., A Novel Method for Assessment of Natural Killer Cell Cytotoxicity Using Image Cytometry. *PLOS ONE* **2015,** *10* (10), e0141074.

160. Shamir, M.; Bar-On, Y.; Phillips, R.; Milo, R., SnapShot: Timescales in Cell Biology. *Cell* **2016,** *164* (6), 1302-1302 e1.

161. Li, M. J.; Wang, X.; Chen, Y.; Li, G. J.; Zhao, G. Q.; Xiang, B. Q.; Wei, X. Q.; Lei, Y. J.; Huang, Y. C., The influences of TGF-beta1 upon the human adenocarcinoma cell of lung A549 and cellular immunity. *Ann Transl Med* **2020,** *8* (17), 1076.

162. Mao, Y.; Sarhan, D.; Steven, A.; Seliger, B.; Kiessling, R.; Lundqvist, A., Inhibition of tumor-derived prostaglandin-e2 blocks the induction of myeloid-derived suppressor cells and recovers natural killer cell activity. *Clin Cancer Res* **2014,** *20* (15), 4096-106.

163. Angelo, L. S.; Banerjee, P. P.; Monaco-Shawver, L.; Rosen, J. B.; Makedonas, G.; Forbes, L. R.; Mace, E. M.; Orange, J. S., Practical NK cell phenotyping and variability in healthy adults. *Immunol Res* **2015,** *62* (3), 341-56.

164. Millard, A. L.; Valli, P. V.; Stussi, G.; Mueller, N. J.; Yung, G. P.; Seebach, J. D., Brief Exercise Increases Peripheral Blood NK Cell Counts without Immediate Functional Changes, but Impairs their Responses to ex vivo Stimulation. *Front Immunol* **2013,** *4*, 125.

165. Alisson-Silva, F.; Freire-de-Lima, L.; Donadio, J. L.; Lucena, M. C.; Penha, L.; Sa-Diniz, J. N.; Dias, W. B.; Todeschini, A. R., Increase of O-glycosylated oncofetal fibronectin in high glucose-induced epithelial-mesenchymal transition of cultured human epithelial cells. *PLoS One* **2013,** *8* (4), e60471.

166. Luo, X.; Liu, Y.; Wang, R.; Hu, H.; Zeng, R.; Chen, H., A high-quality secretome of A549 cells aided the discovery of C4b-binding protein as a novel serum biomarker for non-small cell lung cancer. *J Proteomics* **2011,** *74* (4), 528-38.

167. Bello, T.; Gujral, T. S., KInhibition: A Kinase Inhibitor Selection Portal. *iScience* **2018,** *8*, 49-53.

168. Grisan, F.; Iannucci, L. F.; Surdo, N. C.; Gerbino, A.; Zanin, S.; Di Benedetto, G.; Pozzan, T.; Lefkimmiatis, K., PKA compartmentalization links cAMP signaling and autophagy. *Cell Death Differ* **2021,** *28* (8), 2436-2449.

169. Ugland, H.; Naderi, S.; Brech, A.; Collas, P.; Blomhoff, H. K., cAMP induces autophagy via a novel pathway involving ERK, cyclin E and Beclin 1. *Autophagy* **2011,** *7* (10), 1199-211.

170. Robke, L.; Laraia, L.; Carnero Corrales, M. A.; Konstantinidis, G.; Muroi, M.; Richters, A.; Winzker, M.; Engbring, T.; Tomassi, S.; Watanabe, N.; Osada, H.; Rauh, D.; Waldmann, H.; Wu, Y. W.; Engel, J., Phenotypic Identification of a Novel Autophagy Inhibitor Chemotype Targeting Lipid Kinase VPS34. *Angew Chem Int Ed Engl* **2017,** *56* (28), 8153-8157.

171. Virginie Rabolli, M. M., Ariane Scoumanne, Marie-Claire Letellier, Stefano Crosignani, Christophe Quéva, Michel Detheux, Jakub M. Swiercz, Sandra CauwenberghsVirginie Rabolli, Murielle Martini, Ariane Scoumanne, Marie-Claire Letellier, Stefano Crosignani, Christophe Quéva, Michel Detheux, Jakub M. Swiercz, Sandra Cauwenberghs, Development and validation of a phenotypic screening platform for the identification of novel immuno-oncology targets [abstract]. *AACR; Cancer Immunol Res, International Cancer Immunotherapy Conference* **2016,** *4* (Abstract nr B030).

172. Guo, W.; Yao, S.; Sun, P.; Yang, T. B.; Tang, C. P.; Zheng, M. Y.; Ye, Y.; Meng, L. H., Discovery and characterization of natural products as novel indoleamine 2,3-dioxygenase 1 inhibitors through high-throughput screening. *Acta Pharmacol Sin* **2020,** *41* (3), 423-431.

173. Rohrig, U. F.; Majjigapu, S. R.; Chambon, M.; Bron, S.; Pilotte, L.; Colau, D.; Van den Eynde, B. J.; Turcatti, G.; Vogel, P.; Zoete, V.; Michielin, O., Detailed analysis and follow-up studies of a high-throughput screening for indoleamine 2,3-dioxygenase 1 (IDO1) inhibitors. *Eur J Med Chem* **2014,** *84*, 284-301.

174. Crosignani, S.; Bingham, P.; Bottemanne, P.; Cannelle, H.; Cauwenberghs, S.; Cordonnier, M.; Dalvie, D.; Deroose, F.; Feng, J. L.; Gomes, B.; Greasley, S.; Kaiser, S. E.; Kraus, M.; Negrerie, M.; Maegley, K.; Miller, N.; Murray, B. W.; Schneider, M.; Soloweij, J.; Stewart, A. E.; Tumang, J.; Torti, V. R.; Van Den Eynde, B.; Wythes, M., Discovery of a Novel and Selective Indoleamine 2,3-Dioxygenase (IDO-1) Inhibitor 3-(5-Fluoro-1H-indol-3-yl)pyrrolidine-2,5-dione (EOS200271/PF-06840003) and Its Characterization as a Potential Clinical Candidate. *J Med Chem* **2017,** *60* (23), 9617-9629.

175. Peng, Y. H.; Liao, F. Y.; Tseng, C. T.; Kuppusamy, R.; Li, A. S.; Chen, C. H.; Fan, Y. S.; Wang, S. Y.; Wu, M. H.; Hsueh, C. C.; Chang, J. Y.; Lee, L. C.; Shih, C.; Shia, K. S.; Yeh, T. K.; Hung, M. S.; Kuo, C. C.; Song, J. S.; Wu, S. Y.; Ueng, S. H., Unique Sulfur-Aromatic Interactions Contribute to the Binding of Potent Imidazothiazole Indoleamine 2,3-Dioxygenase Inhibitors. *J Med Chem* **2020,** *63* (4), 1642-1659.

176. Van den Eynde, B. J.; van Baren, N.; Baurain, J.-F., Is There a Clinical Future for IDO1 Inhibitors After the Failure of Epacadostat in Melanoma? *Annual Review of Cancer Biology* **2020,** *4* (1), 241-256.

177. Schneider, W. M.; Chevillotte, M. D.; Rice, C. M., Interferon-stimulated genes: a complex web of host defenses. *Annu Rev Immunol* **2014,** *32*, 513-545.

178. Tian, C. Q.; Chen, L.; Chen, H. D.; Huan, X. J.; Hu, J. P.; Shen, J. K.; Xiong, B.; Wang, Y. Q.; Miao, Z. H., Inhibition of the BET family reduces its new target gene IDO1 expression and the production of L-kynurenine. *Cell Death Dis* **2019,** *10* (8), 557.

179. Zengerle, M.; Chan, K.-H.; Ciulli, A., Selective Small Molecule Induced Degradation of the BET Bromodomain Protein BRD4. *ACS chemical biology* **2015,** *10* (8), 1770-1777.

180. Reeder, B. J.; Grey, M.; Silaghi-Dumitrescu, R.-L.; Svistunenko, D. A.; Bülow, L.; Cooper, C. E.; Wilson, M. T., Tyrosine Residues as Redox Cofactors in Human Hemoglobin. *Journal of Biological Chemistry* **2008,** *283* (45), 30780-30787.

181. Aschenbrenner, B.; Druyan, R.; Albin, R.; Rabinowitz, M., Haem a, cytochrome c and total protein turnover in mitochondria from rat heart and liver. *Biochem J* **1970,** *119* (2), 157-60.

182. Troester, M. A.; Lindstrom, A. B.; Kupper, L. L.; Waidyanatha, S.; Rappaport, S. M., Stability of Hemoglobin and Albumin Adducts of Benzene Oxide and 1,4-Benzoquinone after Administration of Benzene to F344 Rats. *Toxicological Sciences* **2000,** *54* (1), 88-94.

183. Stevens, J. M.; Uchida, T.; Daltrop, O.; Ferguson, S. J., Covalent cofactor attachment to proteins: cytochrome c biogenesis. *Biochemical Society Transactions* **2005,** *33* (4), 792-795.

184. Shimizu, T.; Lengalova, A.; Martinek, V.; Martinkova, M., Heme: emergent roles of heme in signal transduction, functional regulation and as catalytic centres. *Chem Soc Rev* **2019,** *48* (24), 5624-5657.

185. Kennel, K. B.; Greten, F. R., Immune cell - produced ROS and their impact on tumor growth and metastasis. *Redox Biology* **2021,** *42*, 101891.

186.   Fiorito, V.; Chiabrando, D.; Petrillo, S.; Bertino, F.; Tolosano, E., The Multifaceted Role of Heme in Cancer. *Front Oncol* **2019,** *9*, 1540.

187.   Ferreira, G. C., Heme Synthesis. In *Encyclopedia of Biological Chemistry (Second Edition)*, Lennarz, W. J.; Lane, M. D., Eds. Academic Press: Waltham, 2013; pp 539-542.

188.   Mezrich, J. D.; Fechner, J. H.; Zhang, X.; Johnson, B. P.; Burlingham, W. J.; Bradfield, C. A., An interaction between kynurenine and the aryl hydrocarbon receptor can generate regulatory T cells. *J Immunol* **2010,** *185* (6), 3190-8.

189.   Röhrig, U. F.; Zoete, V.; Michielin, O., Inhibitors of the Kynurenine Pathway. In *Cancer II*, Waring, M. J., Ed. Springer International Publishing: Cham, 2018; pp 371-371.

190.   Tomek, P.; Palmer, B. D.; Flanagan, J. U.; Sun, C.; Raven, E. L.; Ching, L. M., Discovery and evaluation of inhibitors to the immunosuppressive enzyme indoleamine 2,3-dioxygenase 1 (IDO1): Probing the active site-inhibitor interactions. *Eur J Med Chem* **2017,** *126*, 983-996.

191.   Schapira, M.; Calabrese, M. F.; Bullock, A. N.; Crews, C. M., Targeted protein degradation: expanding the toolbox. *Nature Reviews Drug Discovery* **2019,** *18* (12), 949-963.

192.   Mondanelli, G.; Coletti, A.; Greco, F. A.; Pallotta, M. T.; Orabona, C.; Iacono, A.; Belladonna, M. L.; Albini, E.; Panfili, E.; Fallarino, F.; Gargaro, M.; Manni, G.; Matino, D.; Carvalho, A.; Cunha, C.; Maciel, P.; Di Filippo, M.; Gaetani, L.; Bianchi, R.; Vacca, C.; Iamandii, I. M.; Proietti, E.; Boscia, F.; Annunziato, L.; Peppelenbosch, M.; Puccetti, P.; Calabresi, P.; Macchiarulo, A.; Santambrogio, L.; Volpi, C.; Grohmann, U., Positive allosteric modulation of indoleamine 2,3-dioxygenase 1 restrains neuroinflammation. *Proc Natl Acad Sci U S A* **2020,** *117* (7), 3848-3857.

193.   Nelp, M. T.; Zheng, V.; Davis, K. M.; Stiefel, K. J. E.; Groves, J. T., Potent Activation of Indoleamine 2,3-Dioxygenase by Polysulfides. *J Am Chem Soc* **2019,** *141* (38), 15288-15300.

194.   Pallotta, M. T.; Orabona, C.; Volpi, C.; Vacca, C.; Belladonna, M. L.; Bianchi, R.; Servillo, G.; Brunacci, C.; Calvitti, M.; Bicciato, S.; Mazza, E. M.; Boon, L.; Grassi, F.; Fioretti, M. C.; Fallarino, F.; Puccetti, P.; Grohmann, U., Indoleamine 2,3-dioxygenase is a signaling protein in long-term tolerance by dendritic cells. *Nat Immunol* **2011,** *12* (9), 870-8.

195.   Albini, E.; Rosini, V.; Gargaro, M.; Mondanelli, G.; Belladonna, M. L.; Pallotta, M. T.; Volpi, C.; Fallarino, F.; Macchiarulo, A.; Antognelli, C.; Bianchi, R.; Vacca, C.; Puccetti, P.; Grohmann, U.; Orabona, C., Distinct roles of immunoreceptor tyrosine-based motifs in immunosuppressive indoleamine 2,3-dioxygenase 1. *Journal of Cellular and Molecular Medicine* **2017,** *21* (1), 165-176.

196.   Daniels, D. L.; Riching, K. M.; Urh, M., Monitoring and deciphering protein degradation pathways inside cells. *Drug Discovery Today: Technologies* **2019,** *31*, 61-68.

197.   Bond, M. J.; Crews, C. M., Proteolysis targeting chimeras (PROTACs) come of age: entering the third decade of targeted protein degradation. *RSC Chem Biol* **2021,** *2* (3), 725-742.

198.   Naito, M.; Ohoka, N.; Shibata, N.; Tsukumo, Y., Targeted Protein Degradation by Chimeric Small Molecules, PROTACs and SNIPERs. *Front Chem* **2019,** *7*, 849.

199.   Osborne, C. K.; Wakeling, A.; Nicholson, R. I., Fulvestrant: an oestrogen receptor antagonist with a novel mechanism of action. *British Journal of Cancer* **2004,** *90* (1), S2-S6.

200.   Lindner, S.; Krönke, J., The molecular mechanism of thalidomide analogs in hematologic malignancies. *J Mol Med (Berl)* **2016,** *94* (12), 1327-1334.

201.   Yu, F.; Cai, M.; Shao, L.; Zhang, J., Targeting Protein Kinases Degradation by PROTACs. *Frontiers in Chemistry* **2021,** *9* (498).

202.   Mullard, A., Targeted protein degraders crowd into the clinic. *Nat Rev Drug Discov* **2021,** *20* (4), 247-250.

203.   Sakamoto, K. M.; Kim, K. B.; Verma, R.; Ransick, A.; Stein, B.; Crews, C. M.; Deshaies, R. J., Development of Protacs to Target Cancer-promoting Proteins for Ubiquitination and Degradation*. *Molecular & Cellular Proteomics* **2003,** *2* (12), 1350-1358.

204.   Hu, M.; Zhou, W.; Wang, Y.; Yao, D.; Ye, T.; Yao, Y.; Chen, B.; Liu, G.; Yang, X.; Wang, W.; Xie, Y., Discovery of the first potent proteolysis targeting chimera (PROTAC) degrader of indoleamine 2,3-dioxygenase 1. *Acta Pharm Sin B* **2020,** *10* (10), 1943-1953.

205.   Endo, R.; Nakamura, T.; Kawakami, K.; Sato, Y.; Harashima, H., The silencing of indoleamine 2,3-dioxygenase 1 (IDO1) in dendritic cells by siRNA-loaded lipid nanoparticles enhances cell-based cancer immunotherapy. *Scientific Reports* **2019,** *9* (1), 11335.

206.   Park, Y.; Yoon, S. K.; Yoon, J.-B., TRIP12 functions as an E3 ubiquitin ligase of APP-BP1. *Biochemical and Biophysical Research Communications* **2008,** *374* (2), 294-298

207.   Huang, F.; Feng, Y.; Peterlin, B. M.; Fujinaga, K., P-TEFb is degraded by Siah1/2 in quiescent cells. *bioRxiv* **2022**, 2021.12.30.474394.
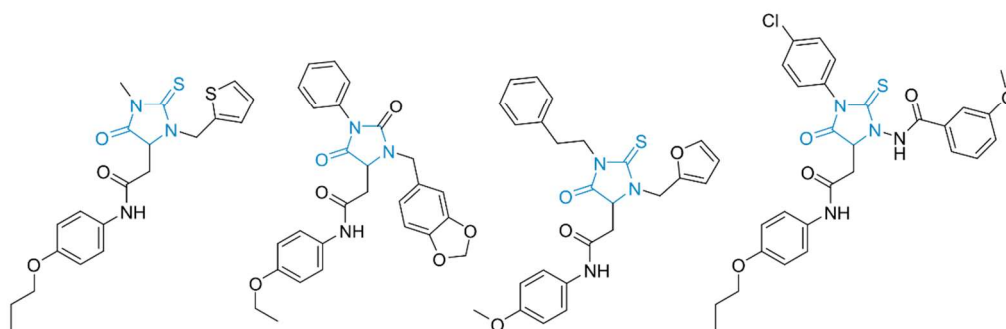
# 9. Appendix

9.1 Supplementary figures

A
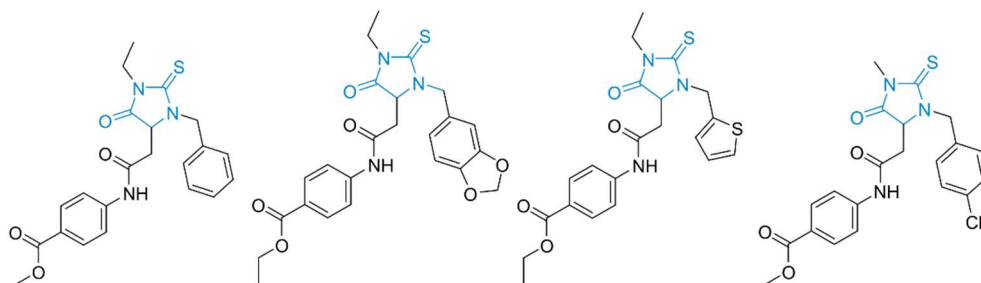
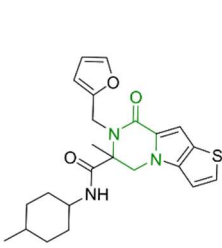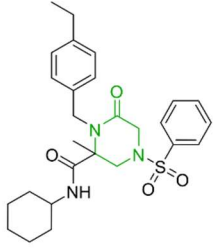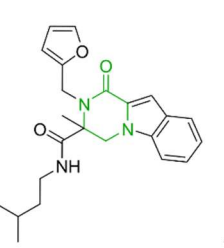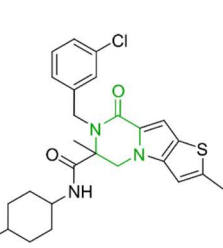| Compound	**9**	**13**	**14**	**15**
Kyn assay IC$_{50}$ / μM	0.006 ± 0.003	0.008 ± 0.005	0.013 ± 0.01	0.23 ± 0.06
IDO1 activity assay IC$_{50}$ / μM	0.44 ± 0.18	0.62 ± 0.48	0.55 ± 0.23	4.43 ± 1.13
Cell count IC$_{50}$ / μM	inactive	inactive	inactive	inactive

----

Compound	**16**	**17**	**18**	**19**
Kyn assay IC$_{50}$ / μM	1.08 ± 0.003	1.11 ± 0.22	≥ 10	inactive
IDO1 activity assay IC$_{50}$ / μM	≥ 30	8.39 ± 1.71	inactive	inactive
Cell count IC$_{50}$ / μM	inactive	inactive	inactive	inactive
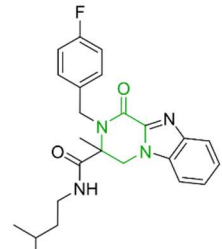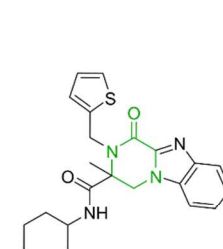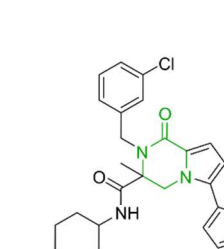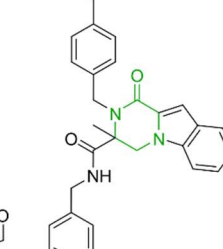
B
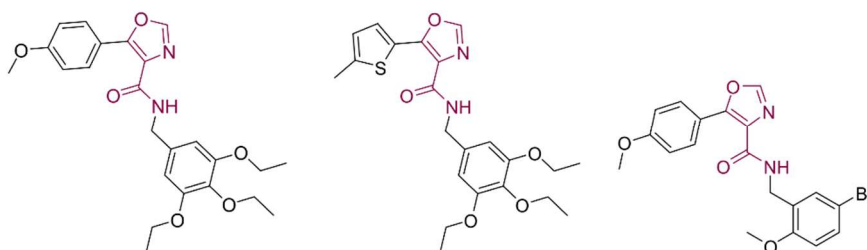
Compound	**10**	**20**	**21**
Kyn assay IC$_{50}$ / μM	0.005 ± 0.001	0.008 ± 0.002	1.01 ± 0.20
IDO1 activity assay IC$_{50}$ / μM	0.73 ± 0.45	1.45 ± 0.39	inactive
Cell count IC$_{50}$ / μM	inactive	inactive	inactive

C

Compound	**11**	**22**	**23**	**24**
Kyn assay IC$_{50}$ / µM	0.05 ± 0.02	0.09 ± 0.03	0.30 ± 0.11	0.40 ± 0.23
IDO1 activity assay IC$_{50}$ / µM	2.35 ± 1.83	1.85 ± 1.06	≥ 60	≥ 60
Cell count IC$_{50}$ / µM	inactive	inactive	inactive	inactive

Compound	**25**	**26**	**27**	**28**
Kyn assay IC$_{50}$ / µM	0.44 ± 0.22	0.53 ± 0.07	0.90 ± 0.37	2.60 ± 0.48
IDO1 activity assay IC$_{50}$ / µM	≥ 30	≥ 30	≥ 30	inactiv
Cell count IC$_{50}$ / µM	inactive	inactive	inactive	inactive
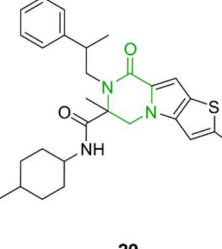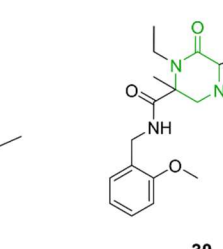
Compound	**29**	**30**
Kyn assay IC$_{50}$ / µM	≥ 10	inactive
IDO1 activity assay IC$_{50}$ / µM	inactive	inactive
Cell count IC$_{50}$ / µM	inactive	inactive

Figure S1: **Further derivatives of IDO1 inhibitors 9, 10 and 11.** Kyn was detected utilizing sensor 6 in the Kyn assay as well as in the IDO1 activity assay. (A) Structures and IC$_{50}$ values of derivatives of compound **9**. (B) Structures and IC$_{50}$ values of derivatives of compound **10**. (C) Structures and IC$_{50}$ values of derivatives of compound **11**. IC$_{50}$ values in the automated Kyn assay were determined in BxPC3 cells. IC$_{50}$ values in the IDO1 activity assay were determined with recombinant human IDO1 protein. Cell count was evaluated using Hoechst 33342 for compound cytotoxicity. Data are mean values ± SD, n ≥ 3.
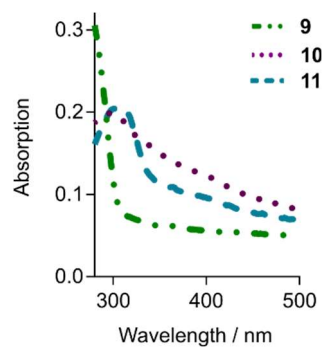
Figure S2: **UV-VIS spectrum of compounds 9, 10 and 11**. Compounds were diluted to 200 µM in 100 mM K-PO$_4$ buffer and UV-VIS spectrum was monitored.
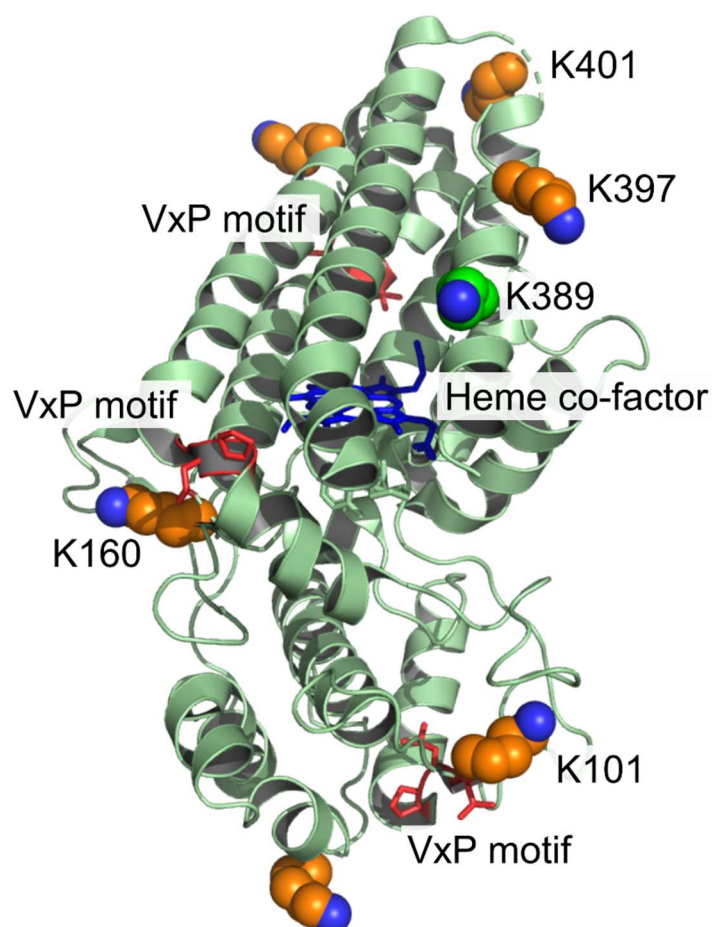
Figure S 3: **IDO1 crystal structure that highlights the not identified lysines and VxP motifs**. Crystal structure of IDO1 (PDB: 5ek4) in which lysine residues are highlighted that were not identified by MS (orange), K389 is the lysine residue that was found to be polyubiquitinated (green) and VxP motif is highlighted in red. The heme cofactor of IDO1 is shown in the catalytic pocket.

9.2 Abbreviations

Abbreviation	Meaning
1-NMPP	N-methyl protoporphyrin IX
A549Green	A549 cells expressing Histone H2B type 1-J-eGFP
AhR	Aryl hydrocarbon receptor
APS	Ammonium persulfate
BRD4	Bromodomain-containing protein 4
CAR	Chimeric antigen receptor
CETSA	Cellular thermal shift assay
CFZ	Carfilzomib
CHX	Cycloheximide
Co-IP	Co-immunoprecipitation
COMAS	Compound management and screening center
CRBN	Cereblon
CREB	cAMP response element-binding protein
CRL	cullin-RING E3 ligases
CTL	Control
CUL2	Cullin 2
Da	Dalton
DC	Dendritic cell
DC_{50}	Half-maximal degrading concentration
D_{max}	Maximal degradation percentage
DMEM	Dulbecco's Modified Eagle Medium
DMSO	Dimethyl sulfoxide
DNA-PK	DNA-dependent protein kinase
DTE	Dithioerythritol
DTT	Dithiotreitol
DVL3	Dishevelled
E:T	Effector to target ratio
E2	Ubiquitin-conjugating enzyme
E3	E3 ubiquitin ligase
Em	Emission wavelength
Ex	Excitation wavelength
FBS	Fetal bovine serum
GFP	green fluorescent protein
GPDH	Glycerol-3-phosphate dehydrogenase
GzmB	Granzyme B

Abbreviation	Meaning
h	Hours
HPG	L-homopropargylglycine
HPLC	High performance liquid chromatography
HRP	Horseradish peroxidase
HTS	High-throughput screen
IC_{50}	Half-maximal inhibitory concentration
iDeg-1	Induced IDO degradation compound-1
IDO1	Indoleamine 2,3-dioxygenase 1
IFNγ	Interferon gamma
IMiDs	Immunomodulatory imide drugs
ITIM	immunoreceptor tyrosine-based inhibitory motif
K	Lysine
Kyn	Kynurenine
LC-MS/MS	Liquid Chromatography with tandem mass spectrometry
LFQ	Label-free quantification
L-Trp	L-Tryptophan
M	Molar
min	Minutes
MoA	mode-of-action
MS	Mass spectrometry
mTOR	Mammalian target of rapamycin
mTORC1	mTOR complex 1
NFK	*N*-formylkynurenine
NK cells	Natural killer cells
NKG2D	Natural killer group 2-member D
NKp	Natural killer protein
nm	Nanometers
PAGE	Polyacrylamide gel electrophoresis
PAINS	Pan-assay interference
PBMC	Peripheral blood mononuclear cells
PBS	Phosphate-buffered saline
pDC	plasmacytoid DC
p-DMAB	*p*-dimethylamino benzaldehyde
PEX10	Peroxisome biogenesis factor 10
PGE2	Prostaglandin E2
PHF1	PHD finger protein 1
PRICKLE1	Prickle-like protein 1
PSMD14	26S proteasome non-ATPase regulatory subunit 14
PTGER1-4	PGE receptor EP1 - EP4 subtypes

Abbreviation	Meaning
RBX1	E3 ubiquitin-protein ligase RBX1
RFPL4AL1	Ret finger protein-like 4A-like protein 1
rhIDO1	Recombinant human IDO1
S/B	Signal to background
SA	Succinylacetone
SD	Standard deviations
sec	Seconds
SHP1 / SHP2	Src homology 2 domain phosphatases
SIAH2	Seven in Absentia Homolog 2, E3 ubiquitin-protein ligase
SKP2	S-phase kinase-associated protein 2
SOCS3	Suppressor of cytokine signaling 3
TRIP12	Thyroid hormone Receptor Interacting Protein 12; E3 ubiquitin-protein ligase
TUBE	Tandem ubiquitin binding entity
Ub	Ubiquitin
UBA6	Ubiquitin-like modifier-activating enzyme 6
UPS	Ubiquitin-proteasome-system
USP44	Ubiquitin carboxyl-terminal hydrolase 44
VHL	Von Hipple Lindau

9.3 Acknowledgements